OXIDATIVE STRESS RELATED TO CELLULAR METABOLISM IN LUNG HEALTH AND DISEASES

EDITED BY: Arunachalam Karuppusamy, Anand Krishnan, Palanisamy Subramanian and Vikas Anathy

PUBLISHED IN: Frontiers in Pharmacology

frontiers Research Topics

frontiers

ISSN 1664-8714
ISBN 978-2-83250-810-7
DOI 10.3389/978-2-83250-810-7

About Frontiers

Frontiers is more than just an open-access publisher of scholarly articles: it is a pioneering approach to the world of academia, radically improving the way scholarly research is managed. The grand vision of Frontiers is a world where all people have an equal opportunity to seek, share and generate knowledge. Frontiers provides immediate and permanent online open access to all its publications, but this alone is not enough to realize our grand goals.

Frontiers Journal Series

The Frontiers Journal Series is a multi-tier and interdisciplinary set of open-access, online journals, promising a paradigm shift from the current review, selection and dissemination processes in academic publishing. All Frontiers journals are driven by researchers for researchers; therefore, they constitute a service to the scholarly community. At the same time, the Frontiers Journal Series operates on a revolutionary invention, the tiered publishing system, initially addressing specific communities of scholars, and gradually climbing up to broader public understanding, thus serving the interests of the lay society, too.

Dedication to Quality

Each Frontiers article is a landmark of the highest quality, thanks to genuinely collaborative interactions between authors and review editors, who include some of the world's best academicians. Research must be certified by peers before entering a stream of knowledge that may eventually reach the public - and shape society; therefore, Frontiers only applies the most rigorous and unbiased reviews.
Frontiers revolutionizes research publishing by freely delivering the most outstanding research, evaluated with no bias from both the academic and social point of view. By applying the most advanced information technologies, Frontiers is catapulting scholarly publishing into a new generation.

What are Frontiers Research Topics?

Frontiers Research Topics are very popular trademarks of the Frontiers Journals Series: they are collections of at least ten articles, all centered on a particular subject. With their unique mix of varied contributions from Original Research to Review Articles, Frontiers Research Topics unify the most influential researchers, the latest key findings and historical advances in a hot research area! Find out more on how to host your own Frontiers Research Topic or contribute to one as an author by contacting the Frontiers Editorial Office: frontiersin.org/about/contact

OXIDATIVE STRESS RELATED TO CELLULAR METABOLISM IN LUNG HEALTH AND DISEASES

Topic Editors:
Arunachalam Karuppusamy, Chinese Academy of Sciences (CAS), China
Anand Krishnan, University of the Free State, South Africa
Palanisamy Subramanian, Gangneung–Wonju National University, South Korea
Vikas Anathy, University of Vermont, United States

Citation: Karuppusamy, A., Krishnan, A., Subramanian, P., Anathy, V., eds. (2022). Oxidative Stress Related to Cellular Metabolism in Lung Health and Diseases. Lausanne: Frontiers Media SA. doi: 10.3389/978-2-83250-810-7

Table of Contents

frontiers | Frontiers in Pharmacology

TYPE Editorial
PUBLISHED 03 November 2022
DOI 10.3389/fphar.2022.1015423

OPEN ACCESS

EDITED AND REVIEWED BY
Paolo Montuschi,
Catholic University of the Sacred Heart, Italy

*CORRESPONDENCE
Karuppusamy Arunachalam,
arunachalam04@gmail.com

SPECIALTY SECTION
This article was submitted to Respiratory Pharmacology, a section of the journal Frontiers in Pharmacology

RECEIVED 09 August 2022
ACCEPTED 05 October 2022
PUBLISHED 03 November 2022

CITATION
Arunachalam K, Anand K, Palanisamy S and Anathy V (2022), Editorial: Oxidative stress related to cellular metabolism in lung health and diseases.
Front. Pharmacol. 13:1015423.
doi: 10.3389/fphar.2022.1015423

Editorial: Oxidative stress related to cellular metabolism in lung health and diseases

Karuppusamy Arunachalam[1,2,3]*, Krishnan Anand[4], Subramanian Palanisamy[5,6] and Vikas Anathy[7]

[1]Key Laboratory of Economic Plants and Biotechnology and the Yunnan Key Laboratory for Wild Plant Resources, Kunming Institute of Botany, Chinese Academy of Sciences, Kunming, China, [2]Southeast Asia Biodiversity Research Institute, Chinese Academy of Sciences, Naypyidaw, Myanmar, [3]Centro de Estudos em Células Tronco, Terapia Celular e Genética Toxicológica (CeTroGen), Programa de Pós-graduação em Saúde e Desenvolvimento na Região Centro-Oeste, Faculdade de Medicina Dr. Hélio Mandetta (FAMED), Universidade Federal de Mato Grosso do Sul (UFMS), Campo Grande, Mato Grosso do Sul, Brazil, [4]Department of Chemical Pathology, School of Pathology, Faculty of Health Sciences, University of the Free State, Bloemfontein, South Africa, [5]Department of Marine Food Science and Technology, Gangneung-Wonju National University, Gangneung, Gangwon, South Korea, [6]East Coast Life Sciences Institute, Gangneung-Wonju National University, Gangneung, Gangwon, South Korea, [7]Department of Pathology, University of Vermont, Burlington, VT, United States

KEYWORDS

reactive oxygen species, oxidative stress, lung disease, respiratory illness, drug toxicity and therapy

Editorial on the Research Topic
Oxidative stress related to cellular metabolism in lung health and diseases

Cellular metabolism is constantly exposed to oxidants that are produced either endogenously (e.g., by mitochondrial electron transport during respiration or the activation of phagocytes) or exogenously (e.g., by air pollutants and cigarette smoke) (Wilson et al., 2002; Sharifi-Rad et al., 2020). ROS-mediated damage to the lungs is facilitated by the high oxygen concentration in the lungs as well as their large surface area and blood supply. Due to an imbalance of oxidants/antioxidants favoring oxidants, oxidative stress causes the oxidation of proteins, DNA, and lipids, and causes secondary metabolic ROS production in cells (Sies, 1991; Park et al., 2009). The role of oxidative stress in lung diseases such as asthma, bronchial asthma (BA), chronic obstructive pulmonary disease (COPD), acute respiratory distress syndrome (ARDS), acute lung injury, and pulmonary fibrosis has now been established (Park et al., 2009).

According to Adeloye et al. (2022), COPD was the third leading cause of death among people aged 30–79 in 2019, affecting approximately 391.9 million people worldwide. In 2015, 0.4 million people died from asthma, making it the most prevalent chronic childhood medical condition (Maurer, 2016; Soriano et al., 2017; The Global Asthma Report, 2018; Mitra et al., 2021). In children under 5 years of age, pneumonia is the most common cause of death. Millions of people are affected by pneumonia each year. The World Health Organization estimates that over 10 million people worldwide die from

tuberculosis (TB) every year, making it the most common infectious disease that causes death (WHO, 2016). Globally, lung cancer incidence, mortality, and prevalence are increasing. According to GLOBOCAN estimates, 2.09 million new cases (11.6%) of lung cancer and 1.76 million deaths (18.4%) occur each year (Bade and Cruz, 2020).Worldwide, 545 million people suffered from chronic respiratory diseases in 2017 (Labaki, and Han, 2020).

Respiratory and lung disease medicine is one of the least developed therapeutic fields, with few innovative pharmaceutical products under development. The reasons for this may be a lack of interest among pharmaceutical firms (despite the prevalence of respiratory disorders in the general population), a lack of funding for fundamental research, inadequate and nonpredictive animal models, or a lack of useful biomarkers. Natural chemicals such as epinephrine, herbal anticholinergics, and adrenal corticosteroids are the most commonly used medications nowadays and perhaps in the future. Unfortunately, novel medications have been unsuccessful in treating asthma (leukotriene receptor antagonists and anti-IgE) and COPD (roflumilast) (Gross and Barnes, 2017).

In recent years, ethnopharmacological studies focused on the bioactivities of natural products [(Aescin (*Aesculus hippocastanum* L.), Baicalin (*Scutellaria baicalensis* Georgi), Bavachinin (*Psoralea corylifolia* L.), Capsaicin (Chilli), Carnosic acid (Rosemary), Celastrol (*Tripterygium wilfordii* Hook.f.), Corylifol A (*Psoralea corylifolia* L.), Curcumin (*Curcuma longa* L.), Emodin (*Polygonum cuspidatum* Siebold & Zucc.), Eriodictyol (*Dracocephalum rupestre* Hance), Ginkgetin (*Ginkgo biloba* L.), Glycyrrhizin (*Glycyrrhiza glabra* L.), Jubanine G (*Ziziphus jujuba* Mill.), Kaempferol (Tea), Luteolin (peppermint), Naringenin (Citrus fruits), Resveratrol (Grapes), Salinomycin (*Streptomyces albus*), and Vanillin (*Vanilla planifolia* Andrews)] against metabolic disorders in lung diseases, since many non-natural, synthetic drugs cause various side effects. Several natural remedies have been shown to possess remarkable bioactivities and are considered to be excellent treatments for lung disease (Rahman et al., 2022). The compounds present in these natural remedies function as antioxidants thereby reducing the risk of asthma, COPD, ALI, lung fibrosis, and lung cancer. However, many natural functional metabolites remain unexplored, and the mechanisms related to their beneficial properties remain unclear. In view of the emerging advances in ethnopharmacology for drug discovery, Frontiers in Pharmacology is presenting a Research Topic entitled *Oxidative stress related to cellular metabolism in lung disease and health* to exhibit recent advances concerning natural products and oxidative stress in inflammatory pulmonary diseases, and possible mechanisms of action. A total of eight original research articles and one review article are included in this Research Topic, having generated 6,709 views and 1,358 downloads to date.

This Research Topic includes a review article by Cui et al., which summarizes current research on the molecular mechanisms of ER stress in pulmonary disease, offering several likely therapeutic causes of pulmonary disease including pulmonary fibrosis, pulmonary infection, asthma, COPD, and lung cancer. In addition, the latest interventions to target ER stress and ROS in pulmonary diseases were discussed.

In the medical management of patients with chronic obstructive pulmonary disease (COPD), herbal supplements exhibiting antioxidant and anti-inflammatory properties have proven to be incredibly effective. In the study by Ghobadi et al., COPD patients in the intervention group received crocin supplementation (30 mg/day for 12 weeks), derived from Saffron (*Crocus sativus* L.). Intervention with crocin for 12 weeks decreased the serum levels of TOS and NF-κB and increased TAOC. Crocin supplementation appears to improve inflammatory conditions and establish an oxidant/antioxidant balance in COPD patients.

In a similar study, Liu et al. evaluated the efficacy of Number 2 Feibi Recipe (N2FBR, a traditional Chinese medicine formula) for treating idiopathic pulmonary fibrosis. As a result of N2FBR treatment, interstitial fibrosis and collagen deposition were effectively alleviated, primarily through upregulation of SOD, GSH-Px, and TAOC, and downregulation of MDA. In addition, N2FBR increased the expressions of LC3B, Beclin-1, LAMP1, and TFEB, and downregulated the expressions of p62 and legumain. TEM observations showed that the N2FBR treatment boosted autophagosome production. In addition, the authors revealed the antioxidative stress and proautophagy effects of N2FBR through GSK-3β/mTOR signaling.

Antioxidant products show promise in the treatment and prevention of respiratory tract diseases. Due to its high nutritional value and pharmacological properties such as hypolipidemicity, hypoglycemicity, and antihypertensivity, as well as its antioxidant and anti-inflammatory properties, *Spirulina platensis*, a filamentous cyanobacterium, has been used as a food supplement by humans for many years (Appel et al., 2018). Brito et al. supplemented rats with *S. platensis* at doses of 50 (SG50), 150 (SG150), and 500 mg/kg (SG500) and the nitrite levels, lipid peroxidation, and antioxidant activity were evaluated through biochemical analysis. The authors observed a decrease in lipid peroxidation in the plasma as well as an increase in oxidation inhibition in the trachea and lung for the SG150 and SG500 doses, suggesting enhanced antioxidant activity. Additionally, the antioxidant activity and nitrite levels increased, and the inflammatory responses were modulated, resulting in a decreased contractile response and an increase in relaxation. Fan et al. used C57B6/J mice and human pulmonary microvascular endothelial cells (HPMECs) to investigate the effects of ventilator-induced lung injury (VILI) and Intermedin (IMD), a member of the calcitonin gene-related peptide (CPRP) superfamily. They also evaluated the potential mechanism by investigating anti-apoptotic and antioxidant stress in mice and HPMECs, in this study discovered that

IMD decreased VILI as well as suppression of the JAK2/STAT3 signaling pathway was a mediator of the anti-apoptotic and antioxidant stress effects of IMD.

A multidisciplinary approach was used to study the effects of *Thuja occidentalis* L. (TO) homeopathic mother tincture and TO-mediated PDT (TO-PDT) on A549 lung cancer cells using photodynamic therapy (PDT). In cells treated with TO and TO-PDT, morphological changes in the nucleus and cell membrane were evident. A dose-dependent increase in LDH release was observed, as well as a decrease in ATP levels and cell viabilities in these groups, indicating the cytotoxic and antiproliferative properties of TO. At the same doses, TO enhanced anticancer responses when photoactivated in PDT, outperforming TO tincture alone. The results demonstrate that TO can be used as a photosensitizer during PDT to enhance its direct cytotoxic effects on cancer cells Loonat et al.

Evidence suggests that chloroquine (an agonist of bitter taste receptors) improves the cell function of ASM cells, which are involved in asthma. Mice were administered chloroquine or dexamethasone before being introduced to house dust mites (HDMs). According to an *in vitro* study, chloroquine markedly reduced maladaptive changes in the ASM phenotype, combined with a reduction in ROS production. In ASM cells, chloroquine inhibits the ROS-AKT response *via* inhibition of oxidative stress levels and PI3K signaling (LY294002). This may constitute a potential mechanism for restoring the phenotypic imbalance caused by H_2O_2 and PI3K inhibition. The findings suggest that chloroquine improves asthmatic airway function by controlling the change in the ASM cell phenotype, providing a new therapeutic profile for airway remodelling Ren et al.

The effects of montelukast and fluticasone on sodium arsenite-induced EMT changes in normal human bronchial cells were investigated. Montelukast was effective in reducing arsenic-induced EMT in human bronchial epithelial cells. Montelukast hindered arsenic-induced cell migration as well as the expressions of extracellular matrix proteins and NF-kB, critical for arsenic-induced EMT, by inhibiting ROS generation and NF-kB activation. In combination with fluticasone, montelukast reversed the inhibitory effects of arsenic on EMT. The purpose of this study was to provide therapeutic strategies and mechanisms for lung epithelia damage caused by arsenic.

Clinical trials have confirmed that the Huashi Baidu Formula (HSBDF) exhibits remarkable clinical efficacy in treating acute lung injury (ALI); it has been approved by the National Medical Products Administration of China. A network pharmacology approach was used to identify the potential regulatory mechanisms of plasma compounds. In order to identify the active compounds, a series of experimental assays was conducted, which included CCK-8, EdU staining, TNF-α, IL-6, MDA, and T-SOD tests, as well as flow cytometry. The pharmacokinetic properties of the active compounds were also predicted. Molecular docking revealed that HSBDF hampered inflammation by inhibiting IL-6R and TNF-α. In the plasma, six key compounds may ameliorate ALI by regulating inflammation and oxidative damage: piceatannol, emodin, aloe-emodin, rhein, luteolin, and quercetin. In addition, the authors found that HSBDF can enhance anti-inflammation and anti-oxidative defenses, as well as decrease cell apoptosis Wang et al.

To summarize, in recent years numerous studies have been performed to analyze the impact of natural products derived from plants and animals. Polyhydroxy compounds such as flavonoids, alkaloids, and terpenoids derived from plants exhibit a variety of *in vitro* and *in vivo* biological effects. These include anti-inflammatory, antiviral, antiplatelet, anti-tumor, anti-allergic, antioxidant, and immunomodulatory effects. Substances with different chemical structures have different biological effects. However, many of these natural drugs do not pass clinical trials due to their toxicities and low bioavailabilities. Acceptable drugs for lung diseases must be screened using pharmacokinetics and pharmacodynamic studies. The literature does not contain many clinical trials using these compounds, and further research is required to confirm their safety and efficacy. In the future, research should focus on the identification and isolation of more effective compounds, their mechanisms of action, formulations, dosage forms, pharmacokinetics, and safety profiles, in order to develop more effective multi-target drugs for respiratory and lung diseases.

Author contributions

KA, contributed to the conceptualization, design, and drafting of the manuscript; AK, contributed to the concept and critical revision of the manuscript; SP and VA, reviewed the manuscript.

Acknowledgments

The guest editors of this Research Topic gratefully acknowledge the efforts and contributions of authors, reviewers, and senior/special editors in Frontiers in Pharmacology.

Conflict of interest

The authors declare that the research was conducted in the absence of any commercial or financial relationships that could be construed as a potential conflict of interest.

Publisher's note

References

Adeloye, D., Song, P., Zhu, Y., Campbell, H., Sheikh, A., and Rudan, I.NIHR RESPIRE Global Respiratory Health Unit (2022). Global, regional, and national prevalence of, and risk factors for, chronic obstructive pulmonary disease (COPD) in 2019: A systematic review and modelling analysis. *Lancet. Respir. Med.* 10, 447–458. doi:10.1016/S2213-2600(21)00511-7

Appel, K., Munoz, E., Navarrete, C., Cruz-Teno, C., Biller, A., and Thiemann, E. (2018). Immunomodulatory and inhibitory effect of Immulina®, and Immunloges® in the ig-E mediated activation of RBL-2H3 cells. A new role in allergic inflammatory responses. *Plants (Basel)* 7 (1), 13. doi:10.3390/plants7010013

Bade, B. C., and Cruz, C. S. D. (2020). Lung cancer 2020: Epidemiology, etiology, and prevention. *Clin. Chest Med.* 41 (1), 1–24. doi:10.1016/j.ccm.2019.10.001

Gross, N. J., and Barnes, P. J. (2017). New therapies for asthma and chronic obstructive pulmonary disease. *Am. J. Respir. Crit. Care Med.* 195 (2), 159–166. doi:10.1164/rccm.201610-2074PP

Labaki, W. W., and Han, M. K. (2020). Chronic respiratory diseases: A global view. *Lancet. Respir. Med.* 8 (6), 531–533. doi:10.1016/S2213-2600(20)30157-0

Maurer, J. R. (2016). Global and regional trends in COPD mortality, 1990-2010. *Yearb. Pulm. Dis.* 2016, 60–61. doi:10.1016/j.ypdi.2016.02.029

Mitra, S., Prova, S. R., Sultana, S. A., Das, R., Nainu, F., Emran, T. B., et al. (2021). Therapeutic potential of indole alkaloids in respiratory diseases: A comprehensive review. *Phytomedicine.* 90, 153649. doi:10.1016/j.phymed.2021.153649

Park, H. S., Kim, S. R., and Lee, Y. C. (2009). Impact of oxidative stress on lung diseases. *Respirology* 14 (1), 27–38. doi:10.1111/j.1440-1843.2008.01447.x

Rahman, M. M., Bibi, S., Rahaman, M. S., Rahman, F., Islam, F., Khan, M. S., et al. (2022). Natural therapeutics and nutraceuticals for lung diseases: Traditional significance, phytochemistry, and pharmacology. *Biomed. Pharmacother.* 150, 113041. doi:10.1016/j.biopha.2022.113041

Sharifi-Rad, M., Anil Kumar, N. V., Zucca, P., Varoni, E. M., Dini, L., Panzarini, E., et al. (2020). Lifestyle, oxidative stress, and antioxidants: Back and forth in the pathophysiology of chronic diseases. *Front. Physiol.* 11, 694. doi:10.3389/fphys.2020.00694

Sies, H. (1991). "Oxidative stress: Introduction," in *Oxidative stress: Oxidants and antioxidants*. Editor H. Sies (London: Academic Press), xv–xxii.

Soriano, J. B., Abajobir, A. A., and Abate, K. H., (2017). Global, regional, and national deaths, prevalence, disability-adjusted life years, and years lived with disability for chronic obstructive pulmonary disease and asthma, 1990–2015: A systematic analysis for the global burden of disease study 2015. *Lancet. Respir. Med.* 5, 691–706. doi:10.1016/S2213-2600(17)30293-X

The Global Asthma Report (2018). Global asthma network 92. Available at: http://globalasthmareport.org/(Accessed date 09 August, 2022).

WHO (2016). *Global tuberculosis report 2016 (WHO/HTM/TB/2016.13)*. Geneva, Switzerland: WHO, 1–214.

Wilson, M., Lightbody, J. H., Donaldson, K., Sales, J., and Stone, V. (2002). Interactions between ultrafine particles and transition metals *in vivo* and *in vitro*. *Toxicol. Appl. Pharmacol.* 84, 172–179. doi:10.1006/taap.2002.9501

frontiers in Pharmacology

ORIGINAL RESEARCH
published: 24 January 2022
doi: 10.3389/fphar.2021.817874

Intermedin Reduces Oxidative Stress and Apoptosis in Ventilator-Induced Lung Injury via JAK2/STAT3

Shulei Fan, Jing He, Yanli Yang and Daoxin Wang**

Department of Respiratory Medicine, Second Affiliated Hospital of Chongqing Medical University, Chongqing, China

Mechanical ventilation is an effective treatment for acute respiratory distress syndrome (ARDS), which can improve the prognosis of ARDS to a certain extent. However, it may further aggravate lung tissue injury, which is defined as ventilator-induced lung injury (VILI). Intermedin (IMD) belongs to the calcitonin gene-related peptide (CPRP) superfamily. Our previous studies have found that IMD reduces the expression proinflammatory cytokines, down-regulates nuclear translocation and improves the integrity of endothelial barrier in ARDS. However, the effect of IMD on VILI has not been clarified. Oxidative stress imbalance and apoptosis are the main pathophysiological characteristics of VILI. In the current study, we used C57B6/J mice and human pulmonary microvascular endothelial cells (HPMECs) to establish a VILI model to analyze the effects of IMD on VILI and explore its potential mechanism. We found that IMD alleviated lung injury and inflammatory response in VILI, mainly in reducing ROS levels, upregulating SOD content, downregulating MDA content, reducing the expression of Bax and caspase-3, and increasing the expression of Bcl-2. In addition, we also found that IMD played its anti-oxidative stress and anti-apoptotic effects via JAK2/STAT3 signaling. Our study may provide some help for the prevention and treatment of VILI.

Keywords: intermedin (IMD), ventilator-induced lung injury, oxidative stress, apoptosis, JAK-STAT signaling pathway

OPEN ACCESS

Edited by:
Anand Krishnan, University of the Free State, South Africa

Reviewed by:
Vivek P. Chavda, L. M. College of Pharmacy, India
Vadivalagan Chithravel, Akfa University, Uzbekistan

****Correspondence:***
Yanli Yang
502613685@qq.com
Daoxin Wang
wangdaoxin0163@163.com

Specialty section:
This article was submitted to Respiratory Pharmacology, a section of the journal Frontiers in Pharmacology

Received: *18 November 2021*
Accepted: *30 December 2021*
Published: *24 January 2022*

Citation:
Fan S, He J, Yang Y and Wang D (2022) Intermedin Reduces Oxidative Stress and Apoptosis in Ventilator-Induced Lung Injury via JAK2/STAT3. Front. Pharmacol. 12:817874. doi: 10.3389/fphar.2021.817874

INTRODUCTION

Acute respiratory distress syndrome (ARDS) is one of the most common critical diseases of the respiratory system, with high mortality and a heavy social burden (Matthay et al., 2019). Mechanical ventilation (MV) restores respiratory muscles and provides sufficient gas exchange, which improves the prognosis of ARDS to a certain extent (Slutsky and Ranieri, 2013; Gaver et al., 2020). However, mechanical ventilation may aggravate lung tissue injury, mainly manifested in infiltration of neutrophils, formation of hyaline membrane, increase of apoptosis, up-regulation of vascular endothelial permeability and formation of pulmonary edema, which is called ventilator-related lung injury (Curley et al., 2016). Endothelial cells (ECs) are the earliest effector cells in lung injury (Matthay et al., 2019). Therefore, reducing endothelial cell injury and maintaining endothelial cell function is the key to alleviating endothelial permeability, reducing pulmonary edema, and reducing mortality (Qi et al., 2016; Huang et al., 2017).

Intermedin (IMD) is a novel polypeptide belonging to the calcitonin superfamily. IMD is widely expressed throughout the body, and its sequence is highly conserved among different species (Hong et al., 2012; Holmes et al., 2020; Sohn et al., 2020). IMD is a homeostasis regulating peptide involved in many life activities, such as glucose and lipid metabolism, inhibition of inflammation, maintaining

cardiovascular system stability, tissue repair, and other aspects (Wang et al., 2020; Ren et al., 2021). Our previous study found that IMD reduced inflammation, improved pulmonary microvascular endothelial cell barrier integrity and function, eased pulmonary edema, and alleviated vascular leakage in LPS-induced ARDS (Fan et al., 2020). However, the effects of IMD on VILI is unclear.

In the present study, we used 18% cyclic stretching (CS)-induced human pulmonary microvascular endothelial cells (HPMECs) and mechanical ventilation (MV)-induced C57BL/6J mice as VILI models to clarify the anti-apoptotic and anti-oxidative stress effects of IMD. Our study may provide some help for the prevention and treatment of VILI.

MATERIALS AND METHODS

1. VILI animal model

Healthy C57BL/6J mice (8–10-week-old, male) were purchased from the Experimental Animal Center of Chongqing Medical University (Chongqing, China). All mice were housed at a 12/12 h dark/light cycles and were allowed access to food and water. Establishment of the VILI mouse model (Yu et al., 2020): After endotracheal intubation, an animal ventilator (Alcott Biotechnology, Shanghai, China) for MV was calibrated as follows: the tidal volume was 30 ml/kg, the respiratory rate was 75 times/min, the positive end expiratory pressure (PEEP) was 0 cmH_2O, and the duration of MV was 4 h. IMD1-53 (the active fragment of IMD peptide, containing 53 amino acids) (50 ng/kg) or an IMD inhibitor [IMD17-47, a truncated fragment of IMD peptide with 31 amino acid residues, that was used as the competitive inhibitor of IMD (Xiao et al., 2018; Zhang and Xu, 2018)] (100 ng/kg) was subcutaneously injected 1 h before the MV. IMD1-53 and IMD inhibitor (IMDinh) were purchased from Phoenix Pharmaceuticals (CA, United States). In some experiments, the JAK2/STAT3 agonist Colivelin TFA (MedChemExpress, Shanghai, China, 1 mg/kg) was injected intraperitoneally into the mice 30 min before the IMD1-53 injection. All *in vivo* experimental procedures were performed in accordance with the guidelines for the Care and Use of Laboratory Animals by the National Institutes of Health, and were approved by the Ethics Committee of the Second Affiliated Hospital of Chongqing Medical University (Chongqing, China).

2. Cell culture

HPMECs (from ScienCell) were cultured in EC medium containing 1% EC growth supplement, 10% fetal bovine serum and 1% penicillin–streptomycin in an incubator. Cyclic stretching (CS) was performed for 4 h to establish EC models (18% CS for VILI model and 5% CS for the spontaneous breathing model) using a Flexcell FX-4000 Tension System (Flexcell, Burlington, United States) (Yu et al., 2020). In addition, HPMECs were cultured in IMD1-53 (10^{-7} mol/L) or IMDinh (10^{-6} mol/L) 1 h before CS. In some experiments, which detected the potential effects of the JAK2/STAT3 pathway in IMD-mediated protection, Colivelin TFA (MedChemExpress, Shanghai, China, 1 μM) was administrated half an hour before IMD1-53 pretreatment.

3. Hematoxylin and eosin (H&E) staining and lung histology injury evaluation

The mice lung tissues were soaked in 4% paraformaldehyde. Next, the specimens were embedded in paraffin, cut into sections and stained with hematoxylin and eosin (H&E). The stained slides were analyzed using a microscope (Olympus, Tokyo, Japan). The lung injury score was measured as previously described (Wang et al., 2014).

4. Measurement of SOD and MDA

The levels of SOD and MDA were measured using SOD or MDA assay kit (Solarbio, Beijing, China) followed by the manufacturer's instructions.

5. Immunohistochemistry

Lung tissue sections from the left mice were deparaffinized with xylene, rehydrated in ethanol, and incubated in 3% H_2O_2 for 15 min. Then sections were washed and then blocked with goat serum for 1 h and incubated overnight at 4°C with the anti-primary antibody (Bax, caspase-3 and Bcl-2, all from servicebio, Hubei, China). Then, the sections were washed and incubated with secondary antibody (servicebio, Hubei, China) for 30 min, and then stained with DAB solution. Sections were counterstained with hematoxylin, dehydrated, vitrified and sealed.

6. Flow cytometry for reactive oxygen species (ROS)

An ROS detection kit (Beyotime, Shanghai, China) was used to detect ROS levels. The ECs were cultured in DCFH-DA solution at 37°C for 20 min, washed with serum-free cell culture medium. Then, the cell suspensions were collected. Finally, ROS levels were analyzed using a flow cytometer (Beckman, Georgia, United States).

7. Quantitative real-time PCR (qRT-PCR)

Total RNA was isolated from the cells and mice lung tissues using RNAiso Plus (Takara, Beijing, China). Then, 1 μg of total RNA was used as a template for amplifying the cDNA using the PrimeScript™ RT reagent kit (Takara, Beijing, China). cDNA was used for qPCR amplification using TB Green™ Premix Ex Taq™ II (Takara, Beijing, China). All data were calculated using the 2-ΔΔCt method and normalized to β-actin. Primer sequences for the mice were as follows: Bax (sense:5′-CCTCCTCTCCTACTTTGGGAC-3′, antisense:5′-GAAAAACACAGTCCAAGGCAG-3′); caspase-3 (sense:5′-GGACTCTGGAATATCCCTGGAC-3′, antisense:5′-TTTGCTGCATCGACATCTGTAC-3′); Bcl-2 (sense:5′-GTGGCCTTCTTTGAGTTCGG-3′, antisense:5′-

GGTGCCGGTTCAGGTACTCA-3′); IL-6 (sense 5′-ATGAGGAGACTTGCCTGGTGAA -3′, antisense 5′-GTTGGGTCAGGGGTGGTTATT-3′); TNF-α (sense 5′-TCATCTACTCCCAGGTCCTCTTCA-3′, antisense 5′-TCTGGCAGGGGCTCTTGATG-3′); β-Catenin (sense: 298 5′-GTTCTACGCCATCACGACACTG-3′, antisense: 5′-TTGCTCTCTTGATTGCCATAAGC-3′).

8. Western blotting

Total proteins were extracted from tissues and ECs using RIPA, and the concentration was detected by BCA kit (Solarbio, Beijing, China). Equal amounts of protein were loaded into each well for separation via SDS-PAGE and electrophoresed onto PVDF membranes. The membranes were blocked with 5% skim milk or 5% BSA for 1 h, incubated with primary antibodies (Bax, caspase-3, Bcl-2, JAK2, p-JAK2, STAT3, p-STAT3 and β-actin) (β-actin purchases from Bioworld Technology, Nanjing, China, and others from Abcam, Cambridge, United Kingdom) overnight at 4°C, and then incubated with secondary antibodies (Bioworld, Nanjing, China). Finally, the protein bands were measured using the ECL Substrate kit (BioGround Biotechnology, China) and images were captured using Imaging System (Bio-Rad, CA, United States).

9. ROS staining

Fresh lung tissues were embedded in the OTC and sliced. The sections were rewarmed to room temperature while controlling the moisture content, after which an autofluorescence quenching agent was added and cleaned. Thereafter, the sections were stained with ROS dye and kept away from light for 30 min. Finally, they were counterstained with DAPI, sealed, and observed under a fluorescence microscope.

10. Flow cytometry

An apoptosis detection kit was used to access cell apoptosis. All processes were in accordance with the manufacturer's requirements. A flow cytometer (Beckman, Georgia, United States) was used to analyzed the data.

11. Statistical analysis

Continuous data are displayed as the mean ± standard deviation (SD). T-test or ANOVA is performed to detected significance between groups if the data are normally distributed, while the Mann-Whitney U test or Kruskal-Wallis test is used if the data are non-normally distributed. To assess subgroup analysis, Tukey test or Dunn's multiple comparisons test is measured. The chi-squared test is used to compare categorical variables between groups. Statistical significance is set at $p < 0.05$.

RESULTS

1. IMD attenuated lung injury and inflammation in VILI

In vivo, IMD or IMDinh (inhibitor of IMD) was administered 1 h before MV and then MV was administered for 4 h. H&E and lung injury score results showed that IMD pretreatment significantly attenuated lung tissue injury caused by MV, mainly manifesting as narrowing of the alveolar septum, reduction of neutrophil infiltration, perivascular edema, protein edema fluid exudation, and patchy bleeding. IMDinh was truncated structure of IMD, which was worked as a competitive inhibitor of IMD. It inhibited the biological functions of endogenous IMD and aggravated lung tissue injury caused by MV (**Figure 1A**). ELISA for IL-6 and TNF-α of lung homogenates showed that IMD pretreatment significantly reduced the increase in IL-6 and TNF-α levels induced by MV. However, IMD inhibitor played the opposite role (**Figures 1A–C**). *In vitro*, HPMECs were subjected to 18% CS (VILI model) or 5% CS (spontaneous breathing, control model) for 4 h. IMD or IMDinh was given 1 h before 18% CS. PCR results showed that compared with the VILI group, the mRNA levels of IL-6 and TNF-α in the VILI + IMD group were significantly alleviated. However, IMDinh further exacerbated the mRNA levels of proinflammatory cytokines (IL-6 and TNF-α) (**Figures 1D,E**). The above data demonstrated that IMD attenuated lung injury and inflammation both *in vivo* and *in vitro*.

2. IMD alleviated apoptosis in mice and in ECs

The expression of apoptosis related protein (Bax, caspase-3, and Bcl-2) was detected by western blotting, PCR, and immunohistochemistry to evaluate the anti-apoptotic role of IMD in VILI. Western blotting and qPCR showed that in the VILI model group, the expression of Bax and caspase-3 increased significantly while the expression of Bcl-2 decreased significantly (**Figures 2A–C**). However, compared with the VILI group, IMD pretreatment significantly reduced the expression of Bax and caspase-3 and increased the expression of Bcl-2 (**Figures 2A–C**). Immunohistochemistry showed a significant alleviation of histopathologic damage in the lungs after IMD treatment (**Figure 2D**). We also found that compared with the VILI group, if IMD pretreatment was given in advance, it could significantly reduce the expression of Bax and caspase-3 and increase the expression of Bcl-2. In addition, flow cytometry analyses demonstrated that the administration of IMD voided ECs from apoptosis (**Figure 2E**). However, IMDinh displayed the opposite effect (**Figures 2A–E**). These findings indicated that IMD reduced ventilator-induced apoptosis *in vivo* and *in vitro*.

3. IMD alleviated oxidative stress

Excessive oxidative stress generated by injured ECs is widely involved in the progression of lung damage during VILI (Fodor et al., 2021). The imbalance of ROS is the main driving factor for oxidative stress (Piera-Velazquez and Jimenez, 2021). In mice, frozen sections of the lungs were prepared, and ROS were measured by detecting the fluorescence intensity of O_{13}. We found that IMD significantly reduced the generation of ROS in the VILI group (**Figure 3A**). In HPMECs, ROS was measured by

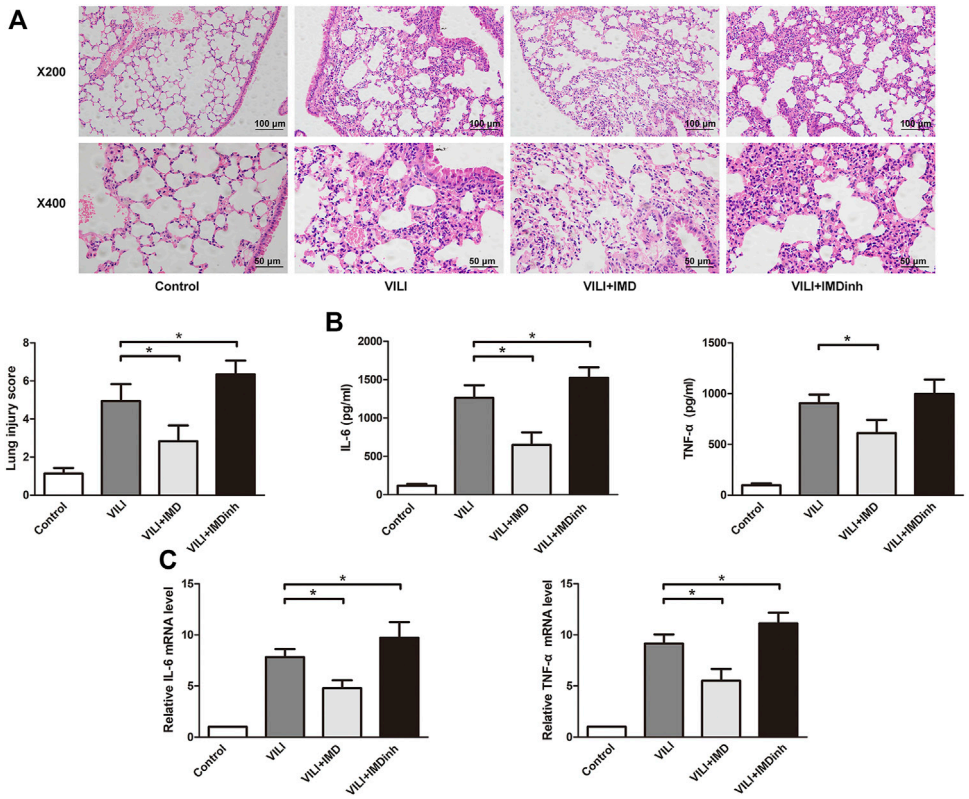

FIGURE 1 | IMD alleviated lung injury inflammation *in vivo* and *in vitro*. **(A)** H&E staining (×200 and ×400), lung injury score was used to evaluate lung histopathological injury. **(B)** The concentration of IL-6 and TNF-α in mice lung tissues. **(C)** The expression of IL-6 mRNA and TNF-α in HPMECs. *$p < 0.05$.

detecting the fluorescence intensity of DCF, and we found that IMD significantly alleviated the generation of ROS induced by VILI (**Figure 3B**). SOD and MDA are important indices for evaluating the antioxidant and oxidative capacities of oxidative stress (Fodor et al., 2021). *In vivo* and *in vitro*, compared with the VILI group, IMD pretreatment significantly increased SOD levels and decreased MDA levels (**Figures 3C,D**). However, IMDinh had the opposite effect and aggravated oxidative stress. These data demonstrated that IMD alleviated oxidative stress *in vivo* and *in vitro*.

4. JAK2/STAT3 pathway was involved in IMD-mediated protection

To further clarify the participation of the JAK2/STAT3 signaling in VILI, the phosphorylation of JAK2 and STAT3 was measured by western blotting. In both mice and ECs, compared with the control group, the phosphorylation of JAK2 and STAT3 in the VILI group was significantly higher, and IMD reduced VILI-induced phosphorylation of JAK2 and STAT3 (**Figures 4A,B**). Future, we used Colivelin TFA (CT), an activator of the JAK2/STAT3 signaling pathway, to explore whether JAK2/STAT3 was involved in the IMD-mediated protective effects on VILI. Western blotting showed that in tissues, compared with the VILI + IMD group, the expression of Bax and caspase-3 increased significantly, and the expression of Bcl-2 declined significantly in the VILI + IMD + CT group (**Figure 5A**). In ECs, Flow cytometry results suggested that the activator of the JAK2/STAT3 significantly up-regulated the level of cell apoptosis (**Figure 5B**). We also found that CT partially reversed the antioxidant stress effects of IMD on VILI, manifesting in up-regulating EC ROS (**Figure 5C**). These findings suggested that IMD exerted anti-apoptotic and anti-oxidant stress effects via inhibiting JAK/STAT3 signaling.

DISCUSSION

In the current study, we used C57B6/J mice and HPMECs to establish a VILI model to analyze the effect of IMD on VILI and its potential mechanism. We found, for the first time, that IMD improved lung injury and alleviated inflammatory factor expression in VILI. In addition, IMD also reduced oxidative stress by reducing ROS levels, upregulating SOD content, and downregulating MDA content. Western blot and immunohistochemical results showed that IMD also alleviated apoptosis, mainly by reducing the expression of Bax and caspase-3 and increasing the expression of Bcl-2. IMD exerted protective effects against VILI via JAK2/STAT3 signaling (**Figure 6**).

The IMD gene is located on human chromosome 22q13.33, and the encoded polypeptide chain is composed of 148 amino acids (Zhang and Xu, 2018). The N-terminal of IMD is an

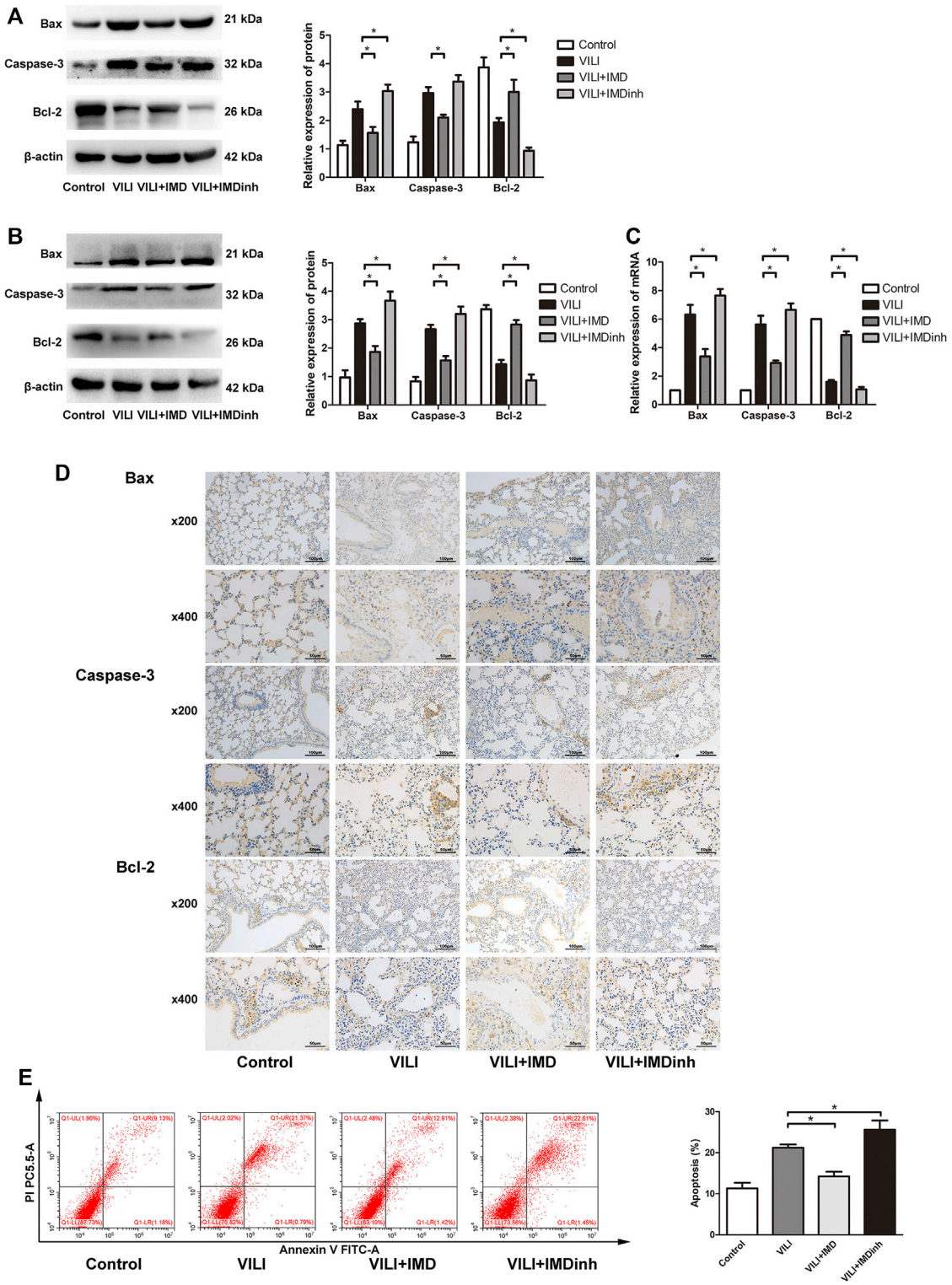

FIGURE 2 | IMD alleviated apoptosis in mice and in ECs. Western blot analysis of Bax, caspase-3, Bcl-2 and β-actin in lung tissues **(A)** and ECs **(B)**. **(C)** Immunohistochemistry of Bax, caspase-3, Bcl-2 and β-actin in lung tissues. **(D)** Cell apoptosis rate was detected using flow cytometry. *$p < 0.05$.

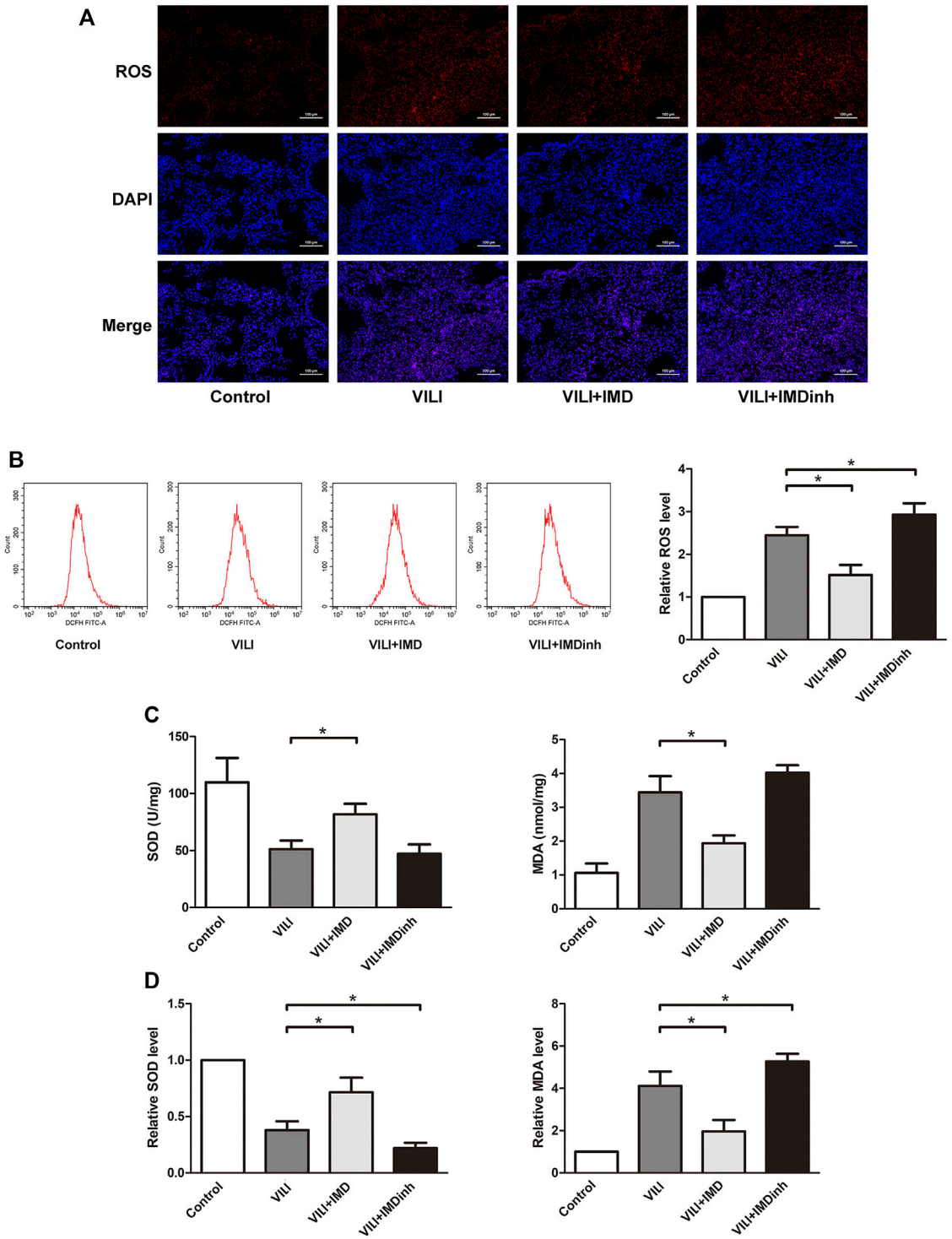

FIGURE 3 | IMD alleviated oxidative stress in mice and in ECs. **(A)** ROS staining of mice lung tissues. **(B)** Cell ROS was detected using flow cytometry. **(C)** The expression of SOD and MDA in mice lung tissues was measured by ELISA. **(D)** The expression of SOD and MDA in ECs was measured by ELISA. *$p < 0.05$.

intramolecular ring composed of six amino acids and an α-helical structure (Takei et al., 2004; Holmes et al., 2020; Sohn et al., 2020). Human IMD sequences are 60% similar to fish and 87% similar to rodents (Roh et al., 2004). The high conservation of IMD also shows that it has important biological functions in the body. Through identification, it was found that IMD has three potential active cleavage fragments: IMD1-53 (Arg94-His95), IMD1-47 (Arg100-Thr101), and IMD1-40 (Arg107-Val108). The effects

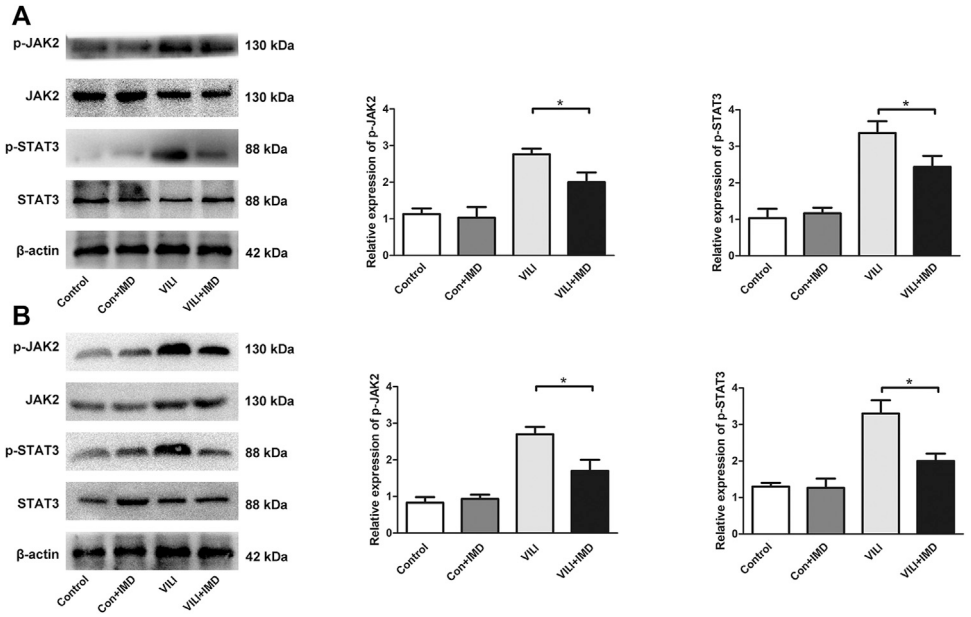

FIGURE 4 | IMD inhibited the JAK2/STAT3 pathway in VILI. Western blot analysis of p-JAK2, JAK2, p-STAT3, STAT3 and β-actin in lung tissues **(A)** and ECs **(B)**. *$p < 0.05$.

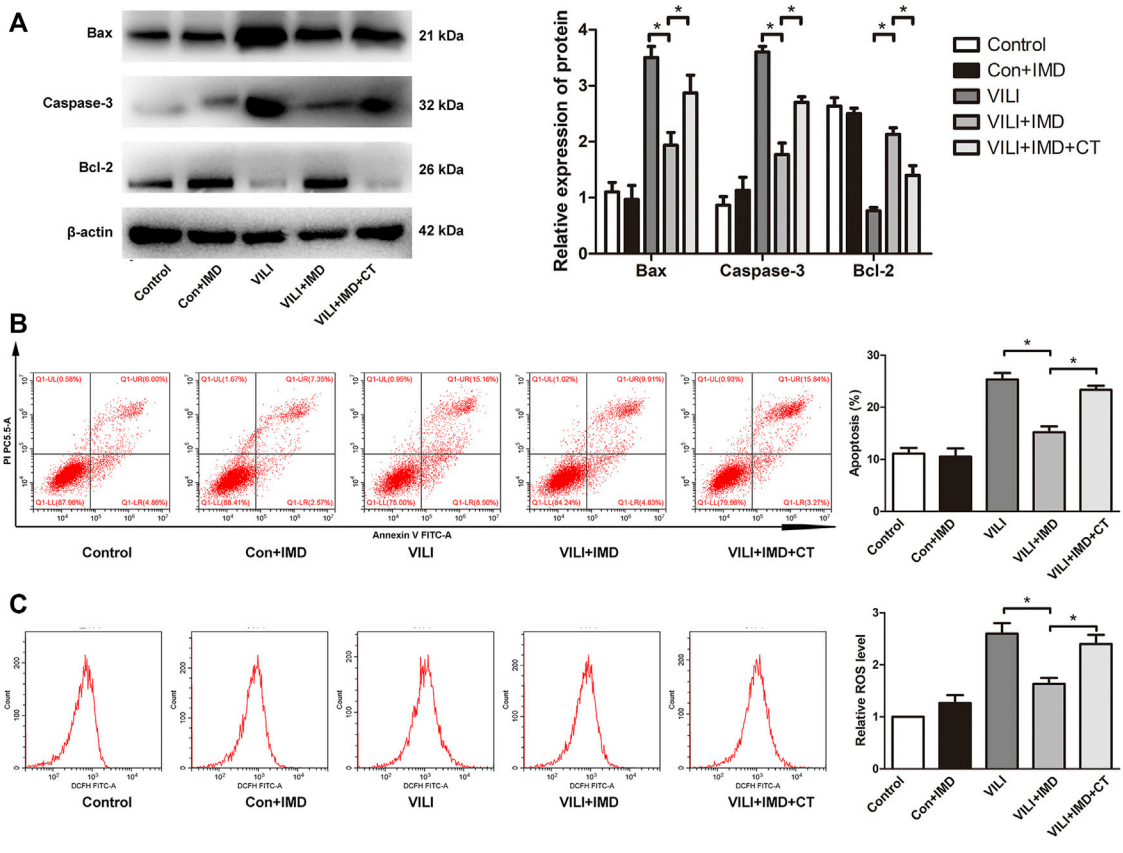

FIGURE 5 | JAK2/STAT3 pathway was involved in IMD-mediated protection. **(A)** Western blot analysis of p-JAK2, JAK2, p-STAT3, STAT3 and β-actin in lung tissues. **(B)** Cell apoptosis rate was detected using flow cytometry. **(C)** Cell ROS was detected using flow cytometry. *$p < 0.05$.

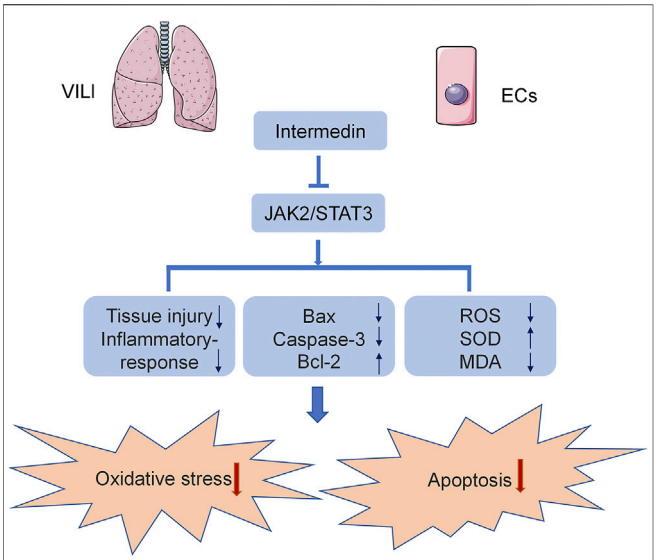

FIGURE 6 | The diagram of mechanism we explored in the current study.

of different fragments may be different *in vivo*, and IMD1-53 has strong biological activity (Roh et al., 2004; Hirose et al., 2011; Zhu et al., 2016). IMD is widely expressed in the lung, heart, brain, kidney, and other tissues and organs, and produces various effects in the body through paracrine or autocrine processes. For example, IMD decreased orchitis in rats, alleviated macrophage aggregation and inflammatory cytokine levels in septic mice, and reduced acute organ injury (Li et al., 2013; Xiao et al., 2018). IMD also significantly eased chronic inflammation of adipose tissue by inhibiting AMPK phosphorylation and maintaining the balance of M1/M2 macrophages (Pang et al., 2016). In septic mice, IMD promoted the co-localization of Rab11 and VE-cadherin, repaired cell adhesion, and reduced vascular leakage (Xiao et al., 2018). Our previous studies have also shown that IMD reduced endothelial cell inflammation and improved the endothelial barrier integrity and functionality in LPS-induced ARDS (Fan et al., 2020). In the current study, we used IMD and IMD inhibitor to comprehensively confirm our hypothesis - IMD protected against VILI by alleviating oxidative stress and apoptosis. And we found that, on the one hand, compared with the VILI group, the VILI + IMD group had down-regulated inflammatory response, repaired lung injury, and reduced apoptosis and oxidative stress, suggesting that the administration of exogenous IMD had a protective effect on VILI. On the other hand, because IMD is widely expressed *in vivo*, we used IMD inhibitor to interfere the effect of endogenous IMD. Compared with the VILI group, the VILI + IMDinh group had more severe lung injury, more expression of inflammatory factors, and higher levels of apoptosis and oxidative stress. These results indicated that IMD inhibitor counteracted the protective effect of endogenous IMD. Overall, we confirmed the protective effect of IMD on VILI.

ECs are widely distributed throughout the body and have a large surface area. They mainly regulate the body's homeostasis through six functions: regulating vasodilation-contraction, vascular permeability, cell growth, immunity and inflammation, coagulation function, cell growth, and lipid metabolism (Daiber et al., 2017; Fodor et al., 2021). Because the ability of endothelial cells to resist external stimulation is weak, endothelial cells are the firs to be affected and changed in acute lung injury (Wiener-Kronish et al., 1991; Matthay et al., 2019). EC activation may lead to mediator generation and leukocyte accumulation in the pulmonary capillary, further aggravating tissue injury. Studies have shown that EC dysfunction is mainly related to the decrease in the bioavailability of vasodilator substances (especially nitric oxide, NO) and the increase in vasoconstrictor substances (Lind et al., 2017; Cyr et al., 2020). However, excessive degradation or inactivation of NO caused by the increase in ROS is one of the main reasons for the decrease in NO bioavailability (Lind et al., 2017; Yepuri and Ramasamy, 2019). Upon injury, the production of ROS may be excessive, and the balance between oxidative stress and antioxidant stress is broken, EC function is destroyed, and apoptosis increases, which has a negative impact on cell and tissue function (Kuzkaya et al., 2003; Landmesser et al., 2003; Fodor et al., 2021). Therefore, it is essential to detect the oxidative and antioxidant stress functions of ECs in VILI. SOD is an antioxidant enzyme that scavenges superoxide anion free radicals and protects cells from damage caused by oxygen free radicals. MDA is a product formed by the reaction between lipids and oxygen free radicals, and its content represents the degree of lipid peroxidation (Abdelzaher et al., 2021). In the current study, we used frozen sections to detect the level of ROS in mouse lung tissue, flow cytometry to detect ROS content, and ELISA to detect the levels of SOD and MDA; we found that IMD could inhibit the oxidative stress in VILI. Consistent with our study, IMD alleviated oxidative stress and apoptosis in a NO-dependent manner in brain ECs (Chen et al., 2006). In cardiomyocytes, IMD inhibited oxidative stress and reduced ischemia-reperfusion injury through PI3K/Akt pathway (Song et al., 2009; Zhao et al., 2012).

The JAK2/STAT3 pathway is an intracellular signal transduction pathway that is involved in various biological processes and provides a direct mechanism for the regulation of gene expression by extracellular factors. Cytokines bind to receptors, resulting in receptor-coupled JAK aggregation and the activation of adjacent JAKs through mutual phosphorylation. The activated JAKs phosphorylate the tyrosine site on the receptor, causing the receptor to generate a STAT binding region and then phosphorylate STATs (O'Shea et al., 2015; Johnson et al., 2018; Xiong et al., 2021). In a septic mouse model, blocking the JAK2/STAT3 signaling pathway significantly reduced the levels of HMGB1 and key cytokines and alleviated multi-organ injury (Hui et al., 2009; Xin et al., 2020). In addition, the JAK2/STAT3 pathway affects cell apoptosis by altering the levels of Bcl-2 and Bax and influencing oxidative stress (Li et al., 2017; Raut et al., 2021). Therefore, we hypothesized that IMD could reduce oxidative stress and apoptosis through the JAK2/STAT3 pathway and protected against VILI. Consistent with previous studies, in the current study, we found that IMD inhibited the phosphorylation of JAK2 and STAT3 in VILI. The agonist of JAK2/STAT3 significantly reversed the anti-apoptotic and antioxidant stress effects mediated by IMD. However, the

effects of STAT3 on lung tissue were not dogmatic. Previous study found that vagus nerve stimulation played a protective role in acute respiratory distress syndrome by increasing STAT3 and regulating macrophage transformation (Li et al., 2021). The diverse functions of STAT3 may be related to the different mechanisms of STAT3 in different cells types.

However, this study had some limitations. We found a protective effect of IMD on VILI, which indicated that IMD may be a potential target for the prevention and treatment of VILI. However, its mechanism remains unclear. In addition, although EC injury is vital in VILI, the pathogenesis of VILI is complex and diverse, and other injury mechanisms should not be ignored. Basic and clinical follow-up studies are essential to further clarify the potential role of IMD in VILI.

In conclusion, we found for the first time that IMD reduced VILI through anti-apoptotic and antioxidant stress in mice and HPMECs. In addition, we found that the anti-apoptotic and antioxidant stress effects of IMD were mediated by the inhibition of the JAK2/STAT3 signaling pathway.

DATA AVAILABILITY STATEMENT

The original contributions presented in the study are included in the article/Supplementary Material, further inquiries can be directed to the corresponding authors.

ETHICS STATEMENT

The animal study was reviewed and approved by Ethics Committee of the Second Affiliated Hospital of Chongqing Medical University.

AUTHOR CONTRIBUTIONS

SF, YY, and DW designed the study; SF and JH performed experiments; SF, JH, and YY analyzed all data; SF drafted the manuscript; DW revised the manuscript. All authors have read and approved the final submitted manuscript.

FUNDING

This study was supported by the National Natural Science Foundation of China (Grant no. 81670071) and Natural Science Foundation of Chongqing, China (Grant no. cstc2019jcyj-zdxmX0031).

ACKNOWLEDGMENTS

Thanks to all those who offered help.

REFERENCES

Abdelzaher, W. Y., Mohammed, H. H., Welson, N. N., Batiha, G. E., Baty, R. S., and Abdel-Aziz, A. M. (2021). Rivaroxaban Modulates TLR4/Myd88/NF-Kβ Signaling Pathway in a Dose-Dependent Manner with Suppression of Oxidative Stress and Inflammation in an Experimental Model of Depression. *Front. Pharmacol.* 12, 715354. doi:10.3389/fphar.2021.715354

Chen, L., Kis, B., Hashimoto, H., Busija, D. W., Takei, Y., Yamashita, H., et al. (2006). Adrenomedullin 2 Protects Rat Cerebral Endothelial Cells from Oxidative Damage *In Vitro*. *Brain Res.* 1086 (1), 42–49. doi:10.1016/j.brainres.2006.02.128

Curley, G. F., Laffey, J. G., Zhang, H., and Slutsky, A. S. (2016). Biotrauma and Ventilator-Induced Lung Injury: Clinical Implications. *Chest* 150 (5), 1109–1117. doi:10.1016/j.chest.2016.07.019

Cyr, A. R., Huckaby, L. V., Shiva, S. S., and Zuckerbraun, B. S. (2020). Nitric Oxide and Endothelial Dysfunction. *Crit. Care Clin.* 36 (2), 307–321. doi:10.1016/j.ccc.2019.12.009

Daiber, A., Steven, S., Weber, A., Shuvaev, V. V., Muzykantov, V. R., Laher, I., et al. (2017). Targeting Vascular (Endothelial) Dysfunction. *Br. J. Pharmacol.* 174 (12), 1591–1619. doi:10.1111/bph.13517

Fan, S., Qi, D., Yu, Q., Tang, X., Wen, X., Wang, D., et al. (2020). Intermedin Alleviates the Inflammatory Response and Stabilizes the Endothelial Barrier in LPS-Induced ARDS through the PI3K/Akt/eNOS Signaling Pathway. *Int. Immunopharmacol* 88, 106951. doi:10.1016/j.intimp.2020.106951

Fodor, A., Tiperciuc, B., Login, C., Orasan, O. H., Lazar, A. L., Buchman, C., et al. (2021). Endothelial Dysfunction, Inflammation, and Oxidative Stress in COVID-19-Mechanisms and Therapeutic Targets. *Oxid Med. Cel Longev* 2021, 8671713. doi:10.1155/2021/8671713

Gaver, D. P., 3rd, Nieman, G. F., Gatto, L. A., Cereda, M., Habashi, N. M., and Bates, J. H. T. (2020). The POOR Get POORer: A Hypothesis for the Pathogenesis of Ventilator-Induced Lung Injury. *Am. J. Respir. Crit. Care Med.* 202 (8), 1081–1087. doi:10.1164/rccm.202002-0453CP

Hirose, T., Totsune, K., Nakashige, Y., Metoki, H., Kikuya, M., Ohkubo, T., et al. (2011). Influence of Adrenomedullin 2/Intermedin Gene Polymorphism on Blood Pressure, Renal Function and Silent Cerebrovascular Lesions in Japanese: the Ohasama Study. *Hypertens. Res.* 34 (12), 1327–1332. doi:10.1038/hr.2011.131

Holmes, D., Corr, M., Thomas, G., Harbinson, M., Campbell, M., Spiers, P., et al. (2020). Protective Effects of Intermedin/Adrenomedullin-2 in a Cellular Model of Human Pulmonary Arterial Hypertension. *Peptides* 126, 170267. doi:10.1016/j.peptides.2020.170267

Hong, Y., Hay, D. L., Quirion, R., and Poyner, D. R. (2012). The Pharmacology of Adrenomedullin 2/Intermedin. *Br. J. Pharmacol.* 166 (1), 110–120. doi:10.1111/j.1476-5381.2011.01530.x

Huang, R. T., Wu, D., Meliton, A., Oh, M. J., Krause, M., Lloyd, J. A., et al. (2017). Experimental Lung Injury Reduces Krüppel-Like Factor 2 to Increase Endothelial Permeability via Regulation of RAPGEF3-Rac1 Signaling. *Am. J. Respir. Crit. Care Med.* 195 (5), 639–651. doi:10.1164/rccm.201604-0668OC

Hui, L., Yao, Y., Wang, S., Yu, Y., Dong, N., Li, H., et al. (2009). Inhibition of Janus Kinase 2 and Signal Transduction and Activator of Transcription 3 Protect against Cecal Ligation and Puncture-Induced Multiple Organ Damage and Mortality. *J. Trauma* 66 (3), 859–865. doi:10.1097/TA.0b013e318164d05f

Johnson, D. E., O'Keefe, R. A., and Grandis, J. R. (2018). Targeting the IL-6/JAK/STAT3 Signalling Axis in Cancer. *Nat. Rev. Clin. Oncol.* 15 (4), 234–248. doi:10.1038/nrclinonc.2018.8

Kuzkaya, N., Weissmann, N., Harrison, D. G., and Dikalov, S. (2003). Interactions of Peroxynitrite, Tetrahydrobiopterin, Ascorbic Acid, and Thiols: Implications for Uncoupling Endothelial Nitric-Oxide Synthase. *J. Biol. Chem.* 278 (25), 22546–22554. doi:10.1074/jbc.M302227200

Landmesser, U., Dikalov, S., Price, S. R., McCann, L., Fukai, T., Holland, S. M., et al. (2003). Oxidation of Tetrahydrobiopterin Leads to Uncoupling of Endothelial Cell Nitric Oxide Synthase in Hypertension. *J. Clin. Invest.* 111 (8), 1201–1209. doi:10.1172/JCI14172

Li, L., Ma, P., Liu, Y., Huang, C., O, W. S., Tang, F., et al. (2013). Intermedin Attenuates LPS-Induced Inflammation in the Rat Testis. *PLoS One* 8 (6), e65278. doi:10.1371/journal.pone.0065278

Li, S., Qi, D., Li, J. N., Deng, X. Y., and Wang, D. X. (2021). Vagus Nerve Stimulation Enhances the Cholinergic Anti-Inflammatory Pathway to Reduce

Lung Injury in Acute Respiratory Distress Syndrome via STAT3. *Cell Death Discov* 7 (1), 63. doi:10.1038/s41420-021-00431-1

Li, Y., Shi, X., Li, J., Zhang, M., and Yu, B. (2017). Knockdown of KLF11 Attenuates Hypoxia/Reoxygenation Injury via JAK2/STAT3 Signaling in H9c2. *Apoptosis* 22 (4), 510–518. doi:10.1007/s10495-016-1327-1

Lind, M., Hayes, A., Caprnda, M., Petrovic, D., Rodrigo, L., Kruzliak, P., et al. (2017). Inducible Nitric Oxide Synthase: Good or Bad? *Biomed. Pharmacother.* 93, 370–375. doi:10.1016/j.biopha.2017.06.036

Matthay, M. A., Zemans, R. L., Zimmerman, G. A., Arabi, Y. M., Beitler, J. R., Mercat, A., et al. (2019). Acute Respiratory Distress Syndrome. *Nat. Rev. Dis. Primers* 5 (1), 18. doi:10.1038/s41572-019-0069-0

O'Shea, J. J., Schwartz, D. M., Villarino, A. V., Gadina, M., McInnes, I. B., and Laurence, A. (2015). The JAK-STAT Pathway: Impact on Human Disease and Therapeutic Intervention. *Annu. Rev. Med.* 66, 311–328. doi:10.1146/annurev-med-051113-024537

Pang, Y., Li, Y., Lv, Y., Sun, L., Zhang, S., Li, Y., et al. (2016). Intermedin Restores Hyperhomocysteinemia-Induced Macrophage Polarization and Improves Insulin Resistance in Mice. *J. Biol. Chem.* 291 (23), 12336–12345. doi:10.1074/jbc.M115.702654

Piera-Velazquez, S., and Jimenez, S. A. (2021). Oxidative Stress Induced by Reactive Oxygen Species (ROS) and NADPH Oxidase 4 (NOX4) in the Pathogenesis of the Fibrotic Process in Systemic Sclerosis: A Promising Therapeutic Target. *J. Clin. Med.* 10 (20), 4791. doi:10.3390/jcm10204791

Qi, D., Tang, X., He, J., Wang, D., Zhao, Y., Deng, W., et al. (2016). Omentin Protects against LPS-Induced ARDS through Suppressing Pulmonary Inflammation and Promoting Endothelial Barrier via an Akt/eNOS-Dependent Mechanism. *Cell Death Dis* 7 (9), e2360. doi:10.1038/cddis.2016.265

Raut, P. K., Lee, H. S., Joo, S. H., and Chun, K. S. (2021). Thymoquinone Induces Oxidative Stress-Mediated Apoptosis through Downregulation of Jak2/STAT3 Signaling Pathway in Human Melanoma Cells. *Food Chem. Toxicol.* 157, 112604. doi:10.1016/j.fct.2021.112604

Ren, J. L., Chen, Y., Zhang, L. S., Zhang, Y. R., Liu, S. M., Yu, Y. R., et al. (2021). Intermedin1-53 Attenuates Atherosclerotic Plaque Vulnerability by Inhibiting CHOP-Mediated Apoptosis and Inflammasome in Macrophages. *Cel Death Dis* 12 (5), 436. doi:10.1038/s41419-021-03712-w

Roh, J., Chang, C. L., Bhalla, A., Klein, C., and Hsu, S. Y. (2004). Intermedin Is a Calcitonin/Calcitonin Gene-Related Peptide Family Peptide Acting through the Calcitonin Receptor-Like Receptor/Receptor Activity-Modifying Protein Receptor Complexes. *J. Biol. Chem.* 279 (8), 7264–7274. doi:10.1074/jbc.M305332200

Slutsky, A. S., and Ranieri, V. M. (2013). Ventilator-Induced Lung Injury. *N. Engl. J. Med.* 369 (22), 2126–2136. doi:10.1056/NEJMra1208707

Sohn, I., Sheykhzade, M., Edvinsson, L., and Sams, A. (2020). The Effects of CGRP in Vascular Tissue - Classical Vasodilation, Shadowed Effects and Systemic Dilemmas. *Eur. J. Pharmacol.* 881, 173205. doi:10.1016/j.ejphar.2020.173205

Song, J. Q., Teng, X., Cai, Y., Tang, C. S., and Qi, Y. F. (2009). Activation of Akt/GSK-3beta Signaling Pathway Is Involved in Intermedin(1-53) Protection against Myocardial Apoptosis Induced by Ischemia/Reperfusion. *Apoptosis* 14 (11), 1061–1069. doi:10.1007/s10495-009-0398-7

Takei, Y., Inoue, K., Ogoshi, M., Kawahara, T., Bannai, H., and Miyano, S. (2004). Identification of Novel Adrenomedullin in Mammals: A Potent Cardiovascular and Renal Regulator. *FEBS Lett.* 556 (1-3), 53–58. doi:10.1016/s0014-5793(03)01368-1

Wang, Q., Zheng, X., Cheng, Y., Zhang, Y. L., Wen, H. X., Tao, Z., et al. (2014). Resolvin D1 Stimulates Alveolar Fluid Clearance through Alveolar Epithelial Sodium Channel, Na,K-ATPase via ALX/cAMP/PI3K Pathway in Lipopolysaccharide-Induced Acute Lung Injury. *J. Immunol.* 192 (8), 3765–3777. doi:10.4049/jimmunol.1302421

Wang, Y., Mi, Y., Tian, J., Qiao, X., Su, X., Kang, J., et al. (2020). Intermedin Alleviates Renal Ischemia-Reperfusion Injury and Enhances Neovascularization in Wistar Rats. *Drug Des. Devel Ther.* 14, 4825–4834. doi:10.2147/DDDT.S253019

Wiener-Kronish, J. P., Albertine, K. H., and Matthay, M. A. (1991). Differential Responses of the Endothelial and Epithelial Barriers of the Lung in Sheep to *Escherichia C* Endotoxin. *J. Clin. Invest.* 88 (3), 864–875. doi:10.1172/JCI115388

Xiao, F., Wang, D., Kong, L., Li, M., Feng, Z., Shuai, B., et al. (2018). Intermedin Protects against Sepsis by Concurrently Re-Establishing the Endothelial Barrier and Alleviating Inflammatory Responses. *Nat. Commun.* 9 (1), 2644. doi:10.1038/s41467-018-05062-2

Xin, P., Xu, X., Deng, C., Liu, S., Wang, Y., Zhou, X., et al. (2020). The Role of JAK/STAT Signaling Pathway and its Inhibitors in Diseases. *Int. Immunopharmacol* 80, 106210. doi:10.1016/j.intimp.2020.106210

Xiong, Y., Wang, Y., Xiong, Y., and Teng, L. (2021). Protective Effect of Salidroside on Hypoxia-Related Liver Oxidative Stress and Inflammation via Nrf2 and JAK2/STAT3 Signaling Pathways. *Food Sci. Nutr.* 9 (9), 5060–5069. doi:10.1002/fsn3.2459

Yepuri, G., and Ramasamy, R. (2019). Significance and Mechanistic Relevance of SIRT6-Mediated Endothelial Dysfunction in Cardiovascular Disease Progression. *Circ. Res.* 124 (10), 1408–1410. doi:10.1161/CIRCRESAHA.119.315098

Yu, Q., Wang, D., Wen, X., Tang, X., Qi, D., He, J., et al. (2020). Adipose-Derived Exosomes Protect the Pulmonary Endothelial Barrier in Ventilator-Induced Lung Injury by Inhibiting the TRPV4/Ca2+ Signaling Pathway. *Am. J. Physiology-Lung Cell Mol. Physiol.* 318, L723–L741. doi:10.1152/ajplung.00255.2019

Zhang, S. Y., Xu, M. J., and Wang, X. (2018). Adrenomedullin 2/Intermedin: A Putative Drug Candidate for Treatment of Cardiometabolic Diseases. *Br. J. Pharmacol.* 175 (8), 1230–1240. doi:10.1111/bph.13814

Zhao, L., Peng, D. Q., Zhang, J., Song, J. Q., Teng, X., Yu, Y. R., et al. (2012). Extracellular Signal-Regulated Kinase 1/2 Activation Is Involved in Intermedin1-53 Attenuating Myocardial Oxidative Stress Injury Induced by Ischemia/reperfusion. *Peptides* 33 (2), 329–335. doi:10.1016/j.peptides.2011.12.016

Zhu, Y., Wu, H., Wu, Y., Zhang, J., Peng, X., Zang, J., et al. (2016). Beneficial Effect of Intermedin 1-53 in Septic Shock Rats: Contributions of Rho Kinase and BKCA Pathway-Mediated Improvement in Cardiac Function. *Shock* 46 (5), 557–565. doi:10.1097/shk.0000000000000639

Conflict of Interest: The authors declare that the research was conducted in the absence of any commercial or financial relationships that could be construed as a potential conflict of interest.

Publisher's Note: All claims expressed in this article are solely those of the authors and do not necessarily represent those of their affiliated organizations, or those of the publisher, the editors and the reviewers. Any product that may be evaluated in this article, or claim that may be made by its manufacturer, is not guaranteed or endorsed by the publisher.

frontiers | Frontiers in Pharmacology

ORIGINAL RESEARCH
published: 19 April 2022
doi: 10.3389/fphar.2022.877125

Effects of Montelukast on Arsenic-Induced Epithelial-Mesenchymal Transition and the Role of Reactive Oxygen Species Production in Human Bronchial Epithelial Cells

Huang-Chi Chen[1,2], *Hsin-Ying Clair Chiou*[3,4], *Mei-Lan Tsai*[5,6], *Szu-Chia Chen*[1,7,8], *Ming-Hong Lin*[5,9,10,11], *Tzu-Chun Chuang*[12], *Chih-Hsing Hung*[5,6,13,14]* and *Chao-Hung Kuo*[1,8,15]*

[1]Department of Internal Medicine, Kaohsiung Municipal Siaogang Hospital, Kaohsiung Medical University, Kaohsiung, Taiwan, [2]Division of Pulmonary and Critical Care Medicine, Department of Internal Medicine, Kaohsiung Medical University Hospital, Kaohsiung Medical University, Kaohsiung, Taiwan, [3]Teaching and Research Center, Kaohsiung Municipal Siaogang Hospital, Kaohsiung Medical University, Kaohsiung, Taiwan, [4]Kaohsiung Medical University Hospital, Kaohsiung Medical University, Kaohsiung, Taiwan, [5]Graduate Institute of Medicine, College of Medicine, Kaohsiung Medical University, Kaohsiung, Taiwan, [6]Department of Pediatrics, School of Medicine, College of Medicine, Kaohsiung Medical University, Kaohsiung, Taiwan, [7]Division of Nephrology, Department of Internal Medicine, Kaohsiung Medical University Hospital, Kaohsiung Medical University, Kaohsiung, Taiwan, [8]Faculty of Medicine, College of Medicine, Kaohsiung Medical University, Kaohsiung, Taiwan, [9]Department of Microbiology and Immunology, School of Medicine, College of Medicine, Kaohsiung Medical University, Kaohsiung, Taiwan, [10]Department of Medical Research, Kaohsiung Medical University Hospital, Kaohsiung Medical University, Kaohsiung, Taiwan, [11]M.Sc. Program in Tropical Medicine, College of Medicine, Kaohsiung Medical University, Kaohsiung, Taiwan, [12]Department of Respiratory Therapy, College of Medicine, Kaohsiung Medical University, Kaohsiung, Taiwan, [13]Research Center for Environmental Medicine, Kaohsiung Medical University, Kaohsiung, Taiwan, [14]Department of Pediatrics, Kaohsiung Municipal Siaogang Hospital, Kaohsiung Medical University, Kaohsiung, Taiwan, [15]Division of Gastroenterology, Department of Internal Medicine, Kaohsiung Medical University Hospital, Kaohsiung, Taiwan

OPEN ACCESS

Edited by:
Arunachalam Karuppusamy, Chinese Academy of Sciences (CAS), China

Reviewed by:
Yap Hui Min, Putra Malaysia University, Malaysia
Dona Sinha, Chittaranjan National Cancer Institute, India
Ganapasam Sudhandiran, University of Madras, India

***Correspondence:**
Chih-Hsing Hung
pedhung@gmail.com
Chao-Hung Kuo
kjh88kmu@gmail.com

Specialty section:
This article was submitted to Respiratory Pharmacology, a section of the journal Frontiers in Pharmacology

Received: *16 February 2022*
Accepted: *25 March 2022*
Published: *19 April 2022*

Citation:
Chen H-C, Chiou H-YC, Tsai M-L, Chen S-C, Lin M-H, Chuang T-C, Hung C-H and Kuo C-H (2022) Effects of Montelukast on Arsenic-Induced Epithelial-Mesenchymal Transition and the Role of Reactive Oxygen Species Production in Human Bronchial Epithelial Cells. Front. Pharmacol. 13:877125. doi: 10.3389/fphar.2022.877125

Background: Epithelial-mesenchymal transition (EMT) of airway lung epithelial cells is considered a major driver of fibrosis and airway remodeling. Arsenic exposure is well known to cause the malignant transformation of cells, including those in the lung. Accumulating studies have shown that arsenic exposure is associated with chronic pulmonary diseases. However, clinical treatment for arsenic-induced pulmonary damage has not been well investigated.

Materials and Methods: The therapeutic effects of montelukast and its combination with fluticasone on sodium arsenite-induced EMT changes in normal human bronchial cells were investigated. The cell migration ability was evaluated by Transwell and wound healing assays. EMT marker expression was determined by immunoblotting. Furthermore, the role of reactive oxygen species (ROS) generation in arsenic-induced EMT and the effect of montelukast on this process were determined by ROS inhibitor treatment and ROS measurement, respectively.

Results: Montelukast was effective at reducing arsenic-induced cell migration and mesenchymal protein (fibronectin, MMP-2, N-cadherin, β-catenin, and SMAD2/3) expression. Arsenic-induced ROS production was attenuated by pretreatment with

montelukast. Treatment with the ROS inhibitor N-acetyl cysteine reduced arsenic-induced NF-kB phosphorylation and the mesenchymal protein expression, indicating that ROS production is critical for arsenic-induced EMT. In addition, combined treatment with montelukast and fluticasone reversed the inhibitory effects of montelukast on cell migration. The expression of fibronectin, MMP-2 induced by arsenic was further enhanced by the combination treatment compared with montelukast treatment only.

Conclusion: This study demonstrated that montelukast is effective at reducing arsenic-induced EMT in human bronchial epithelial cells. Through the inhibition of arsenic-induced ROS generation and NF-kB activation, which is critical for arsenic-induced EMT, montelukast inhibited arsenic-induced cell migration and the expression of extracellular matrix proteins and several EMT-regulating transcription factors. The combination of fluticasone with montelukast reversed the inhibitory effect of montelukast on arsenic-induced EMT. This study provides therapeutic strategies and mechanisms for arsenic-induced pulmonary epithelial damage.

Keywords: montelukast, epithelial-mesenchymal transition, oxidative stress, bronchial epithelium, NF-κB

INTRODUCTION

Arsenic contamination is a major public health concern and threatens the health of millions of people worldwide. Previous studies have shown that chronic exposure to arsenic damages several organs, including the lung. Arsenic is classified as a group I carcinogen by the International Agency for Research on Cancer. The association between arsenic exposure and lung cancer has been well established (Straif et al., 2009). In addition, accumulating studies have shown that chronic arsenic exposure is positively correlated with the incidence of respiratory symptoms, chronic lung disease mortality (Sanchez et al., 2016), and lung function decrements (Parvez et al., 2013; Sanchez et al., 2018). Arsenic exposure is positively associated with nonmalignant lung diseases such as chronic obstructive pulmonary disease, bronchiectasis (Guha Mazumder, 2007), lung fibrosis (Assad et al., 2018; Wang P. et al., 2021; Xiao et al., 2021), and asthma (Siddique et al., 2020). Currently, the most popular options for the treatment of chronic arsenic overexposure include chelating and antioxidant therapies. However, the therapeutic effects, in terms of relieving lung symptoms caused by arsenic exposure, are inconsistent with chelating agents (Bjorklund et al., 2020). The usefulness of different therapies for arsenic-associated pulmonary diseases warrants further study.

Epithelial-mesenchymal transition (EMT) is characterized by loss of the epithelial phenotype and acquisition of the mesenchymal phenotype and is important in the regulation of not only the invasion and migration of tumor cells but also development and wound repair processes. The major events of EMT include the loss of cell–cell junctions and epithelial polarity, cytoskeletal reorganization, and an increase in the ability of the extracellular matrix (ECM) to regulate invasion (Kalluri and Weinberg, 2009). EMT is induced by extracellular factors/stimuli (Liu et al., 2010; Sohal et al., 2010) and is considered a universal process in lung diseases that promotes tissue remodeling (Hackett, 2012; Pain et al., 2014) and fibrosis (Jia and Kim, 2017; Rout-Pitt et al., 2018). Chronic exposure to arsenic induces neoplastic transformation of several tissues through the induction of cancer-related type III EMT (Jiang et al., 2013; Chang and Singh, 2019a; Tryndyak et al., 2020; Zhou et al., 2021). Moreover, arsenic was reported to perturb type I EMT in a chick embryo heart during development (Lencinas et al., 2010). In our previous studies, arsenic exposure at 10^{-6} M promoted cell migration and the expression of several mesenchymal proteins, especially ECM proteins, in human bronchial epithelial cells. In addition, several studies have demonstrated that sodium arsenite exposure could induce pulmonary fibrosis *in vitro* and *in vivo* (Dai et al., 2019; Wang P. et al., 2021; Xiao et al., 2021). These results provide evidence that EMT may be the critical mechanism by which arsenic induces pulmonary diseases.

Montelukast is a cysteinyl leukotriene receptor (CysLT1R) antagonist that was approved as an effective therapeutic agent for asthma as well as allergic rhinitis. It was reported to have antitumor activity through the induction of apoptosis and growth arrest (Zovko et al., 2018). It was also found to inhibit cell migration and invasion by inhibiting MMP-2 and MMP-9 expression in human glioblastoma cells (Piromkraipak et al., 2018). CysLT1R antagonists have been demonstrated to suppress EMT and fibrotic protein expression. Montelukast (10^{-4} M) suppresses EMT induced by eosinophils through the inhibition of TGF-β signaling (Hosoki et al., 2014). The expression of profibrotic cytokines, including IL-6, IL-10, IL-13, and TGF-β, was inhibited by montelukast in a bleomycin-induced pulmonary fibrosis mouse model (Shimbori et al., 2011). Pranlukast was shown to reduce airway remodeling through the inhibition of TGF-β/Smad signaling in an OVA-sensitized and challenged asthma mouse model (Hur et al., 2018).

In this study, we evaluated the therapeutic potential and mechanism of montelukast in treating arsenic-induced lung

damage using normal human bronchial epithelial cells. The effects of montelukast on arsenic-induced EMT and ROS generation was examined. Furthermore, the combination of montelukast with fluticasone was assessed.

MATERIALS AND METHODS

Cell Culture, Drugs, and Reagents

Normal human bronchial epithelial cells (NHBE, Lonza) were maintained in Keratinocyte SFM basal medium supplemented with 5 μg/L human recombinant epithelial growth factor (EGF), 50 mg/L bovine pituitary extract (BPE), 5 mg/L insulin, and 25 nM hydrocortisone at 37°C in a 5% CO_2 atmosphere. Cells were passaged every 3 days and plated for experimental treatment within 6 passages.

$NaAsO_2$, montelukast, fluticasone, N-acetylcysteine, and BAY117082 were purchased from Sigma–Aldrich (United States). Antibodies against fibronectin (Sigma, F3648), MMP-2 (GeneTex, GTX 104577), GAPDH (GeneTex, GTX100118), SMAD2/3 (GeneTex, GTX111123), β-catenin (R&D, AF1329), N-Cadherin (GeneTex, GTX127345), and E-Cadherin (GeneTex, GTX100443) were used.

Western Blotting

Cells were pretreated with drugs or inhibitors (montelukast, fluticasone, BAY117082, NAC) for 2 h, and then combined treated with sodium arsenite for additional 24 h. After treatments, the cells were washed twice with ice-cold PBS and lysed with RIPA buffer containing protease inhibitor (cOmplete™, Mini, EDTA-free Protease Inhibitor Cocktail, Sigma–Aldrich) and phosphatase inhibitor (PhosStop™, Sigma–Aldrich). The protein lysate was harvested by centrifugation at 14,000 rpm at 4°C for 15 min to pellet the cell debris. The protein concentration was determined using the BCA Dual-Range BCA Protein Assay Kit (Visual Protein, Taiwan). A total of 10 μg of protein lysate was separated by 6 ~ 13% SDS–PAGE and transferred onto PVDF membranes (Millipore, United States). After blocking with 5% skim milk at room temperature for 1 h, the membranes were incubated with primary antibody at 4°C overnight. After three washes with 0.1% TBST, the membrane was incubated with HRP-conjugated anti-rabbit IgG or anti-goat secondary antibody (Jackson ImmunoResearch Laboratories, West Grove, PA). The membrane was developed by reacting with chemiluminescence HRP substrate (Merck, Germany), and the protein bands were visualized and captured using a ChemiDoc-It 810 Imager (Ultra-Violet Products, United States). The protein bands were quantified using ImageJ.

DCFH-DA Staining of Total ROS

The staining protocol was performed as described (Li et al., 2013). HBE cells were seeded on a dark, clear bottom 96-well microplate with 15,000 cells per well. The cells were pretreated with montelukast for 2 h and then treated with $NaAsO_2$ for 3 h. The cells were then stained with 10 μM DCFH-DA at 37°C for 30 min by added the dye into the well. After DCFH-DA staining, the cells were washed with PBS and immediately assessed on a fluorescence microplate reader (Ex/Em = 485/535 nm). The result was represented as a subtraction of the tested well and the unstained well. Fluorescence was also observed under a fluorescence microscope (Leica).

Wound Healing Assay

NHBE cells were plated in 12-well plates and allowed to grow to confluence. Inhibitors were pretreated 2 h before arsenic treatment. After arsenic treatment for 24 h, wounds were made with 200-μl tips and washed twice with PBS to remove the floating cells. $NaAsO_2$ was added in the presence of inhibitors and incubated for analysis at 6, 9, 12 h as indicated. Images were captured using a microscope (magnification, ×200; Olympus, Tokyo, Japan), and the wound area was analyzed by ImageJ. The wound area was normalized to that at 0 h as 100% and expressed as wound coverage%. The calculation was performed as $[(\text{wound area}_{0h} - \text{wound area}_{\text{after incubation}})/\text{wound area}_{0h}]\text{x}100\%$.

Transwell Migration Assay

NHBE cells were exposed to asthma drugs for 2 h, followed by $NaAsO_2$ exposure for 24 h. The cells were then detached and replated onto the upper chamber of a Transwell with 8-μm pores (BD Biosciences, Franklin Lakes, NJ, United States) at a density of 5×10^4 cells in 200 μl of supplement-free Keratinocyte SFM. The lower chamber was filled with Keratinocyte SFM containing 100 ng/ml EGF, 50 mg/L bovine pituitary extract (BPE), 5 mg/L insulin, and 25 nM hydrocortisone. After incubation, the cells were fixed with methanol for 10 min at room temperature followed by staining with 0.2% crystal violet for 10 min at room temperature. All cells on the membrane were imaged and counted to ensure that an equal number of cells were seeded. After that, the cells in the upper side of the chamber were removed with a cotton swab, and the migrated cells on the bottom side of the membrane were imaged for quantitative analysis. Five randomly selected areas (×200) were selected under a light microscope. The cell migration activity was quantitated by determining the occupied area *via* ImageJ and applying the following formula: (the bottom side cell occupied area/total cell occupied area).

Cell Morphology Analysis

Cell morphology change was analyzed by radius-ratio method (Ren et al., 2015). Briefly, NHBE cells were pretreated with montelukast for 2 h, and followed by combined treatment with sodium arsenite for another 48 h. The cell images of each group were observed in ×200 magnification and acquired using Leica Flexacam C1 (Leica microsystems, Germany). The radius ratio was determined using Ratio between max radius and min radius of the cells. Total of 60 cells were analyzed in each group for statistical analysis.

Statistical Analysis

The unpaired Student t-test and one way ANOVA test were used for the statistical analysis. Values are presented as

means ± S.E.M. Statistical signifcance was determined as $p < 0.05$.

RESULTS

Montelukast Inhibits the Arsenic-Induced Migration of Human Bronchial Epithelial Cells

Cell migration is a critical property of EMT. The effects of montelukast on arsenic-induced cell migration were determined by Transwell and wound healing assays in human bronchial epithelial (NHBE) cells. In the Transwell migration assay, cell migration was increased upon 1 μM $NaAsO_2$ treatment. Pretreatment with montelukast at 0.1 and 1 μM had inhibitory effects on arsenic-induced cell migration compared with treatment with arsenic alone (**Figure 1A**) In the wound healing assay, arsenic treatment increased wound closure compared with untreated cells. Pretreatment with montelukast reduced the migration ability, as shown by reduced wound coverage (**Figure 1B**). Treatment with montelukast alone did not alter the migration ability of NHBE cells (**Figure 1A**). These results demonstrated that montelukast was effective for reducing arsenic-induced cell migration.

Montelukast Reduces Arsenic-Induced Mesenchymal Protein Expression

To examine the effects of arsenic on EMT marker expression, NHBE cells were treated with $NaAsO_2$ for 24 h, and the protein lysate was harvested for western blot analysis. Arsenic treatment significantly induced the expression of several mesenchymal markers, such as extracellular matrix-regulating proteins [fibronectin and matrix metalloproteinase 2 (MMP-2)], cytoskeletal protein (N-cadherin), and transcription factors (β-catenin and SMAD2/3). The expression of E-cadherin was not altered by arsenic. The dose-response effects of arsenic on EMT marker expressions were performed. The results show that 1 uM of arsenic most significantly increased the mesenchymal proteins expressions (**Supplementary Figures S1A-E**). Moreover, 1 μM of $NaAsO_2$ equals 75 ppb of arsenic, which is about the environmental relevant concentration in the drinking water of arsenic contaminated region (>50 ppb) (Smith et al., 2000). Thus, we had treated with 1 μM of sodium arsenite for 24 h on NHBE cells to evaluate the effect of montelukast on EMT. Montelukast treatment from 10^{-8}~10^{-6} M caused no significant changes on cell viability (**Supplementary Figure S1G**). Pretreatment with montelukast at 0.1 and 1 μM was effective in reducing the expression of these mesenchymal proteins (**Figures 2A–G**). Moreover, the treatment of 0.1 and 1 μM of montelukast alone or in combination with arsenic do not affect cell viability (**Supplementary Figures S1G,H**). Consistent with the

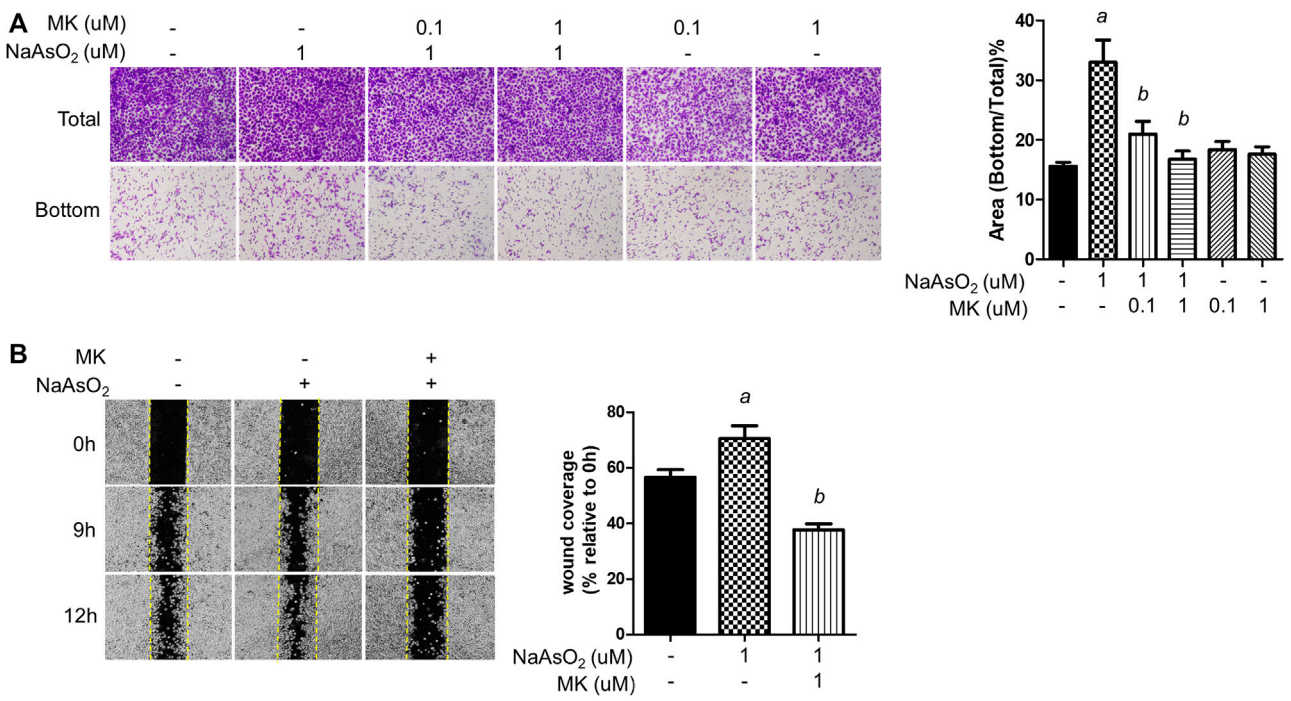

FIGURE 1 | The effect of montelukast on the arsenic-induced migration of NHBE cells. **(A)** Cells were treated with montelukast (MK, 0.1 and 1 μM) 2 h prior to $NaAsO_2$ stimulation followed by combined treatment for 24 h. The cells were subjected to a Transwell migration assay. Twenty-seven hours later, the cells were fixed and stained with crystal violet. The representative image (left panel) and the quantitative results (right panel) are shown. **(B)** The cells were pretreated with 1 μM montelukast for 2 h and then arsenic was added. After 24 h, a wound was made, and images were taken at different time points as indicated. The representative image (left panel) and the quantitative results (right panel) are shown. *a*: $p < 0.05$ compared with the vehicle control group. *b*: $p < 0.05$ compared with the $NaAsO_2$ group.

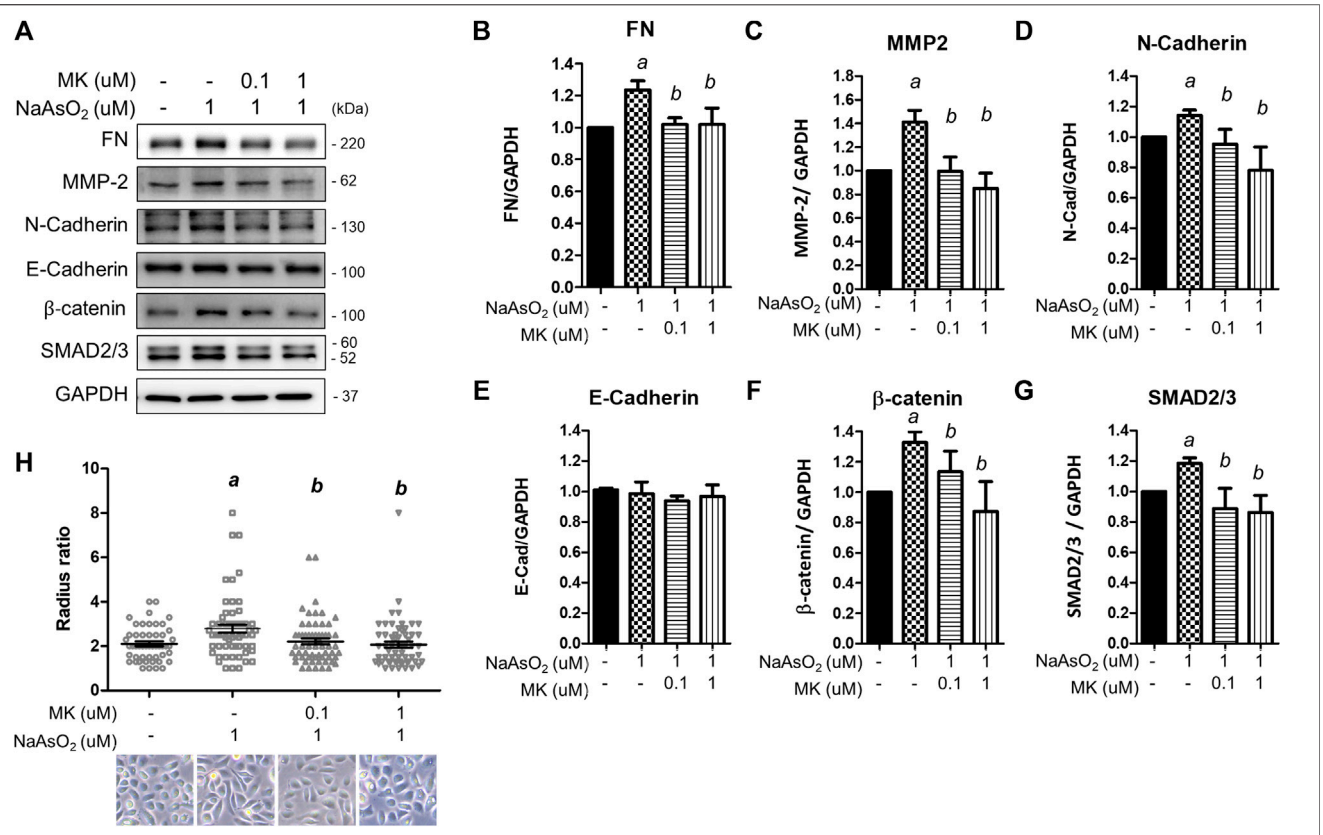

FIGURE 2 | The effect of montelukast on arsenic-induced EMT marker expression in NHBE cells. Cells were pretreated with montelukast for 2 h, followed by combined treatment with 1 μM $NaAsO_2$. After 24 h of treatment, the cells were harvested for protein expression analysis by western blotting. **(A)** Representative western blot images. **(B–G)** The quantitative results of protein expression changes are shown in **(C–G)**. *a*: $p < 0.05$ compared with the vehicle control group. *b*: $p < 0.05$ compared with the $NaAsO_2$ group. **(H)** The cell morphology changes. NHBE cells were pretreated with 0.1 or 1 μM montelukast respectively for 2 h and followed by sodium arsenite for another 48 h. The cell morphology was analyzed by radius-ratio methods. *a*: $p < 0.05$ compared with the vehicle control group. *b*: $p < 0.05$ compared with the $NaAsO_2$ group.

mesenchymal protein expressions, arsenic induced morphological changes of the cell. The cells morphology become spindle shape after sodium arsenite treatment compared to vehicle control. Arsenic treatment significantly increased the radius-ratio of NHBE cells, which was reversed by pretreatment of montelukast (**Figure 2H**).

Montelukast Reduces ROS Generation to Regulate Arsenic-Induced EMT

Oxidative stress is a widely accepted mechanism of arsenic toxicity (Hu et al., 2020). Here, we aimed to elucidate whether montelukast regulates arsenic-induced ROS generation, which is reported to be associated with EMT progression (Jiang et al., 2017).

First, the effect of montelukast on arsenic-induced ROS generation was examined. NHBE cells were treated with arsenic and montelukast alone or in combination for 3 h, and ROS generation was determined by staining with DCFH-DA followed by quantitation of the fluorescence intensity of each well with a plate reader. The DCFH-DA was known to react with H_2O_2, $ONOO^-$, lipid hydroperoxide and O_2^-, and was considered a general indicator for total ROS generation. The results indicated that arsenic treatment increased the fluorescence intensity compared with that in control cells (**Figure 3A**). The cells pretreated with montelukast showed reduced arsenic-induced ROS generation compared with those treated with arsenic only. Representative images showing the reduced fluorescent signal induced by montelukast are shown in the right panel (**Figure 3A**). These results demonstrated that montelukast reduced the ROS generation induced by arsenic in NHBE cells.

Moreover, to determine the role of ROS generation in the EMT of NHBE cells, we pretreated cells with the ROS scavenger N-acetylcysteine (NAC), and the effects on arsenic-induced EMT were examined. Pretreatment with NAC significantly inhibited arsenic-induced wound closure (**Figure 3B**) and reduced the expression levels of fibronectin, matrix metalloproteinase-2 (MMP-2), N-cadherin, β-catenin, SMAD2/3, and SNAIL, which were increased with arsenic treatment (**Figure 3C**). These results demonstrated that the induction of oxidative stress is involved in the arsenic-induced EMT of NHBE cells. Altogether, these results suggested that montelukast-mediated

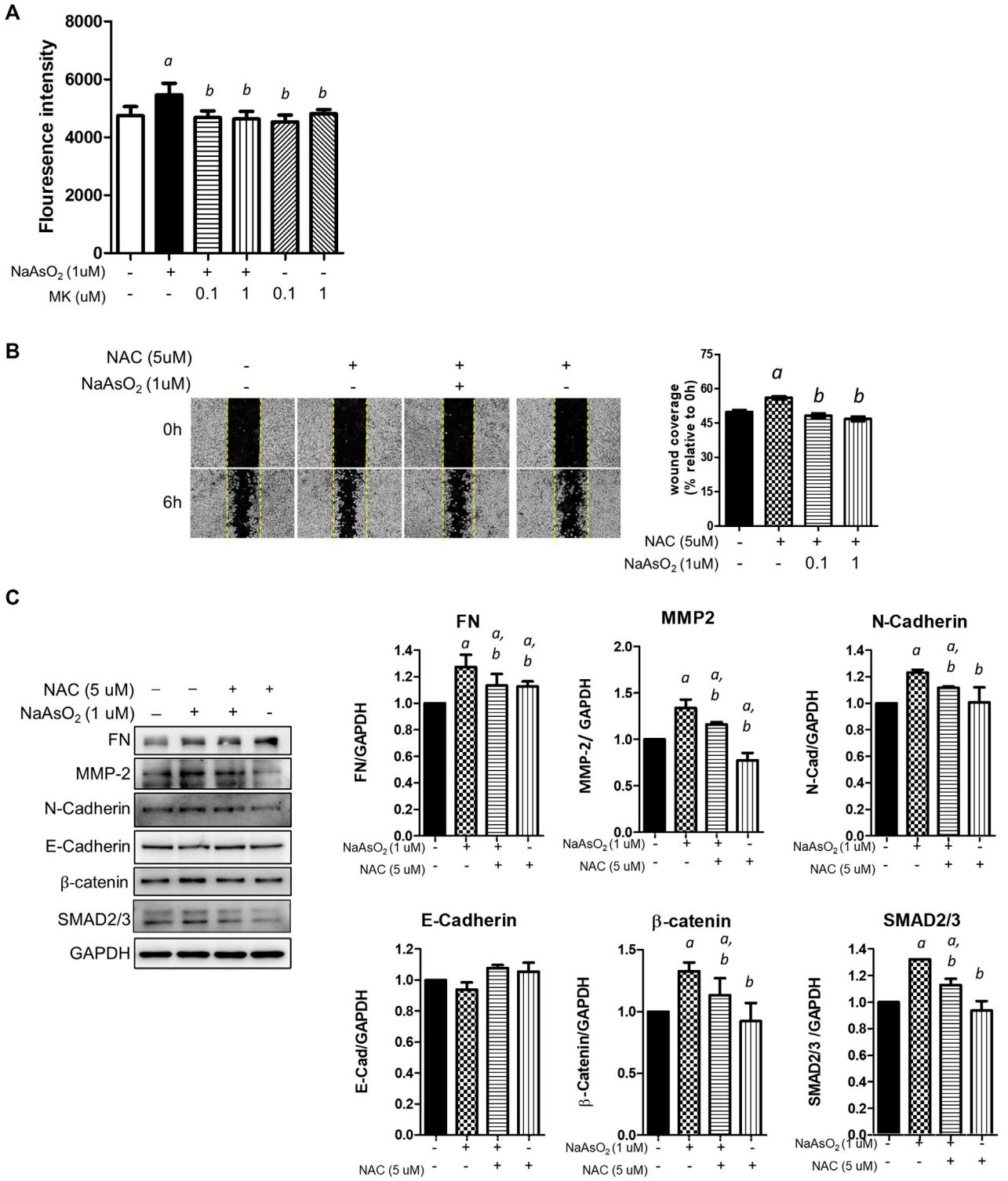

FIGURE 3 | The effects of montelukast on ROS generation and of the inhibition of ROS generation on arsenic-induced EMT of NHBE cells. **(A)** Cells seeded in 96-well plates were pretreated with montelukast at 0.1 and 1 μM for 2 h, and then 1 μM $NaAsO_2$ was applied for combination treatment. After 3 h of treatment, the cells were stained with 10 μM DCFH-DA for 30 min. After washing out the residue dye, the fluorescent signal was measured immediately. The quantitative results (left panel) and representative images (right panel) are shown. a: $p < 0.05$ compared with the vehicle control group. b: $p < 0.05$ compared with the NaAsO2 group. **(B)** Cells were pretreated with NAC for 2 h, and then 1 μM NaAsO2 for another 24 h. A wound was made with a 200-μl tip, and the wound coverage was analyzed 6 h after the wound was made. a: $p < 0.05$ compared with the vehicle control group. b: $p < 0.05$ compared with the NaAsO2 group. **(C)** Cells were pretreated with NAC for 2 h, and then 1 μM $NaAsO_2$ was added for another 24 h. The cells were harvested for protein expression analysis by western blotting. *a*: $p < 0.05$ compared with the vehicle control group. *b*: $p < 0.05$ compared with the $NaAsO_2$ group.

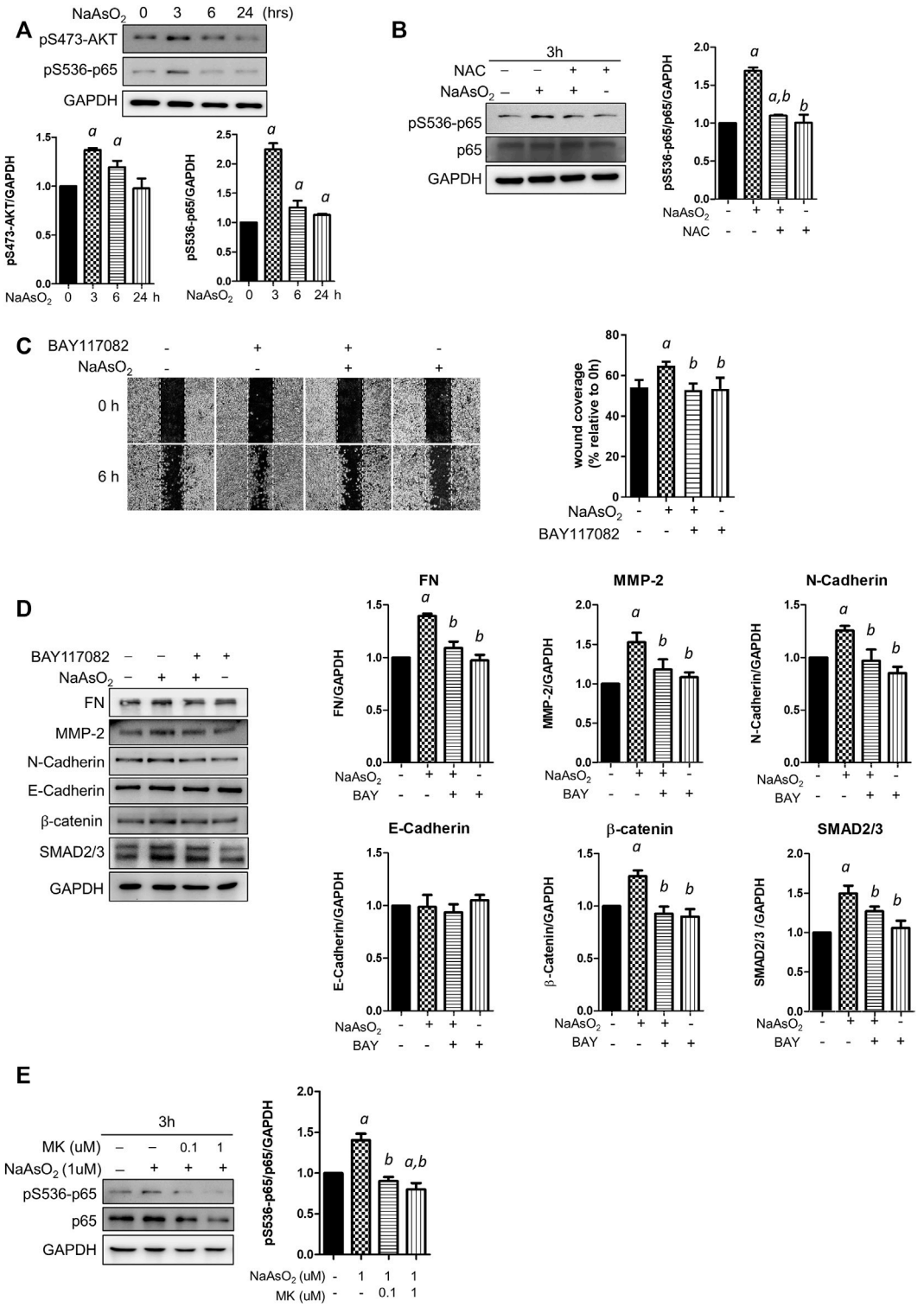

FIGURE 4 | The effects of montelukast on NF-κB activation and of the inhibition of NF-κB on mediated arsenic-induced EMT of NHBE cells. **(A)** Arsenic induced the phosphorylation of AKT and p65. Cells were treated with 1 μM $NaAsO_2$ for different time intervals, and the cells were harvested and subjected to western blot analysis using a phospho-antibody. **(B)** NAC treatment inhibited arsenic-induced phospho-p65. Cells were pretreated with NAC for 2 h, and then $NaAsO_2$ was added for another 3 h. The expression of phospho-p65 was determined with a phospho-Ser536-p65 antibody. GAPDH served as the internal control. **(C)** Treatment with an NF-κB inhibitor reduced arsenic-induced cell migration. Cells were pretreated with 2 μM BAY117082 for 2 h and then treated with 1 μM $NaAsO_2$ for another 24 h. A wound was made with a 200-μl tip, and the wound coverage was analyzed by comparing the cell-occupied area at 0 h versus that 6 h after the wound was made. The representative

(*Continued*)

FIGURE 4 | image (left panel) and the quantitative results (right panel) are shown. *a*: $p < 0.05$ compared with the vehicle control group. *b*: $p < 0.05$ compared with the $NaAsO_2$ group. **(D)** Treatment with an NF-κB inhibitor reduced arsenic-induced mesenchymal marker expression. Cells were pretreated with 2 μM BAY117082 for 2 h, and then 1 μM $NaAsO_2$ was added for another 24 h. The cells were harvested for protein expression analysis by western blotting. **(E)** Montelukast inhibited arsenic-induced phospho-p65 expression. Cells were pretreated with montelukast for 2 h, and then arsenic was added for another 3 h. The cells were harvested for protein expression analysis by western blotting. GAPDH served as the internal control.

inhibition of ROS generation is critical for arsenic-induced EMT in NHBE cells.

Montelukast Inhibits the Activation of NF-κB to Regulate Arsenic-Induced EMT

To explore the downstream molecules mediating arsenic-ROS signaling for EMT regulation, the involvement of AKT-NF-κB, which is known as critical signaling for EMT regulation, was examined. Cells were treated with $NaAsO_2$ for 3, 6, and 24 h, and the results showed that the phosphorylation of AKT and the NF-κB subunit p65 was induced at 3 h and then decreased at 24 h after $NaAsO_2$ treatment (**Figure 4A**). The arsenic-induced phosphor-Ser536-p65 is inhibited by pre-treatment of NAC (**Figure 4B**), indicating that arsenic induced NF-kB activation through ROS generation.

To elucidate the role of NF-κB activation in arsenic-induced EMT, the cells were pretreated with the NF-κB inhibitor BAY117082, and cell migration and mesenchymal protein expression were analyzed. The results indicated that wound coverage was significantly induced by arsenic, which was reversed by combined treatment with BAY117082 (**Figure 4C**). The mesenchymal protein expression induced by arsenic was reversed by pretreatment with BAY117082, including fibronectin, MMP-2, N-cadherin, β-catenin, and SMAD2/3 (**Figure 4D**). These results indicate that NF-κB is an important mediator of arsenic-induced cell migration in NHBE cells.

To elucidate whether montelukast inhibits arsenic-induced EMT through the regulation of NF-κB activation, the effects of montelukast on arsenic-induced Ser536 phosphorylation of p65 were determined by western blotting. The results indicated that treatment with montelukast significantly reduced arsenic-induced phospho-Ser536-p65 expression (**Figure 4E**). These results indicated that montelukast inhibits arsenic-induced EMT through the regulation of NF-κB activation.

Effects of the Combination of Montelukast and Fluticasone on Cell Migration and Mesenchymal Protein Expression

Since montelukast is frequently used in combination with fluticasone in the clinic, the effect of the combination of montelukast and fluticasone on arsenic-induced EMT in NHBE cells was examined. Considering the plasma concentration in human (average ~ 0.2 μM within 8 h after single oral dose) (Balani et al., 1997), we had chosen the lower concentration of montelukast (0.1 μM) to combined with fluticasone.

Consistently, treatment with 0.1 μM montelukast reduced cell migration in the Transwell migration assay. However, the combination of montelukast with fluticasone at either 0.01 μM or 0.1 μM reversed the inhibitory effects of montelukast on cell migration (**Figures 5A,B**). Treatment of fluticasone show to increase the arsenic-induced cell migration. For the mesenchymal protein expressions, montelukast treatment consistently inhibit the arsenic-induced mesenchymal protein expressions. Fluticasone treatment increased the arsenic-induced fibronectin expressions but the arsenic-induced MMP-2, N-cadherin, b-catenin, and SNAD2/3 were not changed. For the combine treatment with montelukast and fluticasone, the effects of montelukast on inhibiting arsenic-induced fibronectin (FN) and MMP-2 expression was reversed, and the N-cadherin, β-catenin, SMAD2/3 expressions were not changed (**Figures 5C–I**). This result suggested that the addition of fluticasone blocks the inhibitory effect of montelukast on arsenic-induced EMT, possibly by reversing the expression of fibronectin.

DISCUSSION

Arsenic exposure causes both malignant and nonmalignant transformation of the pulmonary system and threatens the health of millions of people around the world. In this study, we examined the therapeutic effects of the clinical drug montelukast on arsenic-induced bronchial epithelial changes *in vitro*. We have demonstrated that through the inhibition of ROS generation and downstream AKT-NF-κB signaling activation, montelukast inhibits arsenic-induced EMT in human bronchial epithelial cells. These results provide a possible effective therapeutic agent for arsenic-induced pulmonary malfunctions.

EMT is a critical mechanistic change that contributes to tissue fibrosis, airway remodeling, and carcinogenesis. The major changes in epithelial cells undergoing EMT include 1) diminished cell junctions and loss of apical-basal cell polarity, 2) cytoskeletal remodeling and acquisition of cell motility, and 3) ECM remodeling and deposition. Several EMT changes were reported to be affected by arsenic. Arsenic trioxide (40 μM, 12 h) treatment induced tight junction damage to intestinal epithelial cells, which resulted in the downregulation of claudin-1 and claudin-5 (Jeong et al., 2017). The excess production of ECM caused by EMT contributes to fibrotic disorders. Arsenic exposure causes fibrotic-related changes in several organs, such as the kidney (Chang and Singh, 2019b), lung (Wang P. et al., 2021; Xiao et al., 2021), and liver (Wu et al., 2008). These studies demonstrated that arsenic significantly induced the expression of markers for fibrosis, such as fibronectin, collagen I, transforming

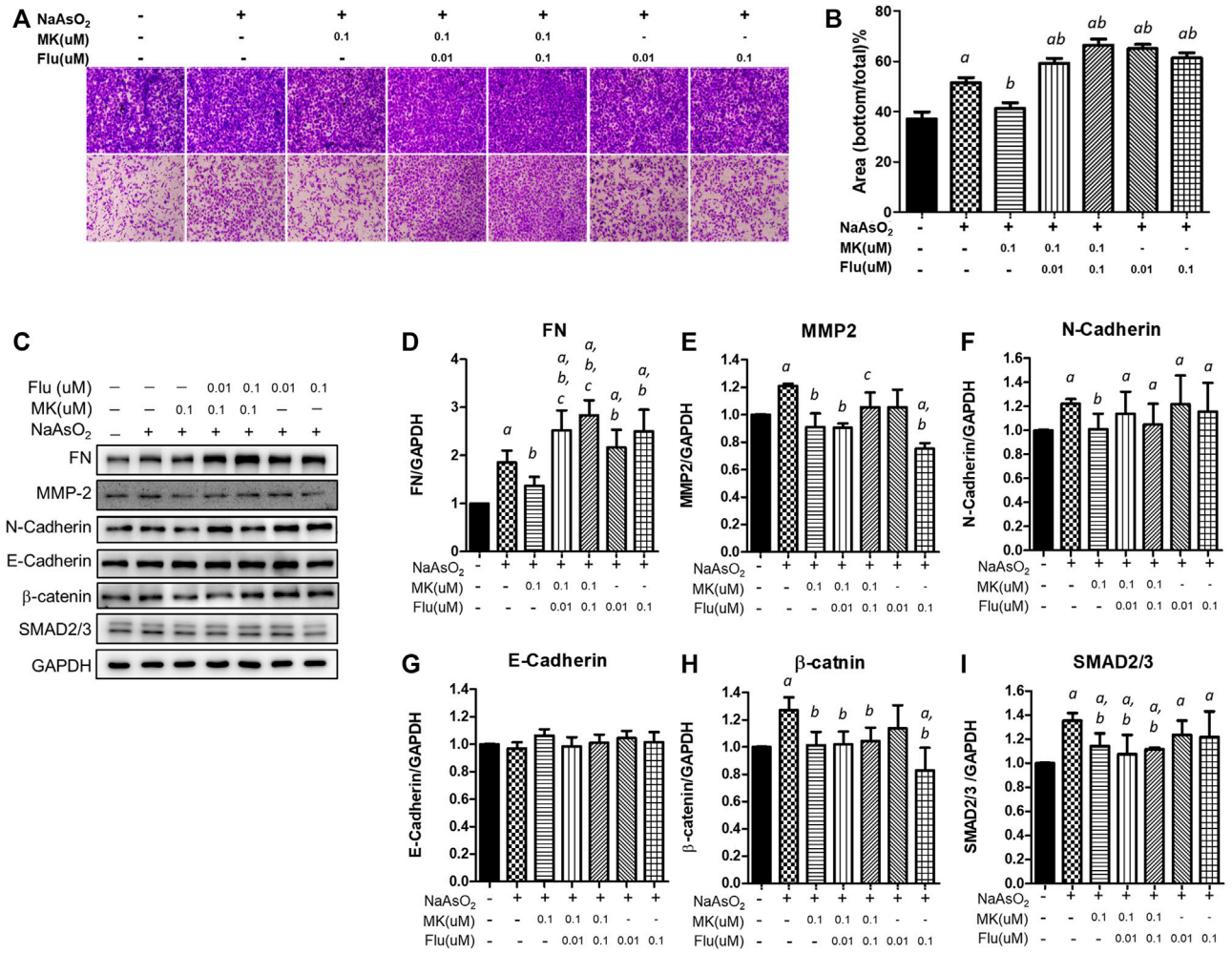

FIGURE 5 | Effect of the combination of montelukast and fluticasone on $NaAsO_2$-induced cell migration of NHBE cells. Cells were pretreated with medications for 2 h and then arsenic was added. **(A,B)** After 24 h of incubation, the cells were trypsinized, plated onto the inner side of the Transwell chamber and incubated for 36 h. The migrated cells were analyzed by the ratio of the bottom/total of the cell occupied area. Representative images (left panel) and the quantitative results are shown (right panel). **(C–I)** After 24 of incubation, the protein lysates were extracted and applied to western blot analysis. The representative image was shown in **(C)**, and the quantitative results were shown, respectively **(D–I)**. *a*: $p < 0.05$ compared with the vehicle control group. *b*: $p < 0.05$ compared with the $NaAsO_2$ group. *c*: $p < 0.05$ compared with the montelukast plus $NaAsO_2$ group.

growth factor β, and α-smooth muscle actin. These studies are consistent with our study: using normal human bronchial epithelial cells, we observed that sodium arsenite (1 μM, 24 h) promotes cell migration and the expression of mesenchymal proteins, including the adherent junction protein N-cadherin, and extracellular matrix-regulating proteins, including fibronectin and MMP-2. However, the epithelial marker protein E-cadherin was not significantly altered under this condition. Downregulation of E-cadherin has been considered as the hallmark of EMT. However, some studies have also found that E-Cadherin expression is preserved in several types of cancer cells that undergo EMT, and downregulation of E-Cadherin is not sufficient to induce EMT (Hollestelle et al., 2013; Chen et al., 2020; Nilsson et al., 2014; Wong et al., 2018). Holestelle's study has reported that E-Cadherin was downregulated by the EMT process itself *via* downstream epigenetic silencing. Thus, it is suggested that E-Cadherin downregulation may not be necessary for the development and progression of arsenic-induced EMT. Moreover, for junctional proteins such as occludin and ZO-1, there were no significant expression changes with treatment (data not shown). It is suggested that our cell culture model does not include well-differentiated epithelial cells to represent an intact functional junction structure. This issue can be further addressed by using an air-liquid interface culture system, which has been widely accepted for assessing epithelial junction integrity.

Montelukast is a leukotriene receptor antagonist that acts as both a bronchodilator and an anti-inflammatory agent to ameliorate asthma symptoms. The activity of montelukast in EMT regulation has been reported. In a rat model of bronchopulmonary dysplasia (BPD), montelukast treatment inhibited the expression of hyperoxia-induced mesenchymal markers, such as collagen I (Col I), metalloproteinase-1

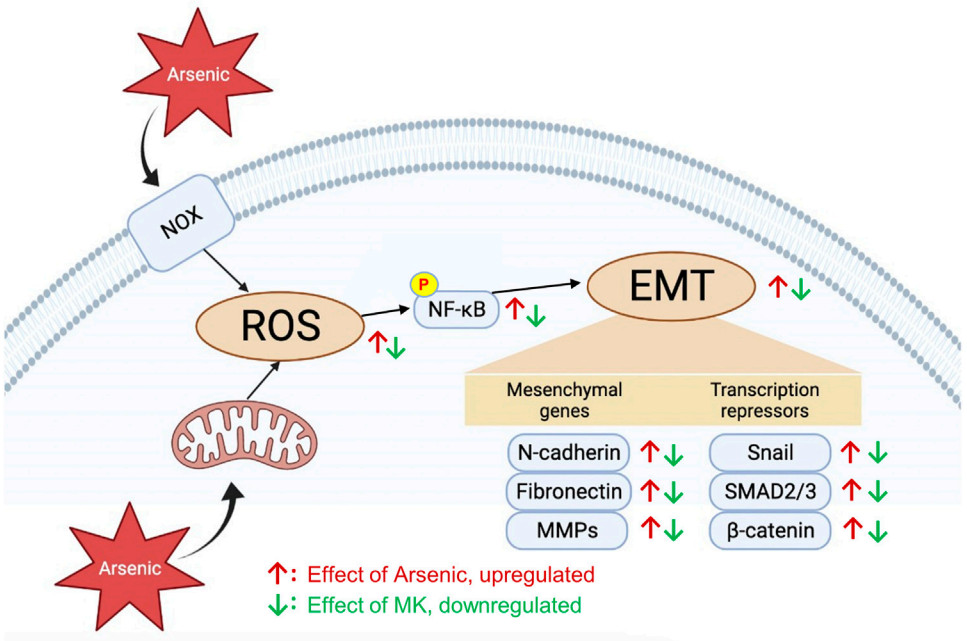

FIGURE 6 | The effects and signaling molecules involved in montelukast-mediated attenuation of arsenic-induced EMT changes in human bronchial epithelial cells.

(MMP-1), MMP-3, TGF-β1, and Smad3, in lung tissues by inactivating the TGF-β1/Smad signaling pathway (Chen et al., 2020). Consistently, in this study, we showed that montelukast downregulates SMAD2/3 signaling to suppress arsenic-induced EMT. Moreover, we demonstrated that montelukast suppresses arsenic-induced β-catenin expression, which is a key effector of the WNT signaling pathway known to regulate EMT. In a meta-analysis, arsenic was reported to upregulate the WNT/β-catenin signaling pathway in normal cells and downregulate it in cancer cells. Arsenic at concentrations ranging from 0 to 7.5 μM has been demonstrated to have a dose-dependent effect on WNT/β-catenin signaling (Li and Ren, 2020). This is consistent with our results that arsenic (1 μM, 24 h) upregulates β-catenin expression. These results suggested that montelukast reduced arsenic-induced EMT through the suppression of multiple EMT-promoting pathways, including TGFβ/SMAD and WNT/β-catenin. Since TGFβ/SMAD and WNT/β-catenin pathways were also critical for type III EMT in the regulation of tumorigenesis, it is suggested that montelukast may have the potential for the prevention or therapy of lung cancer.

While the toxicity mechanisms of arsenic are complex and not fully understood, ROS generation is considered a common pathway in arsenic toxicity. ROS are important cellular secondary messengers that mediated diverse biological processes through the regulation of signaling pathways involved in cell proliferation, apoptosis, cell migration, and inflammation. Arsenic induces ROS generation in several ways: 1) activation of mitochondrial complexes I and III in the electron transport chain to increase O_2- production, 2) activation of nicotinamide adenine dinucleotide phosphate oxidase (Nox), 3) the process of arsenic metabolism, 4) activation of the endoplasmic reticulum by trivalent dimethylarsinic acid, and 5) indirect induction of ROS generation by interfering with antioxidants (Hu et al., 2020). Excess ROS generation has been demonstrated to promote bronchial hyperresponsiveness (Jiang et al., 2014) and EMT progression (Jiang et al., 2017). Montelukast has been previously demonstrated to have powerful anti-ROS activity for H_2O_2-induced ROS generation in human monocyte cells (Tsai et al., 2018). In our study, pretreatment with montelukast suppressed arsenic-induced ROS generation. Simultaneously, the activation of AKT-NF-κB signaling is also attenuated by montelukast. NF-κB is a critical transcription factor that is activated by ROS to transactivate the expression of several mesenchymal proteins, such as MMPs, Snail, and Twist. Our results demonstrated that inhibition of NF-κB activation blocked arsenic-induced EMT. These results indicate that montelukast inhibits arsenic-induced total ROS generation, thus inhibiting AKT-NF-κB signaling activation and downstream mesenchymal changes. The scheme summarizing our findings is shown in **Figure 6**.

Montelukast leads to clinical improvement in asthma-related symptoms both as a monotherapy and in combination with inhaled corticosteroids. Combining oral montelukast with an inhaled corticosteroid, fluticasone, is the most common maintenance therapy for asthmatic children. Glucocorticoids were reported to ameliorate TGF-β-induced EMT in airway epithelial cells (Yang et al., 2017). Treatment with fluticasone decreased TGF-β-induced cell migration and mesenchymal protein (α-SMA, vimentin, and fibronectin) expression. One contrary, the other study has also shown that Fluticasone further enhanced TGF-β-induced fibronectin expression at

both the transcriptional and protein levels in fibroblasts (Degen et al., 2009). In our study, fluticasone promoted arsenic-induced cell migration and the expression fibronectin. These results indicated that corticosteroid treatment and the combination of corticosteroid and montelukast may worsen arsenic-induced pulmonary damage.

Taken together, this study revealed novel potential therapeutic agents for treating arsenic-induced pulmonary damage and provides usage guidelines for combination of these agents with corticosteroids. Since our results have shown that montelukast reversed the arsenic-induced EMT in pulmonary epithelial cells, which is believed a mechanism for induction of pulmonary fibrosis, it still needs further *in vivo* studies to validate the therapeutic effect of montelukast for arsenic-induced lung damage. Besides, arsenic exposure-induced airway inflammation is observed in both human (Shih et al., 2019) and rodent (Wang P. et al., 2021; Wang W. et al., 2021; Xiao et al., 2021), and is believed one of the critical mechanisms for arsenic-induced pulmonary damages. For example, arsenic exposure is associated with an increase in eosinophil number in human (Maiti et al., 2012). Notably, montelukast was shown to decrease eosinophil inflammation of asthma patients (Schaper et al., 2011). Therefore, the systemic effects of montelukast on arsenic-induced pulmonary damages *in vivo* is worth for further study.

DATA AVAILABILITY STATEMENT

The original contributions presented in the study are included in the article/**Supplementary Material**, further inquiries can be directed to the corresponding author.

AUTHOR CONTRIBUTIONS

H-CC and H-YC: conception and design, acquisition of data, analysis and interpretation, literature searching, generating figures, and drafting manuscript. C-HH and C-HK: conception and design, data collection, analysis and interpretation, revising manuscript, final approval of the version. M-LT: conception and design, literature searching, and drafting manuscript. S-CC and M-HL: literature searching, generating figures, and drafting manuscript. T-CC: acquisition of data, analysis and interpretation.

FUNDING

This study was supported partially by Kaohsiung Municipal Siaognag Hospital, [KMHK-DK(C)111001, KMHK-S-110-10, KMHK-H-110-008], the Research Center for Environmental Medicine, Kaohsiung Medical University, Kaohsiung, Taiwan from The Featured Areas Research Center Program within the framework of the Higher Education Sprout Project by the Ministry of Education (MOE) in Taiwan and by Kaohsiung Medical University Research Center Grant (KMU-TC109A01-1, KMU-TC111A01-1, and KMUTC111IFSP01).

SUPPLEMENTARY MATERIAL

The Supplementary Material for this article can be found online at: https://www.frontiersin.org/articles/10.3389/fphar.2022.877125/full#supplementary-material

REFERENCES

Assad, N., Sood, A., Campen, M. J., and Zychowski, K. E. (2018). Metal-Induced Pulmonary Fibrosis. *Curr. Environ. Health Rep.* 5, 486–498. doi:10.1007/s40572-018-0219-7

Balani, S. K., Xu, X., Pratha, V., Koss, M. A., Amin, R. D., Dufresne, C., et al. (1997). Metabolic Profiles of Montelukast Sodium (Singulair), a Potent Cysteinyl Leukotriene1 Receptor Antagonist, in Human Plasma and Bile. *Drug Metab. Dispos* 25, 1282–1287.

Bjørklund, G., Oliinyk, P., Lysiuk, R., Rahaman, M. S., Antonyak, H., Lozynska, I., et al. (2020). Arsenic Intoxication: General Aspects and Chelating Agents. *Arch. Toxicol.* 94, 1879–1897. doi:10.1007/s00204-020-02739-w

Chang, Y. W., and Singh, K. P. (2019b). Arsenic Induces Fibrogenic Changes in Human Kidney Epithelial Cells Potentially through Epigenetic Alterations in DNA Methylation. *J. Cel. Physiol.* 234, 4713–4725. doi:10.1002/jcp.27244

Chang, Y. W., and Singh, K. P. (2019a). Arsenic-Induced Neoplastic Transformation Involves Epithelial-Mesenchymal Transition and Activation of the β-Catenin/c-Myc Pathway in Human Kidney Epithelial Cells. *Chem. Res. Toxicol.* 32, 1299–1309. doi:10.1021/acs.chemrestox.9b00089

Chen, X., Peng, W., Zhou, R., Zhang, Z., and Xu, J. (2020). Montelukast Improves Bronchopulmonary Dysplasia by Inhibiting Epithelial-Mesenchymal Transition via Inactivating the TGF-β1/Smads Signaling Pathway. *Mol. Med. Rep.* 22, 2564–2572. doi:10.3892/mmr.2020.11306

Dai, J., Xu, M., Zhang, X., Niu, Q., Hu, Y., Li, Y., et al. (2019). Bi-directional Regulation of TGF-β/Smad Pathway by Arsenic: A Systemic Review and Meta-Analysis of *In Vivo* and *In Vitro* Studies. *Life Sci.* 220, 92–105. doi:10.1016/j.lfs.2019.01.042

Degen, M., Goulet, S., Ferralli, J., Roth, M., Tamm, M., and Chiquet-Ehrismann, R. (2009). Opposite Effect of Fluticasone and Salmeterol on Fibronectin and Tenascin-C Expression in Primary Human Lung Fibroblasts. *Clin. Exp. Allergy* 39, 688–699. doi:10.1111/j.1365-2222.2009.03220.x

Guha Mazumder, D. N. (2007). Arsenic and Non-Malignant Lung Disease. *J. Environ. Sci. Health A. Tox. Hazard. Subst. Environ. Eng.* 42, 1859–1867. doi:10.1080/10934520701566926

Hackett, T. L. (2012). Epithelial-Mesenchymal Transition in the Pathophysiology of Airway Remodelling in Asthma. *Curr. Opin. Allergy Clin. Immunol.* 12, 53–59. doi:10.1097/ACI.0b013e32834ec6eb

Hollestelle, A., Peeters, J. K., Smid, M., Timmermans, M., Verhoog, L. C., Westenend, P. J., et al. (2013). Loss of E-Cadherin Is Not a Necessity for Epithelial to Mesenchymal Transition in Human Breast Cancer. *Breast Cancer Res. Treat.* 138, 47–57. doi:10.1007/s10549-013-2415-3

Hosoki, K., Kainuma, K., Toda, M., Harada, E., Chelakkot-Govindalayathila, A. L., Roeen, Z., et al. (2014). Montelukast Suppresses Epithelial to Mesenchymal Transition of Bronchial Epithelial Cells Induced by Eosinophils. *Biochem. Biophys. Res. Commun.* 449, 351–356. doi:10.1016/j.bbrc.2014.05.033

Hu, Y., Li, J., Lou, B., Wu, R., Wang, G., Lu, C., et al. (2020). The Role of Reactive Oxygen Species in Arsenic Toxicity. *Biomolecules* 10. doi:10.3390/biom10020240

Hur, J., Kang, J. Y., Rhee, C. K., Kim, Y. K., and Lee, S. Y. (2018). The Leukotriene Receptor Antagonist Pranlukast Attenuates Airway

Remodeling by Suppressing TGF-β Signaling. *Pulm. Pharmacol. Ther.* 48, 5–14. doi:10.1016/j.pupt.2017.10.007

Jeong, C. H., Seok, J. S., Petriello, M. C., and Han, S. G. (2017). Arsenic Downregulates Tight Junction Claudin Proteins Through P38 and NF-κB in Intestinal Epithelial Cell Line, HT-29. *Toxicology* 379, 31–39. doi:10.1016/j.tox.2017.01.011

Jia, S., and Kim, K. K. (2017). "The Function of Epithelial Cells in Pulmonary Fibrosis," in *Lung Epithelial Biology in the Pathogenesis of Pulmonary Disease*. Editors V. K. Sidhaye and M. Koval (Boston: Academic Press), 103–131. doi:10.1016/b978-0-12-803809-3.00007-5

Jiang, J., Wang, K., Chen, Y., Chen, H., Nice, E. C., and Huang, C. (2017). Redox Regulation in Tumor Cell Epithelial-Mesenchymal Transition: Molecular Basis and Therapeutic Strategy. *Signal. Transduct. Target Ther.* 2, 17036. doi:10.1038/sigtrans.2017.36

Jiang, L., Diaz, P. T., Best, T. M., Stimpfl, J. N., He, F., and Zuo, L. (2014). Molecular Characterization of Redox Mechanisms in Allergic Asthma. *Ann. Allergy Asthma Immunol.* 113, 137–142. doi:10.1016/j.anai.2014.05.030

Jiang, R., Li, Y., Xu, Y., Zhou, Y., Pang, Y., Shen, L., et al. (2013). EMT and CSC-Like Properties Mediated by the IKKβ/IκBα/RelA Signal Pathway via the Transcriptional Regulator, Snail, Are Involved in the Arsenite-Induced Neoplastic Transformation of Human Keratinocytes. *Arch. Toxicol.* 87, 991–1000. doi:10.1007/s00204-012-0933-0

Kalluri, R., and Weinberg, R. A. (2009). The Basics of Epithelial-Mesenchymal Transition. *J. Clin. Invest* 119, 1420–1428. doi:10.1172/JCI39104

Lencinas, A., Broka, D. M., Konieczka, J. H., Klewer, S. E., Antin, P. B., Camenisch, T. D., et al. (2010). Arsenic Exposure Perturbs Epithelial-Mesenchymal Cell Transition and Gene Expression in a Collagen Gel Assay. *Toxicol. Sci.* 116, 273–285. doi:10.1093/toxsci/kfq086

Li, B., Li, X., Zhu, B., Zhang, X., Wang, Y., Xu, Y., et al. (2013). Sodium Arsenite Induced Reactive Oxygen Species Generation, Nuclear Factor (Erythroid-2 Related) Factor 2 Activation, Heme Oxygenase-1 Expression, and Glutathione Elevation in Chang Human Hepatocytes. *Environ. Toxicol.* 28, 401–410. doi:10.1002/tox.20731

Li, S., and Ren, Q. (2020). Effects of Arsenic on Wnt/β-Catenin Signaling Pathway: A Systematic Review and Meta-Analysis. *Chem. Res. Toxicol.* 33, 1458–1467. doi:10.1021/acs.chemrestox.0c00019

Liu, Y., Gao, W., and Zhang, D. (2010). Effects of Cigarette Smoke Extract on A549 Cells and Human Lung Fibroblasts Treated with Transforming Growth Factor-Beta1 in a Coculture System. *Clin. Exp. Med.* 10, 159–167. doi:10.1007/s10238-009-0081-x

Maiti, S., Chattopadhyay, S., Deb, B., Samanta, T., Maji, G., Pan, B., et al. (2012). Antioxidant and Metabolic Impairment Result in DNA Damage in Arsenic-Exposed Individuals with Severe Dermatological Manifestations in Eastern India. *Environ. Toxicol.* 27, 342–350. doi:10.1002/tox.20647

Nilsson, G. M., Akhtar, N., Kannius-Janson, M., and Baeckström, D. (2014). Loss of E-Cadherin Expression Is Not a Prerequisite for C-erbB2-Induced Epithelial-Mesenchymal Transition. *Int. J. Oncol.* 45, 82–94. doi:10.3892/ijo.2014.2424

Pain, M., Bermudez, O., Lacoste, P., Royer, P. J., Botturi, K., Tissot, A., et al. (2014). Tissue Remodelling in Chronic Bronchial Diseases: from the Epithelial to Mesenchymal Phenotype. *Eur. Respir. Rev.* 23, 118–130. doi:10.1183/09059180.00004413

Parvez, F., Chen, Y., Yunus, M., Olopade, C., Segers, S., Slavkovich, V., et al. (2013). Arsenic Exposure and Impaired Lung Function. Findings from a Large Population-Based Prospective Cohort Study. *Am. J. Respir. Crit. Care Med.* 188, 813–819. doi:10.1164/rccm.201212-2282OC

Piromkraipak, P., Sangpairoj, K., Tirakotai, W., Chaithirayanon, K., Unchern, S., Supavilai, P., et al. (2018). Cysteinyl Leukotriene Receptor Antagonists Inhibit Migration, Invasion, and Expression of MMP-2/9 in Human Glioblastoma. *Cell Mol. Neurobiol.* 38, 559–573. doi:10.1007/s10571-017-0507-z

Ren, Z. X., Yu, H. B., Li, J. S., Shen, J. L., and Du, W. S. (2015). Suitable Parameter Choice on Quantitative Morphology of A549 Cell in Epithelial-Mesenchymal Transition. *Biosci. Rep.* 35 (3), e00202. doi:10.1042/BSR20150070

Rout-Pitt, N., Farrow, N., Parsons, D., and Donnelley, M. (2018). Epithelial Mesenchymal Transition (EMT): A Universal Process in Lung Diseases with Implications for Cystic Fibrosis Pathophysiology. *Respir. Res.* 19, 136. doi:10.1186/s12931-018-0834-8

Sanchez, T. R., Perzanowski, M., and Graziano, J. H. (2016). Inorganic Arsenic and Respiratory Health, from Early Life Exposure to Sex-Specific Effects: A Systematic Review. *Environ. Res.* 147, 537–555. doi:10.1016/j.envres.2016.02.009

Sanchez, T. R., Powers, M., Perzanowski, M., George, C. M., Graziano, J. H., and Navas-Acien, A. (2018). A Meta-Analysis of Arsenic Exposure and Lung Function: Is There Evidence of Restrictive or Obstructive Lung Disease? *Curr. Environ. Health Rep.* 5, 244–254. doi:10.1007/s40572-018-0192-1

Schäper, C., Noga, O., Koch, B., Ewert, R., Felix, S. B., Gläser, S., et al. (2011). Anti-Inflammatory Properties of Montelukast, a Leukotriene Receptor Antagonist in Patients with Asthma and Nasal Polyposis. *J. Investig. Allergol. Clin. Immunol.* 21, 51–58.

Shih, Y. H., Argos, M., and Turyk, M. E. (2019). Urinary Arsenic Concentration, Airway Inflammation, and Lung Function in the U.S. Adult Population. *Environ. Res.* 175, 308–315. doi:10.1016/j.envres.2019.05.031

Shimbori, C., Shiota, N., and Okunishi, H. (2011). Effects of Montelukast, a Cysteinyl-Leukotriene Type 1 Receptor Antagonist, on the Pathogenesis of Bleomycin-Induced Pulmonary Fibrosis in Mice. *Eur. J. Pharmacol.* 650, 424–430. doi:10.1016/j.ejphar.2010.09.084

Siddique, A. E., Rahman, M., Hossain, M. I., Karim, Y., Hasibuzzaman, M. M., Biswas, S., et al. (2020). Association Between Chronic Arsenic Exposure and the Characteristic Features of Asthma. *Chemosphere* 246, 125790. doi:10.1016/j.chemosphere.2019.125790

Smith, A. H., Lingas, E. O., and Rahman, M. (2000). Contamination of Drinking-Water by Arsenic in Bangladesh: a Public Health Emergency. *Bull. World Health Organ.* 78, 1093–1103.

Sohal, S. S., Reid, D., Soltani, A., Ward, C., Weston, S., Muller, H. K., et al. (2010). Reticular Basement Membrane Fragmentation and Potential Epithelial Mesenchymal Transition Is Exaggerated in the Airways of Smokers with Chronic Obstructive Pulmonary Disease. *Respirology* 15, 930–938. doi:10.1111/j.1440-1843.2010.01808.x

Straif, K., Benbrahim-Tallaa, L., Baan, R., Grosse, Y., Secretan, B., El Ghissassi, F., et al. (2009). A Review of Human Carcinogens-Part C: Metals, Arsenic, Dusts, and Fibres. *Lancet Oncol.* 10, 453–454. doi:10.1016/s1470-2045(09)70134-2

Tryndyak, V. P., Borowa-Mazgaj, B., Steward, C. R., Beland, F. A., and Pogribny, I. P. (2020). Epigenetic Effects of Low-Level Sodium Arsenite Exposure on Human Liver HepaRG Cells. *Arch. Toxicol.* 94, 3993–4005. doi:10.1007/s00204-020-02872-6

Tsai, M. K., Lin, Y. C., Huang, M. Y., Lee, M. S., Kuo, C. H., Kuo, P. L., et al. (2018). The Effects of Asthma Medications on Reactive Oxygen Species Production in Human Monocytes. *J. Asthma* 55, 345–353. doi:10.1080/02770903.2017.1339798

Wang, P., Xiao, T., Li, J., Wang, D., Sun, J., Cheng, C., et al. (2021). miR-21 in EVs from Pulmonary Epithelial Cells Promotes Myofibroblast Differentiation via Glycolysis in Arsenic-Induced Pulmonary Fibrosis. *Environ. Pollut.* 286, 117259. doi:10.1016/j.envpol.2021.117259

Wang, W., Zheng, F., and Zhang, A. (2021). Arsenic-Induced Lung Inflammation and Fibrosis in a Rat Model: Contribution of the HMGB1/RAGE, PI3K/AKT, and TGF-B1/SMAD Pathways. *Toxicol. Appl. Pharmacol.* 432, 115757. doi:10.1016/j.taap.2021.115757

Wong, S. H. M., Fang, C. M., Chuah, L. H., Leong, C. O., and Ngai, S. C. (2018). E-Cadherin: Its Dysregulation in Carcinogenesis and Clinical Implications. *Crit. Rev. Oncol. Hematol.* 121, 11–22. doi:10.1016/j.critrevonc.2017.11.010

Wu, J., Liu, J., Waalkes, M. P., Cheng, M. L., Li, L., Li, C. X., et al. (2008). High Dietary Fat Exacerbates Arsenic-Induced Liver Fibrosis in Mice. *Exp. Biol. Med. (Maywood)* 233, 377–384. doi:10.3181/0710-RM-269

Xiao, T., Zou, Z., Xue, J., Syed, B. M., Sun, J., Dai, X., et al. (2021). LncRNA H19-Mediated M2 Polarization of Macrophages Promotes Myofibroblast Differentiation in Pulmonary Fibrosis Induced by Arsenic Exposure. *Environ. Pollut.* 268, 115810. doi:10.1016/j.envpol.2020.115810

Yang, H. W., Lee, S. A., Shin, J. M., Park, I. H., and Lee, H. M. (2017). Glucocorticoids Ameliorate TGF-B1-Mediated Epithelial-To-Mesenchymal Transition of Airway Epithelium Through MAPK and Snail/Slug Signaling Pathways. *Sci. Rep.* 7, 3486. doi:10.1038/s41598-017-02358-z

Zhou, Q., Jin, P., Liu, J., Li, S., Liu, W., and Xi, S. (2021). HER2 Overexpression Triggers the IL-8 to Promote Arsenic-Induced EMT and Stem Cell-Like Phenotypes in Human Bladder Epithelial Cells. *Ecotoxicol Environ. Saf.* 208, 111693. doi:10.1016/j.ecoenv.2020.111693

Zovko, A., Yektaei-Karin, E., Salamon, D., Nilsson, A., Wallvik, J., and Stenke, L. (2018). Montelukast, a Cysteinyl Leukotriene Receptor Antagonist, Inhibits the Growth of Chronic Myeloid Leukemia Cells Through Apoptosis. *Oncol. Rep.* 40, 902–908. doi:10.3892/or.2018.6465

Conflict of Interest: The authors declare that the research was conducted in the absence of any commercial or financial relationships that could be construed as a potential conflict of interest.

Publisher's Note: All claims expressed in this article are solely those of the authors and do not necessarily represent those of their affiliated organizations, or those of the publisher, the editors and the reviewers. Any product that may be evaluated in this article, or claim that may be made by its manufacturer, is not guaranteed or endorsed by the publisher.

frontiers | Frontiers in Pharmacology

ORIGINAL RESEARCH
published: 20 April 2022
doi: 10.3389/fphar.2022.884710

Effect of Crocin From Saffron (*Crocus sativus* L.) Supplementation on Oxidant/Antioxidant Markers, Exercise Capacity, and Pulmonary Function Tests in COPD Patients: A Randomized, Double-Blind, Placebo-Controlled Trial

Hassan Ghobadi[1,2], *Nasim Abdollahi*[2], *Hanieh Madani*[3] *and Mohammad Reza Aslani*[1,4]*

[1]*Lung Diseases Research Center, Ardabil University of Medical Sciences, Ardabil, Iran,* [2]*Department of Internal Medicine, Faculty of Medicine, Ardabil University of Medical Sciences, Ardabil, Iran,* [3]*Faculty of Medicine, Ardabil University of Medical Sciences, Ardabil, Iran,* [4]*Applied Biomedical Research Center, Mashhad University of Medical Sciences, Mashhad, Iran*

OPEN ACCESS

Edited by:
Arunachalam Karuppusamy, Chinese Academy of Sciences, China

Reviewed by:
Abhijit Dey, Presidency University, India
Annalisa Chiavaroli, University of Studies G d'Annunzio Chieti and Pescara, Italy

***Correspondence:**
Mohammad Reza Aslani
mraslani105@yahoo.com

Specialty section:
This article was submitted to Respiratory Pharmacology, a section of the journal Frontiers in Pharmacology

Received: *26 February 2022*
Accepted: *04 April 2022*
Published: *20 April 2022*

Citation:
Ghobadi H, Abdollahi N, Madani H and Aslani MR (2022) Effect of Crocin From Saffron (Crocus sativus L.) Supplementation on Oxidant/Antioxidant Markers, Exercise Capacity, and Pulmonary Function Tests in COPD Patients: A Randomized, Double-Blind, Placebo-Controlled Trial. Front. Pharmacol. 13:884710. doi: 10.3389/fphar.2022.884710

Background: Chronic obstructive pulmonary disease (COPD) is a progressive and chronic respiratory disorder characterized by reversible airflow limitation and lung parenchyma destruction. The main feature of COPD is inflammation and disturbance of the oxidant/antioxidant balance in the airways. The therapeutic use of herbal supplements with antioxidant and anti-inflammatory properties seems to be very useful in the medical management of patients with COPD.

Method: COPD patients were divided into placebo and intervention groups (each group n = 23) in a clinical trial study. The intervention group received crocin supplementation (30 mg/day for 12 weeks), and the control group received a placebo. Pre- and after the intervention, pulmonary function tests (PFTs), exercise capacity (using a 6-min walking distance test (6MWD)), and serum levels of total oxidant status (TOS), total antioxidant capacity (TAOC), and NF-kB were assessed using the ELISA test.

Results: Intervention with crocin for 12 weeks in COPD patients decreased serum levels of TOS and NF-κB as well as increased TAOC. In addition, the results of the 6MWD test reveal an improvement in patients' exercise capacity.

Conclusion: Crocin supplementation appears to effectively establish oxidant/antioxidant balance and improve inflammatory conditions in patients with COPD.

Keywords: crocin, oxidative stress, COPD, 6MWD (6minute walking distance), NF-kB

Iranian Registration of Clinical Trials No: IRCT20110109005579N2.

INTRODUCTION

Chronic obstructive pulmonary disease (COPD) is a progressive and chronic respiratory disorder characterized by reversible airflow limitation and destruction of lung parenchyma (Decramer et al., 2012). Various factors are involved in the development and progression of COPD, such as sex, age, genetic factors, chronic bronchitis, exposure to particles, and infection (Halpin et al., 2021). Smoking is a predominant risk factor in patients with COPD, as it contains various harmful substances that stimulate reactive oxygen species (ROS) production and induce oxidative damage (Bernardo et al., 2015). Although the pathophysiological mechanism of COPD has not been well clarified, certain factors have been reported, including neutrophil airway inflammation, oxidative stress, protease–antiprotease imbalance, and apoptosis (Amani et al., 2017; Barnes, 2017; Ghobadi et al., 2017).

Oxidative stress is caused by an imbalance in ROS-induced oxidants and endogenous antioxidants (Marotta et al., 2011). Environmental sources for ROS production include cigarette smoking, car exhaust fumes, industrial pollution, and occupational exposure to dust (Antunes et al., 2021). In contrast, cellular sources for ROS production include activation of xanthine oxidase (XO) and nicotine adenine disphosphonucleotide (NADPH) oxidase (Taniguchi et al., 2021). Inflammation of the airways is closely related to oxidative stress processes in COPD patients. ROS-induced airway inflammation leads to the recruitment of inflammatory cells to the airways and the production of pro-inflammatory cytokines, which increase the severity of inflammation and increase ROS production (Kirkham and Barnes, 2013). Transcription factors such as nuclear factor kappa B (NF-kB) play a significant role in the interaction between inflammation and ROS in chronic inflammatory diseases (Mahmoud et al., 2021). Therefore, one of the critical therapeutic targets of COPD patients is the management of inflammation and oxidative stress.

Therapeutic use of some foods and herbs has been of interest to humans throughout history for the prevention and treatment of diseases and health problems (Boskabady et al., 2007; Ghasemi et al., 2021; Khazdair et al., 2021; Saadat et al., 2021). Saffron (Crocus sativus L.) is a valuable plant used as a food additive and medicinal plant (Boskabady and Aslani, 2006). Therapeutic effects of saffron have been reported in various disorders such as cardiovascular, asthma, diabetes, and autoimmune (Hashemzaei et al., 2020; Aslani et al., 2021). Major compounds of saffron include crocin, crocetin, safranal and picrocrocin (Kermani et al., 2017a; Saadat et al., 2019). The antioxidant and anti-inflammatory properties of crocin have been proven in animal and human studies (Kermani et al., 2017a; Aslani et al., 2021). In chronic inflammatory diseases such as diabetes and asthma, clinical studies have reported the protective role of saffron in reducing inflammatory markers (Hosseini et al., 2018; Shahbazian et al., 2019). Recently, Krocina™ tablets, a 98% purified crocin from saffron, have been used in clinical trial studies (Poursamimi et al., 2020). The anti-inflammatory effects of Krocina™ have been identified in patients with osteoarthritis by reducing C-reactive protein (CRP) and interleukin (IL)-17 levels (Poursamimi et al., 2020).

Accordingly, the primary aim of the current study was to evaluate the effects of 12 weeks of crocin from saffron intervention on oxidant/antioxidant and inflammatory markers in COPD patients. Secondary objectives were determined for exercises capacity and pulmonary function tests (PFTs).

SUBJECTS AND METHODS

Design

The current study was a randomized, double-blind, placebo-controlled clinical trial.

Participants

The study was carried out in 2020 at Ardabil Imam Khomeini Hospital in northwestern Iran. Male patients with COPD were eligible to participate in the study by having the following conditions: one- clinical criteria such as shortness of breath, sputum, and cough, and two- spirometric findings (Forced expiratory volume (FEV1) <80% and FEV1/Forced vital capacity (FVC) < 70%). Exclusion criteria were one-hospitalization history during the last 3 months, two- any lung disease other than COPD, three- infectious diseases, 4-rheumatoid arthritis, 5-cancer, 6- history of drug use other than COPD-related drugs, and 7- patients with structured physical activity or planned exercise. Exclusion criteria were selected based on previous clinical trial studies that may have influenced the results of oxidant/antioxidant factors, such as supplements and medications, mentioned inflammatory diseases, and daily physical activity.

Randomization

Using a practical sampling methodology, patients were included in the study and randomized into two groups (placebo and intervention, n = 23). In order to randomize patients, the RANDBETWEEN command was done in Excel. A placebo and intervention tablets were placed in numbered bags by one of the investigators who did not participate in the study. Numbered bags were assigned to participants unaware of random sequences by another researcher. Random codes blinded all study subjects (both researchers and patients).

Intervention

After obtaining permission from the university authorities in the intervention group, the samples that were eligible for entering the study were included in the study. The intervention group was

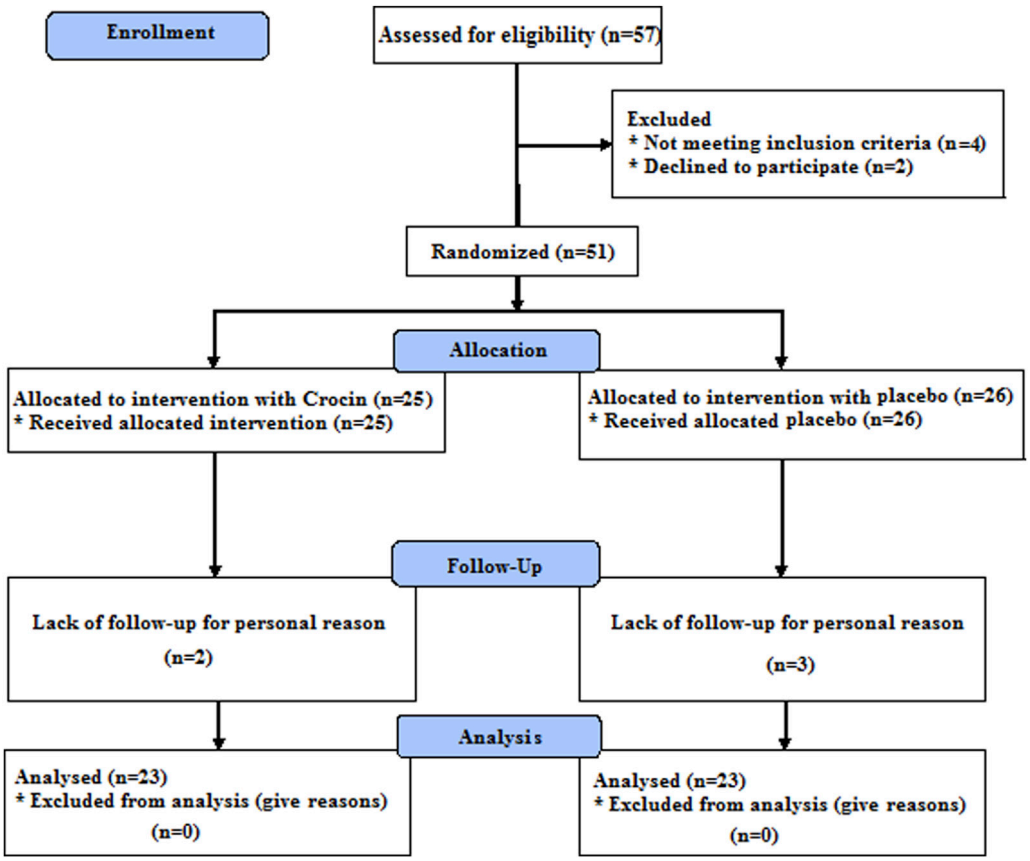

FIGURE 1 | Flow diagram of the trial.

given crocin at a 30 mg/day concentration for 12 weeks (Talaei et al., 2015), while the control group received a placebo with the same form and concentration of the drug. Crocin and placebo tablets were prepared by Sina Pooyesh Drug Company (www.samisaz.com, Registration Number 486769) (Poursamimi et al., 2020). Participants were recommended to avoid fast foods, saffron, sausages, and canned foods during the study.

Outcomes and Relevant Measures

The primary outcome was determined by serum levels of oxidant/antioxidant markers and NF-kB, and the secondary outcome was pulmonary function tests and a 6-min walking distance test (6MWD) test.

Demographic and Clinical Assessments Questionnaire

Demographic information on age, height, and weight was completed for everyone. Body mass index (BMI) at the beginning and the end of the study was calculated based on height and weight. The pulmonary function test (including FEV1, FVC, and FEV1/FVC) and the 6MWD test were also evaluated before and after the intervention.

Biochemical Examinations

At the beginning and end of the study, blood samples were taken from patients to evaluate serum levels of total antioxidant capacity (TAOC), total oxidant status (TOS), and NF-kB. The ELISA technique and commercial kits (Crystal day, China) were used to determine TAOC, TOS, and NF-kB serum levels.

Sample Size Estimation

According to the previous study, the sample size in this study was estimated at 22 subjects, of which 25 individuals were included in each group (Hosseini et al., 2018). Twenty-three individuals in each group completed the study (**Figure 1**).

Ethical Considerations

The current study was approved by the Human Ethics Committee of Ardabil University of Medical Sciences with an ethics code: IR. ARUMS.REC.1398.428 and was registered in the Iranian Registration of Clinical Trials No.: IRCT20110109005579N2. Informed written consent was obtained from all individuals. All patients were free to leave the study at any study stage.

TABLE 1 | Baseline parameters in the study groups.

Variables	Placebo (n = 23)	Crocin (n = 23)	*p*-value
	Baseline	Baseline	
Age (year)	61.72 ± 8.54	62.04 ± 8.83	0.904
Weight (kg)	68.81 ± 12.12	74.82 ± 10.99	0.089
Height (m^2)	1.71 ± 0.05	1.72 ± 0.05	0.842
BMI (kg/m^2)	23.18 ± 4.31	25.13 ± 3.62	0.109
FEV1 (%)	58.26 ± 15.95	55.39 ± 13.91	0.519
FVC (%)	76.21 ± 15.85	70.34 ± 14.92	0.203
FEV1/FVC ratio	62.23 ± 9.82	64.67 ± 9.25	0.391
6MWD (m/min)	380.68 ± 113.64	397.61 ± 64.91	0.546
TAOC (ng/ml)	2.48 ± 0.60	2.57 ± 1.49	0.787
TOS (ng/ml)	4.87 ± 1.61	5.04 ± 0.82	0.661
NF-kB (ng/ml)	4.57 ± 1.27	4.79 ± 1.04	0.543

BMI: body mass index, FEV1: forced expiratory volume in the first second, FVC: forced vital capacity, 6MWD: 6-min walking distance test, IL-6: interleukin-6, TNF-α: tumor necrosis factor alpha.

Statistical Analysis

The normal distribution of the data was determined from the Kolmogorov-Smirnov test. Parametric data were reported using the mean ± standard deviation (SD), and non-parametric data were reported using the 25th-75th percentiles. Paired *t*-test (parametric) and Wilcoxon (non-parametric) tests were used to analyze each group's data before and after the intervention. Independent t-tests and Mann-Whitney tests were used for comparing data between placebo and intervention groups. $p < 0.05$ was defined as statistically significant. SPSS version 21 and Graph Pad Prism 7 software were used for the statistical analysis.

RESULTS

Characteristics of Subjects

The parameters considered in the current study are presented in **Table 1**. There was no significant difference between the placebo and intervention groups at the beginning of the study regarding age, BMI, FEV1, FVC, FEV1/FVC, 6MWD, and serum levels of TAOC, TOS, and NF-kB variables.

Effects of Crocin-Intervention on PFTs and 6MWD

In both placebo and Crocin-treated groups, it was found that there was no significant difference in the mean FEV1, FVC, and FEV1/FVC ratio (**Figures 2A,C,E**). In addition, the mean changes of FEV1, FVC, and FEV1/FVC ratio also did not reveal a significant difference between the two groups (**Figures 2B,D,F**).

In the placebo group, despite the increase in mean 6MWD at the end of the study, no significant difference was observed, while in the intervention group, a significant increase was evident ($p < 0.01$, **Figure 3A**). Mean changes of 6MWD were not significantly different between the placebo and intervention groups (**Figure 3B**).

Effects of Crocin-Intervention on Serum TOS, TAOC, and NF-kB Levels

Significantly increased levels of TOS were seen in the placebo group at the end of the study compared to the beginning of the study ($p < 0.05$, **Figure 4A**), but there was no significant difference in the intervention group. The mean TOS changes between the placebo and Crocin-treated groups were insignificant (**Figure 4B**).

After the intervention, the mean serum TAOC levels in the intervention group were significantly higher than in pre-intervention ($p < 0.05$, **Figure 4C**), but no significant differences were observed in the placebo group. Furthermore, the mean changes in serum TAOC concentrations were significantly higher in the intervention group than in the placebo group ($p < 0.05$, **Figure 4D**).

Serum NF-κB levels were not significantly different in the placebo and intervention groups after the intervention than pre-intervention (**Figure 4E**). However, the results of mean changes in serum NF-κB levels showed a significant decrease in the Crocin-treated group compared to the placebo group ($p < 0.05$, **Figure 4F**).

Side Effects

No drug side effects were observed in individuals receiving the crocin intervention. Individuals who withdrew from the study for personal reasons and the study coincided with the COVID-19 pandemic.

DISCUSSION

The most important results of the current clinical trial study were: one- decreased serum TOS and NF-kB levels, two- increased serum TAOC levels, and three- improved 6MWD tolerance.

COPD is an inflammatory disease characterized by the involvement of the lung parenchyma, airways, and pulmonary vasculature (Halpin et al., 2021). The pathophysiology of COPD is thought to be involved in oxidant/antioxidant and protease/antiprotease imbalances (Boukhenouna et al., 2018). As a result of increased activity of oxidants and proteases, destruction of air sacs has been reported in patients with COPD (Boukhenouna et al., 2018). PFT changes are critical diagnostic, grading and monitoring criteria for COPD patients (Halpin et al., 2021). There is evidence of a decrease in FEV1 in COPD patients due to inflammatory responses and airway obstruction. The intervention with Crocin showed that FEV1 in COPD patients was enhanced, although it was not significant. One of the factors that may have influenced the PFT results of the current study is the duration of the intervention for 3 months. The effectiveness of most supplements has been reported in clinical trial studies with more than 3 months of intervention. Hosseini et al. demonstrated that saffron intervention improves pulmonary function tests in asthmatic patients (Hosseini et al., 2018). Although the exact mechanism of saffron and its active ingredient (Crocin) is poorly understood, its anti-inflammatory and antioxidant effects may

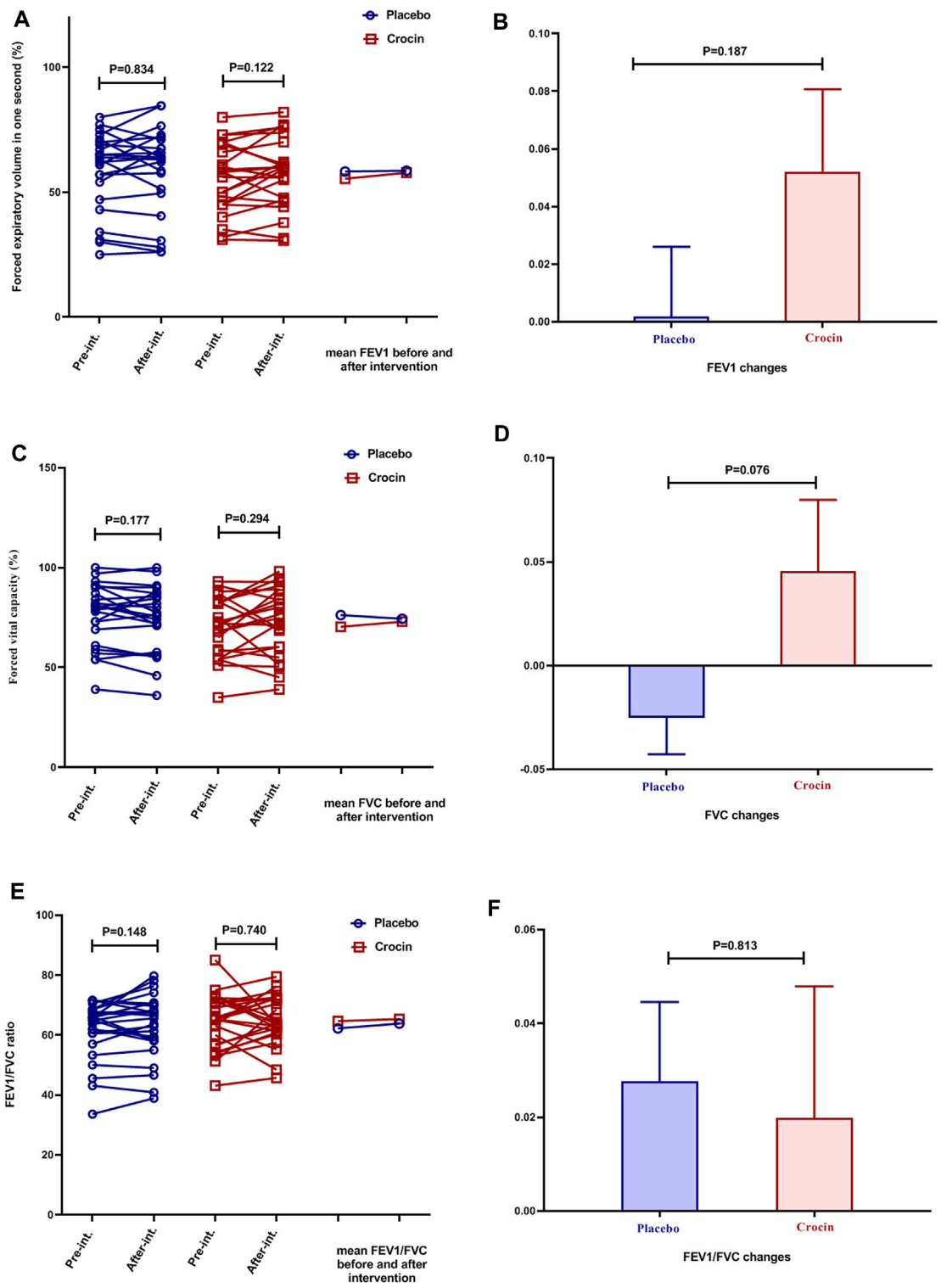

FIGURE 2 | Individual values and mean of **(A)**: FEV1 **(B)**: FEV1 changes **(C)** FVC **(D)**: FVC changes **(E)**: FVE1/FVC, and **(F)**: FEV1/FVC changes in placebo (blue color) and crocin-treated (red color) group's pre-intervention and after 12 weeks of intervention. FEV1: Forced expiratory volume in the first second, FVC: Forced vital capacity.

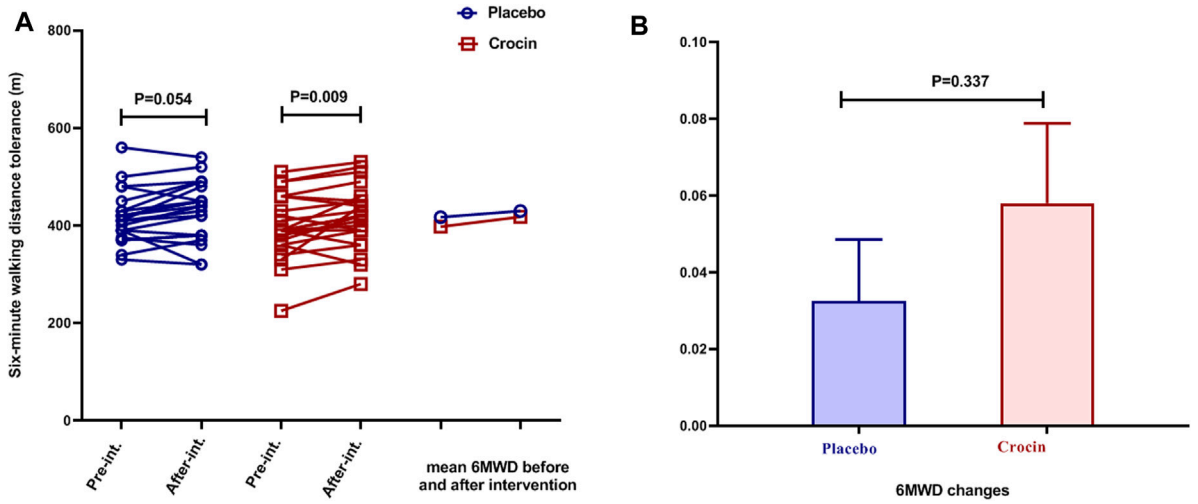

FIGURE 3 | Individual values and mean of **(A)**: 6MWD and **(B)**: 6MWD changes in placebo (blue color) and crocin-treated groups (red color) pre-intervention and after 12 weeks of intervention. 6MWD: 6-min walking distance test.

play a key role (Kermani et al., 2017b). Most animal studies have shown the protective effects of saffron and Crocin in the ovalbumin-induced asthma model (Saadat et al., 2019; Aslani et al., 2021). However, further human studies are required to elucidate the effects of Crocin on PFTs in chronic lung diseases.

Oxidative stress is a critical factor in promoting COPD inflammation (Zinellu et al., 2021). Oxidative stress occurs when endogenous antioxidant defenses are impaired, or reactive oxygen species (ROS) activity is enhanced (Kirkham and Barnes, 2013). ROS production originates from environmental (cigarette smoke) or cellular (inflammatory and structural cells) sources (Kirkham and Barnes, 2013). Pulmonary inflammation induced by ROS leads to the production of pro-inflammatory markers and the recruitment of inflammatory cells into the airways, thereby increasing the production of ROS (Zinellu et al., 2021). In patients with COPD, oxidative stress is typically caused by prolonged exposure to cigarettes smoke or by a variety of inflammatory and immune stimuli in the airways (Taniguchi et al., 2021). Elevated levels of oxidants and decreased antioxidant levels are present locally (in lung tissue) and systemically in patients with COPD (Elmasry et al., 2015). Patients with COPD showed increased levels of oxidative products such as malonyl dialdehyde (MDA) and TOS compared to healthy subjects (Zeng et al., 2013). Decreased antioxidants may also contribute to increased oxidative stress in COPD conditions, such as SOD, GSH-Px, reduced GSH, TAOC, thioredoxin, and nuclear factor erythroid two– related factor 2 (Nrf2) (Taniguchi et al., 2021).

The study showed that Crocin treatment in COPD patients caused a significant reduction in serum TOS levels. On the other hand, Crocin treatment also increased TAOC levels in COPD patients. In fact, the results suggest that Crocin treatment reversed the oxidant/antioxidant imbalance created by COPD. Saffron has potent anti-inflammatory and antioxidant effects with various components such as Crocin, crocetin, and safranal (Assimopoulou et al., 2005). Invitro, *in vivo*, and human studies have shown the antioxidant effects of saffron and Crocin in various pathological conditions, including asthma, COPD, myocardial infarction, and cancer (Tsantarliotou et al., 2013; Al-Gubory, 2014). The saffron and its effective compounds exert their antioxidant effects by reducing the production of oxidative factors such as MDA, lipid peroxidation (LPO), inducible nitric oxide synthase (iNOS), nitric oxide (NO), XO, myeloperoxidase (MPO), and protein carbonyls (PC) as well as by increasing antioxidant factors such as reduced glutathione (GSH), total antioxidant capacity (TAOC), superoxide dismutase (SOD), glutathione peroxidase (GPx), catalase (CAT), and glutathione-S-transferase (GST) (Boskabady and Farkhondeh, 2016).

Different clinical trial studies have examined the effects of saffron on oxidative markers in various diseases. Intervention with saffron in type 2 diabetic patients reduced serum MDA concentrations while no effect was observed on TAOC and F2-isoprostane levels (Azimi et al., 2014; Ebrahimi et al., 2019; Shahbazian et al., 2019). In patients with ulcerative sclerosis, it was revealed that intervention with saffron for 8 weeks resulted in increased TAOC, GPX, and SOD while preventing an increase in serum MDA concentration compared with the placebo group (Tahvilian et al., 2021). Also, in patients with multiple sclerosis, a 4-weeks intervention with saffron decreased MDA levels and increased TAOC (Ghiasian et al., 2019). In addition, similar results occurred in patients with nonalcoholic fatty liver diseases due to intervention with saffron for 12 weeks, decreasing MDA and increasing TAOC levels (Pour et al., 2020). In patients with metabolic syndrome, it has been reported that intervention with saffron for 12 weeks can modulate pro-oxidant-antioxidant serum levels (Kermani et al., 2015). However, in patients with rheumatoid arthritis, Hamidi et al. did not observe significant differences in MDA and TAOC levels after 12 weeks of saffron intervention (Hamidi et al.,

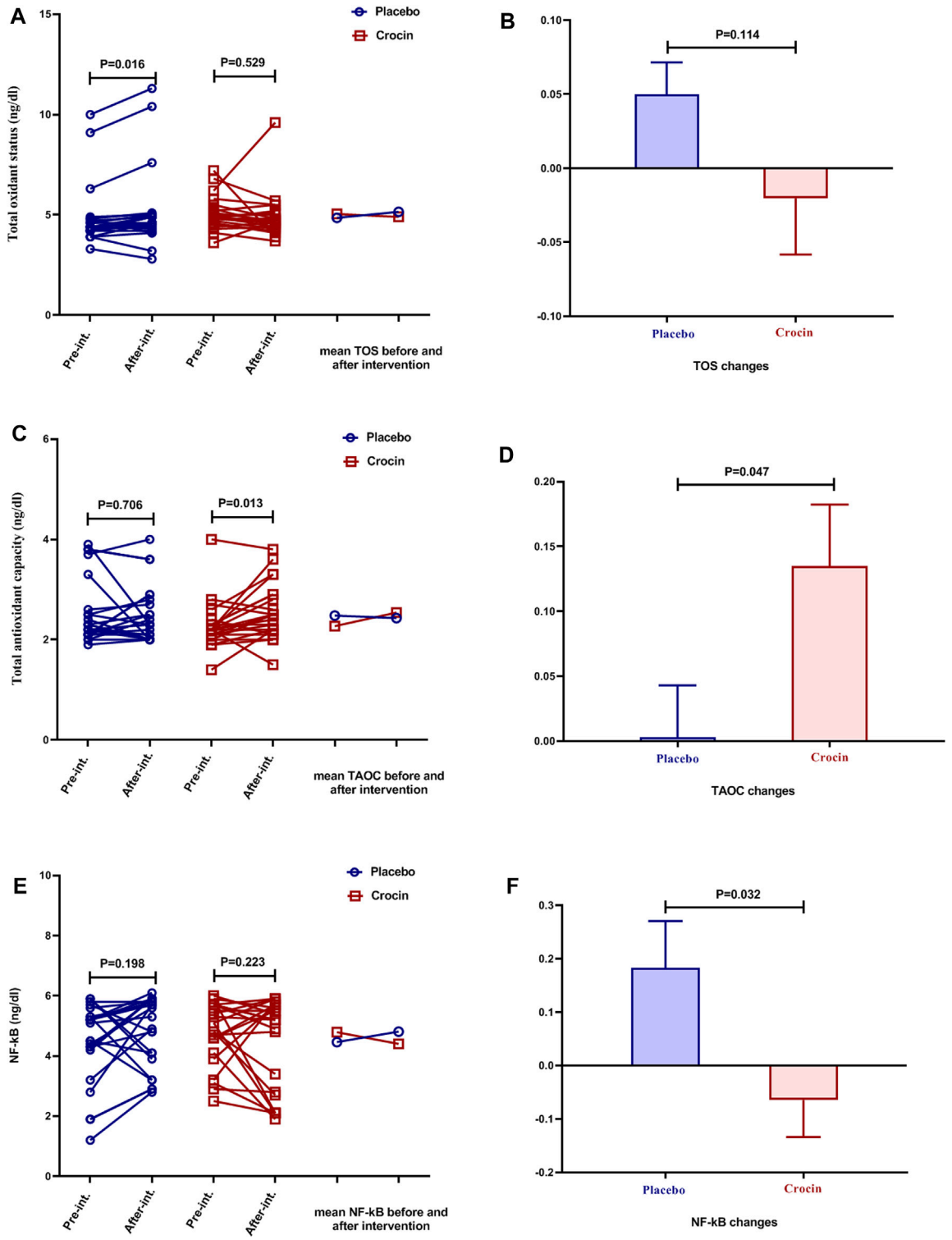

FIGURE 4 | Individual values and mean of serum levels of **(A)**: TOS **(B)**: TOS changes **(C)**: TAOC **(D)**: TAOC changes **(E)**: NF-kB, and **(F)**: NF-kB changes in placebo (blue color) and crocin-treated groups (red color) pre-intervention and after 12 weeks of intervention. TOS: total oxidant status, TAOC: total antioxidant capacity.

2020). For the first time in a clinical trial study on COPD patients, the results of our study reported the reducing effects of Crocin on oxidative factors and the increasing effects of antioxidant factors.

Recently, there has been much evidence that oxidative stress and inflammation play a vital role in the pathogenesis of various diseases, including diabetes, cancer, obesity, metabolic syndrome, and chronic respiratory disease (Mahmoud et al., 2021). By activating inflammatory signaling pathways, ROS causes the release of different inflammatory mediators such as cytokines, chemokines, and eicosanoids (Mahmoud et al., 2021). Activation of some protein kinases and signaling pathways (nuclear factor-kappaB (NF-kB), p38 mitogen-activated protein kinases (MAPK), and protein kinase C) as a result of oxidative stress also has a double effect on inflammatory processes (Canty et al., 1999; Khan et al., 2020). NF-κB activation in patients with COPD occurs in response to inflammatory mediators such as IL-1β and TNF-α or due to activation of Toll-like receptors (TLRs) following bacterial or viral infections (Edwards et al., 2009). The redox pathway regulates NF-κB signaling due to oxidant/antioxidant imbalance in inflammatory diseases of the airways (Rajendrasozhan et al., 2008). In patients with COPD, regulation of NF-κB signaling activity is one of the essential therapeutic criteria, so the therapeutic use of corticosteroids inhibits NF-κB activity and consequently reduces the levels of inflammatory cytokines.

The present study showed that the Crocin intervention had a protective effect on the serum NF-κB concentration since there was a significant increase in the placebo group at the end of the study. Also, the mean changes in serum NF-κB concentration in the placebo group were higher than in the Crocin-treated group. The results revealed that Crocin intervention had inhibitory effects on NF-κB activity in patients with COPD. Similar results have been reported from human and animal studies about the effects of saffron and Crocin on NF-κB levels (Boskabady and Farkhondeh, 2016). Saffron and crocin exert anti-inflammatory and antioxidant effects through various mechanisms, including modulation of phosphoinositide-3-kinase (PI3K)/Akt, protein kinase C (PKC), mitogen-activated protein kinases (MAPK/ERK), Nrf2, NF-κB p65, c-Jun N-terminal kinases (JNK), Ca2+/calmodulin dependent protein kinase 4 (CAMK4), inducible nitric oxide synthase (iNOS), signal transducer and activator of transcription 6 (STAT6), ER-stress markers, and high-mobility group box 1 (HMGB-1) pathways (Kim et al., 2014; Xiong et al., 2015; Yosri et al., 2017; Dianat et al., 2018; Xie et al., 2019; Zhang et al., 2020; Aslani et al., 2021).

One of the most critical health indicators is cardiorespiratory preparations (Oliveira et al., 2016). n exercise test below the maximum 6-min walk-in for patients with COPD is a crucial activity for assessing cardiovascular and respiratory rehabilitation. With this test, patients' exercise capacity and health-related quality of life (HRQL) can be evaluated (Wouters et al., 2020). COPD patients have reported reduced levels of 6MWD and quality of life compared with healthy individuals (Puhan et al., 2008). Intervention with Crocin for 12 weeks significantly increased 6MWD in patients with COPD. Crocin with anti-inflammatory and antioxidant effects may have led to increased exercise capacity and quality of life satisfaction in patients with COPD, which requires further studies.

This study had some limitations. First, the current study had no female patients, and the extraction results can only be used in men with COPD. Second, the sample size was moderate considering the COVID-19 conditions and may have masked the significant results of crocin. Finally, although most studies have reported duration of ≥12 weeks for saffron (crocin) supplementation, it is advisable to evaluate a more extended intervention with saffron in future studies.

In summary, the association between oxidative stress and inflammation affects patients with COPD, such as decreased pulmonary function tests, exercise capacity, and quality of life. Under COPD conditions, increased oxidative and inflammatory markers (such as TOS and NF-kB) combined with decreased antioxidant factors (TAOC) may have been associated with decreased exercise capacity and PFT. Intervention with Crocin (one of the main compounds of saffron) increased exercise capacity and PFTs of patients with COPD, possibly by modulating oxidant/antioxidant and inflammatory pathways.

DATA AVAILABILITY STATEMENT

The original contributions presented in the study are included in the article/Supplementary Materials, further inquiries can be directed to the corresponding author.

ETHICS STATEMENT

The studies involving human participants were reviewed and approved by Human Ethics Committee of Ardabil University of Medical Sciences with an ethics code: IR. ARUMS.REC.1398.428. The patients/participants provided their written informed consent to participate in this study.

AUTHOR CONTRIBUTIONS

MA and HG: Literature search, Proposal writing, Data collection, Analysis of data, Interpretation of data, Manuscript preparation, Review of manuscript NA and HM: Proposal writing, Data collection, Analysis of data, Review of manuscript.

ACKNOWLEDGMENTS

The authors would like to thank the staff of the spirometerys' clinic of Ardabil Imam Khomeini Hospital.

REFERENCES

Al-Gubory, K. H. (2014). Environmental Pollutants and Lifestyle Factors Induce Oxidative Stress and Poor Prenatal Development. *Reprod. Biomed. Online* 29, 17–31. doi:10.1016/j.rbmo.2014.03.002

Amani, M., Ghadimi, N., Aslani, M. R., and Ghobadi, H. (2017). Correlation of Serum Vascular Adhesion Protein-1 with Airflow Limitation and Quality of Life in Stable Chronic Obstructive Pulmonary Disease. *Respir. Med.* 132, 149–153. doi:10.1016/j.rmed.2017.10.011

Antunes, M. A., Lopes-Pacheco, M., and Rocco, P. R. M. (2021). Oxidative Stress-Derived Mitochondrial Dysfunction in Chronic Obstructive Pulmonary Disease: A Concise Review. *Oxid. Med. Cel Longev.* 2021, 6644002. doi:10.1155/2021/6644002

Aslani, M. R., Amani, M., Masrori, N., Boskabady, M. H., Ebrahimi, H. A., and Chodari, L. (2021). Crocin Attenuates Inflammation of Lung Tissue in Ovalbumin-Sensitized Mice by Altering the Expression of Endoplasmic Reticulum Stress Markers. *Biofactors* 48, 204–215. doi:10.1002/biof.1809

Assimopoulou, A. N., Sinakos, Z., and Papageorgiou, V. P. (2005). Radical Scavenging Activity of Crocus Sativus L. Extract and its Bioactive Constituents. *Phytother Res.* 19, 997–1000. doi:10.1002/ptr.1749

Azimi, P., Ghiasvand, R., Feizi, A., Hariri, M., and Abbasi, B. (2014). Effects of Cinnamon, Cardamom, Saffron, and Ginger Consumption on Markers of Glycemic Control, Lipid Profile, Oxidative Stress, and Inflammation in Type 2 Diabetes Patients. *Rev. Diabet. Stud.* 11, 258–266. doi:10.1900/RDS.2014.11.258

Barnes, P. J. (2017). Cellular and Molecular Mechanisms of Asthma and COPD. *Clin. Sci. (Lond)* 131, 1541–1558. doi:10.1042/CS20160487

Bernardo, I., Bozinovski, S., and Vlahos, R. (2015). Targeting Oxidant-dependent Mechanisms for the Treatment of COPD and its Comorbidities. *Pharmacol. Ther.* 155, 60–79. doi:10.1016/j.pharmthera.2015.08.005

Boskabady, M. H., and Aslani, M. R. (2006). Relaxant Effect of Crocus Sativus (Saffron) on guinea-pig Tracheal Chains and its Possible Mechanisms. *J. Pharm. Pharmacol.* 58, 1385–1390. doi:10.1211/jpp.58.10.0012

Boskabady, M. H., and Farkhondeh, T. (2016). Antiinflammatory, Antioxidant, and Immunomodulatory Effects of Crocus Sativus L. And its Main Constituents. *Phytother Res.* 30, 1072–1094. doi:10.1002/ptr.5622

Boskabady, M. H., Aslani, M. R., Mansuri, F., and Amery, S. (2007). Relaxant Effect of Satureja Hortensis on guinea Pig Tracheal Chains and its Possible Mechanism(s). *DARU J. Pharm. Sci.* 15, 199.

Boukhenouna, S., Wilson, M. A., Bahmed, K., and Kosmider, B. (2018). Reactive Oxygen Species in Chronic Obstructive Pulmonary Disease. *Oxid. Med. Cel Longev.* 2018, 5730395. doi:10.1155/2018/5730395

Canty, T. G., Boyle, E. M., Farr, A., Morgan, E. N., Verrier, E. D., and Pohlman, T. H. (1999). Oxidative Stress Induces NF-κB Nuclear Translocation without Degradation of IκBα. *Circulation* 100, II-361–II-364. doi:10.1161/01.cir.100.suppl_2.ii-361

Decramer, M., Janssens, W., and Miravitlles, M. (2012). Chronic Obstructive Pulmonary Disease. *Lancet* 379, 1341–1351. doi:10.1016/S0140-6736(11)60968-9

Dianat, M., Radan, M., Badavi, M., Mard, S. A., Bayati, V., and Ahmadizadeh, M. (2018). Crocin Attenuates Cigarette Smoke-Induced Lung Injury and Cardiac Dysfunction by Anti-oxidative Effects: the Role of Nrf2 Antioxidant System in Preventing Oxidative Stress. *Respir. Res.* 19, 58–20. doi:10.1186/s12931-018-0766-3

Ebrahimi, F., Sahebkar, A., Aryaeian, N., Pahlavani, N., Fallah, S., Moradi, N., et al. (2019). Effects of Saffron Supplementation on Inflammation and Metabolic Responses in Type 2 Diabetic Patients: A Randomized, Double-Blind, Placebo-Controlled Trial. *Diabetes Metab. Syndr. Obes.* 12, 2107–2115. doi:10.2147/DMSO.S216666

Edwards, M. R., Bartlett, N. W., Clarke, D., Birrell, M., Belvisi, M., and Johnston, S. L. (2009). Targeting the NF-kappaB Pathway in Asthma and Chronic Obstructive Pulmonary Disease. *Pharmacol. Ther.* 121, 1–13. doi:10.1016/j.pharmthera.2008.09.003

Elmasry, S. A., Al-Azzawi, M. A., Ghoneim, A. H., Nasr, M. Y., and Abozaid, M. M. N. (2015). Role of Oxidant-Antioxidant Imbalance in the Pathogenesis of Chronic Obstructive Pulmonary Disease. *Egypt. J. Chest Dis. Tuberculosis* 64, 813–820. doi:10.1016/j.ejcdt.2015.06.001

Ghasemi, Z., Rezaee, R., Aslani, M. R., and Boskabady, M. H. (2021). Anti-inflammatory, Anti-oxidant, and Immunomodulatory Activities of the Genus Ferula and Their Constituents: A Review. *Iran. J. Basic Med. Sci.* 24, 1613–1623. doi:10.22038/ijbms.2021.59473.13204

Ghiasian, M., Khamisabadi, F., Kheiripour, N., Karami, M., Haddadi, R., Ghaleiha, A., et al. (2019). Effects of Crocin in Reducing DNA Damage, Inflammation, and Oxidative Stress in Multiple Sclerosis Patients: A Double-Blind, Randomized, and Placebo-Controlled Trial. *J. Biochem. Mol. Toxicol.* 33, e22410. doi:10.1002/jbt.22410

Ghobadi, H., Aslani, M. R., Hosseinian, A., and Farzaneh, E. (2017). The Correlation of Serum Brain Natriuretic Peptide and Interleukin-6 with Quality of Life Using the Chronic Obstructive Pulmonary Disease Assessment Test. *Med. Princ Pract.* 26, 509–515. doi:10.1159/000484900

Halpin, D. M. G., Criner, G. J., Papi, A., Singh, D., Anzueto, A., Martinez, F. J., et al. (2021). Global Initiative for the Diagnosis, Management, and Prevention of Chronic Obstructive Lung Disease. The 2020 GOLD Science Committee Report on COVID-19 and Chronic Obstructive Pulmonary Disease. *Am. J. Respir. Crit. Care Med.* 203, 24–36. doi:10.1164/rccm.202009-3533so

Hamidi, Z., Aryaeian, N., Abolghasemi, J., Shirani, F., Hadidi, M., Fallah, S., et al. (2020). The Effect of Saffron Supplement on Clinical Outcomes and Metabolic Profiles in Patients with Active Rheumatoid Arthritis: A Randomized, Double-Blind, Placebo-Controlled Clinical Trial. *Phytother Res.* 34, 1650–1658. doi:10.1002/ptr.6633

Hashemzaei, M., Mamoulakis, C., Tsarouhas, K., Georgiadis, G., Lazopoulos, G., Tsatsakis, A., et al. (2020). Crocin: A Fighter against Inflammation and Pain. *Food Chem. Toxicol.* 143, 111521. doi:10.1016/j.fct.2020.111521

Hosseini, S. A., Zilaee, M., Shoushtari, M. H., and Ghasemi Dehcheshmeh, M. (2018). An Evaluation of the Effect of Saffron Supplementation on the Antibody Titer to Heat-Shock Protein (HSP) 70, hsCRP and Spirometry Test in Patients with Mild and Moderate Persistent Allergic Asthma: A Triple-Blind, Randomized Placebo-Controlled Trial. *Respir. Med.* 145, 28–34. doi:10.1016/j.rmed.2018.10.016

Kermani, T., Mousavi, S. H., Shemshian, M., Norouzy, A., Mazidi, M., Moezzi, A., et al. (2015). Saffron Supplements Modulate Serum Pro-oxidant-antioxidant Balance in Patients with Metabolic Syndrome: A Randomized, Placebo-Controlled Clinical Trial. *Avicenna J. Phytomed* 5, 427–433. doi:10.22038/ajp.2015.4672

Kermani, T., Kazemi, T., Molki, S., Ilkhani, K., Sharifzadeh, G., and Rajabi, O. (2017a). The Efficacy of Crocin of Saffron (Crocus Sativus L.) on the Components of Metabolic Syndrome: A Randomized Controlled Clinical Trial. *J. Res. Pharm. Pract.* 6, 228–232. doi:10.4103/jrpp.JRPP_17_26

Kermani, T., Zebarjadi, M., Mehrad-Majd, H., Mirhafez, S. R., Shemshian, M., Ghasemi, F., et al. (2017b). Anti-Inflammatory Effect of Crocus Sativus on Serum Cytokine Levels in Subjects with Metabolic Syndrome: A Randomized, Double-Blind, Placebo- Controlled Trial. *Curr. Clin. Pharmacol.* 12, 122–126. doi:10.2174/1574884712666170622082737

Khan, M. S., Khan, A., Ahmad, S., Ahmad, R., Rehman, I. U. R., Ikram, M., et al. (2020). Inhibition of JNK Alleviates Chronic Hypoperfusion-Related Ischemia Induces Oxidative Stress and Brain Degeneration via Nrf2/HO-1 and NF-κB Signaling. *Oxid. Med. Cel Longev.* 2020, 5291852. doi:10.1155/2020/5291852

Khazdair, M. R., Saadat, S., Aslani, M. R., Shakeri, F., and Boskabady, M. H. (2021). Experimental and Clinical Studies on the Effects of Portulaca Oleracea L. And its Constituents on Respiratory, Allergic, and Immunologic Disorders, a Review. *Phytother Res.* 35, 6813–6842. doi:10.1002/ptr.7268

Kim, J. H., Park, G. Y., Bang, S. Y., Park, S. Y., Bae, S. K., and Kim, Y. (2014). Crocin Suppresses LPS-Stimulated Expression of Inducible Nitric Oxide Synthase by Upregulation of Heme Oxygenase-1 via Calcium/calmodulin-dependent Protein Kinase 4. *Mediators Inflamm.* 2014, 728709. doi:10.1155/2014/728709

Kirkham, P. A., and Barnes, P. J. (2013). Oxidative Stress in COPD. *Chest* 144, 266–273. doi:10.1378/chest.12-2664

Mahmoud, A. M., Wilkinson, F. L., Sandhu, M. A., and Lightfoot, A. P. (2021). The Interplay of Oxidative Stress and Inflammation: Mechanistic Insights and Therapeutic Potential of Antioxidants. *Oxid. Med. Cel Longev.* 2021, 9851914. doi:10.1155/2021/9851914

Marotta, F., Naito, Y., Padrini, F., Xuewei, X., Jain, S., Soresi, V., et al. (2011). Redox Balance Signalling in Occupational Stress: Modification by Nutraceutical Intervention. *J. Biol. Regul. Homeost Agents* 25, 221–229.

Oliveira, M. F., Zanussi, G., Sprovieri, B., Lobo, D. M., Mastrocolla, L. E., Umeda, I. I. K., et al. (2016). Alternatives to Aerobic Exercise Prescription in Patients with Chronic Heart Failure. *Arq Bras Cardiol.* 106, 97–104. doi:10.5935/abc.20160014

Pour, F. K., Aryaeian, N., Mokhtare, M., Mirnasrollahi Parsa, R. S., Jannani, L., Agah, S., et al. (2020). The Effect of Saffron Supplementation on Some Inflammatory and Oxidative Markers, Leptin, Adiponectin, and Body Composition in Patients with Nonalcoholic Fatty Liver Disease: A Double-Blind Randomized Clinical Trial. *Phytother Res.* 34, 3367–3378. doi:10.1002/ptr.6791

Poursamimi, J., Shariati-Sarabi, Z., Tavakkol-Afshari, J., Mohajeri, S. A., Ghoryani, M., and Mohammadi, M. (2020). Immunoregulatory Effects of Krocina™, a Herbal Medicine Made of Crocin, on Osteoarthritis Patients: A Successful Clinical Trial in Iran. *Iran J. Allergy Asthma Immunol.* 19, 253. doi:10.18502/ijaai.v19i3.3453

Puhan, M. A., Mador, M. J., Held, U., Goldstein, R., Guyatt, G. H., and Schünemann, H. J. (2008). Interpretation of Treatment Changes in 6-minute Walk Distance in Patients with COPD. *Eur. Respir. J.* 32, 637–643. doi:10.1183/09031936.00140507

Rajendrasozhan, S., Yang, S. R., Edirisinghe, I., Yao, H., Adenuga, D., and Rahman, I. (2008). Deacetylases and NF-kappaB in Redox Regulation of Cigarette Smoke-Induced Lung Inflammation: Epigenetics in Pathogenesis of COPD. *Antioxid. Redox Signal.* 10, 799–811. doi:10.1089/ars.2007.1938

Saadat, S., Yasavoli, M., Gholamnezhad, Z., Aslani, M. R., and Boskabady, M. H. (2019). The Relaxant Effect of Crocin on Rat Tracheal Smooth Muscle and its Possible Mechanisms. *Iran. J. Pharm. Sci.* 18, 1358. doi:10.22037/ijpr.2019.1100713

Saadat, S., Aslani, M. R., Ghorani, V., Keyhanmanesh, R., and Boskabady, M. H. (2021). The Effects of Nigella Sativa on Respiratory, Allergic and Immunologic Disorders, Evidence from Experimental and Clinical Studies, a Comprehensive and Updated Review. *Phytother Res.* 35, 2968–2996. doi:10.1002/ptr.7003

Shahbazian, H., Moravej Aleali, A., Amani, R., Namjooyan, F., Cheraghian, B., Latifi, S. M., et al. (2019). Effects of Saffron on Homocysteine, and Antioxidant and Inflammatory Biomarkers Levels in Patients with Type 2 Diabetes Mellitus: A Randomized Double-Blind Clinical Trial. *Avicenna J. Phytomed* 9, 436–445. doi:10.22038/ajp.2019.12854

Tahvilian, N., Masoodi, M., Faghihi Kashani, A., Vafa, M., Aryaeian, N., Heydarian, A., et al. (2021). Effects of Saffron Supplementation on Oxidative/antioxidant Status and Severity of Disease in Ulcerative Colitis Patients: A Randomized, Double-Blind, Placebo-Controlled Study. *Phytother Res.* 35, 946–953. doi:10.1002/ptr.6848

Talaei, A., Hassanpour Moghadam, M., Sajadi Tabassi, S. A., and Mohajeri, S. A. (2015). Crocin, the Main Active Saffron Constituent, as an Adjunctive Treatment in Major Depressive Disorder: A Randomized, Double-Blind, Placebo-Controlled, Pilot Clinical Trial. *J. Affect Disord.* 174, 51–56. doi:10.1016/j.jad.2014.11.035

Taniguchi, A., Tsuge, M., Miyahara, N., and Tsukahara, H. (2021). Reactive Oxygen Species and Antioxidative Defense in Chronic Obstructive Pulmonary Disease. *Antioxidants* 10, 1537. doi:10.3390/antiox10101537

Tsantarliotou, M. P., Poutahidis, T., Markala, D., Kazakos, G., Sapanidou, V., Lavrentiadou, S., et al. (2013). Crocetin Administration Ameliorates Endotoxin-Induced Disseminated Intravascular Coagulation in Rabbits. *Blood Coagul. Fibrinolysis* 24, 305–310. doi:10.1097/MBC.0b013e32835bdc8f

Wouters, E. F., Posthuma, R., Koopman, M., Liu, W. Y., Sillen, M. J., Hajian, B., et al. (2020). An Update on Pulmonary Rehabilitation Techniques for Patients with Chronic Obstructive Pulmonary Disease. *Expert Rev. Respir. Med.* 14, 149–161. doi:10.1080/17476348.2020.1700796

Xie, Y., He, Q., Chen, H., Lin, Z., Xu, Y., and Yang, C. (2019). Crocin Ameliorates Chronic Obstructive Pulmonary Disease-Induced Depression via PI3K/Akt Mediated Suppression of Inflammation. *Eur. J. Pharmacol.* 862, 172640. doi:10.1016/j.ejphar.2019.172640

Xiong, Y., Wang, J., Yu, H., Zhang, X., and Miao, C. (2015). Anti-asthma Potential of Crocin and its Effect on MAPK Signaling Pathway in a Murine Model of Allergic Airway Disease. *Immunopharmacol. Immunotoxicol.* 37, 236–243. doi:10.3109/08923973.2015.1021356

Yosri, H., Elkashef, W. F., Said, E., and Gameil, N. M. (2017). Crocin Modulates IL-4/IL-13 Signaling and Ameliorates Experimentally Induced Allergic Airway Asthma in a Murine Model. *Int. Immunopharmacol.* 50, 305–312. doi:10.1016/j.intimp.2017.07.012

Zeng, M., Li, Y., Jiang, Y., Lu, G., Huang, X., and Guan, K. (2013). Local and Systemic Oxidative Stress Status in Chronic Obstructive Pulmonary Disease Patients. *Can. Respir. J.* 20, 35–41. doi:10.1155/2013/985382

Zhang, D., Qi, B. Y., Zhu, W. W., Huang, X., and Wang, X. Z. (2020). Crocin Alleviates Lipopolysaccharide-Induced Acute Respiratory Distress Syndrome by Protecting against Glycocalyx Damage and Suppressing Inflammatory Signaling Pathways. *Inflamm. Res.* 69, 267–278. doi:10.1007/s00011-019-01314-z

Zinellu, E., Zinellu, A., Fois, A. G., Pau, M. C., Scano, V., Piras, B., et al. (2021). Oxidative Stress Biomarkers in Chronic Obstructive Pulmonary Disease Exacerbations: A Systematic Review. *Antioxidants (Basel)* 10, 710. doi:10.3390/antiox10050710

Conflict of Interest: The authors declare that the research was conducted in the absence of any commercial or financial relationships that could be construed as a potential conflict of interest.

Publisher's Note: All claims expressed in this article are solely those of the authors and do not necessarily represent those of their affiliated organizations, or those of the publisher, the editors and the reviewers. Any product that may be evaluated in this article, or claim that may be made by its manufacturer, is not guaranteed or endorsed by the publisher.

frontiers | Frontiers in Pharmacology

REVIEW
published: 26 April 2022
doi: 10.3389/fphar.2022.879204

ROS and Endoplasmic Reticulum Stress in Pulmonary Disease

Xiangning Cui[1†], *Yang Zhang*[2*†], *Yingdong Lu*[1†] *and Mi Xiang*[1†]

[1]*Department of Cardiovascular, Guang'anmen Hospital, China Academy of Chinese Medical Sciences, Beijing, China,* [2]*First Clinical Medical School, Shandong University of Traditional Chinese Medicine, Jinan, China*

Pulmonary diseases are main causes of morbidity and mortality worldwide. Current studies show that though specific pulmonary diseases and correlative lung-metabolic deviance own unique pathophysiology and clinical manifestations, they always tend to exhibit common characteristics including reactive oxygen species (ROS) signaling and disruptions of proteostasis bringing about accumulation of unfolded or misfolded proteins in the endoplasmic reticulum (ER). ER is generated by the unfolded protein response. When the adaptive unfolded protein response (UPR) fails to preserve ER homeostasis, a maladaptive or terminal UPR is engaged, leading to the disruption of ER integrity and to apoptosis, which is called ER stress. The ER stress mainly includes the accumulation of misfolded and unfolded proteins in lumen and the disorder of Ca^{2+} balance. ROS mediates several critical aspects of the ER stress response. We summarize the latest advances in of the UPR and ER stress in the pathogenesis of pulmonary disease and discuss potential therapeutic strategies aimed at restoring ER proteostasis in pulmonary disease.

Keywords: er stress, unfolded protein response, pulmonary disease, reactive oxygen spieces, oxidative stress

OPEN ACCESS

Edited by:
Arunachalam Karuppusamy, Chinese Academy of Sciences (CAS), China

Reviewed by:
Lingrui Zhang, Purdue University, United States
Duxan Arancibia, Universidad de Antofagasta, Chile

***Correspondence:**
Yang Zhang
yanghedonghai@163.com

†These authors share first authorship and share co-first authorship

Specialty section:
This article was submitted to Respiratory Pharmacology, a section of the journal Frontiers in Pharmacology

Received: *19 February 2022*
Accepted: *11 March 2022*
Published: *26 April 2022*

Citation:
Cui X, Zhang Y, Lu Y and Xiang M (2022) ROS and Endoplasmic Reticulum Stress in Pulmonary Disease. Front. Pharmacol. 13:879204. doi: 10.3389/fphar.2022.879204

1 INTRODUCTION

The endoplasmic reticulum (ER) is a membrane organelle widely found. In eukaryotic cells with multiple functions. The ER coordinates secretory and transmembrane proteins folding and translocation, serves as a place to regulate the cellular stress response (Chen and Cubillos-Ruiz, 2021). The ER controls cellular Ca^{2+} uptake, storage and signaling, keeping the intracellular Ca^{2+} homeostasis. Meanwhile, the ER takes part in the generation of phospholipids including cholesterol (Sozen and Ozer, 2017). The ER lumen is the main site where proteins synthesize in cells. The accumulation of some misfold or unfolded proteins within the ER or the disruption of Ca^{2+} homeostasis can lead to the disequilibrium of ER homeostasis, which is called ER stress (Di Conza and Ho, 2020). The stability of the environment within the ER is the guarantee of regulating its normal function. In the early stage of ER stress, the induction of unfolded protein response (UPR) can reduce protein synthesis and enhance the degradation function of ER, thus lowering the burden of ER and maintaining intracellular homeostasis, which is a pro-survival response. With the aggravation of ER, the activation of UPR is inhibited, resulting in Ca^{2+} uptake/release barrier of ER or protein processing/transporting obstacle (Song et al., 2018). The signaling is accordingly transformed from survival to apoptosis, and the expression of ER stress-specific pro-apoptotic transcription factor CHOP is activated, further inhibiting the activity of AKT, and promoting cell apoptosis (Sen, 2019). The normal physiological function of ER is closely related to the redox state, and increasing studies suggest the production of ROS has become a primary part of ER stress response, possibly acting as an upstream signaling (Zhang et al., 2019a). The lung is in direct contact with the outside world, and external stimuli can easily lead to mis-synthetic proteins and cause the

occurrence of pulmonary diseases including pulmonary fibrosis, pulmonary infections, asthma, COPD (chronic obstructive pulmonary disease) and lung cancer (Liu et al., 2017; Katzen and Beers, 2020). Several pathophysiological factors such as hypoxia, inflammation, and metabolic disorders can trigger ER stress. Conversely, ER stress induces inflammation and oxidative stress, maladaptive UPR induces apoptosis, and disruption of interaction between the ER and other organelles in epithelial cells can negatively affect pulmonary disease. In this context, we introduced the relationship between ROS and ER stress, summarized current research on the molecular mechanisms of ER stress in pulmonary disease, and raised several promising therapeutic strategies targeting ER stress that might prevent or treat pulmonary disease.

2 THE PHYSIOLOGICAL MECHANISM OF REACTIVE OXYGEN SPECIES

ROS are oxygen radicals in organisms, including oxygen and oxygen-containing highly reactive molecules (such as superoxide anions, tissue peroxides, and free radicals), serving as an intracellular and inter-cellular messenger which regulates many signaling molecules (Incalza et al., 2018). ROS are generated as a byproduct in cells by mitochondria and other cellular organelles (Boengler et al., 2017). ROS modulate different cell signaling pathways, which are mostly mediated by these transcription factors NF-κB and STAT3, hypoxia-inducible factor-1α, kinases, cytokines, and other proteins; these signaling pathways have been demonstrated to be related with inflammation, proliferation, cellular transformation, angiogenesis, as well as cell metabolism in cancer cells (Prasad et al., 2017). Continuous studies have confirmed ROS production in hypoxia and ischemia models, and found that ER proteins were oxidized and modified, suggesting that ER functions can be destroyed by ROS (Xu et al., 2017; Wang et al., 2018a; Singh-Mallah et al., 2019). ROS production on ER is generated by delivering electrons to O^2 by NADH-cytochrome P450 reductase to form O^{2-}, with electrons delivered to O^2 by the electron transport chain on the nuclear membrane, assisted by NADH (Delaunay-Moisan and Appenzeller-Herzog, 2015; Zeeshan et al., 2016). Changes of intracellular redox state promotes the production of oxygen radicals and apoptosis inducer activation, resulting in apoptosis and aggravate intracellular redox state variation, then affect cell physiological state, initiate oxidative stress, and trigger the activation of apoptotic signal activation. Furtherly, calcium imbalance, oxidative stress are also important factors to induce ER stress (Kaminskyy and Zhivotovsky, 2014; Prasad et al., 2017).

3 ENDOPLASMIC RETICULUM FUNCTION AND HOMEOSTASIS

The ER is a multifunctional organelle that forms the access into the secretory pathway which is made up of smooth and rough endoplasmic reticulum. The ER is crucial in maintaining cellular calcium homeostasis, lipid biosynthesis and secretory, and transmembrane protein folding and translocation (Rowland and Voeltz, 2012; Schwarz and Blower, 2016).The oxidative environment of ER lumen promotes disulfide bond formation, allowing complex secretion and transmembrane protein folding. The process of protein folding is regulated by a variety of chaperones, folding enzymes and cofactors (Kim et al., 2013a; Saibil, 2013). The ER takes part in lipids production in cells such as cholesterol and glycerophospholipids regulated by multiple ER-localized lipid biosynthetic enzymes including GTPase SAR1B and SURF4 (Wang et al., 2021). When cholesterol levels in the ER turn too high, SREBP undergo conformational changes that hinder it from leaving the ER. Correspondingly, homeostasis of cholesterol is restored (Brown et al., 2018; Lim et al., 2019). The ER also participates in mediating calcium homeostasis in cells. In quiescent cells, the level of free Ca^{2+} in cytoplasm was lower than that in extracellular space and ER lumen. Disruption of intracellular Ca^{2+} homeostasis is related with inflammatory responses. Research suggest that increase in IP3R (inositol 1,4,5-trisphosphate receptor) mediated Ca^{2+} release can cause inflammatory pathophysiology of ventilator-induced lung injury in mice models *via* ER stress (Ye et al., 2021). During chaperone-assisted disulfide bond formation between polypeptide chain substrates, two electrons are provided to the cysteine residue within the PDI active site. This transfer of electrons results in the reduction of the PDI active site and oxidation of the substrate, suggesting main ER-originating ROS production process. Studies have confirmed that the ER membrane-associated protein ERO1 (Endoplasmic reticulum oxidoreductin-1) oxidizes PDI, indicating that ERO1 is closely associated with protein load in the ER and can trigger ROS generation and contribute to ER stress. In addition, experimental analysis revealed that UP to 25% of ROS is produced by disulfide bonds in the endoplasmic reticulum during mass oxidation. Therefore, the close relationship between ROS and endoplasmic reticulum homeostasis is further suggested.

4 REACTIVE OXYGEN SPECIES AND ENDOPLASMIC RETICULUM STRESS

As is illustrated above, accumulation of some misfolded or unfolded proteins within the ER or disruption of Ca^{2+} homeostasis can cause ER stress. Under normal circumstance, the stability of the environment within ER is the guarantee for the normal function of ER. In the early stage, ER stress reduces protein biosynthesis and enhances ER degradation function by inducing unfolded protein response (UPR), thus reducing ER burden, and maintaining intracellular homeostasis, which in essence is a protective means. Changes of intracellular redox state initiate oxidative stress and trigger the activation of apoptosis signals. Meanwhile, Ca^{2+} imbalance and oxidative stress are also important factors to induce ER stress.

4.1 Reactive Oxygen Species and UPR

4.1.1 Unfolded Protein Reaction and its Relevant Signaling Pathways (Figure 1)

ER is an important site for secretory protein folding and various post-translational modifications such as glycosylation and

disulfide bond formation. The homeostasis regulation of ER ensures that correctly folded proteins proceed to the next step of modification, while slowly folded or unfolded proteins are retained in the ER for proteasome degradation through ER related protein degradation, which is the unfolded protein response (UPR).

Under physiological conditions, three independent branches regulate the UPR, mediated by ER stress receptor proteins, PERK (RNA-dependent protein kinase (PKR)-like ER kinase), ATF6 (activating transcription factor 6), and IRE1α (Inositol-requiring enzyme-1α). These three individual proteins respectively bind to ER chaperone GRP78 (glucose-regulated protein 78) and remain inactive and serve as sensors and effectors for enhanced ER stress (Oakes and Papa, 2015; Kopp et al., 2019). When the nucleotide-binding domain of GRP78 coordinates with luminal domains of IRE1α and PERK, GRP78 is converted from a molecular chaperone to an ER stress sensor, accelerating further UPR activation (Kopp et al., 2019). These mechanisms can monitor the deviant conditions on the ER lumen, deliver signals to the cytosol, then transfer them the nucleus and activate corresponding downstream responses (**Figure 1**) (Schwarz and Blower, 2016).

PERK, a crucial ER stress sensor of the UPR, is particularly enriched at the MAMs (mitochondria-associated ER membranes), and capable of preventing mRNA translation under ER stress, thus inhibiting protein synthesis, and folding (Verfaillie et al., 2012). ATF4 (activating transcription factor 4) is a stress-induced transcription factor which is at always upregulated in cells, controls the expression of several adaptive genes that protect cells from stress, such as hypoxia or amino acid limitation. But under sustained stress conditions, ATF4 can initiate the transcription of CHOP (C/EBP homologous protein) to induce cell apoptosis (Wortel et al., 2017). PERK phosphorylates eIF2α (eukaryotic initiation factor 2) to decrease the GTP-bound (guanosine triphosphate, GTP) form and allow translation of ATF4 (Han et al., 2013; Luhr et al., 2019; Vanhoutte et al., 2021). Meanwhile, CHOP can bind to BOK (B-cell lymphoma 2 varian killer) and Caspase to act as an antiapoptotic agent (Carpio et al., 2015).

ATF6 is a type II transmembrane protein that induces ER stress response. As an up-regulating chaperone, it is an important element of the ERAD (endoplasmic reticulum—associated degradation) pathway (Jin et al., 2017). The unfolded proteins in the ER lumen separate ATF6 from GRP78, then ATF6 is transferred from the ER membrane to the Golgi apparatus as vesicles; the lumen domain of ATF6 is cleaved by S1P (serine protease site-1), the n-terminal is cleaved by metalloproteinase S2P (site-2 protease), forming the ATF6f with n-terminal cytoplasmic domain. As a result, several ER stress response element genes such as GRP78, GRP94, CHOP can be activated, and promote the ER associated protein degradation gene XBP1 (X-box binding protein 1) transcription. The ATF6f can bind XBP1 and control the expression of some specific genes (Zhang et al., 2019b; Pachikov et al., 2021).

IRE1α is a transmembrane protein, which is composed of n-terminal ER lumen sensor domain, a single transmembrane domain, and c-terminal cytoplasmic protein kinase effector, responsible for protein kinase and endonuclease activity. When ER stress happens, IRE1α cavity structure domain is dissociative with GRP78, causing cavity structure domain two polymerization to further activate the activity of enzymes, catalyze the transcription of XBP1 to upregulate multiple folding enzymes, including glycosylation, redox enzymes degradation to rectify ER homeostasis. IRE1α also degrades specific mRNA in a tissue-specific manner through RIDD (regulated IRE1-dependent mRNA decay) and activates related kinases through binding of adaptor proteins including JNK (C-Jun amino-terminal kinase) and ASK1 (apoptotic signal-regulated kinase 1) pathways (Lerner et al., 2012; Hwang and Qi, 2018; Huang et al., 2019).

Adaptive UPR is the initial defense against ER stress to keep the balance of ER homeostasis. However, persistent UPR activation can transform into maladaptive UPR, leading to drastic cell injuries even cell death. Incorrectly or terminally misfolded proteins are retained and degraded within the ER. As ER stress cells evolve further with the integrated stress response, cells actively mobilize stress response proteins to resist the deleterious effects caused by stress triggers. Meanwhile, cells adjust ER function to adapt to new internal environmental change requirements. On the other hand, some stress protein regulatory genes that may cause cell death, such as CHOP, will decide according to the situation to finally clear those ER stress cells that are simply unable to return to a normal functional state (Shirakawa et al., 2013; Hotamisligil and Davis, 2016; Urra et al., 2016; Hetz and Papa, 2018). In ER stress response, the activation of IRE-1, PERK, and ATF6 induces CHOP, promotes the activation of CHOP, and significantly increases its expression, leading to apoptosis. IRE-1-mediated splicing of XBP1 induced UPR can promote cell survival, but its overexpression can also promote cell apoptosis. Activated IRE-1 can combine with TRAF2 (TNF-receptor-associated factor 2) and ASK1 (apoptotic signal-regulated kinase 1) to form into the IRE-1-TRAF2-ASK1 complex on ER outer membrane, which activates JNK and P38 MAP (mitogen-activated protein kinase) (Matsuzawa et al., 2002). CHOP expression is induced by phosphorylation of ser78/81 in the transcriptional activation domain of P38 MAP kinase. After ER stress induced GRP78 dissociation from ATF6, the cytoplasmic ATF6 n-terminal domain also dissociated from ER membrane and formed a 50 ku active fragment. It was found that the activated ATF6 entered the nucleus and bound to the NF-Y (nuclear transcription factor-Y) and bound to the promoter ER stress element with homologous or heterologous dimer structure. The complex then induces the transcriptional expression of ER stress genes including CHOP (Feng et al., 2019). PERK is also a transmembrane protein. After dissociation from GRP78, PERK is activated by self-dimerization and phosphorylation of the intracellular domain. Activated PERK phosphorylates serine of the eukaryotic translation initiation factor eIF2α. Phosphorylated eIF2α cannot accept the exchange of GTP-GDP by eIFβ, thus slowing or suspending protein synthesis, thereby promoting the activation of CHOP, and thus inducing cell metabolism and apoptosis (Pillai, 2005; Kopp et al., 2019).

4.1.2 Reactive Oxygen Species Induced Unfolded Protein Reaction

ROS can directly attack the free thionyl group, necessary to maintain the protein foldase activity, leading to oxidative modification of proteins in the ER lumen, and then induce abnormal function of ER molecular chaperones, resulting in the accumulation of unfold proteins and retention in the ER lumen, ultimately triggering ER stress. At the same time, the expression of the chaperone protein GRP78 significantly increased and dissociated from the three transmembrane proteins to bind unfolded proteins to enhance ER protein folding ability and reduce protein accumulation in ER. After dissociation of GRP78, ER stress receptor proteins are activated to trigger UPR generation, reduce the load of ER by limiting the synthesis of unfold proteins, and trigger their respective induced pro-survival response. The PERK-activated-pro-survival pathway inhibits protein translation and synthesis by limiting the entry of abnormally folded proteins into ER and reducing ER's pressure for new protein folding (Borges and Lake, 2014; Hetz et al., 2015; Khanna et al., 2021). PDI (phosphorylation of protein disulfide isomerases), fundamental enzymes involved in ER protein folding, allows these proteins to combine with luminal IRE1α, then moderating excessive IRE1α activity to protect against cell injuries induced by maladaptive UPR (Zhang et al., 2019a). PDI is a kind of oxidoreductase which can catalyze disulfide bonds and it is the correct sequence of cysteine residue pairs with different redox potentials and substrate specificity (Ellgaard and Ruddock, 2005). Cysteine residues within the active site of PDI provide two electrons to assist disulfide bond formation, which results in reduction of the active site of PDI and oxidation of the substrate (Fu et al., 2020). The formation of disulfide bond in the ER is catalyzed by ERO1 (endoplasmic reticulum oxidoreductin 1) family of sulfhydryl oxidases. ERO1 oxidizes PDI and introduces disulfides into ER client proteins. ERO1 can couple disulfide transfer to PDI with reduction of molecular oxygen, forming hydrogen peroxide. Hence, ERO1 activity is a underlying source of ER-derived oxidative stress (Tavender and Bulleid, 2010). Research has found that ROS inhibitor MnTMPyP can inhibit the increase of ROS in ER stress and delay the activation of UPR, suggesting that ROS is the upstream signal molecule that triggers ERS-mediated apoptosis pathway and initiates ER stress-mediated apoptosis (Xu et al., 2018).

UPR as a protective means at the cellular level reduces the accumulation of unfolded or misfolded proteins on the ER. In the early stage of ER stress, ER mainly restore the normal function of ER for survival through activation of UPR to protect cellular damage caused by ER stress, which is a pro-survival response (Senft and Ronai, 2015; Frakes and Dillin, 2017).

4.2 Reactive Oxygen Species and Endoplasmic Reticulum Ca^{2+}

4.2.1 Reactive Oxygen Species Regulates Endoplasmic Reticulum Ca^{2+} Induced Endoplasmic Reticulum Stress

The endoplasmic reticulum is an important calcium reservoir, which regulates ER function, membrane transport and internal homeostasis through maintaining the balance of Ca^{2+} concentration inside and outside the cell. As a messenger molecule, Ca^{2+} participates in cell proliferation, differentiation, movement, muscle contraction, hormone secretion, glycogen metabolism, neuronal excitability, and other physiological activities, and then regulates gene and protein expression, secretion, metabolism, and apoptosis (Frakes and Dillin, 2017). Current studies have shown that disruption of calcium homeostasis in the ER can initiate early apoptosis signals (Rizzuto et al., 2012; Orrenius et al., 2015; Marchi et al., 2018). A study revealed that sodium nitrite (anti-tumor drug) can induce ER stress-mediated apoptosis in human NB4 cells in acute leukemia, certified selenite-induced production of ROS is the upstream of the JNK/ATF2 axis, application of ROS inhibitors partially inhibited the intracellular Ca^{2+} increase caused by sodium nitrite, suggesting that ROS is involved in the sodium nitrite-induced ERS-mediated apoptosis (An et al., 2013). Aoyama elucidated that rotenone, a mitochondrial complex I inhibitor, can cause ER hyperplasia, ER membrane lipid oxidative damage, increase the permeability of ER, cause the increase of cytosol-free Ca^{2+} and then induce ER stress and apoptosis. After using the ER stress inhibitor SUN N8075, mitochondrial ROS production obviously reduced and Ca^{2+} elevation induced by rotenone was significantly weakened, indicating the increase of intracellular free Ca^{2+} induced by rotenone is stimulated by ROS (Aoyama et al., 2021). Although some specific mechanisms are still being studied, ROS production and the increase of ER Ca^{2+} level are both crucial events in ER stress-mediated apoptosis.

4.2.2 Reactive Oxygen Species Regulates IP3R and RyR Mediated Endoplasmic Reticulum Stress

At resting state, the concentration of Ca^{2+} in the ER is higher than that in the cytoplasm. There are three channels related with Ca^{2+} uptake and release for maintaining Ca^{2+} homeostasis on the ER: 1. Ca^{2+}-release channels: RyRs (ryanodine receptors) and IP3Rs; 2. Ca^{2+} -ATPase or SERCA (sarcoplasmic-endoplasmic-reticulum Ca^{2+}-ATPase) in transporting Ca^{2+} from cytoplasm to ER; 3. Ca^{2+}-binding protein in ER cavity (such as calnexin and calreticulin) (Ong and Ambudkar, 2020). Studies have confirmed that the IP3R and RyR distributed on the sarcoplasmic reticulum can be regulated by the redox response (Ong and Ambudkar, 2020). ER includes the NOX subtypes of NADPH oxidase and co-exists with calnexin and calreticulin. The NOX subtype contains the main catalytic subunit GP91Phox (NOX2), which produces ROS mainly involved in cell signaling transduction. Recent studies suggest that NOX1 and NOX4 (NADPH Oxidase 4) can act on PDI, that is, ROS outside the mitochondria may also regulate ER function. Moreover, research has demonstrated NOX4 can act as a proximal signaling intermediate to transduce ER stress-related conditions to the UPR, and sulfonate and modify it through interaction with IRE1 to cause ER stress even cell injuries (Kim et al., 2016; Ochoa et al., 2018; Lee et al., 2020).

4.2.2.1 Reactive Oxygen Species Regulates IP3-Mediated Ca^{2+} Release on Endoplasmic Reticulum

In the phosphatidylinositol signaling pathway, extracellular signaling molecules bind to the G-protein-coupled receptor on

the cell surface to activate phospholipase C on the plasma membrane and hydrolyze PIP2 (4, 5-diphosphate phosphatidylinositol) into 2 s messengers, IP3 (1, 4, 5-triphosphate inositol) and DG (diacylglycerol). Extracellular signals are converted into intracellular signals, and this signaling system is also known as the double messenger system (Kankanamge et al., 2021). IP3R is a widely expressed channel for Ca^{2+} stores. IP3R can control the release of Ca^{2+} from stores into cytoplasm once being activated by IP3 and Ca^{2+} signaling at a lower concentration, and finally trigger downstream events. The closure of the IP3R channel caused by a rise in intracellular Ca^{2+} signals and the activation of the Ca^{2+} pump corporately restores the calcium store to a normal level (Zhang et al., 2020). Activation of NADPH oxidase in ER can improve the sensitivity of ER to IP3. NADPH oxidase-originated ROS can directly act on IP3R distributed on ER, causing its conformational changes, result in increased cytosolic free Ca^{2+} concentration, initiate intracellular Ca^{2+} signaling system, and regulate biological effects through Ca^{2+} dependent protein kinase II activity (Hu et al., 2000; Sakurada et al., 2019).

4.2.2.2 Reactive Oxygen Species Regulates RyR—Mediated Ca^{2+} Release on Endoplasmic Reticulum

RyR is one of the intracellular Ca^{2+} release channels in the sarcoplasmic reticulum of muscle cells and endoplasmic reticulum of other cells and is the largest membrane protein molecule ever known. RyR in mammals can be divided into three subtypes: RyR1 (skeletal muscle type), RyR2 (myocardial type) and RyR3 (brain type). The expression level of RyR1 was highest in skeletal muscle, and RyR2 was mainly expressed in cardiomyocytes (Petrou et al., 2017) and some brain tissues. In cardiomyocytes, Ca^{2+} release of sarcoplasmic reticulum RyR2 is activated by influx of Ca^{2+} release through L-shaped calcium channels in the cell membrane, known as calcium-induced calcium release. RyR3 is widely distributed and expressed in many tissues. It is also activated by calcium-induced calcium release (Berridge, 2016). The increase of intracellular partial redox potential is the trigger point for important cellular functions. Studies found that RyR in the sarcoplasmic reticulum is sensitive to local redox potential, and mild oxidative stress can slightly increase intracellular redox potential, significantly enhance RyR activity and sensitize Ca^{2+} release mechanism, suggesting that ROS bidirectional regulation of ER Ca^{2+} may be concentration-dependent (Santulli et al., 2017; Kushnir et al., 2018). ROS promotes the synthesis of cADPR (cyclic adenosine diphosphate ribose) at low concentrations and opens RyR together with calmodulin. On the contrary, ROS leads to the oxidation of sulfhydryl groups of RyR and sarcoplasmic reticulum-related proteins into disulfide bonds, damaging Ca^{2+} release mechanisms (Avila et al., 2019; Kobayashi et al., 2021).

4.2.3 Reactive Oxygen Species Regulates Endoplasmic Reticulum Ca^{2+} Uptake

In resting conditions, Ca^{2+} is absorbed by the cytoplasm into the ER cavity through SERCA pump and released into the cytoplasm by RyR and IP3R channels. Most of the Ca^{2+} released into the cytoplasm will be recaptured by the Ca^{2+} pump to maintain the Ca^{2+} concentration in the ER. Therefore, Ca^{2+} accumulation in ER is mainly accomplished through the activity of SERCA pump (Ivanova et al., 2020). Ca^{2+}-ATPase, as a known promoter of ER stress, since oxidative damage suppresses Ca^{2+}-ATPase activity, ROS can affect Ca^{2+} storage within ER by inhibiting Ca^{2+}-ATPase, and hence affecting intracellular Ca^{2+} homeostasis and causing ER stress (Krylatov et al., 2018). Studies have revealed ROS production and ER Ca^{2+} pump were sensitive to oxidative damage in ischemia and hypoxia cell models. ROS can make proteins in ER cavity be oxidized and retained, thus inhibiting protein synthesis, and leading to cell apoptosis. Puteney et al. found that Ca^{2+} releasing from the ER *via* IP3R causes decreased ER calcium reserves, Ca^{2+} can enter the cell from the extracellular, a process known as SOCE (store-operated Ca^{2+} entry) (Putney, 1986) Ivan demonstrated that exposure to environmental or cell-intrinsic ROS can affect Ca^{2+} homeostasis, modify multiple pathways and cause cell injuries (Bogeski et al., 2012). ROS production can induce Ca^{2+} release within the ER to cause ER stress, whereas Ca^{2+} release within the ER further stimulates Ca^{2+} aggregation on the mitochondria, causing mitochondrial damage and subsequently inducing apoptosis. As illustrated above, calreticulin is the main Ca^{2+} binding chaperone in the ER lumen, which binds to Ca^{2+} through the C-domain in a high capacity and increases the Ca^{2+} storage capacity of the ER lumen (Venkatesan et al., 2021). Leta found that calreticulin acts directly with SERCA2b glycosylated C-terminal tails to regulate Ca^{2+} storage in ER. When ER Ca^{2+} is sufficient, the activity of ATP-ase can be inhibited and intracellular Ca^{2+} transport to ER stops (Johnson et al., 2014).

Elevated ROS levels send feedback signals that stimulate ER stress. ER stress promotes the correct folding of the wrong proteins and degrades the proteins that cannot be folded. Transient ER stress helps to restore cell homeostasis, but long-term and high-intensity ERS can lead to multiple pulmonary diseases.

5 ENDOPLASMIC RETICULUM STRESS IN PULMONARY DISEASE

As ER stress aggravates, persistent UPR triggers programmed cell death. The occurrence and development of a variety of lung diseases are closely related to intracellular ROS, ER stress and UPR. (**Figure 2**)

5.1 Pulmonary Fibrosis

Pulmonary fibrosis is a kind of lung diseases characterized by inflammatory damage and tissue structure destruction. Pulmonary fibrosis is usually caused by excessive normal tissue repair resulting in vast proliferation of fibroblasts and abnormal accumulation of extracellular matrix. Cells activate UPR signaling to maintain ER homeostasis. Although the short-time UPR is beneficial to maintaining the cellular protein balance, it can cause lung cell dysfunction or even apoptosis when the UPR is stimulation is overwhelmed (Noble et al., 2012; Hetz et al., 2020).

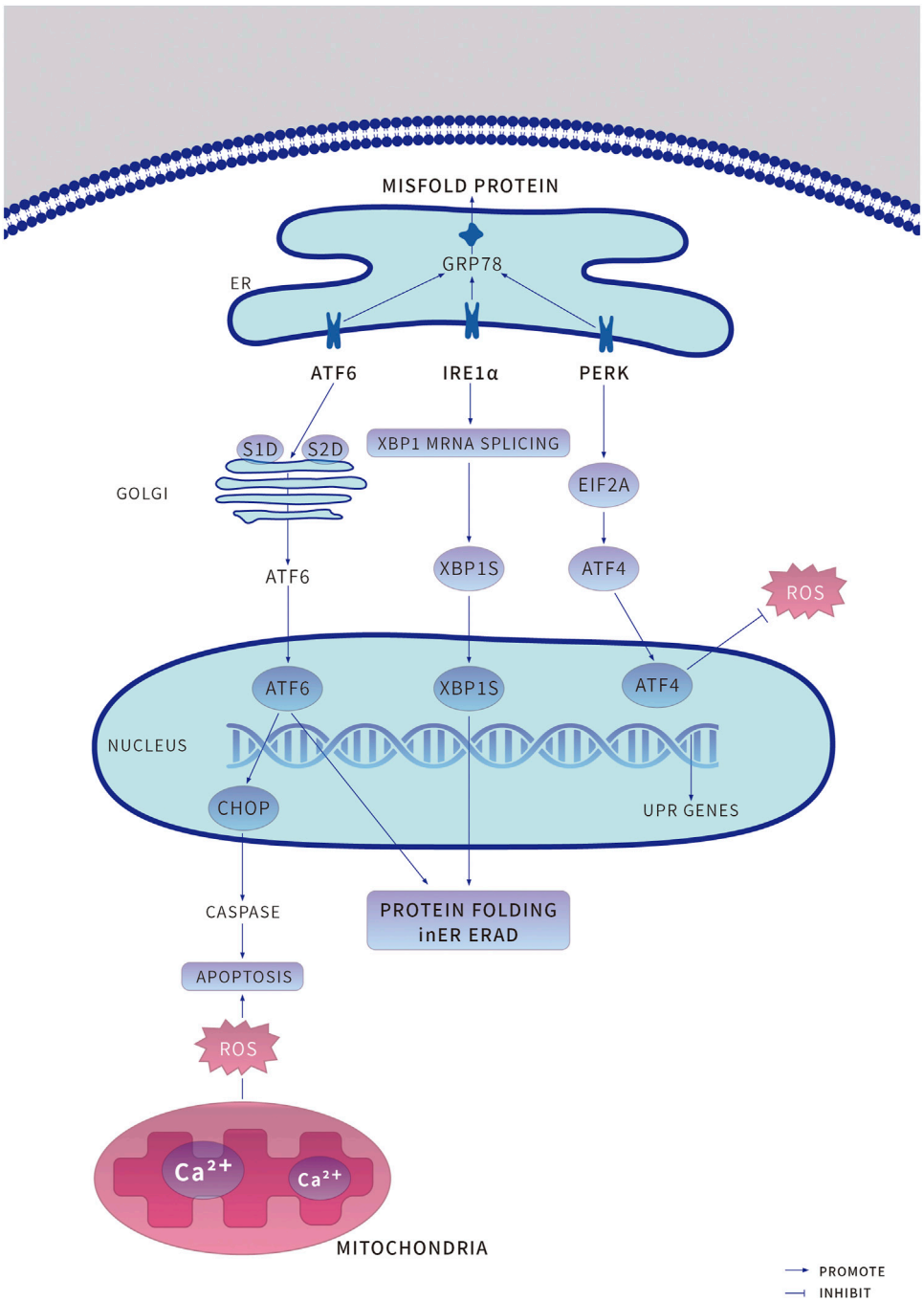

FIGURE 1 | Under endoplasmic reticulum (ER) stress, the adaptive unfolded protein response (UPR) is induced to preserve protein homeostasis and to promote cell survival. An increased accumulation of unfolded or misfolded proteins causes the ER chaperone binding immunoglobulin protein (GRP78) to bind to misfolded proteins accumulated in the ER, resulting in the release of the UPR sensors protein kinase RNA-like ER kinase (PERK), Transcriptional transcription factor 6 (ATF6) and inositol-requiring protein 1α (IRE1α) and initiation of the respective proteins dimerization and phosphorylation of PERK and IRE1α activate their downstream pathways, PERK -- phosphorylated Eukaryotic Initiation factor 2α. Eukaryotic initiation factor 2A (EIF2A) -- ATF4 and IRE1α -- Spliced X-box-binding protein 1 (XBP1s), to promote cell survival. ATF6 is recruited to the Golgi apparatus for processing by the enzymes site-1 proteases (S1P) and site-1 proteases (S2P) to release cleaved ATF6, which enters the nucleus to induce the expression of target genes to promote cell survival. ERAD, ER-associated degradation; ROS, reactive oxygen species.

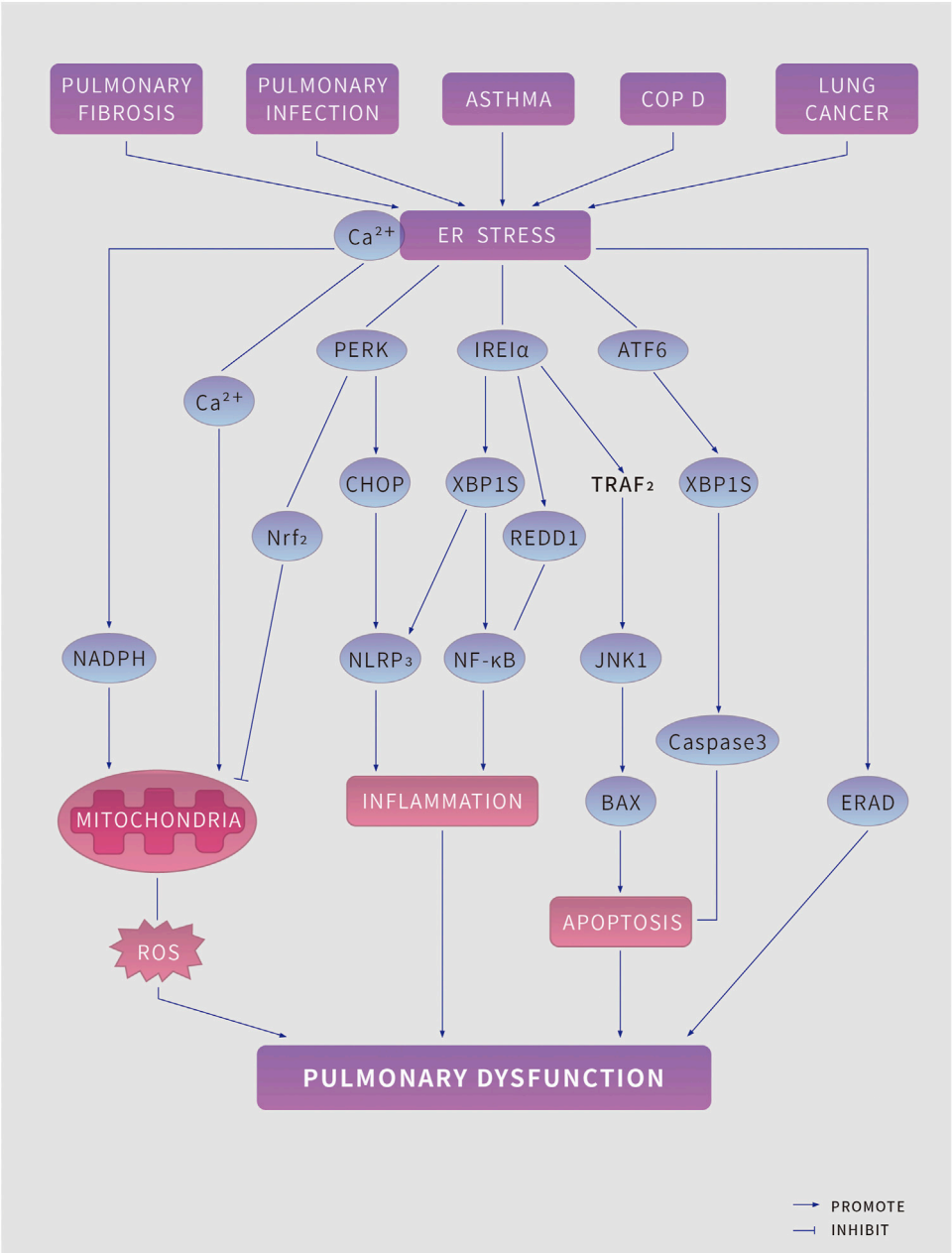

FIGURE 2 | ER stress in pulmonary disease. Pulmonary pathologies, including pulmonary fibrosis, pulmonary infection, asthma, Chronic obstructive pulmonary disease and lung cancer lead to endoplasmic reticulum (ER) stress and induce the unfolded protein response (UPR) (which has three branches, mediated by protein kinase RNA-like ER kinase (PERK), Inositol-requiring protein 1α (IRE1α) and activating factor 6 (ATF6) to tackle ER stress. However, if the UPR fails to restore ER homeostasis, it might induce risk factors for pulmonary disease, including increased reactive oxygen species (ROS) production, inflammation, and apoptosis, which further aggravate pulmonary disease. BAX, BCL-2-associated X protein; CHOP, C/EBP homologous protein; ERAD, ER-associated degradation; JNK1, JUN N-terminal kinase 1; The NK-kappa B, nuclear factor kappa B predominate; NLRP3, NACHT, LRR and PYD domains-containing protein 3; NADPH, nicotinamide adenine dinucleotide phosphate; NRF2, nuclear factor erythroid 2-related factor 2; REDD1, protein regulated in development and DNA damage response 1; TRAF2, TNF receptor associated factor 2; XBP1s, spliced X-box-binding protein 1.

5.1.1 Idiopathic Fibrosis of the Lung

IPF (idiopathic fibrosis of the lung) is a serious interstitial lung disease that can cause progressive loss of lung function, and its pathological mechanism is constantly being updated. Many cells in the lung parenchyma, including alveolar epithelial cells, macrophages, and fibroblasts, are affected by UPR during the pathological process of IPF. CE (Alveolar epithelial cells) are mainly divided into AEC I (alveolar epithelial cells I), and AEC II (alveolar epithelial cells II). AEC II cells are the progenitor cells required to maintain alveolar integrity. Loss of AEC II function

and apoptosis are considered as important processes in the initial stage and development of IPF (Hetz et al., 2020). Researchers took samples of peripheral transplanted lung tissues, analyzed through protein detection, and found that AEC II in IPF can produce much UPR related proteins such as ATF6, ATF4 and CHOP. On the contrary, it does not exist in COPD and normal organ donors, indicating that in IPF patients, UPR activation can lead to the apoptosis of AEC II cells in the inner surface of the fibrotic site and be replaced by fibrous tissue (Korfei et al., 2008; Lawson et al., 2011). Timothy and his colleagues used tunicamycin to induce UPR activation, which enhanced AEC death and pulmonary fibrosis in IPF mice models, demonstrating UPR activation may increase AEC vulnerability, lead to enhanced lung injuries and IPF occurrence. Although UPR cannot directly aggravate the occurrence of IPF, it can improve the incidence probability of IPF in patients (Kropski et al., 2012). In many IPF patients, herpesviruses have been found to be closely associated with the occurrence of IPF. Herpesviruses are frequently found in the IPF lungs and can induce the UPR. Modification and maturation of viral glycosylated envelope proteins during virus replication may induce ER stress, while ER stress play double-acting roles in virus infection. Herpesvirus infection can directly promote UPR activation, causing decreased immune function induced malignant pulmonary fibrosis and IPF (Lee et al., 2009; Tanjore et al., 2012; Liu et al., 2021).

5.1.2 Cystic Fibrosis

Pulmonary cystic fibrosis (CPF or CF) is a congenital disease with familial autosomal recessive inheritance. It is most common among white North Americans and rarely seen in other races. As an exocrine gland lesion, the gastrointestinal tract and respiratory tract are often affected (Elborn, 2016). The airway of patients with CF presents a persistent and intense inflammatory response, and AMs (alveolar macrophage) play key roles in the pathogenesis of CF (Hey et al., 2021). Some AMs can secrete many inflammatory mediators such as TNF-α and IL-6 induction (Lambertsen et al., 2012). XBP1 cut by IRE1 pathway mRNA in UPR affects peripheral macrophages and produces inflammatory effects (Lubamba et al., 2015). It was found that the UPR activated the expression of XBP1 in AMs in CF patients, and lipopolysaccharide was associated with the increased level of transcription factor XBP-1 in the UPR. Knockdown of XBP-1 in cultured dTHP-1 (differentiated human acute monocytic leukemia-1) cells reduced the inflammatory response of CF patients. Inflammatory factors in CF patients can be regulated by the expression of XBP-1 in UPR, and AMs in CF patients can promote the occurrence of airway inflammation in CF patients by upregulating xBP-1-mediated cytokines (Zhu et al., 2012; Lubamba et al., 2015). CFTR (cystic fibrosis transmembrane conductance regulator) is a central regulator of chlorine channel and epithelial function. Loss of CFTR function in airway can lead to mucus thickening, reduced mucosal ciliary clearance, chronic infection, and respiratory failure. UPR can induce the binding of ATF6 to the minimum promoter of CFTR, leading to the inhibition of CFTR transcription and reduce expression of CFTR (Trouvé et al., 2021).

5.2 Pulmonary Infections

Pulmonary infection refers to the infectious disease of pulmonary parenchyma and interstitial tissues, mainly caused by virus, bacteria, or other microbial infection, mainly in the form of pneumonia in clinical. UPR signaling play important roles in the secretion of inflammatory factors. Since inflammatory cells tend to have large secretory requirements and are therefore particularly dependent on a well-developed and abundant ER, the presence of infection-induced stimuli may induce an intracellular UPR response. Inflammatory factors such as TNF- (tumor necrosis factor), IL-1 (interleukin-1), and IL-6 can also cause the activation of three UPR pathways in cells, thus causing the acute phase response of lung inflammation (Grootjans et al., 2016). UPR activation and infection are mutually reinforcing and antagonizing each other (Bettigole and Glimcher, 2015).

5.2.1 Acute Pneumonia

There are many causes of the acute pneumonia response, where acute lung injury is the most important cause. In acute pneumonia caused by acute lung injury, the UPR activation plays an important role in cellular autophagy, as well as in apoptosis (Bettigole and Glimcher, 2015). In lipopolysaccharide-induced acute lung injury mice model and human alveolar epithelial cell model, the UPR inhibitor 4-PBA (4-phenylbutyric acid) blocks the activation of NF-κB pathway and reduces the release of pro-inflammatory mediators including TNF-α, IL-1β and IL-6. 4-PBA reduces the activation of inflammation by inhibiting UPR pathway and the mechanism is likely to be related to PERK-eIF2α-mediated translation reduction promoting NF-κB activation, suggesting that UPR is a crucial promoter of lipopolysaccharide-induced inflammation. 4-PBA leads to decreased autophagy, which plays a protective role in acute pneumonia through the classical AKT/mTOR signaling pathway and exacerbates lipopolysaccharide-induced A549 cytotoxicity through the 3-MA (autophagy inhibitor 3-methyladenine). 4-PBA inhibits UPR activation and has protective effects on autophagy in acute pneumonia models. UPR can stimulate the activation of NF-κB pathway, leading to the translocation of free NF-κB into the nucleus, possibly through conformational changes in cytoplasmic regions induced by IRE1α autophosphorylation. The IREα -TRAF2 complex binds to the adaptor protein TNF-α receptor-associated factor 2 to recruit IκB kinase and phosphorylates IκB, resulting in degradation of IκB and nuclear NF-κB translocation (Urano et al., 2000). Jiang et al. investigated whether ER stress during simulated microgravity induced endothelial inflammation and apoptosis in HUVECs (human umbilical vein endothelial cells), and they found that the increase of apoptosis in HUVECs during clinorotation was significantly suppressed by inhibiting ER stress, iNOS activity, NF-κB/IκB, and the NLRP3 inflammasome signaling pathway, indicating ER stress-dependent activation of iNOS/NO-NF-κB signaling and NLRP3 inflammasome contributes to chronic injury endothelial inflammation and apoptosis associated with microgravity (Jiang et al., 2020).

5.2.2 Allergic Bronchopulmonary Aspergillosis

Aspergillus fumigatus is an opportunistic pathogen that is responsible for a life-threatening fungal infection called as invasive aspergillosis. The sensitization of AF (aspergillus fumigatus) was associated with severe allergic pulmonary inflammation, and allergic bronchopulmonary aspergillosis (ABPA) was the most common disease in allergic mycosis (Krishnan and Askew, 2014). Studies found that in clinical studies, glucoregulatory protein GRP78 was increased in lung tissues of patients with allergic bronchopulmonary aspergillus. Lee found that utilizing of the ER stress inhibitor or a ROS scavenger improved AF-induced allergic inflammation. The PI3K-δ inhibitor reduced AF-induced mitochondrial ROS generation and ER stress accordingly ameliorated. They revealed that PI3K-δ regulates AF-induced steroid-resistant eosinophilic allergic lung inflammation through ER stress (Lee et al., 2016). Wang revealed the effects and mechanisms of resveratrol on fungus-induced allergic airway inflammation, and they demonstrated resveratrol alleviated the AF-exposed allergic inflammation and apoptosis through inhibiting ER stress *via* Akt/mTOR pathway, exerting therapeutic effects on the fungus-induced allergic lung disorder (Wang et al., 2022). These studies revealed the UPR is a critical step in ABPA production.

5.3 Asthma

The bronchial epithelium contains a variety of cell types with high protein synthesis and secretion, which are prone to ER stress (Schögler et al., 2019). In bronchial asthma, the existence of airway inflammation state and other factors are considered to induce UPR, and they are mutually causal and interactive with airway inflammation. Current studies suggest that ER stress is closely related with the dysregulation of Ca^{2+} homeostasis in airway epithelial cells, abnormal secretion of hyaluronic acid and mucin, recruitment of inflammatory cells by cytokines, and abnormal immunomodulatory state in the pathogenesis of bronchial asthma (Russell and Brightling, 2017). The expression of UPR marker protein GRP78 was significantly increased in peripheral blood monocytes and bronchoalveolar lavage fluid of asthmatic mice models, suggesting that the UPR pathway may cause the development of asthma by activating NF-κB, indicating UPR can also stimulate the activity of immune, and get involved in immune response (Kim et al., 2013b; Kim and Lee, 2015). The CHOP protein (also known as GADD153 or DDIT-3) is an important signal molecule in ER stress, and its specific mechanism in asthma has been gradually studied. It has been found that T cells treated with curcumin can induce activation of the PERK and IRE1 pathways in UPR and induce upregulation of stimulating transcription factors XBP-1 and CHOP in $CD4^+$ lymphocytes and T lymphocytes, ultimately leading to apoptosis of T cells (Zhang et al., 2012; Lin et al., 2019). ORMDL3 (Orosomucoid like 3) has been considered as significant regulator of asthma in genetic association studies, David and his colleagues found transfection of ORMDL3s in human bronchial epithelial cells *in vitro* induced expression of metalloproteases (MMP-9), CC chemokines (CCL-20), CXC chemokines (IL-8, CXC-10, CXCL-11) and selectively activated ATF6 and SERCA2B. They furtherly revealed ORMDL3 may be associated with ER-UPR pathway in asthma. It was reported that the expression of ORMDL3 increased UPR response, and related genes signaling pathways of UPR were significantly upregulated. Ca^{2+} released by ER calcium influx decreased in ORMDL3 knockout models, and UPR was correspondingly weakened. The increased expression of ORMDL3 gene in asthmatic patients is probably caused by regulating UPR pathway affecting Ca^{2+} concentration (Cantero-Recasens et al., 2010).

5.4 Chronic Obstructive Pulmonary Disease

COPD (chronic obstructive pulmonary disease) is a kind of pulmonary disease characterized by persistent respiratory symptoms and airflow restriction, which is not completely reversible and develops progressively, mainly affecting the lungs (Labaki and Rosenberg, 2020). COPD is often associated with smoking, and smoking exposure damages the proteasome itself, resulting in massive accumulation of insoluble proteins in airway epithelial cells, alveolar epithelial cells, and macrophages, ultimately causing UPR. COPD patients have more mucus cells in their respiratory tract, often secreting a lot of mucus. IRE1β (inositol-requiring enzyme 1beta) of airway goblet cells plays an important role in mucin cell phenotype and secretion of mucin5AC and mucin5B (Cloots et al., 2021). Michael found that in HEK293 cells models with purified protein, IRE1α is closely related with IRE1β diminishing expression and inhibiting signaling. IRE1β can assemble with and inhibit IRE1α to suppress stress induced XBP1 splicing to affect the UPR (Grey et al., 2020). Research have shown that hypoxic stimulation can activate the dissociation of molecular chaperone GRP78 and activate UPR to repair protease and autophagy functions of cells. Studies also found that the expression of UPR signaling molecules including GRP78, XBP1, CHOP and other proteins were not found in every COPD patient, suggesting that the UPR pathway was activated only in a part of COPD population (Min et al., 2011; van 't Wout et al., 2015). Mitochondrial oxidative stress is specifically significant in COPD, and Nrf2 (nuclear factor-E2-related factor 2) is a major regulator of antioxidant response element-driven cytoprotective protein expression. ER stress-mediated UPR and insufficiency of antioxidant Nrf2 has been implicated in cigarette smoking-induced COPD, suggesting the potential of Nrf2 in the treatment of COPD (Fratta Pasini et al., 2016; Liu et al., 2019).

5.5 Lung Cancer

Lung cancer is the largest tumor threatening human beings (Nasim et al., 2019). Lung cancer cells often tackle ischemia, hypoxia, metabolism, and other changes. To cope with these extreme factors, the cells themselves also produce corresponding changes, resulting in the activation of UPR pathway. The role of ER stress and the UPR is well demonstrated in a lung cancer (Dastghaib et al., 2021).

5.5.1 Lung Adenocarcinoma

The most common type of lung cancer is adenocarcinoma, comprising around 40% of all lung cancer cases, and lung adenocarcinoma is still one of the most aggressive and rapidly

fatal tumor types with overall survival less than 5 years (Denisenko et al., 2018). Many studies have shown that adenocarcinoma is often accompanied by activation of the UPR pathway. Lu found that ER stress can induce the high expression of the transcription factor XBP1 in 2D and 3D culture lung adenocarcinoma cells and promote the proliferation of lung adenocarcinoma in 3D culture *in vitro*. Knockdown the expression of XBP1 can block cell growth induced by Tm/Tg treatment. Meanwhile, LOX gene, as a key downstream sensor of XBP1, can block XBP1-induced cell proliferation by knocking down the expression of LOX, suggesting that XBP1 can regulate the proliferation of lung adenocarcinoma cells through LOX (Yang et al., 2017). It was found that asterosaponin 1 increased ER dilation and cytosolic Ca^{2+} concentration, enhanced the expression of GRP78 and GRP94 in a dose-and-time-dependent manner and increased the expression of CHOP, Caspase-4 and JNK, the three UPR related apoptotic molecules. Finally, the proliferation of A549 cells was inhibited and apoptosis was promoted (Zhao et al., 2011).

5.5.2 Large Cell Carcinoma

Large cell carcinoma is a barely descriptive term indicating a subtype of lung cancer with no specific features of small-cell lung cancer, adenocarcinoma or squamous cell carcinoma (Weissferdt, 2014). Azam et al. have found that GRP78 is closely related to the regulation of large cell carcinoma. The expression of GRP78 in tumor of patients with large cell carcinoma is more than three times that of the negative control. Both miR-495 and miR-199a-5p can promote the malignant transformation of tumor cells. Increased GRP78 in cells can downregulate Mir-495 and Mir-199a-5p in NSCLC, and overexpression or inhibition of miR-495 and miR-199a-5p can also significantly change the expression of GRP78 and XBP1 level. UPR and microRNA interact to promote the occurrence of cancer (Ahmadi et al., 2017). Pau and his colleagues found that the anti-cancer molecule ABTL0812 increases cellular long-chain dihydroceramides by impairing DEGS1 (delta 4-desaturase, sphingolipid 1) activity, which resulted in persistent ER stress and activated UPR *via* ATF4-DDIT3-TRIB3 that ultimately promotes cytotoxic autophagy in cancer cells (Muñoz-Guardiola et al., 2021). Studies have proved that in large-cell lung carcinoma H460 treated with cisplatin, the cell viability is distinctly reduced after adding ERS inhibitor 4-PBA (4-phenylbutyric acid). Intracellular caspase-3 gene and cytochrome C were significantly upregulated and promoted cell apoptosis, confirming that chemotherapy drugs can activate UPR and enhance drug resistance of tumor cells (Shi et al., 2016). Blocking the adaptive pathway of ER stress or promoting the apoptotic pathway could be a promising anti-cancer strategy.

6 POTENTIAL THERAPEUTIC INTERVENTIONS IN PULMONARY DISEASE

Given the significant characteristic in the pathogenesis of pulmonary disease, strategies to target ER proteostasis, UPR signaling, and ROS are crucial for disease intervention. We discuss strategies as following.

6.1 Pharmacotherapy

6.1.1 Chemical Chaperones

4-PBA. 4-phenyl butyric acid, a low-molecular-weight aromatic fatty acid, affect the activation of LPS-induced inflammation human alveolar epithelial cell in acute lung injury models. It further prevents the activation of the NF-κB pathway, decreases the release of the inflammatory mediators through regulating ER stress (Zeng et al., 2017).

TUDCA. TUDCA (Tauroursodeoxycholic) is a hydrophilic bile acid with chaperone properties that is produced endogenously in humans at very low levels. Tong found that the TUDCA can moderate pulmonary ER stress and epithelial-mesenchymal transition in bleomycin-induced lung fibrosis (Tong et al., 2021). TUDCA can inhibit CHOP expression and the bleomycin -induced pulmonary fibrosis and inflammation, suggesting TUDCA may be a promising strategy for preventing pulmonary fibrosis (Tanaka et al., 2015).

6.1.2 Salubrinal

EIF2A phosphorylation levels are controlled by two phosphatase complexes, hydrophobic the protein Phosphatase 1 (PP1) catalytic subunit complexed with either constitutively expressed PPP1R15B (PP1 regulatory subunit 15B) or the ER Stress-inducible isoform PPP1R15A, which is an ATF4 -- CHOP Target (PP1). Salubrinal is a cell-permeable, small-molecule inhibitor of the PP1 complex (Liu et al., 2014). Wang found that Salubrinal attenuated A549 cells from Paraquat-induced damages through upregulating the PERK-eIF2α signaling (Wang et al., 2018b). Salubrinal may be a promising therapeutic strategy to suppress ER stress in pulmonary dysfunctions.

6.1.3 Metformin

Metformin is an antidiabetic drug that has been proved to be beneficial to other diseases independent of its glycaemia effects. Francesca found that metformin may ameliorate cigarette smoke-induced pathologies of emphysematous COPD through the AMPK (AMP-activated protein kinase) pathway (Polverino et al., 2021).

6.1.4 m-TOR Inhibitor

Qin demonstrated ER stress-induced cell death was mediated by autophagy which was partly attributed to the inactivation of the mTOR (mammalian target of rapamycin) (Qin et al., 2010). Tian found that ginkgo biloba leaf extract attenuates atherosclerosis in streptozotocin-induced diabetic $ApoE^{-/-}$ mice by Inhibiting ER stress *via* restoration of autophagy through the mTOR Signaling Pathway (Tian et al., 2019), which inspired us that the mTOR pathway is expected to become a promising target of ER stress-induced lung diseases.

6.1.5 Alanyl Beta Muricholic Acid

AβM acid can resolve the inflammatory and UPR in inflammatory diseases (Vander Zanden et al., 2019). Emily proved that AβM acid-based therapy can inhibit the allergen-

induced UPR and allergic airway disease in mice *via* preferential binding of ATF6α, suggesting a novel avenue to treat allergic asthma using AβM (Nakada et al., 2019).

5.1.6 N-(2-Hydroxy-5-Methylphenyl)-3-Phenylpropanamide (147)

Pharmacologic arm selective UPR signaling pathway activation is emerging as a promising strategy to improve imbalances in ER proteostasis implicated in diverse diseases. The compound 147 was considered to activate ATF6-regulated signaling associated with localized metabolic activation and selective covalent modification of ER stress (Paxman et al., 2018). Therefore, the compound 147 is a promising strategy in preventing ER stress-induced pulmonary disease.

6.1.7 Melatonin

Melatonin is an anti-inflammatory molecule, which has been effective in acute lung injury induced by many conditions (Tordjman et al., 2017). Zhao revealed that melatonin obviously inhibited the activation of NLRP3 inflammation, ER stress and epithelial-mesenchymal transition during bleomycin-mediated pulmonary fibrosis in mice models (Paxman et al., 2018).

6.1.8 Ursolic Acid

Li found that ursolic acid derivative has preventive effects on particulate matter 2.5-induced COPD, causes obvious suppression in PM2.5-induced increase in oxidative stress markers and inflammatory cytokines, suggesting ursolic acid derivative can be a promising therapeutic treatment for PM2.5-induced COPD (Li et al., 2020).

6.1.9 Resveratrol

Resveratrol, a natural polyphenol, is beneficial in supporting its numerous biological properties including antioxidant, anti-inflammatory, ant obesity, antidiabetic, and ant-ischemic activities. The compound also has beneficial effects on cognitive function and lung health (Ahmadi et al., 2021). Wang demonstrated that resveratrol attenuates inflammation and apoptosis through alleviating ER stress *via* Akt/mTOR pathway in fungus-induced allergic airways inflammation, providing therapeutic strategies for fungus-induced allergic lung disease (Wang et al., 2022).

6.2 Strategies Target Reactive Oxygen Species

Diets poor in antioxidants are related with lung dysfunction and a risk factor for the development of COPD. Dietaries include Vitamin C (ascorbic acid), Vitamin E (α-tocopherol), resveratrol, and flavonoids has always been studied in improve lung function or clinical features of COPD (Rana, 2020). Andras implied ascorbate may be involved in oxidative protein folding and creates a link between the disulfide bond formation (oxidative protein folding) and hydroxylation, providing promising strategies in preventing and treating pulmonary disease (Szarka and Lőrincz, 2014).

NRF2-mediated heme oxygenase was upregulated by UPR activation in PC12 cells. and GCLC (glutamate cysteine ligase catalytic) subunit expression increases. Heme oxygenase and GCLC can lead to COPD disease aggravation, indicating increasing Nrf2 activity as a treatment strategy in COPD (Digaleh et al., 2013; Niforou et al., 2014; Wu et al., 2015).

6.3 Lifestyle Adjustments

Lifestyle adjustments including physical exercise, smoking cessation and diet are a novel approach to modulate ER stress to protect against pulmonary disease (Itoh et al., 2013; Pedersen and Saltin, 2015; Schuller, 2019).

ROS-ER stress-associated therapy is becoming recognized as a crucial treatment strategy for pulmonary disease. Efficiently targeting ER stress in an organelle-specific or organ-specific manner holds promise for preventing and treating pulmonary disease.

6 CONCLUSION

Massive attention has been paid to the role of ROS and ER stress in the pathogenesis of pulmonary disease over the past years. The ER coordinates secretory and transmembrane proteins folding and translocation, controls cellular calcium uptake, storage and signaling.

The ER stress promotes the correct folding of faulty proteins and the degradation of misfolding proteins. Transient ER stress contributes to the homeostasis of cells, while sustained and overwhelmed ER stress can lead to several lung diseases. Unfold protein response is the most important reaction in ER stress. UPR and calcium initial signaling are key mechanisms of ER stress-mediated apoptosis. We summarized the mechanisms of ER stress, key regulators, related pathways, and associated lung diseases, including pulmonary fibrosis, pulmonary infections, asthma, COPD, and lung cancers. We also provided latest interventions target ER stress and ROS in pulmonary disease.

ER homeostasis and ER stress, especially the biological entities of ER stress, have been extensively described in many reports. However, there are still many unanswered questions. Although some protein-regulatory promoter compounds targeting ER stress or UPR components have shown potential in preventing and treating lung disease, clinical trials evaluating these agents targeting ER stress or UPR are still lacking. ROS serves as an upstream signal of ER stress, and the study of their internal relationship and mechanism of action need us further understand and provide new ideas for the development of drugs for pulmonary diseases, and further research is needed to provide a new approach for tumor treatment.

AUTHOR CONTRIBUTIONS

YZ researched data for the paper, contributed to discussion of the content, wrote the article, and reviewed the article before the submission. XC had great contribution in subject planning and modified the manuscript. MX and YL retrieved and organized documents.

FUNDING

This work was funded by grants from the National Natural Science Foundation of China (No. 81973842).

REFERENCES

Ahmadi, A., Hayes, A. W., and Karimi, G. (2021). Resveratrol and Endoplasmic Reticulum Stress: A Review of the Potential Protective Mechanisms of the Polyphenol. *Phytother Res.* 35 (10), 5564–5583. doi:10.1002/ptr.7192

Ahmadi, A., Khansarinejad, B., Hosseinkhani, S., Ghanei, M., and Mowla, S. J. (2017). miR-199a-5p and miR-495 Target GRP78 within UPR Pathway of Lung Cancer. *Gene* 620, 15–22. doi:10.1016/j.gene.2017.03.032

An, J. J., Shi, K. J., Wei, W., Hua, F. Y., Ci, Y. L., Jiang, Q., et al. (2013). The ROS/JNK/ATF2 Pathway Mediates Selenite-Induced Leukemia NB4 Cell Cycle Arrest and Apoptosis *In Vitro* and *In Vivo*. *Cell Death Dis* 4, e973. doi:10.1038/cddis.2013.475

Aoyama, Y., Inagaki, S., Aoshima, K., Iwata, Y., Nakamura, S., Hara, H., et al. (2021). Involvement of Endoplasmic Reticulum Stress in Rotenone-Induced Leber Hereditary Optic Neuropathy Model and the Discovery of New Therapeutic Agents. *J. Pharmacol. Sci.* 147 (2), 200–207. doi:10.1016/j.jphs.2021.07.003

Avila, G., de la Rosa, J. A., Monsalvo-Villegas, A., and Montiel-Jaen, M. G. (2019). Ca2+ Channels Mediate Bidirectional Signaling between Sarcolemma and Sarcoplasmic Reticulum in Muscle Cells. *Cells* 9 (1). doi:10.3390/cells9010055

Berridge, M. J. (2016). The Inositol Trisphosphate/Calcium Signaling Pathway in Health and Disease. *Physiol. Rev.* 96 (4), 1261–1296. doi:10.1152/physrev.00006.2016

Bettigole, S. E., and Glimcher, L. H. (2015). Endoplasmic Reticulum Stress in Immunity. *Annu. Rev. Immunol.* 33, 107–138. doi:10.1146/annurev-immunol-032414-112116

Boengler, K., Kosiol, M., Mayr, M., Schulz, R., and Rohrbach, S. (2017). Mitochondria and Ageing: Role in Heart, Skeletal Muscle and Adipose Tissue. *J. Cachexia Sarcopenia Muscle* 8 (3), 349–369. doi:10.1002/jcsm.12178

Bogeski, I., Kilch, T., and Niemeyer, B. A. (2012). ROS and SOCE: Recent Advances and Controversies in the Regulation of STIM and Orai. *J. Physiol.* 590 (17), 4193–4200. doi:10.1113/jphysiol.2012.230565

Borges, C. R., and Lake, D. F. (2014). Oxidative Protein Folding: Nature's Knotty challenge. *Antioxid. Redox Signal.* 21 (3), 392–395. doi:10.1089/ars.2014.5946

Brown, M. S., Radhakrishnan, A., and Goldstein, J. L. (2018). Retrospective on Cholesterol Homeostasis: The Central Role of Scap. *Annu. Rev. Biochem.* 87, 783–807. doi:10.1146/annurev-biochem-062917-011852

Cantero-Recasens, G., Fandos, C., Rubio-Moscardo, F., Valverde, M. A., and Vicente, R. (2010). The Asthma-Associated ORMDL3 Gene Product Regulates Endoplasmic Reticulum-Mediated Calcium Signaling and Cellular Stress. *Hum. Mol. Genet.* 19 (1), 111–121. doi:10.1093/hmg/ddp471

Carpio, M. A., Michaud, M., Zhou, W., Fisher, J. K., Walensky, L. D., and Katz, S. G. (2015). BCL-2 Family Member BOK Promotes Apoptosis in Response to Endoplasmic Reticulum Stress. *Proc. Natl. Acad. Sci. U S A.* 112 (23), 7201–7206. doi:10.1073/pnas.1421063112

Chen, X., and Cubillos-Ruiz, J. R. (2021). Endoplasmic Reticulum Stress Signals in the Tumour and its Microenvironment. *Nat. Rev. Cancer* 21 (2), 71–88. doi:10.1038/s41568-020-00312-2

Cloots, E., Simpson, M. S., De Nolf, C., Lencer, W. I., Janssens, S., and Grey, M. J. (2021). Evolution and Function of the Epithelial Cell-specific ER Stress Sensor IRE1β. *Mucosal Immunol.* 14 (6), 1235–1246. doi:10.1038/s41385-021-00412-8

Dastghaib, S., Kumar, P. S., Aftabi, S., Damera, G., Dalvand, A., Sepanjnia, A., et al. (2021). Mechanisms Targeting the Unfolded Protein Response in Asthma. *Am. J. Respir. Cel Mol Biol* 64 (1), 29–38. doi:10.1165/rcmb.2019-0235TR

Delaunay-Moisan, A., and Appenzeller-Herzog, C. (2015). The Antioxidant Machinery of the Endoplasmic Reticulum: Protection and Signaling. *Free Radic. Biol. Med.* 83, 341–351. doi:10.1016/j.freeradbiomed.2015.02.019

Denisenko, T. V., Budkevich, I. N., and Zhivotovsky, B. (2018). Cell Death-Based Treatment of Lung Adenocarcinoma. *Cel Death Dis* 9 (2), 117. doi:10.1038/s41419-017-0063-y

Di Conza, G., and Ho, P. C. (2020). ER Stress Responses: An Emerging Modulator for Innate Immunity. *Cells* 9 (3). doi:10.3390/cells9030695

Digaleh, H., Kiaei, M., and Khodagholi, F. (2013). Nrf2 and Nrf1 Signaling and ER Stress Crosstalk: Implication for Proteasomal Degradation and Autophagy. *Cell Mol Life Sci* 70 (24), 4681–4694. doi:10.1007/s00018-013-1409-y

Elborn, J. S. (2016). Cystic Fibrosis. *Lancet* 388 (10059), 2519–2531. doi:10.1016/S0140-6736(16)00576-6

Ellgaard, L., and Ruddock, L. W. (2005). The Human Protein Disulphide Isomerase Family: Substrate Interactions and Functional Properties. *EMBO Rep.* 6 (1), 28–32. doi:10.1038/sj.embor.7400311

Feng, K., Ge, Y., Chen, Z., Li, X., Liu, Z., Li, X., et al. (2019). Curcumin Inhibits the PERK-eIF2α-CHOP Pathway through Promoting SIRT1 Expression in Oxidative Stress-Induced Rat Chondrocytes and Ameliorates Osteoarthritis Progression in a Rat Model. *Oxid Med. Cel Longev* 2019, 8574386. doi:10.1155/2019/8574386

Frakes, A. E., and Dillin, A. (2017). The UPRER: Sensor and Coordinator of Organismal Homeostasis. *Mol. Cel* 66 (6), 761–771. doi:10.1016/j.molcel.2017.05.031

Fratta Pasini, A. M., Ferrari, M., Stranieri, C., Vallerio, P., Mozzini, C., Garbin, U., et al. (2016). Nrf2 Expression Is Increased in Peripheral Blood Mononuclear Cells Derived from Mild-Moderate Ex-Smoker COPD Patients with Persistent Oxidative Stress. *Int. J. Chron. Obstruct Pulmon Dis.* 11, 1733–1743. doi:10.2147/COPD.S102218

Fu, J., Gao, J., Liang, Z., and Yang, D. (2020). PDI-regulated Disulfide Bond Formation in Protein Folding and Biomolecular Assembly. *Molecules* 26 (1). doi:10.3390/molecules26010171

Grey, M. J., Cloots, E., Simpson, M. S., LeDuc, N., Serebrenik, Y. V., De Luca, H., et al. (2020). IRE1β Negatively Regulates IRE1α Signaling in Response to Endoplasmic Reticulum Stress. *J. Cel Biol* 219 (2). doi:10.1083/jcb.201904048

Grootjans, J., Kaser, A., Kaufman, R. J., and Blumberg, R. S. (2016). The Unfolded Protein Response in Immunity and Inflammation. *Nat. Rev. Immunol.* 16 (8), 469–484. doi:10.1038/nri.2016.62

Han, J., Back, S. H., Hur, J., Lin, Y. H., Gildersleeve, R., Shan, J., et al. (2013). ER-stress-induced Transcriptional Regulation Increases Protein Synthesis Leading to Cell Death. *Nat. Cel Biol* 15 (5), 481–490. doi:10.1038/ncb2738

Hetz, C., Chevet, E., and Oakes, S. A. (2015). Erratum: Proteostasis Control by the Unfolded Protein Response. *Nat. Cel Biol* 17 (7), 1088–1138. doi:10.1038/ncb3221

Hetz, C., and Papa, F. R. (2018). The Unfolded Protein Response and Cell Fate Control. *Mol. Cel* 69 (2), 169–181. doi:10.1016/j.molcel.2017.06.017

Hetz, C., Zhang, K., and Kaufman, R. J. (2020). Mechanisms, Regulation and Functions of the Unfolded Protein Response. *Nat. Rev. Mol. Cel Biol* 21 (8), 421–438. doi:10.1038/s41580-020-0250-z

Hey, J., Paulsen, M., Toth, R., Weichenhan, D., Butz, S., Schatterny, J., et al. (2021). Epigenetic Reprogramming of Airway Macrophages Promotes Polarization and Inflammation in Muco-Obstructive Lung Disease. *Nat. Commun.* 12 (1), 6520. doi:10.1038/s41467-021-26777-9

Hotamisligil, G. S., and Davis, R. J. (2016). Cell Signaling and Stress Responses. *Cold Spring Harb Perspect. Biol.* 8 (10). doi:10.1101/cshperspect.a006072

Hu, Q., Zheng, G., Zweier, J. L., Deshpande, S., Irani, K., and Ziegelstein, R. C. (2000). NADPH Oxidase Activation Increases the Sensitivity of Intracellular Ca2+ Stores to Inositol 1,4,5-trisphosphate in Human Endothelial Cells. *J. Biol. Chem.* 275 (21), 15749–15757. doi:10.1074/jbc.M000381200

Huang, S., Xing, Y., and Liu, Y. (2019). Emerging Roles for the ER Stress Sensor IRE1α in Metabolic Regulation and Disease. *J. Biol. Chem.* 294 (49), 18726–18741. doi:10.1074/jbc.REV119.007036

Hwang, J., and Qi, L. (2018). Quality Control in the Endoplasmic Reticulum: Crosstalk between ERAD and UPR Pathways. *Trends Biochem. Sci.* 43 (8), 593–605. doi:10.1016/j.tibs.2018.06.005

Incalza, M. A., D'Oria, R., Natalicchio, A., Perrini, S., Laviola, L., and Giorgino, F. (2018). Oxidative Stress and Reactive Oxygen Species in Endothelial Dysfunction Associated with Cardiovascular and Metabolic Diseases. *Vascul Pharmacol.* 100, 1–19. doi:10.1016/j.vph.2017.05.005

Itoh, M., Tsuji, T., Nemoto, K., Nakamura, H., and Aoshiba, K. (2013). Undernutrition in Patients with COPD and its Treatment. *Nutrients* 5 (4), 1316–1335. doi:10.3390/nu5041316

Ivanova, H., Vervliet, T., Monaco, G., Terry, L. E., Rosa, N., Baker, M. R., et al. (2020). Bcl-2-Protein Family as Modulators of IP3 Receptors and Other Organellar Ca2+ Channels. *Cold Spring Harb Perspect. Biol.* 12 (4). doi:10.1101/cshperspect.a035089

Jiang, M., Wang, H., Liu, Z., Lin, L., Wang, L., Xie, M., et al. (2020). Endoplasmic Reticulum Stress-dependent Activation of iNOS/NO-NF-Kb Signaling and NLRP3 Inflammasome Contributes to Endothelial Inflammation and Apoptosis Associated with Microgravity. *FASEB J.* 34 (8), 10835–10849. doi:10.1096/fj.202000734R

Jin, J. K., Blackwood, E. A., Azizi, K., Thuerauf, D. J., Fahem, A. G., Hofmann, C., et al. (2017). ATF6 Decreases Myocardial Ischemia/Reperfusion Damage and Links ER Stress and Oxidative Stress Signaling Pathways in the Heart. *Circ. Res.* 120 (5), 862–875. doi:10.1161/CIRCRESAHA.116.310266

Johnson, J. S., Kono, T., Tong, X., Yamamoto, W. R., Zarain-Herzberg, A., Merrins, M. J., et al. (2014). Pancreatic and Duodenal Homeobox Protein 1 (Pdx-1) Maintains Endoplasmic Reticulum Calcium Levels through Transcriptional Regulation of Sarco-Endoplasmic Reticulum Calcium ATPase 2b (SERCA2b) in the Islet β Cell. *J. Biol. Chem.* 289 (47), 32798–32810. doi:10.1074/jbc.M114.575191

Kaminskyy, V. O., and Zhivotovsky, B. (2014). Free Radicals in Cross Talk between Autophagy and Apoptosis. *Antioxid. Redox Signal.* 21 (1), 86–102. doi:10.1089/ars.2013.5746

Kankanamge, D., Ubeysinghe, S., Tennakoon, M., Pantula, P. D., Mitra, K., Giri, L., et al. (2021). Dissociation of the G Protein $\beta\gamma$ from the Gq-Plcβ Complex Partially Attenuates PIP2 Hydrolysis. *J. Biol. Chem.* 296, 100702. Jan-Jun. doi:10.1016/j.jbc.2021.100702

Katzen, J., and Beers, M. F. (2020). Contributions of Alveolar Epithelial Cell Quality Control to Pulmonary Fibrosis. *J. Clin. Invest.* 130 (10), 5088–5099. doi:10.1172/JCI139519

Khanna, M., Agrawal, N., Chandra, R., and Dhawan, G. (2021). Targeting Unfolded Protein Response: a New Horizon for Disease Control. *Expert Rev. Mol. Med.* 23, e1. doi:10.1017/erm.2021.2

Kim, S. H., Kim, K. Y., Yu, S. N., Seo, Y. K., Chun, S. S., Yu, H. S., et al. (2016). Silibinin Induces Mitochondrial NOX4-Mediated Endoplasmic Reticulum Stress Response and its Subsequent Apoptosis. *BMC Cancer* 16, 452. doi:10.1186/s12885-016-2516-6

Kim, S. R., Kim, D. I., Kang, M. R., Lee, K. S., Park, S. Y., Jeong, J. S., et al. (2013). Endoplasmic Reticulum Stress Influences Bronchial Asthma Pathogenesis by Modulating Nuclear Factor κB Activation. *J. Allergy Clin. Immunol.* 132 (6), 1397–1408. doi:10.1016/j.jaci.2013.08.041

Kim, S. R., and Lee, Y. C. (2015). Endoplasmic Reticulum Stress and the Related Signaling Networks in Severe Asthma. *Allergy Asthma Immunol. Res.* 7 (2), 106–117. doi:10.4168/aair.2015.7.2.106

Kim, Y. E., Hipp, M. S., Bracher, A., Hayer-Hartl, M., and Hartl, F. U. (2013). Molecular Chaperone Functions in Protein Folding and Proteostasis. *Annu. Rev. Biochem.* 82, 323–355. doi:10.1146/annurev-biochem-060208-092442

Kobayashi, T., Kurebayashi, N., and Murayama, T. (2021). The Ryanodine Receptor as a Sensor for Intracellular Environments in Muscles. *Int. J. Mol. Sci.* 22 (19). doi:10.3390/ijms221910795

Kopp, M. C., Larburu, N., Durairaj, V., Adams, C. J., and Ali, M. M. U. (2019). UPR Proteins IRE1 and PERK Switch BiP from Chaperone to ER Stress Sensor. *Nat. Struct. Mol. Biol.* 26 (11), 1053–1062. doi:10.1038/s41594-019-0324-9

Korfei, M., Ruppert, C., Mahavadi, P., Henneke, I., Markart, P., Koch, M., et al. (2008). Epithelial Endoplasmic Reticulum Stress and Apoptosis in Sporadic Idiopathic Pulmonary Fibrosis. *Am. J. Respir. Crit. Care Med.* 178 (8), 838–846. doi:10.1164/rccm.200802-313OC

Krishnan, K., and Askew, D. S. (2014). The Fungal UPR: a Regulatory Hub for Virulence Traits in the Mold Pathogen Aspergillus fumigatus. *Virulence* 5 (2), 334–340. doi:10.4161/viru.26571

Kropski, J. A., Lawson, W. E., and Blackwell, T. S. (2012). Right Place, Right Time: the Evolving Role of Herpesvirus Infection as a "second Hit" in Idiopathic Pulmonary Fibrosis. *Am. J. Physiol. Lung Cel Mol Physiol* 302 (5), L441–L444. doi:10.1152/ajplung.00335.2011

Krylatov, A. V., Maslov, L. N., Voronkov, N. S., Boshchenko, A. A., Popov, S. V., Gomez, L., et al. (2018). Reactive Oxygen Species as Intracellular Signaling Molecules in the Cardiovascular System. *Curr. Cardiol. Rev.* 14 (4), 290–300. doi:10.2174/1573403X14666180702152436

Kushnir, A., Wajsberg, B., and Marks, A. R. (2018). Ryanodine Receptor Dysfunction in Human Disorders. *Biochim. Biophys. Acta Mol. Cel Res* 1865 (11 Pt B), 1687–1697. doi:10.1016/j.bbamcr.2018.07.011

Labaki, W. W., and Rosenberg, S. R. (2020). Chronic Obstructive Pulmonary Disease. *Ann. Intern. Med.* 173 (3), ITC17–ITC32. doi:10.7326/AITC202008040

Lambertsen, K. L., Biber, K., and Finsen, B. (2012). Inflammatory Cytokines in Experimental and Human Stroke. *J. Cereb. Blood Flow Metab.* 32 (9), 1677–1698. doi:10.1038/jcbfm.2012.88

Lawson, W. E., Cheng, D. S., Degryse, A. L., Tanjore, H., Polosukhin, V. V., Xu, X. C., et al. (2011). Endoplasmic Reticulum Stress Enhances Fibrotic Remodeling in the Lungs. *Proc. Natl. Acad. Sci. U S A.* 108 (26), 10562–10567. doi:10.1073/pnas.1107559108

Lee, D. Y., Lee, J., and Sugden, B. (2009). The Unfolded Protein Response and Autophagy: Herpesviruses Rule!. *J. Virol.* 83 (3), 1168–1172. doi:10.1128/JVI.01358-08

Lee, H. Y., Kim, H. K., Hoang, T. H., Yang, S., Kim, H. R., and Chae, H. J. (2020). The Correlation of IRE1α Oxidation with Nox4 Activation in Aging-Associated Vascular Dysfunction. *Redox Biol.* 37, 101727. doi:10.1016/j.redox.2020.101727

Lee, K. S., Jeong, J. S., Kim, S. R., Cho, S. H., Kolliputi, N., Ko, Y. H., et al. (2016). Phosphoinositide 3-Kinase-δ Regulates Fungus-Induced Allergic Lung Inflammation through Endoplasmic Reticulum Stress. *Thorax* 71 (1), 52–63. doi:10.1136/thoraxjnl-2015-207096

Lerner, A. G., Upton, J. P., Praveen, P. V., Ghosh, R., Nakagawa, Y., Igbaria, A., et al. (2012). IRE1α Induces Thioredoxin-Interacting Protein to Activate the NLRP3 Inflammasome and Promote Programmed Cell Death under Irremediable ER Stress. *Cell Metab* 16 (2), 250–264. doi:10.1016/j.cmet.2012.07.007

Li, C., Chen, J., Yuan, W., Zhang, W., Chen, H., and Tan, H. (2020). Preventive Effect of Ursolic Acid Derivative on Particulate Matter 2.5-induced Chronic Obstructive Pulmonary Disease Involves Suppression of Lung Inflammation. *IUBMB Life* 72 (4), 632–640. doi:10.1002/iub.2201

Lim, C. Y., Davis, O. B., Shin, H. R., Zhang, J., Berdan, C. A., Jiang, X., et al. (2019). ER-lysosome Contacts Enable Cholesterol Sensing by mTORC1 and Drive Aberrant Growth Signalling in Niemann-Pick Type C. *Nat. Cel Biol* 21 (10), 1206–1218. doi:10.1038/s41556-019-0391-5

Lin, R., Sun, Y., Ye, W., Zheng, T., Wen, J., and Deng, Y. (2019). T-2 Toxin Inhibits the Production of Mucin *via* Activating the IRE1/XBP1 Pathway. *Toxicology* 424, 152230. doi:10.1016/j.tox.2019.06.001

Liu, G., Pei, F., Yang, F., Li, L., Amin, A. D., Liu, S., et al. (2017). Role of Autophagy and Apoptosis in Non-small-cell Lung Cancer. *Int. J. Mol. Sci.* 18 (2). doi:10.3390/ijms18020367

Liu, Q., Gao, Y., and Ci, X. (2019). Role of Nrf2 and its Activators in Respiratory Diseases. *Oxid Med. Cel Longev* 2019, 7090534. doi:10.1155/2019/7090534

Liu, Y., Li, G., and Wang, B. (2021). Herpesvirus and Endoplasmic Reticulum Stress. *Sheng Wu Gong Cheng Xue Bao* 37 (1), 67–77. doi:10.13345/j.cjb.200226

Liu, Y., Wang, J., Qi, S. Y., Ru, L. S., Ding, C., Wang, H. J., et al. (2014). Reduced Endoplasmic Reticulum Stress Might Alter the Course of Heart Failure *via* Caspase-12 and JNK Pathways. *Can. J. Cardiol.* 30 (3), 368–375. doi:10.1016/j.cjca.2013.11.001

Lubamba, B. A., Jones, L. C., O'Neal, W. K., Boucher, R. C., and Ribeiro, C. M. (2015). X-Box-Binding Protein 1 and Innate Immune Responses of Human Cystic Fibrosis Alveolar Macrophages. *Am. J. Respir. Crit. Care Med.* 192 (12), 1449–1461. doi:10.1164/rccm.201504-0657OC

Luhr, M., Torgersen, M. L., Szalai, P., Hashim, A., Brech, A., Staerk, J., et al. (2019). The Kinase PERK and the Transcription Factor ATF4 Play Distinct and Essential Roles in Autophagy Resulting from Tunicamycin-Induced ER Stress. *J. Biol. Chem.* 294 (20), 8197–8217. doi:10.1074/jbc.RA118.002829

Marchi, S., Patergnani, S., Missiroli, S., Morciano, G., Rimessi, A., Wieckowski, M. R., et al. (2018). Mitochondrial and Endoplasmic Reticulum Calcium Homeostasis and Cell Death. *Cell Calcium* 69, 62–72. doi:10.1016/j.ceca.2017.05.003

Matsuzawa, A., Nishitoh, H., Tobiume, K., Takeda, K., and Ichijo, H. (2002). Physiological Roles of ASK1-Mediated Signal Transduction in Oxidative Stress- and Endoplasmic Reticulum Stress-Induced Apoptosis: Advanced Findings from ASK1 Knockout Mice. *Antioxid. Redox Signal.* 4 (3), 415–425. doi:10.1089/15230860260196218

Min, T., Bodas, M., Mazur, S., and Vij, N. (2011). Critical Role of Proteostasis-Imbalance in Pathogenesis of COPD and Severe Emphysema. *J. Mol. Med. (Berl)* 89 (6), 577–593. doi:10.1007/s00109-011-0732-8

Muñoz-Guardiola, P., Casas, J., Megías-Roda, E., Solé, S., Perez-Montoyo, H., Yeste-Velasco, M., et al. (2021). The Anti-cancer Drug ABTL0812 Induces ER Stress-Mediated Cytotoxic Autophagy by Increasing Dihydroceramide Levels in Cancer Cells. *Autophagy* 17 (6), 1349–1366. doi:10.1080/15548627.2020.1761651

Nakada, E. M., Bhakta, N. R., Korwin-Mihavics, B. R., Kumar, A., Chamberlain, N., Bruno, S. R., et al. (2019). Conjugated Bile Acids Attenuate Allergen-Induced

Airway Inflammation and Hyperresponsiveness by Inhibiting UPR Transducers. *JCI Insight* 4 (9). doi:10.1172/jci.insight.98101

Nasim, F., Sabath, B. F., and Eapen, G. A. (2019). Lung Cancer. *Med. Clin. North. Am.* 103 (3), 463–473. doi:10.1016/j.mcna.2018.12.006

Niforou, K., Cheimonidou, C., and Trougakos, I. P. (2014). Molecular Chaperones and Proteostasis Regulation during Redox Imbalance. *Redox Biol.* 2, 323–332. doi:10.1016/j.redox.2014.01.017

Noble, P. W., Barkauskas, C. E., and Jiang, D. (2012). Pulmonary Fibrosis: Patterns and Perpetrators. *J. Clin. Invest.* 122 (8), 2756–2762. doi:10.1172/JCI60323

Oakes, S. A., and Papa, F. R. (2015). The Role of Endoplasmic Reticulum Stress in Human Pathology. *Annu. Rev. Pathol.* 10, 173–194. doi:10.1146/annurev-pathol-012513-104649

Ochoa, C. D., Wu, R. F., and Terada, L. S. (2018). ROS Signaling and ER Stress in Cardiovascular Disease. *Mol. Aspects Med.* 63, 18–29. doi:10.1016/j.mam.2018.03.002

Ong, H. L., and Ambudkar, I. S. (2020). The Endoplasmic Reticulum-Plasma Membrane Junction: A Hub for Agonist Regulation of Ca2+ Entry. *Cold Spring Harb Perspect. Biol.* 12 (2). doi:10.1101/cshperspect.a035253

Orrenius, S., Gogvadze, V., and Zhivotovsky, B. (2015). Calcium and Mitochondria in the Regulation of Cell Death. *Biochem. Biophys. Res. Commun.* 460 (1), 72–81. doi:10.1016/j.bbrc.2015.01.137

Pachikov, A. N., Gough, R. R., Christy, C. E., Morris, M. E., Casey, C. A., LaGrange, C. A., et al. (2021). The Non-canonical Mechanism of ER Stress-Mediated Progression of Prostate Cancer. *J. Exp. Clin. Cancer Res.* 40 (1), 289. doi:10.1186/s13046-021-02066-7

Paxman, R., Plate, L., Blackwood, E. A., Glembotski, C., Powers, E. T., Wiseman, R. L., et al. (2018). Pharmacologic ATF6 Activating Compounds Are Metabolically Activated to Selectively Modify Endoplasmic Reticulum Proteins. *Elife* 7. doi:10.7554/eLife.37168

Pedersen, B. K., and Saltin, B. (2015). Exercise as Medicine - Evidence for Prescribing Exercise as Therapy in 26 Different Chronic Diseases. *Scand. J. Med. Sci. Sports* 25 Suppl 3 (Suppl. 3), 1–72. doi:10.1111/sms.12581

Petrou, T., Olsen, H. L., Thrasivoulou, C., Masters, J. R., Ashmore, J. F., and Ahmed, A. (2017). Intracellular Calcium Mobilization in Response to Ion Channel Regulators *via* a Calcium-Induced Calcium Release Mechanism. *J. Pharmacol. Exp. Ther.* 360 (2), 378–387. doi:10.1124/jpet.116.236695

Pillai, S. (2005). Birth Pangs: the Stressful Origins of Lymphocytes. *J. Clin. Invest.* 115 (2), 224–227. doi:10.1172/JCI24238

Polverino, F., Wu, T. D., Rojas-Quintero, J., Wang, X., Mayo, J., Tomchaney, M., et al. (2021). Metformin: Experimental and Clinical Evidence for a Potential Role in Emphysema Treatment. *Am. J. Respir. Crit. Care Med.* 204 (6), 651–666. doi:10.1164/rccm.202012-4510OC

Prasad, S., Gupta, S. C., and Tyagi, A. K. (2017). Reactive Oxygen Species (ROS) and Cancer: Role of Antioxidative Nutraceuticals. *Cancer Lett.* 387, 95–105. doi:10.1016/j.canlet.2016.03.042

Putney, J. W., Jr. (1986). A Model for Receptor-Regulated Calcium Entry. *Cell Calcium* 7 (1), 1–12. doi:10.1016/0143-4160(86)90026-6

Qin, L., Wang, Z., Tao, L., and Wang, Y. (2010). ER Stress Negatively Regulates AKT/TSC/mTOR Pathway to Enhance Autophagy. *Autophagy* 6 (2), 239–247. doi:10.4161/auto.6.2.11062

Rana, S. V. S. (2020). Endoplasmic Reticulum Stress Induced by Toxic Elements-A Review of Recent Developments. *Biol. Trace Elem. Res.* 196 (1), 10–19. doi:10.1007/s12011-019-01903-3

Rizzuto, R., De Stefani, D., Raffaello, A., and Mammucari, C. (2012). Mitochondria as Sensors and Regulators of Calcium Signalling. *Nat. Rev. Mol. Cel Biol* 13 (9), 566–578. doi:10.1038/nrm3412

Rowland, A. A., and Voeltz, G. K. (2012). Endoplasmic Reticulum-Mitochondria Contacts: Function of the junction. *Nat. Rev. Mol. Cel Biol* 13 (10), 607–625. doi:10.1038/nrm3440

Russell, R. J., and Brightling, C. (2017). Pathogenesis of Asthma: Implications for Precision Medicine. *Clin. Sci. (Lond)* 131 (14), 1723–1735. doi:10.1042/CS20160253

Saibil, H. (2013). Chaperone Machines for Protein Folding, Unfolding and Disaggregation. *Nat. Rev. Mol. Cel Biol* 14 (10), 630–642. doi:10.1038/nrm3658

Sakurada, R., Odagiri, K., Hakamata, A., Kamiya, C., Wei, J., and Watanabe, H. (2019). Calcium Release from Endoplasmic Reticulum Involves Calmodulin-Mediated NADPH Oxidase-Derived Reactive Oxygen Species Production in Endothelial Cells. *Int. J. Mol. Sci.* 20 (7). doi:10.3390/ijms20071644

Santulli, G., Nakashima, R., Yuan, Q., and Marks, A. R. (2017). Intracellular Calcium Release Channels: an Update. *J. Physiol.* 595 (10), 3041–3051. doi:10.1113/JP272781

Schögler, A., Caliaro, O., Brügger, M., Oliveira Esteves, B. I., Nita, I., Gazdhar, A., et al. (2019). Modulation of the Unfolded Protein Response Pathway as an Antiviral Approach in Airway Epithelial Cells. *Antivir. Res* 162, 44–50. doi:10.1016/j.antiviral.2018.12.007

Schuller, H. M. (2019). The Impact of Smoking and the Influence of Other Factors on Lung Cancer. *Expert Rev. Respir. Med.* 13 (8), 761–769. doi:10.1080/17476348.2019.1645010

Schwarz, D. S., and Blower, M. D. (2016). The Endoplasmic Reticulum: Structure, Function and Response to Cellular Signaling. *Cel Mol Life Sci* 73 (1), 79–94. doi:10.1007/s00018-015-2052-6

Sen, N. (2019). ER Stress, CREB, and Memory: A Tangled Emerging Link in Disease. *Neuroscientist* 25 (5), 420–433. doi:10.1177/1073858418816611

Senft, D., and Ronai, Z. A. (2015). UPR, Autophagy, and Mitochondria Crosstalk Underlies the ER Stress Response. *Trends Biochem. Sci.* 40 (3), 141–148. doi:10.1016/j.tibs.2015.01.002

Shi, S., Tan, P., Yan, B., Gao, R., Zhao, J., Wang, J., et al. (2016). ER Stress and Autophagy Are Involved in the Apoptosis Induced by Cisplatin in Human Lung Cancer Cells. *Oncol. Rep.* 35 (5), 2606–2614. doi:10.3892/or.2016.4680

Shirakawa, J., Togashi, Y., Sakamoto, E., Kaji, M., Tajima, K., Orime, K., et al. (2013). Glucokinase Activation Ameliorates ER Stress-Induced Apoptosis in Pancreatic β-cells. *Diabetes* 62 (10), 3448–3458. doi:10.2337/db13-0052

Singh-Mallah, G., Nair, S., Sandberg, M., Mallard, C., and Hagberg, H. (2019). The Role of Mitochondrial and Endoplasmic Reticulum Reactive Oxygen Species Production in Models of Perinatal Brain Injury. *Antioxid. Redox Signal.* 31 (9), 643–663. doi:10.1089/ars.2019.7779

Song, S., Tan, J., Miao, Y., and Zhang, Q. (2018). Crosstalk of ER Stress-Mediated Autophagy and ER-Phagy: Involvement of UPR and the Core Autophagy Machinery. *J. Cel Physiol* 233 (5), 3867–3874. doi:10.1002/jcp.26137

Sozen, E., and Ozer, N. K. (2017). Impact of High Cholesterol and Endoplasmic Reticulum Stress on Metabolic Diseases: An Updated Mini-Review. *Redox Biol.* 12, 456–461. doi:10.1016/j.redox.2017.02.025

Szarka, A., and Lőrincz, T. (2014). The Role of Ascorbate in Protein Folding. *Protoplasma* 251 (3), 489–497. doi:10.1007/s00709-013-0560-5

Tanaka, Y., Ishitsuka, Y., Hayasaka, M., Yamada, Y., Miyata, K., Endo, M., et al. (2015). The Exacerbating Roles of CCAAT/enhancer-binding Protein Homologous Protein (CHOP) in the Development of Bleomycin-Induced Pulmonary Fibrosis and the Preventive Effects of Tauroursodeoxycholic Acid (TUDCA) against Pulmonary Fibrosis in Mice. *Pharmacol. Res.* 99, 52–62. doi:10.1016/j.phrs.2015.05.004

Tanjore, H., Blackwell, T. S., and Lawson, W. E. (2012). Emerging Evidence for Endoplasmic Reticulum Stress in the Pathogenesis of Idiopathic Pulmonary Fibrosis. *Am. J. Physiol. Lung Cel Mol Physiol* 302 (8), L721–L729. doi:10.1152/ajplung.00410.2011

Tavender, T. J., and Bulleid, N. J. (2010). Molecular Mechanisms Regulating Oxidative Activity of the Ero1 Family in the Endoplasmic Reticulum. *Antioxid. Redox Signal.* 13 (8), 1177–1187. doi:10.1089/ars.2010.3230

Tian, J., Popal, M. S., Liu, Y., Gao, R., Lyu, S., Chen, K., et al. (2019). Erratum to "Ginkgo Biloba Leaf Extract Attenuates Atherosclerosis in Streptozotocin-Induced Diabetic ApoE-/- Mice by Inhibiting Endoplasmic Reticulum Stress *via* Restoration of Autophagy through the mTOR Signaling Pathway". *Oxid Med. Cel Longev* 2019, 3084083. doi:10.1155/2019/3084083

Tong, B., Fu, L., Hu, B., Zhang, Z. C., Tan, Z. X., Li, S. R., et al. (2021). Tauroursodeoxycholic Acid Alleviates Pulmonary Endoplasmic Reticulum Stress and Epithelial-Mesenchymal Transition in Bleomycin-Induced Lung Fibrosis. *BMC Pulm. Med.* 21 (1), 149. doi:10.1186/s12890-021-01514-6

Tordjman, S., Chokron, S., Delorme, R., Charrier, A., Bellissant, E., Jaafari, N., et al. (2017). Melatonin: Pharmacology, Functions and Therapeutic Benefits. *Curr. Neuropharmacol* 15 (3), 434–443. doi:10.2174/1570159X14666161228122115

Trouvé, P., Férec, C., and Génin, E. (2021). The Interplay between the Unfolded Protein Response, Inflammation and Infection in Cystic Fibrosis. *Cells* 10 (11). doi:10.3390/cells10112980

Urano, F., Wang, X., Bertolotti, A., Zhang, Y., Chung, P., Harding, H. P., et al. (2000). Coupling of Stress in the ER to Activation of JNK Protein Kinases by Transmembrane Protein Kinase IRE1. *Science* 287 (5453), 664–666. doi:10.1126/science.287.5453.664

Urra, H., Dufey, E., Avril, T., Chevet, E., and Hetz, C. (2016). Endoplasmic Reticulum Stress and the Hallmarks of Cancer. *Trends Cancer* 2 (5), 252–262. doi:10.1016/j.trecan.2016.03.007

van 't Wout, E. F., van Schadewijk, A., van Boxtel, R., Dalton, L. E., Clarke, H. J., Tommassen, J., et al. (2015). Virulence Factors of *Pseudomonas aeruginosa* Induce Both the Unfolded Protein and Integrated Stress Responses in Airway Epithelial Cells. *Plos Pathog.* 11 (6), e1004946. doi:10.1371/journal.ppat.1004946

Vander Zanden, C. M., Wampler, L., Bowers, I., Watkins, E. B., Majewski, J., and Chi, E. Y. (2019). Fibrillar and Nonfibrillar Amyloid Beta Structures Drive Two Modes of Membrane-Mediated Toxicity. *Langmuir* 35 (48), 16024–16036. doi:10.1021/acs.langmuir.9b02484

Vanhoutte, D., Schips, T. G., Vo, A., Grimes, K. M., Baldwin, T. A., Brody, M. J., et al. (2021). Thbs1 Induces Lethal Cardiac Atrophy through PERK-ATF4 Regulated Autophagy. *Nat. Commun.* 12 (1), 3928. doi:10.1038/s41467-021-24215-4

Venkatesan, A., Satin, L. S., and Raghavan, M. (2021). Roles of Calreticulin in Protein Folding, Immunity, Calcium Signaling and Cell Transformation. *Prog. Mol. Subcell Biol.* 59, 145–162. doi:10.1007/978-3-030-67696-4_7

Verfaillie, T., Rubio, N., Garg, A. D., Bultynck, G., Rizzuto, R., Decuypere, J. P., et al. (2012). PERK Is Required at the ER-Mitochondrial Contact Sites to Convey Apoptosis after ROS-Based ER Stress. *Cell Death Differ* 19 (11), 1880–1891. doi:10.1038/cdd.2012.74

Wang, H. F., Wang, Z. Q., Ding, Y., Piao, M. H., Feng, C. S., Chi, G. F., et al. (2018). Endoplasmic Reticulum Stress Regulates Oxygen-Glucose Deprivation-Induced Parthanatos in Human SH-Sy5y Cells *via* Improvement of Intracellular ROS. *CNS Neurosci. Ther.* 24 (1), 29–38. doi:10.1111/cns.12771

Wang, R., Sun, D.-Z., Song, C.-Q., Xu, Y.-M., Liu, W., Liu, Z., et al. (2018). Eukaryotic Translation Initiation Factor 2 Subunit *α* (eIF2*α*) Inhibitor Salubrinal Attenuates Paraquat-Induced Human Lung Epithelial-like A549 Cell Apoptosis by Regulating the PERK-eIF2*α* Signaling Pathway. *Toxicol. Vitro* 46, 58–65. doi:10.1016/j.tiv.2017.10.006

Wang, S., Gong, L., Mo, Y., Zhang, J., Jiang, Z., Tian, Z., et al. (2022). Resveratrol Attenuates Inflammation and Apoptosis through Alleviating Endoplasmic Reticulum Stress *via* Akt/mTOR Pathway in Fungus-Induced Allergic Airways Inflammation. *Int. Immunopharmacol* 103, 108489. doi:10.1016/j.intimp.2021.108489

Wang, X., Wang, H., Xu, B., Huang, D., Nie, C., Pu, L., et al. (2021). Receptor-Mediated ER Export of Lipoproteins Controls Lipid Homeostasis in Mice and Humans. *Cel Metab* 33 (2), 350–e7. doi:10.1016/j.cmet.2020.10.020

Weissferdt, A. (2014). Large Cell Carcinoma of Lung: On the Verge of Extinction? *Semin. Diagn. Pathol.* 31 (4), 278–288. doi:10.1053/j.semdp.2014.06.005

Wortel, I. M. N., van der Meer, L. T., Kilberg, M. S., and van Leeuwen, F. N. (2017). Surviving Stress: Modulation of ATF4-Mediated Stress Responses in Normal and Malignant Cells. *Trends Endocrinol. Metab.* 28 (11), 794–806. doi:10.1016/j.tem.2017.07.003

Wu, P. S., Yen, J. H., Kou, M. C., and Wu, M. J. (2015). Luteolin and Apigenin Attenuate 4-Hydroxy-2-Nonenal-Mediated Cell Death through Modulation of UPR, Nrf2-ARE and MAPK Pathways in PC12 Cells. *PLoS One* 10 (6), e0130599. doi:10.1371/journal.pone.0130599

Xu, Y., Sun, D., Song, C., Wang, R., and Dong, X. (2018). MnTMPyP Inhibits Paraquat-Induced Pulmonary Epithelial-like Cell Injury by Inhibiting Oxidative Stress. *J. Toxicol. Sci.* 43 (9), 545–555. doi:10.2131/jts.43.545

Xu, Y., Wang, W., Jin, K., Zhu, Q., Lin, H., Xie, M., et al. (2017). Perillyl Alcohol Protects Human Renal Tubular Epithelial Cells from Hypoxia/reoxygenation Injury *via* Inhibition of ROS, Endoplasmic Reticulum Stress and Activation of PI3K/Akt/eNOS Pathway. *Biomed. Pharmacother.* 95, 662–669. doi:10.1016/j.biopha.2017.08.129

Yang, Y., Cheng, B. J., Jian, H., Chen, Z. W., Zhao, Y., Yu, Y. F., et al. (2017). XBP1-LOX Axis Is Critical in ER Stress-Induced Growth of Lung Adenocarcinoma in 3D Culture. *Am. J. Transl Res.* 9 (2), 700–707.

Ye, L., Zeng, Q., Ling, M., Ma, R., Chen, H., Lin, F., et al. (2021). Inhibition of IP3R/Ca2+ Dysregulation Protects Mice from Ventilator-Induced Lung Injury *via* Endoplasmic Reticulum and Mitochondrial Pathways. *Front. Immunol.* 12, 729094. doi:10.3389/fimmu.2021.729094

Zeeshan, H. M., Lee, G. H., Kim, H. R., and Chae, H. J. (2016). Endoplasmic Reticulum Stress and Associated ROS. *Int. J. Mol. Sci.* 17 (3), 327. doi:10.3390/ijms17030327

Zeng, M., Sang, W., Chen, S., Chen, R., Zhang, H., Xue, F., et al. (2017). 4-PBA Inhibits LPS-Induced Inflammation through Regulating ER Stress and Autophagy in Acute Lung Injury Models. *Toxicol. Lett.* 271, 26–37. doi:10.1016/j.toxlet.2017.02.023

Zhang, X., Huang, R., Zhou, Y., Zhou, W., and Zeng, X. (2020). IP3R Channels in Male Reproduction. *Int. J. Mol. Sci.* 21 (23). doi:10.3390/ijms21239179

Zhang, X., Zhang, H. Q., Zhu, G. H., Wang, Y. H., Yu, X. C., Zhu, X. B., et al. (2012). A Novel Mono-Carbonyl Analogue of Curcumin Induces Apoptosis in Ovarian Carcinoma Cells *via* Endoplasmic Reticulum Stress and Reactive Oxygen Species Production. *Mol. Med. Rep.* 5 (3), 739–744. doi:10.3892/mmr.2011.700

Zhang, Y., Cen, J., Jia, Z., Hsiao, C. D., Xia, Q., Wang, X., et al. (2019). Hepatotoxicity Induced by Isoniazid-Lipopolysaccharide through Endoplasmic Reticulum Stress, Autophagy, and Apoptosis Pathways in Zebrafish. *Antimicrob. Agents Chemother.* 63 (5). doi:10.1128/AAC.01639-18

Zhang, Z., Zhang, L., Zhou, L., Lei, Y., Zhang, Y., and Huang, C. (2019). Redox Signaling and Unfolded Protein Response Coordinate Cell Fate Decisions under ER Stress. *Redox Biol.* 25, 101047. doi:10.1016/j.redox.2018.11.005

Zhao, Y., Zhu, C., Li, X., Zhang, Z., Yuan, Y., Ni, Y., et al. (2011). Asterosaponin 1 Induces Endoplasmic Reticulum Stress-Associated Apoptosis in A549 Human Lung Cancer Cells. *Oncol. Rep.* 26 (4), 919–924. doi:10.3892/or.2011.1358

Zhu, X. M., Yao, F. H., Yao, Y. M., Dong, N., Yu, Y., and Sheng, Z. Y. (2012). Endoplasmic Reticulum Stress and its Regulator XBP-1 Contributes to Dendritic Cell Maturation and Activation Induced by High Mobility Group Box-1 Protein. *Int. J. Biochem. Cel Biol* 44 (7), 1097–1105. doi:10.1016/j.biocel.2012.03.018

Conflict of Interest: The authors declare that the research was conducted in the absence of any commercial or financial relationships that could be construed as a potential conflict of interest.

Publisher's Note: All claims expressed in this article are solely those of the authors and do not necessarily represent those of their affiliated organizations, or those of the publisher, the editors and the reviewers. Any product that may be evaluated in this article, or claim that may be made by its manufacturer, is not guaranteed or endorsed by the publisher.

frontiers | Frontiers in Pharmacology

ORIGINAL RESEARCH
published: 31 May 2022
doi: 10.3389/fphar.2022.826649

Supplementation With *Spirulina platensis* Improves Tracheal Reactivity in Wistar Rats by Modulating Inflammation and Oxidative Stress

Aline de F. Brito[1,2], Alexandre S. Silva[2,3], Alesandra A. de Souza[2,4], Paula B. Ferreira[5], Iara L. L. de Souza[6], Layanne C. da C. Araujo[7] and Bagnólia A. da Silva[5,8]*

[1]School of Physical Education, University of Pernambuco, Recife, Brazil, [2]Post-Graduation Program in Physical Education UPE/UFPB, Recife, Brazil, [3]Physical Education Department, Health Sciences Center, Federal University of Paraiba, João Pessoa, Brazil, [4]Federal University of Tocantins, Licentiate in Physical Education, Tocantinopolis, Brazil, [5]Postgraduate Program in Natural and Synthetic Products Bioactive, Health Sciences Center, Federal University of Paraiba, João Pessoa, Brazil, [6]Department of Biological Sciences and Health, Roraima State University, Boa Vista, Brazil, [7]Department of Biophysics and Physiology, Institute of Biomedical Sciences, University of São Paulo, São Paulo, Brazil, [8]Pharmaceutical Sciences Department, Health Sciences Center, Federal University of Paraiba, João Pessoa, Brazil

OPEN ACCESS

Edited by:
Arunachalam Karuppusamy, Chinese Academy of Sciences (CAS), China

Reviewed by:
Nisha Patro, Jiwaji University, India
Kai Guan, Peking Union Medical College Hospital, China
Anurag Varshney, Patanjali Research Foundation, India

***Correspondence:**
Aline de F. Brito
alineebritoo@gmail.com

Specialty section:
This article was submitted to Respiratory Pharmacology, a section of the journal Frontiers in Pharmacology

Received: *01 December 2021*
Accepted: *14 February 2022*
Published: *31 May 2022*

Citation:
Brito AdF, Silva AS, de Souza AA, Ferreira PB, Souza ILLd, Araujo LCdC and da Silva BA (2022) Supplementation With Spirulina platensis Improves Tracheal Reactivity in Wistar Rats by Modulating Inflammation and Oxidative Stress. Front. Pharmacol. 13:826649. doi: 10.3389/fphar.2022.826649

Spirulina platensis has shown effectiveness in the treatment of allergic rhinitis in rats, but its action in tracheal reactivity or on markers of relaxation and antioxidant profile has not yet been possible to determine. In this paper, the animals were divided into the groups healthy (SG) and supplemented with S. platensis at doses of 50 (SG50), 150 (SG150), and 500 mg/kg (SG500). We also evaluated nitrite levels, lipid peroxidation, and antioxidant activity through biochemical analysis. For contractile reactivity, only SG500 (pEC50 = 5.2 ± 0.06 showed reduction in carbachol contractile potency. Indomethacin caused a higher contractile response to carbachol in SG150 and SG500. For relaxation, curves for SG150 (pEC50 = 5.0 ± 0.05) and SG500 (pEC50 = 7:3 ± 0:02) were shifted to the left, more so in SG500. We observed an increase in nitrite in the trachea only with supplementation of 500 mg/kg (54.0 ± 8.0 μM), also when compared to SG50 (37.0 ± 10.0 μM) and SG150 (38.0 ± 7.0 μM). We observed a decrease in lipid peroxidation in the plasma and an increase in oxidation inhibition for the trachea and lung in SG150 and SG500, suggesting enhanced antioxidant activity. S. platensis (150/500 mg/kg) decreased the contractile response and increased relaxation by increasing antioxidant activity and nitrite levels and modulating the inflammatory response.

Keywords: respiratory mucosa, lipid peroxidation, inflammatory response, prostaglandins, epithelium

INTRODUCTION

Allergic diseases of the respiratory tract such as asthma and rhinitis are an inflammatory state in which clinical symptoms such as shortness of breath, wheezing, and tightness in the chest result from either an increased limitation of expired airspace or bronchial hyperreactivity involvement (Fahy, 2015). In this inflammatory context, reactive species are produced, which can cause oxidative stress, resulting in physiological changes in the epithelium and the airway wall structure, in smooth muscle

cells and the immune system, leading to the pulmonary limitations characteristic of these diseases (Lambrecht & Hammad, 2015).

The use of antioxidant products shows promise in the treatment and prevention of respiratory tract diseases. In this context, natural products of *Spirulina platensis*, filamentous cyanobacterium, have been used as a food supplement by humans for many years due to the high nutritional values in *Spirulina platensis*, such as high protein content, amino acids, minerals, and antioxidants. Besides, it has shown hypolipidemic, hypoglycemic, and antihypertensive properties and antioxidant and anti-inflammatory activities (Appel et al., 2018).

Spirulina has shown effectiveness in the treatment and prevention of allergic rhinitis in rats. This treatment acted by reducing inflammatory reactions and the mastocyte number in the nasal mucosa (Chen et al., 2005). As well as improved symptoms of rhinitis in humans (Nourollahian et al., 2020).

Tracheal reactivity has been an experimental model used for investigations that aim to analyze some aspects related to asthma or other allergic diseases of the respiratory tract that present contractile hyperresponsiveness of the tracheal rings (Montaño et al., 2018). The Food supplementation of *Spirulina platensis* proved itself effective in preventing hypercontractility in other smooth muscle models, uterus (Revuelta et al., 1997), aorta (Brito et al., 2018), corpus cavernosum (de Souza et al., 2018) and ileum (Araujo et al., 2020).

Despite the significant evidence on the importance of *S. platensis* in the inhibition of inflammatory markers, so far, this investigation first aimed to analyze the pattern of contraction and relaxation of the health trachea rings to the administration of different doses of S. platensis and to analyze the involvement of the prostanoids and nitric oxide metabolites and lipid peroxidation in health Wistar rats. We study has shown the influence of this cyanobacterium on the response of health trachea rings or relaxation markers and antioxidant profiles.

MATERIALS AND METHODS

We followed the methods of Brito et al. (2018; 2019; 2020).

Substances

Glucose ($C_6H_{12}O_6$), monobasic potassium phosphate (KH_2PO_4), hydrochloric acid (HCl), and magnesium sulfate heptahydrate ($MgSO_4.7H_2O$) were obtained from Nuclear (Brazil). Sodium chloride (NaCl) was purchased from Dinâmica (Brazil). Potassium chloride (KCl), calcium chloride dihydrate ($CaCl_2.2H_2O$), and sodium bicarbonate (NaHCO3) were acquired from Vetec (Brazil) and acetylcholine chloride (ACh) from Merck (Brazil). Phenylephrine (PHE) was obtained from Pfizer (United States) and aminophylline and indomethacin from Sigma Aldrich (Brazil). Ethylenediaminetetraacetic acid (EDTA) (1:250) was purchased from BioTécnica-Advanced Biotechnology (Brazil) and carbogen mixture (95% O_2 and 5% CO_2) from White Martins (Brazil). The weighing of the substances was done with a GEHAKA analytical balance model AG 200 (Brazil).

Preparation and Supplementation With Spirulina platensis

S. platensis in lyophilized powder form was acquired from Bio-Engineering Dongtai Top Co., Ltd. (Nanjing, China) (Lot No. 20130320). the Pharma Nostra Quality Control Laboratory (Anapolis-GO, Brazil) (Lot No. 1308771A) analyzed a sample for certification that the extract was obtained from S. platensis. Then, Dilecta Manipulation Drugstore (João Pessoa-PB, Brazil) (Lot No. 20121025) prepared the used S. platensis. *S. platensis* was dissolved daily in saline in proportions of 0.005, 0.015 and 0.05 g/ml for the preparation of doses of 50, 150 and 500 mg/kg, respectively., which were administered to the animals at the end of the preparation. The preparation of each dose of S. platensis was performed daily on all supplementation days. Supplementations were performed for a period of 8 weeks for all doses (50, 150 and 500 mg/kg/day). The supplements were administered for 8 weeks (adapted from Juarez-Oropeza et al., 2009) with oral administration daily (between 12 and 2 p.m.), using stainless steel gavage needles (BD-12, Insight, Ribeirão Preto-SP, Brazil) and 5 ml syringes with 0.1 ml precision (BD, Higilab, João Pessoa- PB, Brazil).

Animals and Experimental Protocol

For the experimental animal model, the subjects were male Wistar rats (Rattus norvegicus), weighing between 250 and 300 g, from the Prof. Thomas George Bioterium of the Research Institute for Drugs and Medicines from Federal University of Paraiba (UFPB). The animals were weighed on a GEHAKA semi-analytical balance (São Paulo-SP, Brazil). In order to guarantee the reliability during the measurement of the weight of the same, the scale had a cylindrical tube of appropriate size to place the animal, which was effective to contain its movement. All the animals were maintained on a nutritionally balanced feed (Labina®) with free access to water, with controlled temperature (21°C), and a 12 h light-dark cycle (lights on at 6 a.m.). All experiments were conducted between 8 a.m. and 8 p.m., according to the guidelines for the ethical use of animals (Sherwin et al., 2003). The experimental protocol was previously approved by Ethics Committee in Animal Use (CEUA/UFPB) with certificate number 0511/13.

The animals were divided into saline (0.9% NaCl, control) and supplemented with *S. platensis* (50, 150, and 500 mg/kg) groups. Thus, the study was composed of the following groups with 20 rats randomly divided into a saline group (SG, control) and groups supplemented with *S. platensis* at 50 (SG50), 150 (SG150), and 500 mg/kg (SG500). For the reactivity experiments, the sample of each result included five different experiments (n = 5) and for the biochemical experiments we used (n = 10). Each preparation was from different animals. The selected sample size was chosen to avoid using an excessive number of animals, and this number provides enough reliability for the results obtained.

Concentration-Response Curves

Pharmacological Evaluation of Spirulina platensis on Tracheal Reactivity

The rats treated with saline or *S. platensis* at the end of the intervention protocols, the animals were anesthetized with

ketamine 100 mg/kg (i.p.) and xylazine 10 mg/kg (i.p.), followed by a complementary method with were euthanized by cervical dislocation, followed by cervical vessel section. This method was adopted since the tissue to be evaluated in the experiments would be completely damaged if euthanasia were performed by guillotine, in addition to the injury that would be caused to the epithelium of the organ, mechanisms that were also evaluated in our study. The animals' thorax was open and dissected. Their tracheas were carefully removed and cleaned to separate them from all connective and adipose tissue. Then, we separated tracheal segments containing three to four cartilage rings. In addition, lungs were removed for further dosing of oxidative stress. After the removal, the lungs were cleaned in a Krebs solution to remove blood residues, placed in Eppendorf, and stored in a -80°C freezer until analysis.

For isometric responses, the tracheal segments were suspended through stainless steel rods in organ baths (6 ml) containing Krebs solution under a tension of 1 g, maintained at a temperature of 37°C, and remained in rest for 60 min gassed with carbogen. The nutrient solution was renewed every 15 min to prevent interference of metabolites during all the experiments (Sherwin et al., 2003).

After a stabilization period, a tonic contraction was induced by 10^{-6} M Carbachol (CCh). The integrity of the tracheal epithelium was verified by the addition of arachidonic acid (AA) to the organ bath at the concentration of 10^{-4} M during the tonic phase of the first response induced by CCh. In this case, the rings that showed relaxation equal to or greater than 50% were considered with intact epithelium and relaxation equal to or less than 10% without epithelium [18]. The protocols used both the rings with and without the functional epithelium.

Effect of Spirulina platensis on Cumulative Contractions Induced by Carbachol

The procedures quoted in the previous item were followed by the preparation and assembly of the rat tracheal rings. After examination of the epithelium, the preparations were washed every 15 min for 30 min. After 30 min, a CCh-induced cumulative curve (10^{-9}–10^{-3} M) was performed in all groups for further comparison [18]. The contraction was expressed as the percentage of contraction induced by CCh. The negative logarithm of the drug concentration, which produced a half-maximal response (pEC50) value, was obtained from the concentration-response curves obtained on rings with and without functional epithelium of the saline solution or treated with *S. platensis* groups. The efficacy parameters were evaluated through maximum effect (Emax), also under the same conditions.

Effect of Spirulina platensis on Relaxation Induced by Aminophylline

After a stabilization time, a tonic contraction was induced with 10–6 M CCh, and aminophylline (AMF) ($10^{-10} \times 10^{-2}$ M), a non-selective phosphodiesterase inhibitor [19], was cumulatively added to the organ bath in the groups treated with saline solution or *S. platensis* to induce the relaxation of the preparation.

Relaxation was expressed as the reverse percentage of the contraction induced by CCh. The potency parameter was evaluated by pEC50 values from the concentration-response curves obtained in rings with and without functional epithelium of the groups treated with saline solution or *S. platensis*. The efficacy parameters were evaluated through Emax, also under the same conditions.

Evaluation of the prostanoid signaling pathway in the relaxing action of Spirulina platensis in rat trachea: Effect of Spirulina platensis on CCh-induced tonic contractions in the absence and presence of indomethacin.

After the procedures previously cited but before obtaining the CCh induced contraction in trachea rings with and without functional epithelium, 10^{-5} M indomethacin, a non-selective inhibitor of the enzyme cyclooxygenase (COX), was added in independent preparations (Juárez-Oropeza et al., 2009). To ensure the non-interference of prostanoids resulting from COX action, after 30 min, a cumulative curve to CCh (10^{-10}–10^{-3} M) was performed in the presence of indomethacin (INDO) in all groups for further comparison (Tschirhart et al., 1987).

The contraction values were expressed as the percentage of the contraction induced by CCh. The pEC50 values were compared in the absence and presence of indomethacin from the concentration-response curves obtained in the rings of the samples from groups treated with saline solution or *S. platensis*. The efficacy parameters were evaluated through Emax, also under the same conditions.

Biochemical Measurements

After the animals were euthanized, the blood was collected by cardiac puncture (Okafor et al., 2011) and placed in test tubes containing anticoagulant (EDTA) to obtain plasma for quantification of nitrite, malondialdehyde (MDA), and antioxidant activity (Ohkawa et al., 1979; Brand-Williams et al., 1995; Juárez-Oropeza et al., 2009). The samples were centrifuged at 1207 g for 15 min using a Centribio 80-2B-15 ML centrifuge (Guarulhos-SP, Brazil). The plasma was transferred to Eppendorf tubes and stored at -20°C until analysis. The trachea fragments 8 mm long were quickly removed, cleaned with Krebs solution to remove residual blood, and stored inside Eppendorf tubes in a freezer at -80°C until the analysis of the MDA markers, antioxidant activity, and nitrite.

Nitrite Assessment in Plasma and Trachea

Nitrite concentrations were determined by the Griess method as described by Green et al. (1982). Accordingly, the Griess reagent was prepared using equal parts of 5% phosphoric acid, 0.1% N-1-naphthyl ethylenediamine (NEED), 1% sulfanilamide in 5% phosphoric acid, and distilled water. Then, 500 µl volume of plasma or tissue macerate was added to 500 µl of Griess reagent, followed by absorbance reading at 532 nm after 10 min. The blank used was 100 µl of the reagent plus 100 µl of 10% potassium phosphate buffer. The sodium nitrite ($NaNO_2$) standards were made by twofold serial dilutions to obtain: 100, 50, 25, 12.5, 6.25, 3.12, and 1.56 mM solutions. A Biospectro SP-220

spectrophotometer (Curitiba-PR, Brazil) was used for absorbance readings.

Assessment of Lipid Peroxidation

To identify possible changes in the lipid matrix of cell membranes, which results from the indirect effect of the production of reactive oxygen species, we used the oxidant activity technique of measuring thiobarbituric acid reactive substances (TBARS) with lipid hydroperoxides (Okafor et al., 2011). For this, tissue samples (trachea and lung) were homogenized with 10% KCl in 1:1 proportion. Then, tissue homogenate and plasma samples (250 µl) were incubated in a water bath at 37°C for 60 min. After that, the samples were precipitated with 400 µl of 35% perchloric acid and centrifuged at 26,295 g for 10 min at 4°C. The supernatant was transferred to new Eppendorf tubes, and 400 µl of 0.6% thiobarbituric acid was added, followed by incubation at 95–100°C for 30 min. After cooling, the samples were read at 532 nm. MDA concentration in plasma and tissue samples was determined using an MDA standard curve constructed using a standard solution (1 µl of 1,1,3,3-tetramethoxypropane in 70 ml distilled water) diluted in a series of 250, 500, 750, 1000, 1250, 1500, 1750, 2000, 2,250, 2,500, 2,750 and 3,000 µl of distilled water. In the tissue, the absorbance values were normalized to the dry weight present in each sample volume.

Evaluation of Antioxidant Activity

This procedure was based on the method described by Brand-Williams et al. (1995), where 1.25 mg DPPH (2,2-diphenyl-1-picrylhydrazyl) were dissolved in 100 ml of ethanol, kept under refrigeration, and protected from light (aluminum paper or amber glass). Then, a volume of 3.9 ml of DPPH solution and 100 µl of the tissue homogenate or plasma was added to appropriate centrifuge tubes. The tubes were vortexed and allowed to stand for 30 min. They were centrifuged at 13,416 g at 20°C for 15 min, and the absorbance of the supernatant was read at 515 nm. The results were expressed as the percentage of the inhibition of oxidation, where: antioxidant activity (AOA) = 100 - ((DPPH • R) T/(DPPH • R) B 100), where (DPPH • R) and (DPPH • R) B correspond to the concentration of DPPH • remaining after 30 min, measured in the sample (T) and blank (B) prepared with distilled water.

Statistical Analysis

The functional results obtained were expressed as the mean and standard error of the mean (S.E.M.), while the biochemical results as mean and standard deviation (S.D.). These results were statistically analyzed using one-way analysis of variance (ANOVA) followed by Bonferroni's post-test, and the differences between the means were considered significant when $p < 0.05$. pEC50 values were calculated through non-linear regression (Neubig et al., 2003), and Emax was obtained by averaging the maximum percentages of contraction or relaxation. All results were analyzed with the GraphPad Prism® version 5.01 (GraphPad Software Inc., San Diego CA, United States).

RESULTS

Effect of supplementation with S. platensis on the contractile response induced by CCh in the presence of functional epithelium.

Among the healthy groups treated with S. platensis, the 500 mg/kg dose shifted the cumulative concentration-response curve of CCh to the right (pEC50 = 5.2 ± 0.06) compared to SG, SG50, and SG150 (pEC50 = 5.5 ± 0.03, 5.5 ± 0.06 and 5.7 ± 0.06, respectively) in the presence of epithelium (**Figure 1A**). Contractile response induced by CCh in rat trachea without functional epithelium did not change by the supplementation with *S. platensis* (**Figure 1B**).

Effect of supplementation with S. platensis on the relaxation induced by aminophylline.

The relaxing potency of aminophylline increased significantly when the healthy animals received supplementation with *S. platensis* at 150 (pEC50 = 5.0 ± 0.05) and 500 mg/kg (pEC50 = 5.9 ± 0.06) when compared to SG and SG50 (pEC50 = 4.5 ± 0.10 and 4.5 ± 0.02, respectively), but we did not observe changes in Emax (Figura 2A). The relaxing potency of aminophylline in rat trachea without functional epithelium also increased significantly for the group supplemented with S. platensis at 500 mg/kg when compared to healthy animals supplemented with S. platensis at doses of 50 and 150 mg/kg (pEC50 = 4.0 ± 0.04 vs. 3.4 ± 0.04, 3.4 ± 0.02, 3.3 ± 0.02, respectively) (**Figure 2B**).

Effect of supplementation with S. platensis on the cumulative contractions induced by CCh in the absence and presence of indomethacin.

In the presence of indomethacin (INDO), the cumulative concentration-response curve to CCh shifted to the left for the healthy animals supplemented with *S. platensis* at 150 and 500 mg/kg when compared to SG and SG50 in the presence of INDO (pEC50 = 6.3 ± 0.07 and 6.8 ± 0.11 vs. 5.7 ± 0.08 and 5.7 ± 0.08, respectively) (**Figure 3A**). The contractile response induced by CCh in rat trachea without functional epithelium did not change with supplemented with *S. platensis* in healthy animals in the presence of INDO (**Figure 3B**).

Effect of supplementation with S. platensis on nitrite production in plasma and trachea rings.

Nitrite concentration on plasma was higher with supplementation of *S. platensis* at all doses tested, 50, 150, and 500 mg/kg. Values increased from 54.0 ± 11.0 µM (SG) to 70.0 ± 7.0 (SG150) and 88.0 ± 7.0 µM (SG500) (**Figure 4A**). Analyzing the production of nitrite in the trachea, when comparing the healthy (34.0 ± 10.0 µM) and supplemented groups, we only observed the increase in nitrite levels in the group with supplementation of *S. platensis* at 500 mg/kg (54.0 ± 8.0 µM), also when compared to SG50 (37.0 ± 10.0 µM) and SG150 (38.0 ± 7.0 µM) (**Figure 4B**).

Effect of supplementation with S. platensis on MDA production in plasma, trachea rings, and lung.

The concentration of MDA in plasma was lower in healthy animals with supplementation of *S. platensis* at doses of 150 and 500 mg/kg. The values decreased from 8.3 ± 1.1 nmol/L (SG) to 6.8 ± 0.7 (SG150) and 5.0 ± 0.1 nmol/L (SG500) (**Figure 5A**). Furthermore, we observed a reduction in MDA production in the

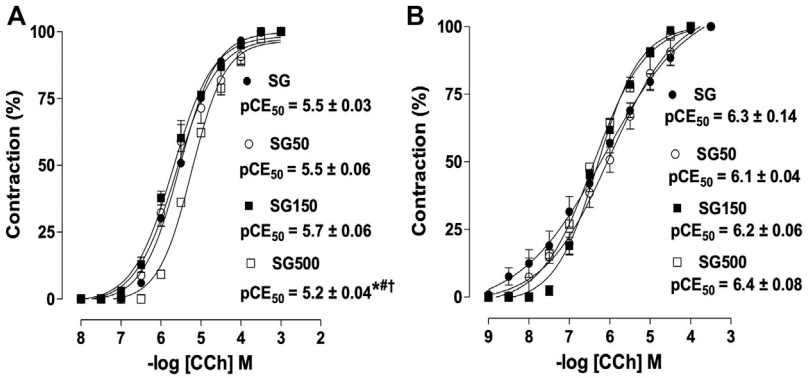

FIGURE 1 | Contractile effect of CCh in SG (●), SG50 (○), SG150 (■) and SG500 groups (.) in rat trachea in the presence **(A)** and absence of epithelium **(B)**. The symbols and vertical bars represent the mean and S.E.M., respectively (n = 5). One-way ANOVA followed by Bonferroni's post-test. *$p < 0.05$ (SG *vs.* SG500), $^{\#}p < 0.05$ (SG50 *vs.* SG500) and $^{\dagger}p < 0.05$ (SG150 *vs.* SG500). CCh = carbachol. Healthy saline group = SG. Healthy group supplemented with *S. platensis* at 50, 150 and 500 mg/kg = SG50, SG150 and SG500, respectively.

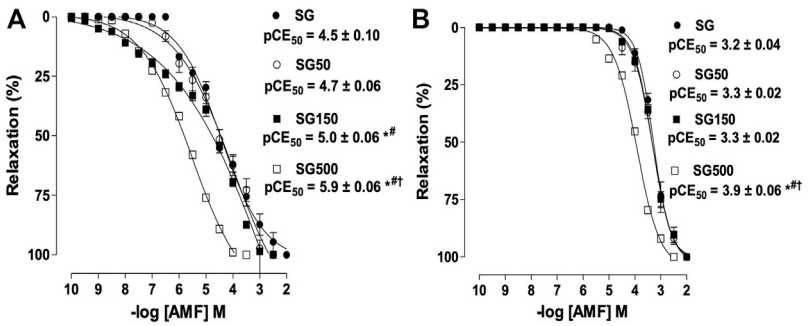

FIGURE 2 | The relaxant effect of AMF on the tonic contractions induced by CCh in SG (●), SG50 (○), SG150 (■) and SG500 groups (.) in rat trachea in the presence **(A)** and absence of epithelium **(B)**. The symbols and vertical bars represent the mean and S.E.M., respectively (n = 5). One-way ANOVA followed by Bonferroni's post-test. *$p < 0.05$ (SG *vs.* SG150 and SG500), $^{\#}p < 0.05$ (SG50 *vs.* SG150 and SG500) and $^{\dagger}p < 0.01$ (SG150 *vs.* SG500). AMF = aminophylline. Healthy saline group = SG. Healthy group supplemented with *S. platensis* at 50, 150 and 500 mg/kg = SG50, SG150 and SG500, respectively.

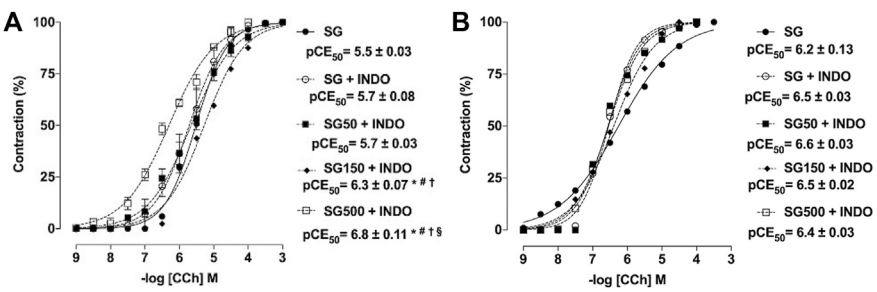

FIGURE 3 | Contractile effect of CCh in the absence SG (●) and presence of indomethacin in SG50 (fx1), SG50 (■) and SG150 (fx2) SG500 groups (fx3) in rat trachea in the presence **(A)** and absence of epithelium **(B)**. The symbols and vertical bars represent the mean and S.E.M., respectively (n = 5). One-way ANOVA followed by Bonferroni's post-test. *$p < 0.05$ (SG *vs.* SG150 + INDO and SG500 + INDO), $^{\#}p < 0.05$ (SG + INDO *vs.* SG150 + INDO and SG500 + INDO), $^{\dagger}p < 0.05$ (SG50 + INDO *vs.* SG150 + INDO and SG500 + INDO) and $^{\S}p < 0.05$ (SG150 + INDO *vs.* SG500 + INDO). INDO = indomethacin. Healthy saline group = SG. Healthy group supplemented with *S. platensis* at 50, 150 and 500 mg/kg = SG50, SG150 and SG500, respectively.

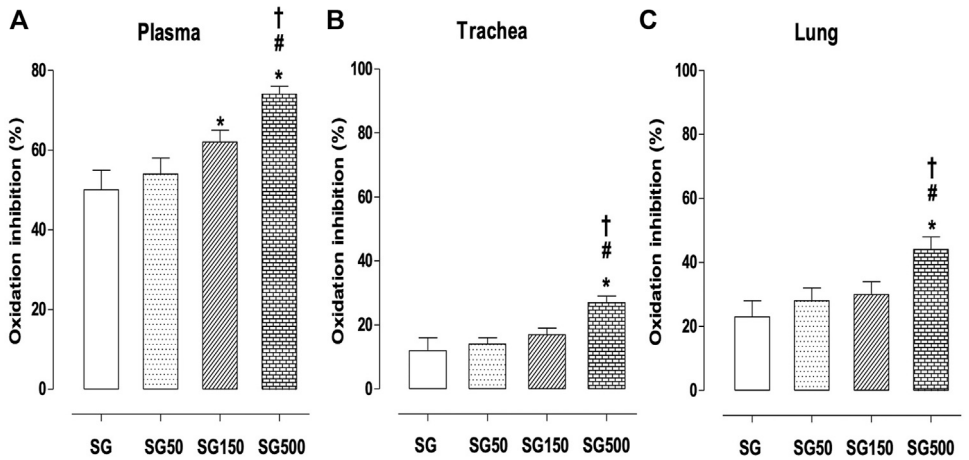

FIGURE 4 | Concentration of nitrite in blood plasma **(A)**, trachea **(B)** and lung **(C)** from SG (fx4), SG50 (fx5), SG150 (fx6), and SG500 groups (fx7). The columns and vertical bars represent the mean and S.D., respectively (n = 10). One-way ANOVA followed by Bonferroni's post-test. *$p < 0.05$ (SG *vs*. SG150 and SG500), #$p < 0.05$ (SG50 *vs.* SG500) and †$p < 0.05$ (SG150 *vs.* SG500). Healthy saline group = SG. Healthy group supplemented with *S. platensis* at 50, 150 and 500 mg/kg = SG50, SG150, and SG500, respectively.

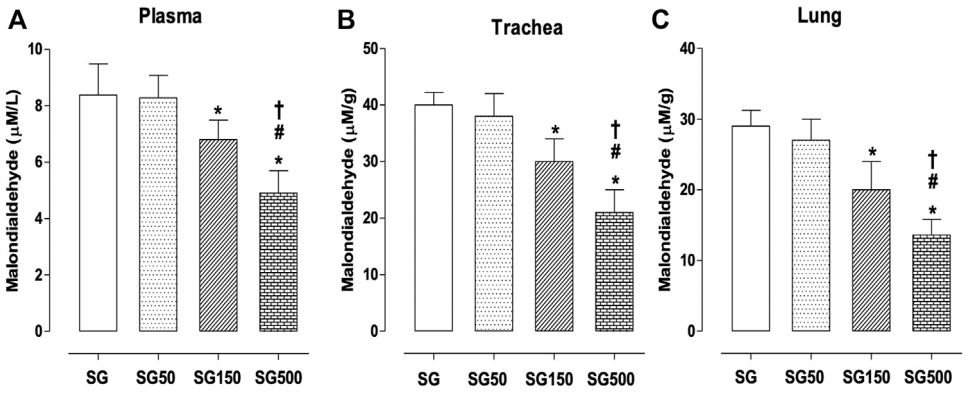

FIGURE 5 | Lipid peroxidation in blood plasma **(A)**, trachea **(B)**, and lung **(C)** from SG (fx4), SG50 (fx5), SG150 (fx6), and SG500 groups (fx7). The columns and vertical bars represent the mean and S.D., respectively (n = 10). One-way ANOVA followed by Bonferroni's post-test. *$p < 0.05$ (SG *vs*. SG150 and SG500), #$p < 0.05$ (SG50 *vs*. SG150 and SG500) and †$p < 0.05$ (SG150 *vs*. SG500). Healthy saline group = SG. Healthy group supplemented with *S. platensis* at 50, 150, and 500 mg/kg = SG50, SG150, and SG500, respectively.

trachea of rats that received supplementation with *S. platensis* at doses of 150 and 500 mg/kg. Values decreased from 40.0 ± 5.0 μM/g (SG) to 29.0 ± 4.0 (SG150) and 21.0 ± 4.0 μM/g (SG500) (**Figure 5B**). Similarly, in the lung, we found a decrease in MDA concentration when comparing SG (29.0 ± 5.0 μM/g) to SG150 (20.0 ± 4.0 μM/g) and SG500 (14.0 ± 2.0 μM/g) (**Figure 5C**).

Effect of supplementation with S. platensis on antioxidant activity in plasma, trachea rings, and lung.

In groups subjected to supplementation with *S. platensis* at doses of 150 and 500 mg/kg, we found a higher percentage of inhibition of plasma oxidation when compared to healthy animals. The values increased from 50.0 ± 5.0% (SG) to 62.0 ± 3.0 (SG150) and 74.0 ± 2.0% (SG500) (**Figure 6A**). In the trachea, the healthy animals showed an increased percentage of oxidation inhibition with the supplementation of *S. platensis* at 500 mg/kg. The values increased from 8.0 ± 4.0% (SG) to 26.0 ± 2.0% (SG500) (**Figure 6B**). Similarly, in the lung, we found an increase in oxidation inhibition when comparing SG (23.0 ± 7.0%) to SG150 (30.0 ± 3.0%) and SG500 (44.0 ± 2.0%) (**Figure 6C**).

DISCUSSION

In the present study, we tested the influence of different doses of Spirulina platensis on the tracheal reactivity of healthy animals. Our main findings are that the doses of 150 and 500 mg/kg of this cyanobacterium promote increase in tracheal rings relaxation. While the dose of 500 mg/kg promote a decrease in contractile

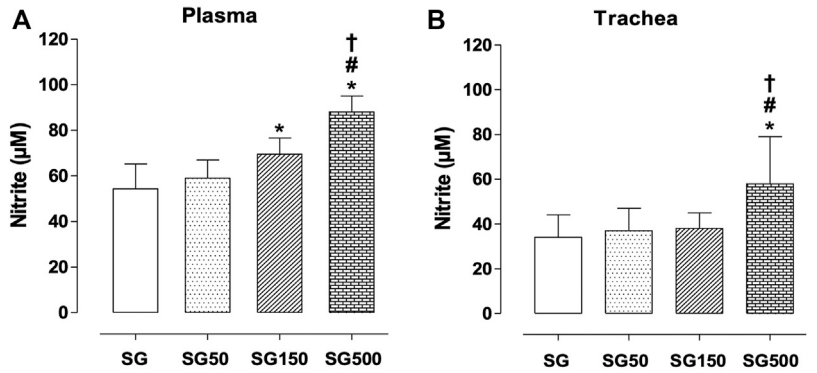

FIGURE 6 | Percentage of oxidation inhibition in blood plasma **(A)**, trachea **(B)** from SG (fx4), SG50 (fx5), SG150 (fx6), and SG500 groups (fx7). The columns and vertical bars represent the mean and S.D., respectively (n = 10). One-way ANOVA followed by Bonferroni's post-test. $^{*}p < 0.05$ (SG *vs*. SG150 and SG500), $^{\#}p < 0.05$ (SG50 *vs*. SG500) and $^{\dagger}p < 0.05$ (SG150 *vs*. SG500). Healthy saline group = SG. Healthy group supplemented with *S. platensis* at 50, 150, and 500 mg/kg = SG50, SG150, and SG500, respectively.

potency and an increase in tracheal rings relaxation. Indicating that in healthy animals higher doses are needed to promote prophylactic effects on physiological responses. In addition, there was a significant contribution of *S. platensis* in the increase in nitrite concentration and the decrease in oxidative stress.

Here, carbachol worked as an inducer of cumulative contraction curves in tracheal rings. The results obtained for the control group demonstrated pEC50 values similar to those verified in previous research by Brito et al. (2015) and Denis et al. (2001). Added to this, Albuquerque et al. (Albuquerque et al., 2016) report that the use of carbachol for contractions induction in tracheal rings was widely verified and accepted to study the reactivity of the trachea as a mimic of cholinergic stimulation.

Albuquerque et al. (2016) also reported that the contraction of trachea smooth muscle has similar mechanisms to those found in the smooth muscle of blood vessels. Thus, the association of agonists with G protein (heterotrimeric complex with α, β, and γ subunits) catalyzes the breakdown of phosphatidylinositol 4,5-bisphosphate resulting in the formation of two intracellular messengers: diacylglycerol and inositol 1,4,5-triphosphate, which promotes an intracellular release of calcium (Juárez-Oropeza et al., 2009). In contrast, the data in the literature have shown that *S. platensis* reduces the contractile potential of aortic rings (Juárez-Oropeza et al., 2009; Albuquerque et al., 2016). Briefly, Mascher et al. (2006) and Juárez-Oropeza et al. (2009) demonstrated that administration of *S. platensis*, in a dose-dependent manner and in obese animals, produced changes in vasomotor reactivity, which led to a decrease in the contractile response to phenylephrine and maximum stress and promoted dose-dependent relaxation in aortic rings. Both authors further suggest that, in addition to *S. platensis* being strongly related to the mechanisms of synthesis and release of nitric oxide by the endothelium in these rings, it also appears to inhibit the process of synthesis/release of a vasodilator dependent on the cyclooxygenase pathway.

From the research done by Mascher et al. (2006) and Juárez-Oropeza et al. (2009) it is noteworthy that the data result from investigations on aortic rings, while we are the pioneers in demonstrating that the tracheal rings of animals submitted to supplementation with *S. platensis* also present lower contractile potency and greater relaxation potential. Thus, the data presented in this investigation corroborate with those previously found but on different physiological systems.

In allergic diseases of the respiratory tract, it is well established in the literature that asthma and allergic rhinitis share the same physiological substrate: the trachea. Therefore, contractions in the smooth muscle of this region trigger different responses according to the disease, for the first one is bronchial hyperreactivity, while the second is upper airway obstruction (Fahy, 2015; Zhong et al., 2018). In this study, we verified the effectiveness of non-drug therapies, such as *Urtica dioica*, *Sambucus nigra*, and *Spirulina platensis*, in the prevention or treatment of contractile reactivity of the trachea (Ibrahim et al., 2013).

The literature shows that the contractile reactivity of the trachea in respiratory allergic diseases is accompanied by an increase in inflammatory markers such as interleukin-4 and -5 and tumor necrosis factor-α (TNF-α) (Joskova et al., 2013; Franova et al., 2016). However, until the present study, it was still not possible to identify whether *S. platensis* would also influence markers of vascular relaxation and oxidative stress such as nitric oxide and malondialdehyde, respectively, on tracheal rings in healthy animals. We based this hypothesis on the fact that C-phycocyanins, active ingredient of S. platensis, and natural dyes used in the pharmaceutical or nutritional industry (Abalde et al., 1998) selectively inhibit the activity of cyclooxygenase-2, the enzyme responsible for the production

of prostaglandins, in addition to their chemical structure possessing antioxidant property functioning as a scavenger of free radicals (Reddy et al., 2000). It was also observed that the high dose of S. platensis actually increased nitrite levels, and that despite it being a precursor to nitrosative stress, concomitantly for the same supplementation doses, we also identified a high rate of inhibition of oxidation in the trachea, ratifying the antioxidant power of Spirulina platensis. We, in this paper, demonstrated that S. platensis positively modulates the production of nitrite, which is the end product of nitric oxide metabolism, increases inhibition of oxidation, and reduces lipid peroxidation in tracheal rings.

The results of the present study confirm the beneficial effect of the frequent use of Spirulina platensis in the prevention of diseases of the respiratory system. As previously demonstrated, S. platensis has been used in humans' diets for many years as a food or supplement in the form of powders, beverages, or capsules (Appel et al., 2018); it received worldwide repercussion when the National Aeronautics and Space Administration (NASA) included it as part of the astronaut's diet both because of its nutritional composition, rich in proteins and minerals, and its anti-inflammatory and antioxidant effects (Karkos et al., 2011; Finamore et al., 2017). Therefore, considering the current scenario with a high incidence of diseases that can affect the respiratory system, having access to a food of ancient use with nutraceutical properties among different ethnic groups is extremely necessary. Despite these findings, it is important to emphasize that our research is a preclinical study. Making further investigation with Spirulina platensis necessary in models that analyze lung function, as well as in standardized models of asthma, is needed to confirm the benefit of algal supplementation on airway reactivity.

DATA AVAILABILITY STATEMENT

The raw data supporting the conclusions of this article will be made available by the authors, without undue reservation.

ETHICS STATEMENT

The animal study was reviewed and approved by The experimental protocol was previously approved by Ethics Committee in Animal Use from Biotechnology Center (CEUA/CBiotec) with certificate number 0511/13.

AUTHOR CONTRIBUTIONS

AB, AS and BS developed the hypothesis and experimental design. AB, IS and LA analyzed the data and wrote the manuscript. AB, IS and PF performed the experimental work. AS contributed to the *in vitro* work. IS and PF contributed to the *in vivo* work.

ACKNOWLEDGMENTS

The authors thank Coordenação de Aperfeiçoamento de Pessoal de Nível Superior (CAPES), Conselho Nacional de Desenvolvimento Científico e Tecnológico (CNPq) and Fundação de Apoio à Pesquisa do Estado da Paraíba (FAPESQ-PB) for their financial support and Federal University of Paraíba for structural support.

REFERENCES

Abalde, J., Betancourt, L., Torres, E., Cid, A., and Barwell, C. (1998). Purification and Characterization of Phycocyanin from the marine Cyanobacterium Synechococcus Sp. IO920. *Plant Sci.* 136, 109–120.

Albuquerque, A. A., Carvalho, M. T., Evora, P. M., de Nadai, T. R., Celotto, A. C., and Evora, P. R. (2016). *In Vitro* reactivity ("organ Chamber") of guinea Pig Tracheal Rings-Methodology Considerations. *Ann. Transl Med.* 4, 216. doi:10.21037/atm.2016.05.18

Appel, K., Munoz, E., Navarrete, C., Cruz-Teno, C., Biller, A., and Thiemann, E. (2018). Immunomodulatory and Inhibitory Effect of Immulina®, and Immunloges® in the Ig-E Mediated Activation of RBL-2H3 Cells. A New Role in Allergic Inflammatory Responses. *Plants (Basel)* 7 (1), 13. doi:10.3390/plants7010013

Araujo, L. C., Brito, A. F., Souza, I. L., Ferreira, P. B., Vasconcelos, L. H. C., Silva, A. S., et al. (2020). Spirulina Platensis Supplementation Coupled to Strength Exercise Improves Redox Balance and Reduces Intestinal Contractile Reactivity in Rat Ileum. *Mar. Drugs* 18 (2), 89. doi:10.3390/md18020089

Brand-Williams, W., Cuvelier, M. E., and Berset, C. (1995). Use of a Free Radical Method to Evaluate Antioxidant Activity. *LWT - Food Sci. Tech.* 28, 25–30. doi:10.1016/s0023-6438(95)80008-5

Brito, A. F., Silva, A. S., de Oliveira, C. V. C., de Souza, A. A., Ferreira, P. B., de Souza, I. L. L., et al. (2020). Spirulina Platensis Prevents Oxidative Stress and Inflammation Promoted by Strength Training in Rats: Dose-Response Relation Study. *Sci. Rep.* 10 (1), 6382. doi:10.1038/s41598-020-63272-5

Brito, A. F., Silva, A. S., de Souza, A. A., Ferreira, P. B., de Souza, I. L. L., Araujo, L. C. D. C., et al. (2018). Aortic Response to Strength Training and Spirulina Platensis Dependent on Nitric Oxide and Antioxidants. *Front. Physiol.* 9, 1522. doi:10.3389/fphys.2018.01522

Brito, A. F., Silva, A. S., Souza, I. L., Pereira, J. C., Martins, I. R., and Silva, B. A. (2015). Intensity of Swimming Exercise Influences Tracheal Reactivity in Rats. *J. Smooth Muscle Res.* 51, 70–81. doi:10.1540/jsmr.51.70

Brito, A. F., Silva, A. S., de Souza, A. A., Ferreira, P. B., de Souza, I. L. L., Araujo, L. C. D. C., et al. (2019). Supplementation with Spirulina Platensis Modulates Aortic Vascular Reactivity through Nitric Oxide and Antioxidant Activity. *Oxid Med. Cel Longev* 24, 7838149. doi:10.1155/2019/7838149

Chen, L. L., Zhang, S. F., Huang, D. N., Tan, J. Q., and He, S. H. (2005). Experimental Study of Spirulina Platensis in Treating Allergic Rhinitis in Rats. *Zhong Nan Da Xue Xue Bao Yi Xue Ban* 30 (1), 96–98.

de Souza, I. L. L., Ferreira, E. D. S., Diniz, A. F. A., Carvalho, M. T. L., Queiroga, F. R., Toscano, L. T., et al. (2018). Effects of Redox Disturbances on Intestinal Contractile Reactivity in Rats Fed with a Hypercaloric Diet. *Oxid Med. Cel Longev* 2018 (2018), 6364821. doi:10.1155/2018/6364821

Denis, D., Fayon, M. J., Berger, P., Molimard, M., De Lara, M. T., Roux, E., et al. (2001). Prolonged Moderate Hyperoxia Induces Hyperresponsiveness and Airway Inflammation in Newborn Rats. *Pediatr. Res.* 50 (4), 515–519. doi:10.1203/00006450-200110000-00015

Fahy, J. V. (2015). Type 2 Inflammation in Asthma-Ppresent in Most, Absent in many. *Nat. Rev. Immunol.* 15 (1), 57–65. doi:10.1038/nri3786

Finamore, A., Palmery, M., Bensehaila, S., and Peluso, I. (2017). Antioxidant, Immunomodulating, and Microbial-Modulating Activities of the Sustainable and Ecofriendly Spirulina. *Oxid. Med. Cel. Longev.* 2017, 3247528. doi:10.1155/2017/3247528

Franova, S., Kazimierova, I., Pappova, L., Joskova, M., Plank, L., and Sutovska, M. (2016). Bronchodilatory, Antitussive and Anti-inflammatory Effect of Morin in the Setting of Experimentally Induced Allergic Asthma. *J. Pharm. Pharmacol.* 68, 1064–1072. doi:10.1111/jphp.12576

Green, L. C., Wagner, D. A., Glogowski, J., Skipper, P. L., Wishnok, J. S., and Tannenbaum, S. R. (1982). Analysis of Nitrate, Nitrite, and [15N]nitrate in

Biological Fluids. *Anal. Biochem.* 126 (1), 131–138. doi:10.1016/0003-2697(82)90118-x

Ibrahim, S., Cemal, C., Fatih, O., Bahadir, B., and Seckin, U. (2013). Complementary Therapies in Allergic Rhinitis. *ISRN Allergy.* 2013, 938751. doi:10.1155/2013/938751

Joskova, M., Sadlonova, V., Nosalova, G., Novakova, E., and Franova, S. (2013). Polyphenols and Their Components in Experimental Allergic Asthma. *Adv. Exp. Med. Biol.* 756, 91–98. doi:10.1007/978-94-007-4549-0_12

Juárez-Oropeza, M. A., Mascher, D., Torres-Durán, P. V., Farias, J. M., and Paredes-Carbajal, M. C. (2009). Effects of Dietary Spirulina on Vascular Reactivity. *J. Med. Food* 12 (1), 15–20. doi:10.1089/jmf.2007.0713

Karkos, P. D., Leong, S. C., Karkos, C. D., Sivaji, N., and Assimakopoulos, D. A. (2011). Spirulina in Clinical Practice: Evidence-Based Human Applications. *Evid. Based Complement. Alternat Med.* 2011, 531053. doi:10.1093/ecam/nen058

Lambrecht, B. N., and Hammad, H. (2015). The Immunology of Asthma. *Nat. Immunol.* 16 (1), 45–56. doi:10.1038/ni.3049

Mascher, D., Paredes-Carbajal, M. C., Torres-Durán, P. V., Zamora-González, J., Díaz-Zagoya, J. C., and Juárez-Oropeza, M. A. (2006). Ethanolic Extract of Spirulina Maxima Alters the Vasomotor Reactivity of Aortic Rings from Obese Rats. *Arch. Med. Res.* 37 (371), 50–57. doi:10.1016/j.arcmed.2005.04.004

Matsuda, F., Sugahara, K., Sugita, M., Sadohara, T., Kiyota, T., and Terasaki, H. (2000). Comparative Effect of Amrinone, Aminophylline and Diltiazem on Rat Airway Smooth Muscle. *Acta Anaesthesiol Scand.* 44, 763–766. doi:10.1034/j.1399-6576.2000.440617.x

Montaño, L. M., Flores-Soto, E., Reyes-García, J., Díaz-Hernández, V., Carbajal-García, A., Campuzano-González, E., et al. (2018). Testosterone Induces Hyporesponsiveness by Interfering with IP3 Receptors in guinea Pig Airway Smooth Muscle. *Mol. Cel Endocrinol.* 473 (473), 17–30. doi:10.1016/j.mce.2017.12.010

Nourollahian, M., Rasoulian, B., Gafari, A., Anoushiravani, M., Jabari, F., and Bakhshaee, M. (2020). Clinical Comparison of the Efficacy of Spirulina Platensis and Cetirizine for Treatment of Allergic Rhinitis. *Acta Otorhinolaryngol. Ital.* 40, 224–229. doi:10.14639/0392-100X-N0139

Ohkawa, H., Ohishi, N., and Yagi, K. (1979). Assay for Lipid Peroxides in Animal Tissues by Thiobarbituric Acid Reaction. *Anal. Biochem.* 95, 351–358. doi:10.1016/0003-2697(79)90738-3

Okafor, O. Y., Erukainure, Ol., Ajiboye, J. A., Adejobi, R. O., Owolabi, F. O., and Kosoko, S. B. (2011). Modulatory Effect of Pineapple Peel Extract on Lipid Peroxidation, Catalase Activity and Hepatic Biomarker Levels in Blood Plasma of Alcohol-Induced Oxidative Stressed Rats. *Asian Pac. J. Trop. Biomed.* 1, 12–14. doi:10.1016/S2221-1691(11)60060-9

Reddy, C. M., Bhat, V. B., Kiranmai, G., Reddy, M. N., Reddanna, P., and Madyastha, K. M. (2000). Selective Inhibition of Cyclooxygenase-2 by C-Phycocyanin, a Biliprotein from Spirulina Platensis. *Biochem. Biophys. Res. Commun.* 277, 599–603. doi:10.1006/bbrc.2000.3725

Revuelta, M. P., Cantabrana, B., and Hidalgo, A. (1997). Depolarization-dependent Effect of Flavonoids in Rat Uterine Smooth Muscle Contraction Elicited by CaCl2. *Gen. Pharmacol.* 29 (5), 847–857. doi:10.1016/s0306-3623(97)00002-5

Tschirhart, E., Frossard, N., Bertrand, C., and Landry, Y. (1987). Arachidonic Acid Metabolites and Airway Epithelium-dependent Relaxant Factor. *J. Pharmacol. Exp. Ther.* 243, 310–316.

Zhong, J., Lai, D., Zheng, Y., and Li, G. (2018). Ma-Huang-Fu-Zi-Xi-Xin Decoction for Allergic Rhinitis: A Systematic ReviewDecoction for Allergic Rhinitis: A Systematic Review. *Evid. Based Complement. Alternat Medevid Based Complement. Alternat Med.* 2018 (2018), 8132798. doi:10.1155/2021/354874010.1155/2018/8132798

Conflict of Interest: The authors declare that the research was conducted in the absence of any commercial or financial relationships that could be construed as a potential conflict of interest.

Publisher's Note: All claims expressed in this article are solely those of the authors and do not necessarily represent those of their affiliated organizations, or those of the publisher, the editors, and the reviewers. Any product that may be evaluated in this article, or claim that may be made by its manufacturer, is not guaranteed or endorsed by the publisher.

frontiers | Frontiers in Pharmacology

ORIGINAL RESEARCH
published: 01 June 2022
doi: 10.3389/fphar.2022.916508

Chloroquine Attenuates Asthma Development by Restoring Airway Smooth Muscle Cell Phenotype *Via* the ROS-AKT Pathway

Yan Ren[1,2†], *Xiuhua Zhong*[1†], *Hongyu Wang*[1], *Zhongqi Chen*[1], *Yanan Liu*[1,3], *Xiaoning Zeng*[1*] *and Yuan Ma*[1*]

[1]*Department of Respiratory and Critical Care Medicine, The First Affiliated Hospital of Nanjing Medical University, Nanjing, China,* [2]*Department of Medical Genetics, Nanjing University School of Medicine, Nanjing, China,* [3]*Department of Respiratory and Critical Care Medicine, Affiliated Hospital of Xuzhou Medical University, Xuzhou, China*

OPEN ACCESS

Edited by:
Arunachalam Karuppusamy, Chinese Academy of Sciences (CAS), China

Reviewed by:
Fangzhou Teng, Fudan University, China
Yap Hui Min, Putra Malaysia University, Malaysia

***Correspondence:**
Xiaoning Zeng
zeng_xiao_ning@hotmail.com
Yuan Ma
mayuan@njmu.edu.cn

[†]*These authors have contributed equally to this work*

Specialty section:
This article was submitted to Respiratory Pharmacology, a section of the journal Frontiers in Pharmacology

Received: *09 April 2022*
Accepted: *18 May 2022*
Published: *01 June 2022*

Citation:
Ren Y, Zhong X, Wang H, Chen Z, Liu Y, Zeng X and Ma Y (2022) Chloroquine Attenuates Asthma Development by Restoring Airway Smooth Muscle Cell Phenotype Via the ROS-AKT Pathway. Front. Pharmacol. 13:916508. doi: 10.3389/fphar.2022.916508

Switching of airway smooth muscle (ASM) cell phenotype from differentiated-contractile to dedifferentiated-proliferative/synthetic state often occurs in asthmatic subjects with airway dysfunction. Evidence has been provided that chloroquine (an agonist of bitter taste receptors) presented benefits to ASM cell function implicated in asthma. However, the underlying mechanism is unclear. House dust mite (HDM)-sensitized mice were administered with chloroquine or dexamethasone before challenge. BALF and lung tissue were obtained for cell counting, histological analysis or ELISA. Primary cultured ASM cells were stimulated with transforming growth factor (TGF)-β1 or H_2O_2. Cells and supernatant were collected for the detection of ASM phenotype, ROS level, and proinflammatory cytokine production. In HDM-sensitized mice, chloroquine attenuated airway hyperresponsiveness (AHR), inflammation and remodeling with an inhibition of immunoglobulin E, IL-4/-13, and TGF-β1 in BALF. ASM cell proliferation (PCNA), hypertrophy (α-SMA), and parasecretion (MMP-9 and MMP-13) were strongly suppressed by chloroquine, hinting the rebalance of the heterogeneous ASM populations in asthmatic airway. Our data *in vitro* indicated that chloroquine markedly restrained maladaptive alteration in ASM phenotype in concert with a remission of ROS. Using H_2O_2 and PI3K inhibitor (LY294002), we found that the inhibition of oxidative stress level and ROS-AKT signal by chloroquine may serve as a potential mechanism that dedicates to the restoration of the phenotypic imbalance in ASM cells. Overall, the present findings suggested that chloroquine improves asthmatic airway function by controlling ASM cell phenotype shift, sketching a novel profile of chloroquine as a new therapeutic candidate for airway remodeling.

Keywords: chloroquine, airway smooth muscle (ASM) cells, bitter taste receptors (TAS2Rs), TGF-β1, asthma

INTRODUCTION

As the major characteristic of asthma (Al-Muhsen et al., 2011), airway remodeling encompasses a range of events such as alterations in airway smooth muscle (ASM), which definitively determine the severity and outcome of the disease (Zhang and Li, 2011). ASM cells retain a remarkable phenotypic plasticity. Insults such as infection, allergens and environmental factors can alter the profile of ASM cells from a differentiated and quiescent "contractile" state to a dedifferentiated and

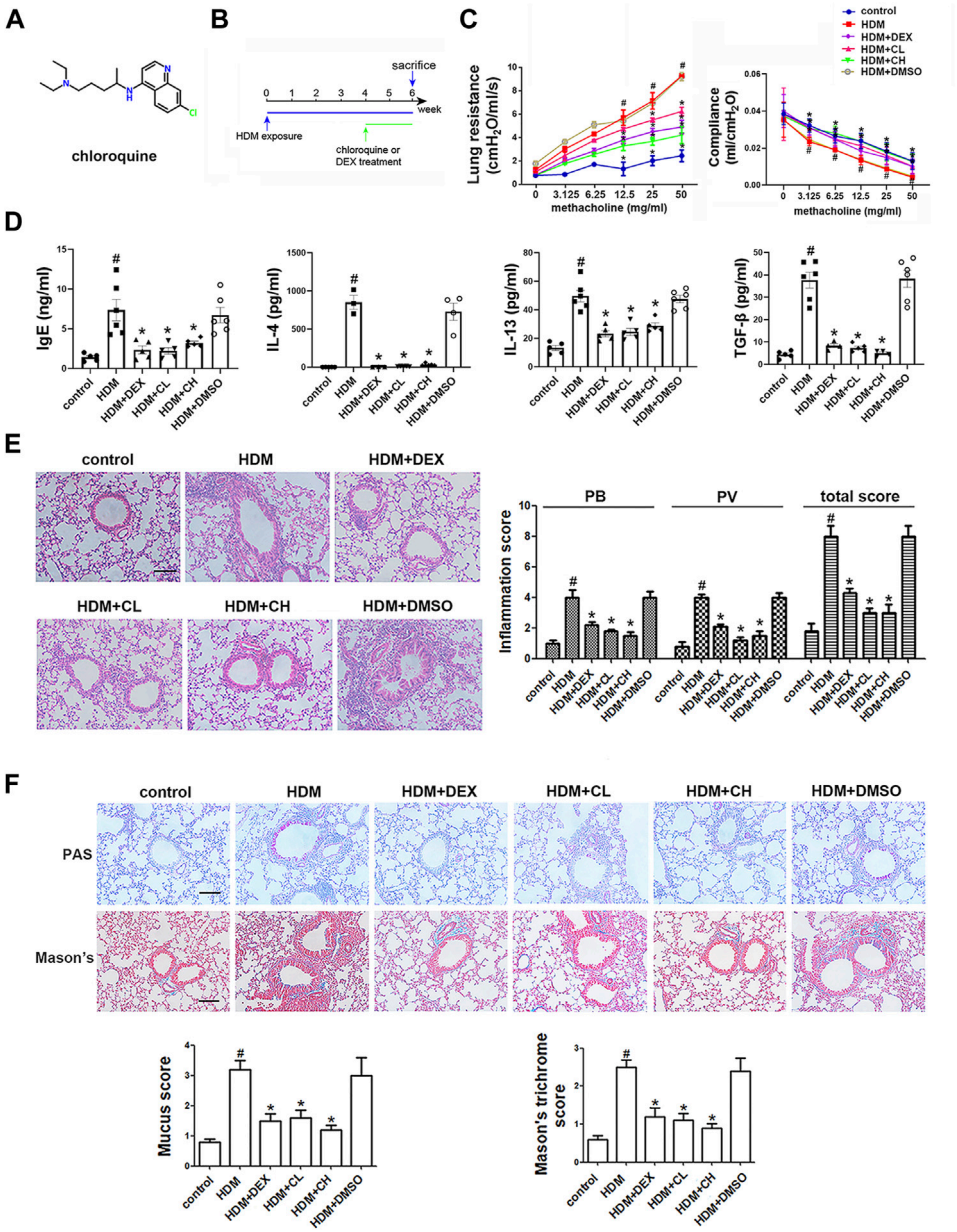

FIGURE 1 | Chemical structure of chloroquine and experimental protocol for the chronic asthma model. Treatment with chloroquine alleviated AHR, ameliorated lung dynamic compliance, decreased the levels of IgE, Th2 cytokines, and TGF-β1 in BALF, and inhibited inflammatory cell infiltration, goblet cell hyperplasia, collagen deposition in lung **(A)** Chemical structure of chloroquine **(B)** Brief scheme of HDM sensitization and challenge **(C)** Increasing inhaled doses of methacholine (3.125–50 mg/ml), lung resistance and dynamic compliance in mice **(D)** The concentrations of HDM-specific IgE, IL-4, IL-13, and TGF-β1 were measured by ELISA **(E)** Lung sections were stained with H&E to analyze the infiltration of inflammatory cells (magnification, ×400; scale bar, 50 μm). Layers of inflammatory cells were counted, and the total inflammation score was summed with the peribronchial (PB) and perivascular (PV) inflammation scores **(F)** Lung sections were stained with PAS to assess goblet cell hyperplasia and Masson's trichrome to evaluate the subepithelial deposition of collagen and fibrosis (magnification, ×400; scale bar, 50 μm). PAS-positive and PAS-negative epithelial cells were counted, and the percentage of PAS-positive cells per bronchiole was calculated. Masson's trichrome staining analysis of collagen deposition was calculated. Values are the mean ± SEM ($n = 6$ per group). #$p < 0.05$ compared with the control group, and *$p < 0.05$ compared with the HDM group.

proliferative "synthetic" state (Liu et al., 2015). The "synthetic" ASM cells involve features such as cell hypertrophy, hyperplasia and parasecretion, which contribute to the persistent AHR, irreversible airway obstruction, and exacerbation of inflammation. Hence, a "vicious cycle" occurs. Many strategies have been developed for asthma management, but few proved effective in stopping "the remodeling clock". Therefore, an urgent need for the development of new therapeutic options targeting airway remodeling has been brought into schedule.

Bitter taste receptors (TAS2Rs) were originally found to be expressed in tongue, responsible for our perception of bitter taste. However, they are also found recently in other tissues including ASM cells which might play a key role in airway remodeling. An upregulation of TAS2Rs was detected in those children with severe asthma. And inhaled bitter tastants helped to decrease the obstruction of asthmatic airway (Deshpande et al., 2010; Pulkkinen et al., 2012). Activation of TAS2Rs by chloroquine and denatonium has been proved to be able to cause the relaxation of ASM (Deshpande et al., 2010; Pulkkinen et al., 2012) and inhibit the secretion of proinflammatory cytokines (Orsmark-Pietras et al., 2013). All these findings suggest TAS2Rs as the potential targets for the management of ASM cell function and open up new avenues for asthma treatment.

Chloroquine (N4-(7-chloroquineolin-4-yl)-1N,N1-diethylpentane-1,4-diamine) (**Figure 1A**) has been proposed as a classic TAS2Rs agonist in digestive system and respiratory system. It was revealed that chloroquine could lead to relaxation of precontracted airways (Becker et al., 1984; Colacone et al., 1990; Kivity et al., 1990; Grassin-Delyle et al., 2015), as well as inhibition of ASM cell growth and cytokine production (Orsmark-Pietras et al., 2013; Ekoff et al., 2014). Although TAS2Rs have got growing attention in respiratory diseases, the actual effects of chloroquine on ASM cells and the precise mechanism involved in asthma have not been clarified.

In this study, the house dust mite (HDM) model was established to illustrate the impacts of chloroquine during asthma progressing. With an emphasis on the modulation of cellular phenotypes, an *in vitro* model of human ASM cells stimulated with TGF-β1 was used to elucidate the underlying mechanism involved.

MATERIALS AND METHODS

Animals

Thirty-six specific pathogen-free female BALB/c mice (18–22 g) aged 6–8 weeks were obtained from the Animal Core Facility of Nanjing Medical University (Nanjing, China). The mice were maintained in a temperature-controlled room under a 12-h dark/12-h light cycle and provided food and water. All experiments involving animal and tissue samples were performed in accordance with the guidelines established by the National Institutes of Health and Nanjing Medical University, and all of the procedures were approved by the Institutional Animal Care and Use Committee of Nanjing Medical University (Nanjing, China). The BALB/c mice were randomly divided into the six groups: control group; HDM group, treated with HDM (Greer Laboratories, Lenoir, NC, United States); HDM + CL group, treated with HDM and 1 mg/kg chloroquine (Sigma-Aldrich, St. Louis, MO, United States); HDM + CH group, treated with HDM and 5 mg/kg chloroquine; HDM + dexamethasone group, treated with HDM and 1 mg/kg DEX (Sigma-Aldrich); and HDM + DMSO group, treated with HDM and 0.5% dimethyl sulfoxide (DMSO, Sigma-Aldrich). The mice received intranasal droplets containing the purified HDM extract [25 μg of protein solubilized in 25 μL of phosphate-buffered saline (PBS)] for 5 days/week for up to six consecutive weeks. During the last 2 weeks of the HDM treatment, the mice were intraperitoneally administered chloroquine, DEX or vehicle (DMSO) 1 h prior to the HDM challenge. All treatments were administered under isoflurane anesthesia and ended 24 h before sacrifice. Bronchoalveolar lavage fluid (BALF) and lung tissues were collected for analyses (**Figure 1B**).

Measurement and Analysis of Airway Responsiveness

The lung function was evaluated from direct measurements of lung resistance and dynamic compliance in restrained, tracheostomized, mechanically ventilated mice using the FinePointe RC system (Buxco Research Systems, Wilmington, NC, United States) under general anesthesia as described previously (Kerzerho et al., 2013).

BALF Collection and Test

The tracheae were exposed, and BALF was collected *via* lavage with ice-cold PBS (400 μL × 3; 85–90% of the lavage volume was recovered) using a tracheal catheter. The lavage samples from each mouse were centrifuged at 1000 rpm at 4°C for 10 min. The supernatant was collected, divided into four equal portions and frozen at −80°C for enzyme-linked immunosorbent assay (ELISA).

Lung Histology

BALF samples were obtained, and the left lung was immersed in 4% paraformaldehyde and then embedded in paraffin. A series of microsections (5 μm) were cut using a microtome and stained with hematoxylin and eosin (H&E) for assessments of inflammatory cell infiltration. An inflammation score was determined as follows: grade 0, no inflammation; grade 1, occasional cuffing with inflammatory cells; and grades 2, 3, and 4, most bronchi or vessels surrounded by a thin layer (1–2 cells), a moderate layer (3–5 cells), or a thick layer (>5 cells) of inflammatory cells, respectively. The total inflammation score was calculated by the addition of the peribronchial (PB) and perivascular (PV) inflammation scores. Periodic acid-Schiff (PAS) staining was used for the quantification of airway goblet cells, and Masson's trichrome staining was used for the visualization of collagen deposition and fibrosis. Both staining methods were scored as follows: 0, none; 1, <25%; 2, 25–50%; 3, 50–75%; and 4, >75% goblet cells (Ma et al., 2016). The sections were also immunohistochemically stained for matrix metalloproteinase (MMP)-9, MMP-13, proliferating cell

nuclear antigen (PCNA) and alpha-smooth muscle actin (α-SMA). For the semiquantitative evaluation of the expression of MMP-9, MMP-13, PCNA and α-SMA, the IOD of the results was analyzed using Image-Pro Plus 6.0 software. The mean percentages of positive epithelial cells in the bronchi were determined in at least five areas at ×400 magnification and assigned to one of the following categories: 0, <5%; 1, 5–25%; 2, 25–50%; 3, 50–75%; and 4, >75% (Ma et al., 2016). The immunostaining intensities of MMP-9, MMP-13, PCNA and α-SMA were scored as 1+ (weak), 2+ (moderate) or 3+ (intense). The percentage of positive epithelial cells and the staining intensities were multiplied to yield a weighted score for each case. Two independent observers who were blinded to the experiment calculated all of the scores, and at least three different fields of each lung section were examined.

In situ Detection of ROS

The *in situ* production of ROS in frozen sections was evaluated microscopically using dihydroethidium (DHE) (Beyotime Institute of Biotechnology, Jinan, Shandong, China) (Boldogh et al., 2005). Briefly, snap-frozen lung tissue samples were embedded in Tissue-Tek OCT compound, cryosectioned at 7 mm, allowed to air-dry at room temperature, and stored at -80°C until needed. The slides were placed in PBS for 30 min at room temperature and stained with DHE (10 mm) in PBS for 30 min in a moist chamber in the dark. The slides were rinsed extensively with PBS, covered with a coverslip, and imaged using a fluorescence microscope (Zeiss LSM 5 LIVE, Germany). The DHE fluorescence was quantified by averaging the mean value of the fluorescence intensity using Image-Pro Plus 6.0. Four sections from each mouse were analyzed using this procedure, and the mean value of the fluorescence was calculated.

Culture and Treatment of Normal Human ASM Cells

Normal human ASM cells were purchased from ScienCell Research Laboratories (Carlsbad, CA, United States) and cultured at 37°C in the presence of 5% CO_2 in smooth muscle cell medium (ScienCell) supplemented with 20 U/l penicillin, 20 μg/ml streptomycin, 1% smooth muscle cell growth supplement and 2% fetal bovine serum (ScienCell). Cells between passages four and eight were used for the experiments. After serum starvation for 6–8 h (**Supplementary Figure S1**), the ASM cells were stimulated with 5 ng/ml TGF-β1 (Peprotech) or H_2O_2 (20 μm, Sigma-Aldrich) alone or in combination with chloroquine (10 μm) or N-acetylcysteine (NAC, 10 mm, Sigma-Aldrich) or LY294002 (10 μm, Sigma-Aldrich). The cells were further cultured for the indicated durations.

Lactate Dehydrogenase Release Assay

LDH assay (Jiancheng, Nanjing, China) was adopted to determine the cytotoxicity of chloroquine in ASM cells. As previously described, ASM cells were planted at a density of 5×10^3 per well in a 96-well plate and treated with chloroquine for 48 h. Then the supernatant was centrifuged and transferred to be mixed with matrix buffer and coenzyme I application solution. After incubation with 2,4-dinitrophenylhydrazine, 0.4 M NaOH was added into the system to terminate the reaction. The release of LDH from ASM cells was then evaluated by colorimetric assay with a microplate reader (CANY, Shanghai, China) at 450 nm. Each sample was tested in triplicate.

Cell Viability Assay

The proliferation of ASM cells was determined using cell counting kits (CCK)-8 and 5-ethynyl-2′-deoxyuridine (EdU) assays. The ASM cells were cultured in a 96-well plate at a density of 5×10^3 cells per well and treated with TGF-β1 and chloroquine at concentrations from 0.1 to 100 μm for 48 h. The CCK-8 solution (Dojindo Molecular Technologies, Inc. Kumamoto, Japan) was added to the cell culture medium at a dilution of 1:10, and the cultures were incubated for another 1–2 h at 37°C. The absorbance at 450 nm (A450) was measured using a microplate reader (CANY, Shanghai, China). For the EdU assay, the ASM cells were cultured using the aforementioned procedure. After 48 h of treatment, the cells were labelled using an EdU assay kit (Ribobio, Guangzhou, China) according to the manufacturer's instructions. Images were obtained using a fluorescence microscope (Olympus IX71, Japan). Each sample was measured in triplicate.

Transmission Electron Microscopy

ASM cell phenotype was observed using TEM. The ASM cell culture medium was discarded, and the cells were fixed with an electron microscope fixative solution at 4°C for 2 h. The ASM cells were centrifuged at low speed, wrapped with 1% agarose, and rinsed with 0.1 M PBS. The cells were fixed with 1% osmium acid at room temperature for 2 h, rinsed with 0.1 M PBS, and dehydrated using an alcohol and acetone gradient for 15 min. The mixture was subsequently combined with acetone and the embedding agent at a ratio of 1:1, infiltrated for 2–4 h, mixed with acetone and the embedding agent at a ratio of 1:2, infiltrated overnight, treated with the pure embedding agent for 5–8 h, poured into an embedding plate and placed overnight in an oven at 37°C. After penetration, the plate was heated in an oven at 60°C for 48 h for polymerization. Ultrathin slices (60–80 nm) were obtained using a tissue slicer. After double staining with uranium (alcohol solution saturated with 2% uranyl acetate, 15 min) and lead (lead citrate, 15 min), the sections were dried overnight at room temperature and observed and analyzed using TEM.

Enzyme-Linked Immunosorbent Assay

To examine the effects of chloroquine on airway inflammation and the microenvironment *in vitro*, the levels of interleukin-8 (IL-8), monocyte chemoattractant protein-1 (MCP-1), soluble intercellular adhesion molecule-1 (ICAM-1), vascular endothelial growth factor (VEGF, R&D Systems, Minneapolis, MN, United States) and isoprostane-8 (IP-8) (Senbeijia Corp. Nanjing, China) were measured. The ASM cells were cultured using the aforementioned procedure. After starvation in serum-free medium, the cells were stimulated with TGF-β1 or H_2O_2

alone or in combination with chloroquine or NAC for 6–8 h and then subjected to ELISA. The level of HDM-specific immunoglobulin E (IgE, Chondrex, Inc. Redmond, WA, United States) in the serum and the levels of TGF-β1, IL-4, and IL-13 (R&D Systems) in the BALF of the mice were also measured using ELISA according to the manufacturer's instructions.

Determination of Malondialdehyde Level

The MDA levels in the cell culture medium were determined using the thiobarbituric acid reacting substances (TBARS) assay (Senbeijia Corp. Nanjing, China) as previously described (Ma et al., 2016). MDA reacts with thiobarbituric acid under acidic conditions at 95°C to form a pink-colored complex that can be measured at 532 nm, and 1,3,3-tetra ethoxy propane (TEP) was used as a standard.

Determination of Intracellular ROS Production

The intracellular ROS level was measured using the 2′,7′-dichlorofluorescin diacetate (DCFH-DA, Sigma-Aldrich) assay. Briefly, 1.5×10^4 ASM cells were seeded into each well of a six-well plate and cultured for 24 h. The cells were then divided into four groups: control group; TGF-β group, treated with 5 ng/ml TGF-β1; TGF-β+C group, treated with 5 ng/ml TGF-β1 and 5 μm chloroquine; and C group, treated with 5 μm chloroquine. The cells were then cultured for an additional 24 h and incubated with 10 μm DCFH-DA for 30 min at 37°C in the dark. The cells were subsequently washed twice with PBS and analyzed within 30 min using a FACScan instrument (Becton Dickinson, San Jose, CA, United States) with an excitation setting of 488 nm. The specific fluorescence signals corresponding to DCFH-DA were determined using a 525-nm bandpass filter.

Western Blot Analysis

The cells were homogenized and lysed in RIPA buffer (Sigma-Aldrich) supplemented with a protease inhibitor and a phosphatase inhibitor (Selleck). Equal amounts of proteins were separated using 10% SDS-PAGE. After electrophoresis, the separated proteins were transferred to polyvinylidene difluoride membranes (Millipore, Billerica, MA, United States) using the wet transfer method. Nonspecific sites were blocked with 5% nonfat milk in TBS Tween 20 [TBST; 25 mm Tris (pH 7.5), 150 mm NaCl, and 0.1% Tween 20] for 2 h, and the blots were incubated with primary antibodies (Cell Signaling Technology, Inc.), including β-actin, anti-phospho-protein kinase B (AKT), anti-AKT, α-SMA, fibronectin and collagen I antibodies overnight at 4°C. Goat anti-rabbit horseradish peroxidase-conjugated IgG (Cell Signaling Technology, Inc.) was used for the detection of antibody binding. The membranes were treated with enhanced chemiluminescence system reagents (Thermo), and the binding of specific antibodies was visualized using a Bio-Rad Gel Doc/ChemiDoc Imaging System and analyzed using Quantity One software.

Statistical Analysis

The data are expressed as the means ± standard errors of the mean (SEM). All of the tests were performed using Prism 6.00 (GraphPad Software, San Diego, CA, United States) and SPSS version 20 (SPSS, Inc. Chicago, IL, United States). To determine the differences between multiple groups, the results were analyzed using one-way analysis of variance for repeated measures followed by Dunnett's post hoc test. The significance level was set to $p < 0.05$.

RESULTS

Chloroquine Relieves AHR and HDM-specific IgE

In this study, HDM was used to establish a mouse model of asthma, and chloroquine-mediated alleviation of asthma was examined (**Figure 1B**; **Supplementary Figure S2**). Our results showed that chloroquine protected lungs from HDM-induced AHR (as assessed by reduced lung resistance) and preserved lung function (as assessed by increased dynamic compliance) (**Figure 1C**; **Supplementary Figure S3**; **Supplementary Video S1**). A high level of IgE is well established as a feature of asthma. After the sensitization and challenge, HDM-specific IgE level in the BALF was significantly elevated in the HDM and HDM + DMSO groups, and the administration of chloroquine and DEX abolished this increase (**Figure 1D**). These findings indicated that the asthma model was successful and chloroquine alleviated AHR and HDM-specific IgE level.

Chloroquine Inhibits Airway Inflammation, Goblet Cell Proliferation and Collagen Deposition/Fibrosis

Extensive infiltration of inflammatory cells was observed around the respiratory tracts and vessels in the HDM and HDM + DMSO groups (**Figure 1E**), which indicated that the HDM and HDM + DMSO groups exhibited more severe airway inflammatory responses than the control group. Similarly, airway challenge with HDM notably increased IL-4 and IL-13 levels in the BALF. The administration of chloroquine dose-dependently reduced the IL-4 and IL-13 levels in the BALF compared to the levels in the HDM group (**Figure 1D**). To evaluate the extent of goblet cell and mucus production, the lung sections were stained with PAS, and the percentage of PAS-positive cells in the airway epithelium was determined. We found that the HDM-challenged mice developed marked goblet cell hyperplasia and mucus hypersecretion in the lumen of the bronchioles (**Figure 1F**). The mice treated with DEX and high doses of chloroquine had fewer goblet cells in the airway epithelium and reduced mucus scores of 1.5 ± 0.24 and 1.2 ± 0.15 ($p < 0.05$), respectively. The area of collagen deposition/fibrosis was assessed using Masson's trichrome staining, and this analysis revealed that the extent of collagen deposition/fibrosis was profoundly enhanced over the interstitia of the airways and vessels of tissues of the HDM-challenged mice compared to the control mice (**Figure 1F**). The administration of 5 mg/kg chloroquine significantly ameliorated these serious

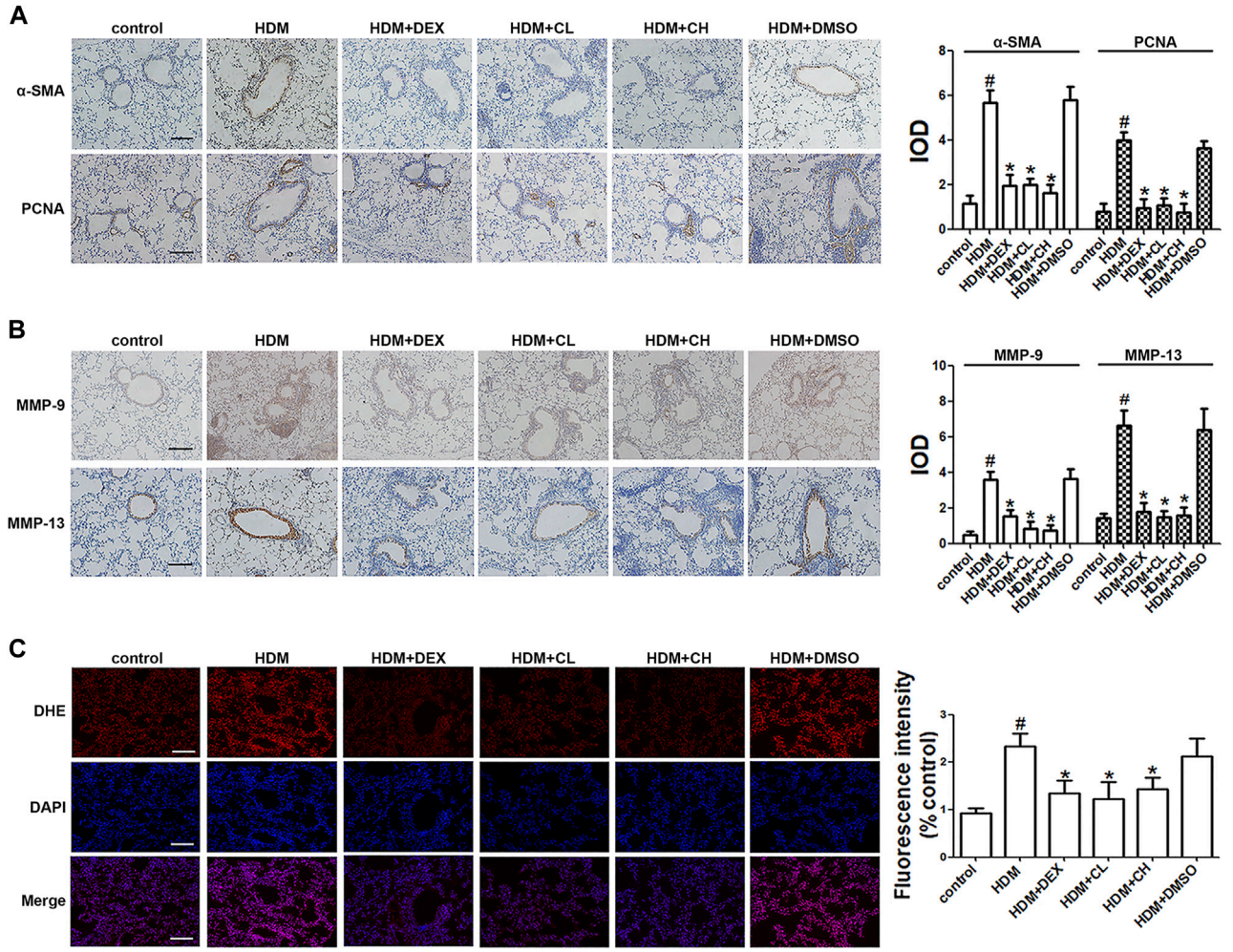

FIGURE 2 | Treatment with chloroquine inhibited the expression of α-SMA, PCNA, MMP-9, MMP-13, and in situ ROS levels in lung tissue **(A,B)** Immunohistochemical staining was performed to assess the distribution of α-SMA, PCNA, MMP-9, and MMP-13 (magnification, ×400; scale bar, 50 μm), and their expression was evaluated, respectively. The staining scores were multiplied by the percentage of positive epithelial cells and staining intensity scores **(C)** Frozen lung sections were stained with DHE, imaged and analyzed by Image-Pro Plus 6.0. The fluorescence values were expressed as the ratio to the levels in the control cells. Values are the mean ± SEM (n = 6 per group). #p < 0.05 compared with the control group, and *p < 0.05 compared with the HDM group.

pathophysiological changes, which resulted in a score of 1.1 ± 0.12 (p < 0.05), and modest effects were observed with the administration of DEX and low doses of chloroquine. These findings indicated that chloroquine inhibited airway inflammation, goblet cell proliferation and collagen deposition/fibrosis in the HDM-induced asthma model.

Chloroquine Decreases the Levels of Proliferation-Associated Proteins and ROS *in vivo*

As a phenotypic marker of ASM cells, a-SMA was detected using immunohistochemical techniques. The α-SMA staining densities in the ASM of the HDM-challenged mice were higher than the control mice (p < 0.05). As shown in **Figure 2A**, the administration of chloroquine markedly decreased the α-SMA-stained smooth muscle layer. Treatment with DEX also decreased the α-SMA staining densities, but these effects were less obvious than the chloroquine effects. The immunohistochemistry assays also showed stronger proliferation-associated protein PCNA, MMP-9 and MMP-13 staining around the bronchioles and in the infiltrated inflammatory cells in the HDM-challenged mice compared to the control mice. The administration of DEX or high doses of chloroquine markedly reversed these increases (**Figures 2A,B**). To determine whether chloroquine inhibited HDM-induced airway inflammation and remodeling *via* the scavenging of free radicals, we detected the *in situ* ROS level in the lung tissue to evaluate the changes resulting from HDM-induced oxidative damage. As shown in **Figure 2C**, DHE staining was used to assess the *in situ* ROS level in the lungs. DHE was predominately detected in the airway epithelium in control mice. Challenge with HDM enhanced the fluorescence not only in the inflammatory cells and epithelium, but also ASM cells around the airway, whereas treatment with chloroquine and DEX weakened

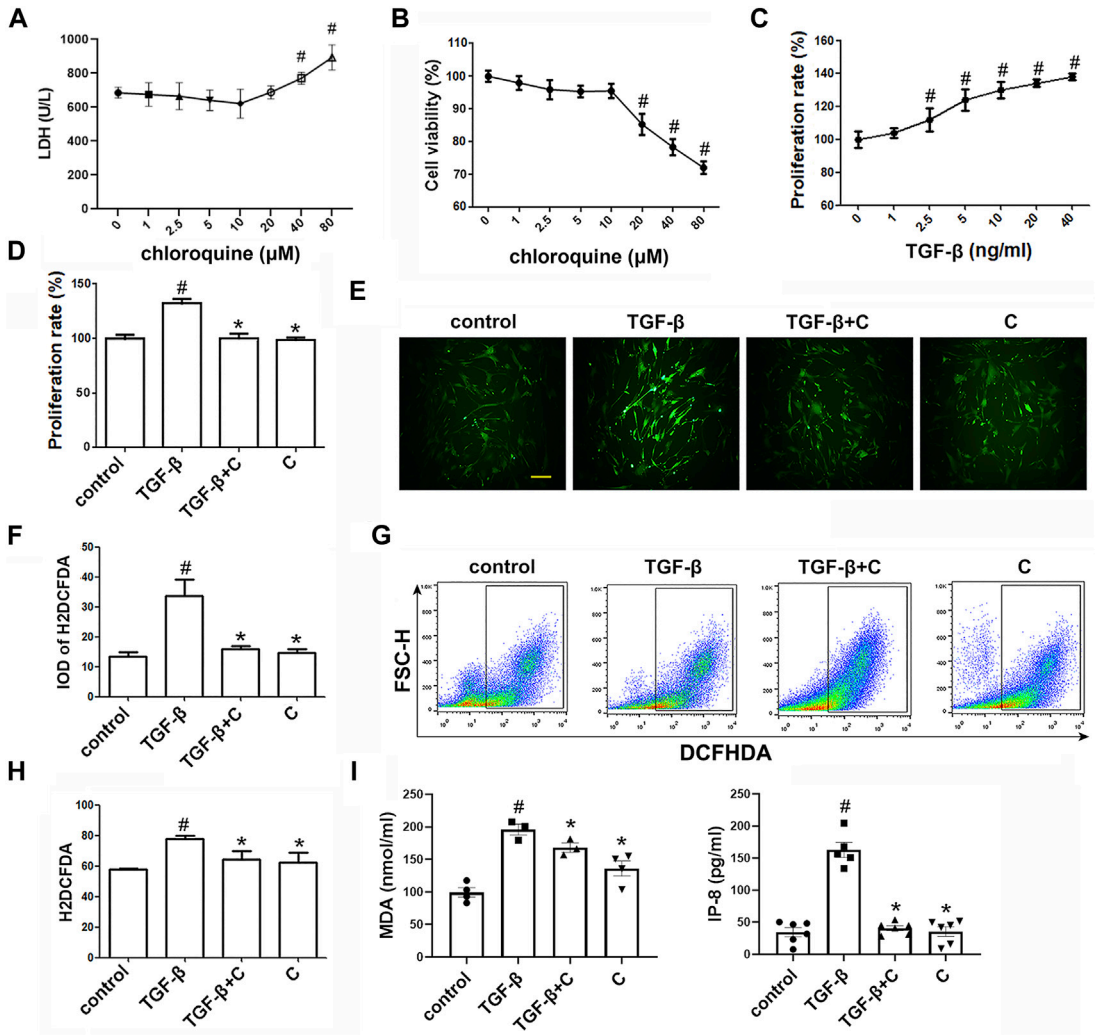

FIGURE 3 | Treatment with chloroquine inhibited ASM cell proliferation, ROS generation and MDA/IP-8 production elicited by TGF-β1 **(A)** Cytotoxicity of chloroquine in human ASM cells (LDH assay) **(B)** Cell viability with diverse concentrations of chloroquine (CCK-8 assay) **(C)** Cell proliferation provoked by TGF-β1 (CCK-8 assay) **(D)** Inhibition of TGF-β1-stimulated cell proliferation by chloroquine **(E,F)** DCFH-DA fluorescence (green) imaging of ROS with a laser scanning confocal microscope (magnification, ×400; scale bar, 50 μm) **(G,H)** Fluorescence-activated cell sorting profile of ROS with DCFH-DA by flow cytometry **(I)** Analysis for MDA and IP-8 content in supernatant. Values are the mean ± SEM of at least four independent experiments performed in triplicate. #$p < 0.05$ compared with the control, and *$p < 0.05$ compared with the TGF-β1 group. C, chloroquine (5 μm); TGF-β, TGF-β1 (5 ng/ml).

the fluorescence in those cells of mice. TGF-β1 is a key mediator in asthmatic airway remodeling. After sensitization and challenge, the TGF-β1 level in the BALF was also upregulated in the HDM and HDM + DMSO groups compared to the control group ($p < 0.05$). Chloroquine and DEX almost reversed this upregulation (**Figure 1D**). These observations suggested that the protective effect of chloroquine was attributed to the downregulation of TGF-β1.

Chloroquine Suppresses TGF-β1-Induced ROS *in vitro*

The toxicity of chloroquine (1, 2.5, 5, 10, 20, 40, and 80 μm) on human ASM cells as shown in **Figure 3A**, and the cell viability after 48 h of treatment with 5 μm chloroquine was 97 ± 3% (**Figure 3B**). Chloroquine decreased the proliferation of ASM cells *in vitro* in a dose-dependent manner, and the proliferation of human ASM cells was enhanced after TGF-β1 stimulation. The concentration of TGF-β1 (5 ng/ml) induced significant ASM cell proliferation, as determined by the CCK-8 assays, after 48 h of treatment (**Figure 3C**). Treatment with 5 μm chloroquine markedly decreased TGF-β1-induced ASM cell proliferation from 132 ± 3%–104 ± 2% ($p < 0.05$) (**Figure 3D**). Then, we used 5 μm chloroquine for further study and determined whether ROS were involved in TGF-β1-induced proliferation. As shown in **Figure 3E**, treatment with TGF-β1 activated ROS. A H2DCFDA analysis was performed to evaluate the level of intracellular ROS in

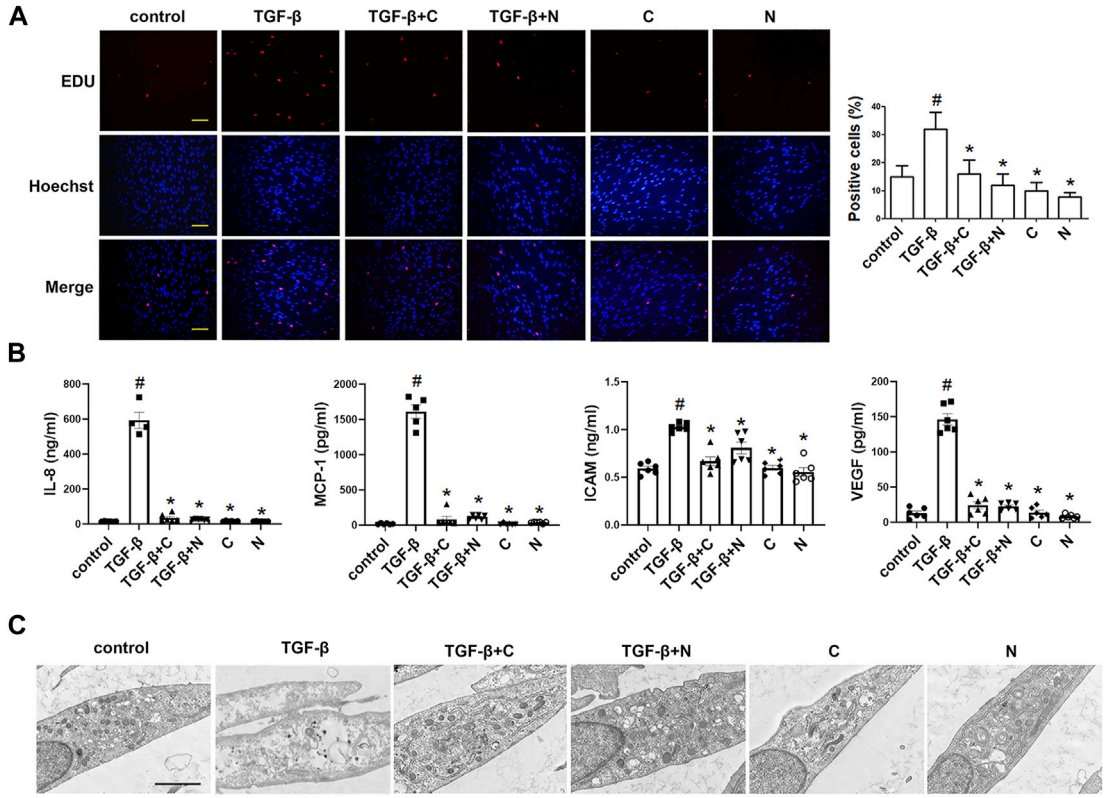

FIGURE 4 | Treatment with chloroquine inhibited TGF-β1-induced proliferation, hypersecretion and hypertrophy in ASM cells **(A)** Effect of chloroquine on TGF-β1-stimulated human ASM cells as assessed by EdU assay (magnification, ×200; scale bar, 100 μm) **(B)** The IL-8, MCP-1, ICAM-1, and VEGF levels in the supernatant were measured by ELISA **(C)** Effect of chloroquine on TGF-β1-stimulated human ASM cells as assessed by transmission electron microscope (TEM) (magnification, ×7000; scale bar, 2 μm). Values are the mean ± SEM of at least four independent experiments performed in triplicate. #$p < 0.05$ compared with the control, and *$p < 0.05$ compared with the TGF-β1 group. C, chloroquine (5 μm); TGF-β, TGF-β1 (5 ng/ml); N, NAC (10 mm).

ASM cells (**Figure 3F**). The results suggested that treatment of ASM cells with chloroquine significantly reduced the TGF-β1-induced fluorescence, which reflects the level of oxidative damage. A flow cytometry analysis showed that treatment with chloroquine decreased the intracellular production of ROS from 79 ± 2%–64 ± 4% ($p < 0.05$) (**Figures 3G,H**). As shown in **Figure 3I**, the concentrations of MDA and IP-8 in the TGF-β1-treated group were significantly higher than the control group ($p < 0.05$), and treatment with chloroquine significantly decreased the increased levels of MDA and IP-8 ($p < 0.05$).

Chloroquine Reverses TGF-β1-Induced Proliferative/Synthetic ASM Cells

We used the EdU incorporation assay, which is a more sensitive and specific method (Yu et al., 2009), to evaluate the effects of chloroquine on TGF-β1-induced cell proliferation. As shown in **Figure 4A**, TGF-β1 stimulation significantly increased the number of cells that incorporated EdU compared to the control, and treatment with chloroquine or NAC (10 mm) clearly limited the TGF-β1-induced proliferation. As previously mentioned, ASM cells tend to proliferative/synthetic phenotype in asthmatic patients, and release chemokines and adhesion molecules to induce inflammatory responses and stimulate eosinophil migration (Zha et al., 2013). To ascertain the anti-inflammatory mechanism of chloroquine, we studied the effects of chloroquine on the TGF-β1-induced upregulation of IL-8, MCP-1, ICAM-1 and VEGF in human ASM cells. The results showed that chloroquine and NAC substantially blocked the TGF-β1-induced upregulation of IL-8, MCP-1, ICAM-1, and VEGF expression in human ASM cells, respectively (**Figure 4B**). The TGF-β1-mediated phenotype switching of ASM cells was assessed by TEM. The proliferative/synthetic ASM cells appeared flattened with numerous cytoplasmic processes and an elongated oval nucleus containing little or no heterochromatin. The cytoplasm contained mitochondria, highly developed Golgi cisternae and numerous profiles of rough endoplasmic reticulum. The results showed that chloroquine and NAC also reversed TGF-β1-induced proliferative/synthetic ASM cells (**Figure 4C**). Based on the above results, we conclude that chloroquine rebalances

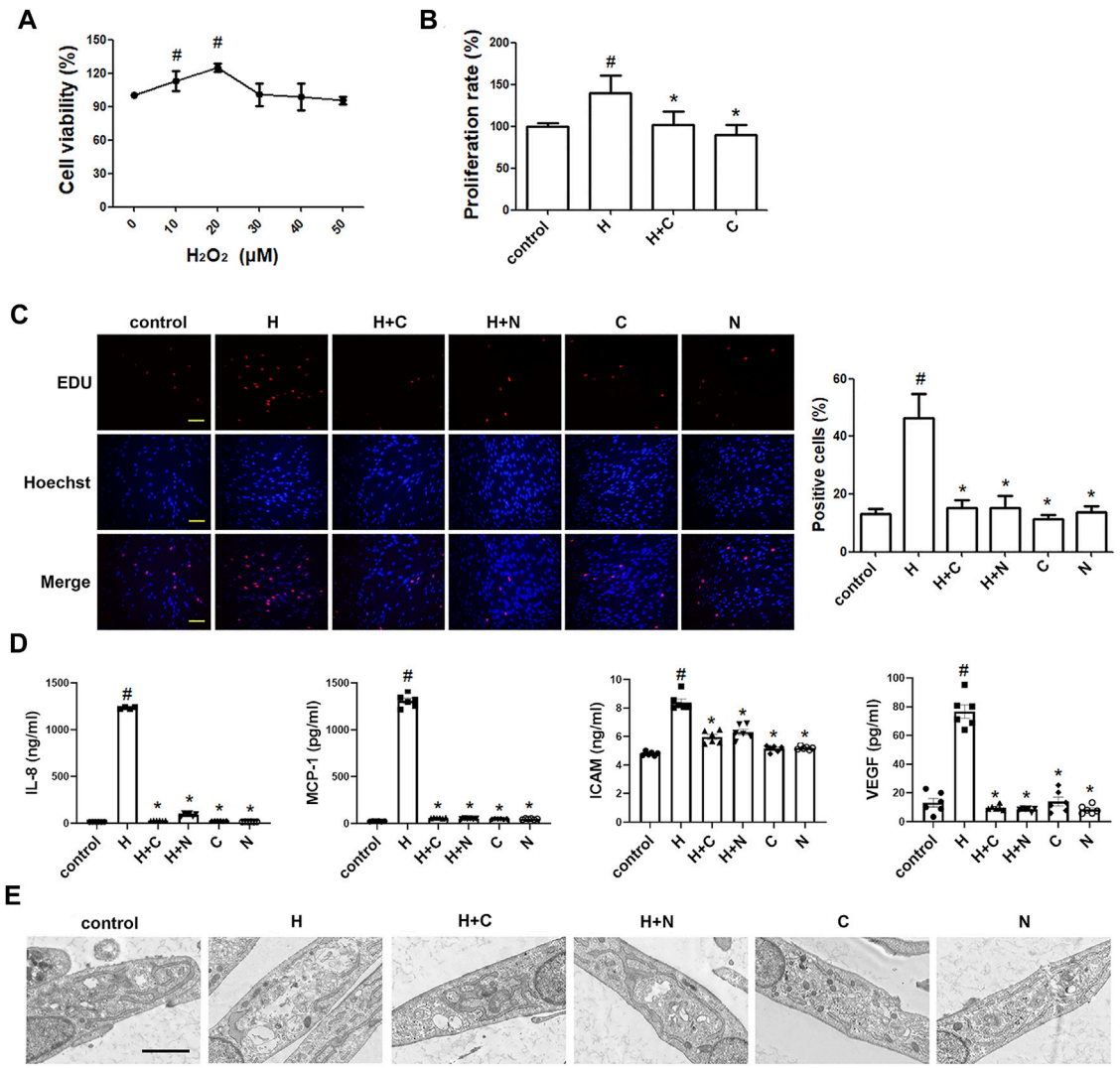

FIGURE 5 | Treatment with chloroquine inhibited the H2O2-induced proliferation, hypersecretion and hypertrophy in ASM cells **(A)** Effect of stimulation with different concentrations of H2O2 on the proliferation of human ASM cells as assessed by CCK-8 assay **(B)** Effect of chloroquine on H2O2-stimulated human ASM cells as assessed by CCK-8 assay **(C)** Effect of chloroquine on H2O2-stimulated human ASM cells as assessed by EdU assay (magnification, ×200; scale bar, 100 μm) **(D)** The IL-8, MCP-1, ICAM-1, and VEGF levels in the supernatant were measured by ELISA **(E)** Effect of chloroquine on H2O2-stimulated human ASM cells as assessed by TEM (magnification, ×7000; scale bar, 2 μm). Values are the mean ± SEM of at least four independent experiments performed in triplicate. #$p < 0.05$ compared with the control, and *$p < 0.05$ compared with the TGF-β1 group. C, chloroquine (5 μm); H, H2O2 (20 μm); N, NAC (10 mm).

ASM cell phenotype, and the mechanism may be related to the regulation of ROS.

Chloroquine Reverses H_2O_2-Induced Proliferative/Synthetic ASM Cells

Furthermore, we studied whether oxidative stress involves in the ASM cell phenotype switching. As shown in **Figures 5A–C**, H_2O_2 (20 μm) stimulation directly increased the number of cells compared to the control, and treatment with chloroquine or NAC clearly limited the H_2O_2-induced proliferation. Chloroquine and NAC also inhibited H_2O_2-induced expression of IL-8, MCP-1, ICAM-1, and VEGF in human ASM cells, respectively (**Figure 5D**). The TEM results showed that the ASM cell phenotype switching induced by H_2O_2 (20 μm) was almost the same as that induced by TGF-β1 (5 ng/ml), and chloroquine also reversed H_2O_2-induced proliferative/synthetic ASM cells (**Figure 5E**). Based on the above results, we conclude that chloroquine rebalances ASM cell phenotype *via* the ROS pathway.

Chloroquine Rebalances ASM Cell Phenotype *via* the AKT Signaling Pathway

To determine the signaling mechanisms underlying the effects of chloroquine on airway remodeling, the phosphorylation status of

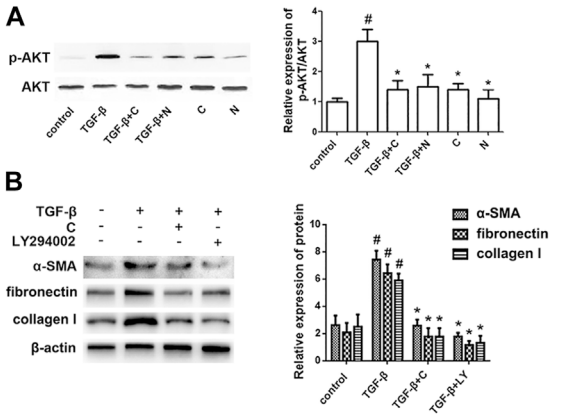

FIGURE 6 | Treatment with chloroquine suppressed the activation of the AKT pathway **(A)** Treatment with chloroquine suppressed the TGF-β1-induced phosphorylation of AKT in ASM cells. The phosphorylation and total protein content of AKT were measured by western blot. The relative density quantification was phosphorylated proteins relative to total proteins **(B)** The contents of α-SMA, fibronectin and collagen I were measured by western blot. Values are the mean ± SEM of at least four independent experiments performed in triplicate. #$p < 0.05$ compared with the control, and *$p < 0.05$ compared with the TGF-β1 group. C, chloroquine (5 μm); TGF-β, TGF-β1 (5 ng/ml); N, NAC (10 mm); LY, LY294002 (10 μm).

AKT was investigated. TGF-β1-induced ASM cells were treated with chloroquine and the AKT signal inhibitor LY294002 (**Supplementary Figure S4**). As shown in **Figure 6A**, treatment with TGF-β1 for 2 h increased the AKT phosphorylation level, whereas chloroquine and NAC inhibited the TGF-β1-mediated induction of AKT phosphorylation. In addition, chloroquine and LY294002 treatment significantly reversed the effects of TGF-β1 on proliferation- and fibrosis-related indicators (**Figure 6B**). Based on the above results, we conclude that chloroquine acts as an inhibitor of the AKT signaling pathway, regulates ASM cell hypertrophy, hypersecretion and proliferation.

DISCUSSION

Asthmatic airway remodeling entails a wide array of pathophysiologic events such as epithelial damage, mucus gland and goblet cell hyperplasia, subepithelial fibrosis, vascular changes, and increased smooth muscle mass (including hyperplasia, parasecretion and hypertrophy) (Wang J et al., 2018). Several studies demonstrated that patients dying from severe asthma exhibited vigorous increases in the apparent smooth muscle mass within the airway wall (Ebina et al., 1993). ASM cell phenotype switching is deeply implicated in this event and favors persistent AHR and irreversible airway obstruction with a decrease in pulmonary function. ASM cells are found to be skewed towards proliferative/synthetic state in asthma and exhibit characteristics of transcription and division. Organelles associated with the synthetic phenotype predominate in the cytoplasm (Hirst, 1996). ASM cell proliferation and synthesis of cytokines or growth factors make a huge contribution to the imbalance of airway microenvironment and perpetuate the chronicity of asthma (Wang L et al., 2018). Our presented data indicated that TAS2Rs agonist chloroquine exhibited a positive effect on asthmatic mice with a significant improvement in AHR, inflammatory cell infiltration, mucus hypersecretion, collagen deposition and fibrosis. It also reduced IgE and Th2-associated cytokines, which are closely involved in the asthmatic airway microenvironment and remodeling.

As a marker of ASM cells, α-SMA is an essential component of microfilaments which connect to cell membranes (Lin et al., 1989; Colpan et al., 2019). It is pivotal for cell proliferation, hypertrophy, contraction and migration which contribute a lot to the development of airway remodeling and airway hyperresponsiveness (AHR) (Bentley and Hershenson, 2008; Xu et al., 2012; Rao et al., 2014). PCNA is also an indicator of ASM cell proliferation devoted to ASM mass (Kesavan et al., 2013; Cabral-Pacheco et al., 2020). Patients with severe asthma were confirmed to present increased levels of α-SMA and PCNA, associated with higher mortality (Kesavan et al., 2013; Zhao et al., 2013; Cabral-Pacheco et al., 2020). Our results further demonstrated that chloroquine pronouncedly downregulated α-SMA and PCNA expression within asthmatic airway walls, implying a reversion of ASM mass by chloroquine. Further study *in vitro* even showed that chloroquine suppressed TGF-β1-induced ASM cell proliferation, providing evidence for chloroquine in ASM cell hyperplasia remission in mice.

ASM cell phenotype shifts are often accompanied by a worse parasecretion state. The influx of inflammatory factors within the airways is proposed as a distinct hallmark of asthma (O'Byrne and Postma, 1999). Increased IL-8 level was observed in severe asthma (Tanabe et al., 2014). It promotes ASM cell contraction and migration (Govindaraju et al., 2006), and changes ASM cell features by eliciting the rate of cell proliferation and survival (Halwani et al., 2011). IL-8 can be secreted from ASM cells accompanied by MCP-1, ICAM-1 and VEGF (Lazaar, 2002; Rose et al., 2003; Mukhopadhyay et al., 2014). As a specific endothelial growth factor, VEGF contributes a lot to nonspecific AHR, exerts chemotactic effects on eosinophils, and enhances ASM cell proliferation (Pei et al., 2016). Previous studies showed that Th2-associated cytokines could increase VEGF production which correlated with the severity of asthma (Makinde et al., 2006). All of these suggests deteriorated airway microenvironment as a critical incentive in asthma progressing, facilitating ASM cells to the proliferative/synthetic phenotype, and aggravating a vicious circle of inflammatory response (Lazaar, 2002; Zha et al., 2013; Faiz et al., 2018). In our study, the *in vitro* findings showed that chloroquine blocked the secretion of these cytokines and adhesion molecules induced by TGF-β1 or H_2O_2, suggesting a novel option for airway remodeling control by rebalancing ASM cell phenotypes.

Along with this phenotype switching, the microstructure of ASM cells profoundly changed. Proliferative/synthetic ASM cells appear hypertrophy with aberrantly increased cytoplasm, organelles and microfilaments (Jones et al., 2014). Abnormal hypertrophy of ASM cells cause cell dysfunction in contraction,

which determines the development and persistence of AHR in asthma (Wang J et al., 2018; Yu et al., 2020). Our TEM results revealed that TGF-β1 or H_2O_2 induced ASM cells to a proliferative/synthetic state, resulting in numerous cytoplasmic processes with increased profiles of organelles, such as mitochondria, highly developed Golgi cisternae and rough endoplasmic reticulum. Chloroquine markedly reversed the growth of these synthetic organelles, implying an inhibition of the high parasecretion of proliferative/synthetic ASM cells in TGF-β1/H_2O_2 model with the rebalance of ASM cell phenotypes.

Hyperplasia, parasecretion and hypertrophy are often present in ASM cell phenotype alterations. Other pathophysiologic events such as extracellular matrix (ECM) deposition and fibrosis involved in airway remodeling are also associated with cell phenotype switching. ECM proteins increased in asthmatic airways, particularly collagen I and fibronectin (Roche et al., 1989; Neil et al., 2007), give strong backing to ASM cell survival and proliferation. They have been proved *in vitro* to enhance the contractile signal (Johnson, 2001; Freyer et al., 2004). In turn, MMPs derived from ASM cells participated actively in ECM deposition and fibrosis (Kesavan et al., 2013; Zhao et al., 2013). Elevated levels of MMP-9 and MMP-13 were found in the serum, sputum and BALF of patients with classic asthma (Greenlee et al., 2007; Mori et al., 2012). MMP-9-deficient animals exhibited reduced airway inflammation, collagen deposition, and peribronchial fibrosis (Halade et al., 2013). Our findings indicated that chloroquine significantly restrained HDM-induced upregulation of MMP-9 and MMP-13, and substantially inhibited the expression of α-SMA, collagen I and fibronectin in ASM cells, sustaining that chloroquine possesses the anti-remodeling potency by controlling ASM cell phenotype. On the other hand, AKT signal inhibitor LY294002 produced the similar effects on the overexpression of α-SMA, collagen I and fibronectin induced by TGF-β1 *in vitro*, suggesting that chloroquine rebalances ASM cell phenotypes through AKT pathway.

As a serine/threonine kinase, AKT is the key mediator in phosphatidylinositol 3 kinase (PI3K)-initiated signaling closely related to ASM cell proliferation (Xu et al., 2017; Li et al., 2018). Once PI3K is activated, AKT could be phosphorylated (p-AKT) and thought as a flare of PI3K activation (Hu et al., 2019). Evidence from our previous study has suggested that ROS play key roles in AKT signal during TGF-β1 stimulation (Ma et al., 2016). ROS triggered PI3K to amplify the downstream signal, and inactivated phosphatase and tensin homolog (PTEN) which negatively regulates AKT activation (Zhang et al., 2016). It has been reported that ROS upregulated mitochondrial E3 ubiquitin protein ligase 1, induced AKT ubiquitination, and promoted proteasome degradation in head and neck cancer (Bae et al., 2012; Kim et al., 2015; Su et al., 2019). ROS-induced miRNAs modulated AKT phosphorylation to promote cellular senescence in uterine leiomyoma (Xu et al., 2018). Since AKT pathway is critical for the phenotype shifts of ASM cells, the suppression of upstream ROS may have potential implications in asthma therapy.

Our results showed that the level of *in situ* ROS was increased in the lung tissue obtained from HDM-challenged mice. And chloroquine treatment significantly attenuated the increase and presented a better benefit than DEX. *In vitro,* our data further demonstrated that chloroquine strongly inhibited the production of intracellular ROS induced by TGF-β1, and reduced the levels of MDA and IP-8. TGF-β1 and increased ROS (H_2O_2) directly induced ASM cell proliferation involved in airway remodeling. Chloroquine and ROS scavenger NAC notably suppressed AKT phosphorylation during the switching of ASM cell phenotype, highlighting a crucial role of ROS-AKT signaling in the phenotype reversal of ASM cells by chloroquine.

By far, the expression of TAS2Rs has been determined in multiple cell types in airway, including resident (macrophages) and migratory (neutrophils, mast cells, lymphocytes) inflammatory cells, epithelial cells, and ASM cells (Shah et al., 2009; Deshpande et al., 2011; Orsmark-Pietras et al., 2013; Ekoff et al., 2014; Maurer et al., 2015; Tran et al., 2018; Nayak et al., 2019). Activation of TAS2Rs in diverse cells may lead to distinct impacts on cell function (Lee et al., 2012; Sharma et al., 2017). As for ASM cells, a previous study has shown that chloroquine could cause their relaxation *via* TAS2Rs (Tan and Sanderson, 2014). It also plays a modulatory role in ERK1/2 phosphorylation, which were closely implicated in ASM cell proliferation (Kim et al., 2019). Besides, an antimitogenic potency of TAS2R agonists has been reported in ASM cells by inhibiting the activities of Akt kinase and S6 kinase (Sharma et al., 2016). Then our present work further provided strong evidences that chloroquine prevents ASM from the aberrant proliferation, hypersecretion and hypertrophy by reversing cellular phenotype. These findings may help to offer a potential option for the treatment of asthma, especially for the remission of airway remodeling. By using H_2O_2 and PI3K inhibitor (LY294002), we further confirmed that the positive effect of chloroquine may rely on the signal of ROS-AKT. The protective properties of chloroquine implicated in asthma should be studied further to determine the value and precise subtype involved in clinical application.

CONCLUSION

We demonstrated the potential therapeutic action of chloroquine in asthma, revealed its properties and underlying mechanism. Collectively, our findings showed that chloroquine (I) abrogated AHR and attenuated inflammatory cell infiltration, goblet cell hyperplasia and fibrotic expression in the airways (II) decreased the overexpression of α-SMA, PCNA, MMP-9, and MMP-13 in HDM-sensitized mice (III) diminished the elevated levels of IgE, IL-4, IL-13, and TGF-β1 in the BALF (IV) reduced the *in situ* ROS in the lungs and MDA and IP-8 levels in the BALF (V) reversed TGF-β1 and H_2O_2-induced proliferative/synthetic ASM cells (proliferation, hypersecretion and hypertrophy); and (VI) suppressed the TGF-β1-induced production of ROS through the inhibition of AKT phosphorylation in human ASM cells. Taken together, our results indicate that chloroquine has the potential to provide beneficial improvements to AHR, airway inflammation and

remodeling, and these beneficial effects are most likely due to ROS-AKT pathways. Based on these findings and its recently described bronchodilator and anti-inflammatory properties, chloroquine, as an TAS2R agonist, may be a new therapeutic approach for the treatment of allergic airway diseases.

DATA AVAILABILITY STATEMENT

The original contributions presented in the study are included in the article/**Supplementary Material**, further inquiries can be directed to the corresponding authors.

ETHICS STATEMENT

The animal study was reviewed and approved by the All animal experiments were conducted according to a protocol approved by the Nanjing Medical University (NJMU) Institutional Animal Care and Use Committee (NJMU IACUC-1711002, Nanjing, Jiangsu, China).

AUTHOR CONTRIBUTIONS

YM and XNZ contributed to the design of the study and wrote the manuscript. YR and XHZ were responsible for the cell culture experiments and performed most of the western blot and immunofluorescent staining experiments. HW, YL, and ZC contributed to animal model establishment, sample collection and detection. HW and YL helped to the acquisition and interpretation of the data.

FUNDING

This work was supported by the National Natural Science Foundation of China (NSFC, No. 81700028, No. 81970016, No. 82170031).

ACKNOWLEDGMENTS

We would like to thank Jiangsu Province Hospital Core Facility Center for the vigorous technical assistance.

SUPPLEMENTARY MATERIAL

The Supplementary Material for this article can be found online at: https://www.frontiersin.org/articles/10.3389/fphar.2022.916508/full#supplementary-material

REFERENCES

Al-Muhsen, S., Johnson, J. R., and Hamid, Q. (2011). Remodeling in Asthma. *J. Allergy Clin. Immunol.* 128 (3), 451–454. doi:10.1016/j.jaci.2011.04.047

Bae, S., Kim, S. Y., Jung, J. H., Yoon, Y., Cha, H. J., Lee, H., et al. (2012). Akt Is Negatively Regulated by the MULAN E3 Ligase. *Cell Res.* 22 (5), 873–885. doi:10.1038/cr.2012.38

Becker, A. B., Simons, K. J., Gillespie, C. A., and Simons, F. E. (1984). The Bronchodilator Effects and Pharmacokinetics of Caffeine in Asthma. *N. Engl. J. Med.* 310 (12), 743–746. doi:10.1056/NEJM198403223101202

Bentley, J. K., and Hershenson, M. B. (2008). Airway Smooth Muscle Growth in Asthma: Proliferation, Hypertrophy, and Migration. *Proc. Am. Thorac. Soc.* 5 (1), 89–96. doi:10.1513/pats.200705-063VS

Boldogh, I., Bacsi, A., Choudhury, B. K., Dharajiya, N., Alam, R., Hazra, T. K., et al. (2005). ROS Generated by Pollen NADPH Oxidase Provide a Signal that Augments Antigen-Induced Allergic Airway Inflammation. *J. Clin. Invest.* 115 (8), 2169–2179. doi:10.1172/JCI24422

Cabral-Pacheco, G. A., Garza-Veloz, I., Castruita-De la Rosa, C., Ramirez-Acuña, J. M., Perez-Romero, B. A., Guerrero-Rodriguez, J. F., et al. (2020). The Roles of Matrix Metalloproteinases and Their Inhibitors in Human Diseases. *Ijms* 21 (24), 9739. doi:10.3390/ijms21249739

Colacone, A., Bertolo, L., Wolkove, N., Cohen, C., and Kreisman, H. (1990). Effect of Caffeine on Histamine Bronchoprovocation in Asthma. *Thorax* 45 (8), 630–632. doi:10.1136/thx.45.8.630

Deshpande, D. A., Robinett, K. S., Wang, W. C., Sham, J. S., An, S. S., and Liggett, S. B. (2011). Bronchodilator Activity of Bitter Tastants in Human Tissue. *Nat. Med.* 17, 776–778. doi:10.1038/nm0711-776b

Deshpande, D. A., Wang, W. C., McIlmoyle, E. L., Robinett, K. S., Schillinger, R. M., An, S. S., et al. (2010). Bitter Taste Receptors on Airway Smooth Muscle Bronchodilate by Localized Calcium Signaling and Reverse Obstruction. *Nat. Med.* 16 (11), 1299–1304. doi:10.1038/nm.2237

Ebina, M., Takahashi, T., Chiba, T., and Motomiya, M. (1993). Cellular Hypertrophy and Hyperplasia of Airway Smooth Muscles Underlying Bronchial Asthma. A 3-D Morphometric Study. *Am. Rev. Respir. Dis.* 148 (3), 720–726. doi:10.1164/ajrccm/148.3.720

Ekoff, M., Choi, J. H., James, A., Dahlén, B., Nilsson, G., and Dahlén, S. E. (2014). Bitter Taste Receptor (TAS2R) Agonists Inhibit IgE-dependent Mast Cell Activation. *J. Allergy Clin. Immunol.* 134 (2), 475–478. doi:10.1016/j.jaci.2014.02.029

Faiz, A., Weckmann, M., Tasena, H., Vermeulen, C. J., Van den Berge, M., Ten Hacken, N. H. T., et al. (2018). Profiling of Healthy and Asthmatic Airway Smooth Muscle Cells Following Interleukin-1β Treatment: a Novel Role for CCL20 in Chronic Mucus Hypersecretion. *Eur. Respir. J.* 52 (2), 1800310. doi:10.1183/13993003.00310-2018

Freyer, A. M., Billington, C. K., Penn, R. B., and Hall, I. P. (2004). Extracellular Matrix Modulates Beta2-Adrenergic Receptor Signaling in Human Airway Smooth Muscle Cells. *Am. J. Respir. Cell Mol. Biol.* 31 (4), 440–445. doi:10.1165/rcmb.2003-0241OC

Govindaraju, V., Michoud, M. C., Al-Chalabi, M., Ferraro, P., Powell, W. S., and Martin, J. G. (2006). Interleukin-8: Novel Roles in Human Airway Smooth Muscle Cell Contraction and Migration. *Am. J. Physiol. Cell Physiol.* 291 (5), C957–C965. doi:10.1152/ajpcell.00451.2005

Grassin-Delyle, S., Naline, E., and Devillier, P. (2015). Taste Receptors in Asthma. *Curr. Opin. Allergy Clin. Immunol.* 15 (1), 63–69. doi:10.1097/ACI.0000000000000137

Greenlee, K. J., Werb, Z., and Kheradmand, F. (2007). Matrix Metalloproteinases in Lung: Multiple, Multifarious, and Multifaceted. *Physiol. Rev.* 87 (1), 69–98. doi:10.1152/physrev.00022.2006

Halade, G. V., Jin, Y. F., and Lindsey, M. L. (2013). Matrix Metalloproteinase (MMP)-9: a Proximal Biomarker for Cardiac Remodeling and a Distal Biomarker for Inflammation. *Pharmacol. Ther.* 139 (1), 32–40. doi:10.1016/j.pharmthera.2013.03.009

Halwani, R., Al-Abri, J., Beland, M., Al-Jahdali, H., Halayko, A. J., Lee, T. H., et al. (2011). CC and CXC Chemokines Induce Airway Smooth Muscle Proliferation and Survival. *J. Immunol.* 186 (7), 4156–4163. doi:10.4049/jimmunol.1001210

Henderson, N., Markwick, L. J., Elshaw, S. R., Freyer, A. M., Knox, A. J., and Johnson, S. R. (2007). Collagen I and Thrombin Activate MMP-2 by MMP-14-

dependent and -independent Pathways: Implications for Airway Smooth Muscle Migration. *Am. J. Physiology-Lung Cell. Mol. Physiology* 292 (4), L1030–L1038. doi:10.1152/ajplung.00317.2006

Hirst, S. J. (1996). Airway Smooth Muscle Cell Culture: Application to Studies of Airway Wall Remodelling and Phenotype Plasticity in Asthma. *Eur. Respir. J.* 9 (4), 808–820. doi:10.1183/09031936.96.09040808

Hu, M., Liu, Y., He, L., Yuan, X., Peng, W., and Wu, C. (2019). Antiepileptic Effects of Protein-Rich Extract from Bombyx Batryticatus on Mice and its Protective Effects against H2O2-Induced Oxidative Damage in PC12 Cells via Regulating PI3K/Akt Signaling Pathways. *Oxid. Med. Cell Longev.* 2019, 7897584. doi:10.1155/2019/7897584

Johnson, P. R. (2001). Role of Human Airway Smooth Muscle in Altered Extracellular Matrix Production in Asthma. *Clin. Exp. Pharmacol. Physiol.* 28 (3), 233–236. doi:10.1046/j.1440-1681.2001.03426.x

Jones, R. L., Elliot, J. G., and James, A. L. (2014). Estimating Airway Smooth Muscle Cell Volume and Number in Airway Sections. Sources of Variability. *Am. J. Respir. Cell Mol. Biol.* 50 (2), 246–252. doi:10.1165/rcmb.2013-0029OC

Kepser, L.-J., Damar, F., De Cicco, T., Chaponnier, C., Prószyński, T. J., Pagenstecher, A., et al. (2019). CAP2 Deficiency Delays Myofibril Actin Cytoskeleton Differentiation and Disturbs Skeletal Muscle Architecture and Function. *Proc. Natl. Acad. Sci. U.S.A.* 116 (17), 8397–8402. doi:10.1073/pnas.1813351116

Kerzerho, J., Maazi, H., Speak, A. O., Szely, N., Lombardi, V., Khoo, B., et al. (2013). Programmed Cell Death Ligand 2 Regulates TH9 Differentiation and Induction of Chronic Airway Hyperreactivity. *J. Allergy Clin. Immunol.* 131 (4), 1048–1057. doi:10.1016/j.jaci.2012.09.027

Kesavan, R., Potunuru, U. R., Nastasijević, B., T, A., Joksić, G., and Dixit, M. (2013). Inhibition of Vascular Smooth Muscle Cell Proliferation by gentiana Lutea Root Extracts. *PLoS One* 8 (4), e61393. doi:10.1371/journal.pone.0061393

Kim, D., Cho, S., Castaño, M. A., Panettieri, R. A., Woo, J. A., and Liggett, S. B. (2019). Biased TAS2R Bronchodilators Inhibit Airway Smooth Muscle Growth by Downregulating Phosphorylated Extracellular Signal-Regulated Kinase 1/2. *Am. J. Respir. Cell Mol. Biol.* 60 (5), 532–540. doi:10.1165/rcmb.2018-0189OC

Kim, S. Y., Kim, H. J., Kang, S. U., Kim, Y. E., Park, J. K., Shin, Y. S., et al. (2015). Non-thermal Plasma Induces AKT Degradation through Turn-On the MUL1 E3 Ligase in Head and Neck Cancer. *Oncotarget* 6 (32), 33382–33396. doi:10.18632/oncotarget.5407

Kivity, S., Ben Aharon, Y., Man, A., and Topilsky, M. (1990). The Effect of Caffeine on Exercise-Induced Bronchoconstriction. *Chest* 97 (5), 1083–1085. doi:10.1378/chest.97.5.1083

Lazaar, A. L. (2002). Airway Smooth Muscle: New Targets for Asthma Pharmacotherapy. *Expert. Opin. Ther. Targets* 6 (4), 447–459. doi:10.1517/14728222.6.4.447

Lee, R. J., Xiong, G., Kofonow, J. M., Chen, B., Lysenko, A., Jiang, P., et al. (2012). T2R38 Taste Receptor Polymorphisms Underlie Susceptibility to Upper Respiratory Infection. *J. Clin. Invest.* 122, 4145–4159. doi:10.1172/JCI64240

Li, H., Tang, Z., Chu, P., Song, Y., Yang, Y., Sun, B., et al. (2018). Neuroprotective Effect of Phosphocreatine on Oxidative Stress and Mitochondrial Dysfunction Induced Apoptosis *In Vitro* and *In Vivo*: Involvement of Dual PI3K/Akt and Nrf2/HO-1 Pathways. *Free Radic. Biol. Med.* 120, 228–238. doi:10.1016/j.freeradbiomed.2018.03.014

Lin, Z. X., Eshleman, J., Grund, C., Fischman, D. A., Masaki, T., Franke, W. W., et al. (1989). Differential Response of Myofibrillar and Cytoskeletal Proteins in Cells Treated with Phorbol Myristate Acetate. *J. Cell Biol.* 108 (3), 1079–1091. doi:10.1083/jcb.108.3.1079

Liu, Y. N., Zha, W. J., Ma, Y., Chen, F. F., Zhu, W., Ge, A., et al. (2015). Galangin Attenuates Airway Remodelling by Inhibiting TGF-B1-Mediated ROS Generation and MAPK/Akt Phosphorylation in Asthma. *Sci. Rep.* 5, 11758. doi:10.1038/srep11758

Ma, Y., Zhang, J. X., Liu, Y. N., Ge, A., Gu, H., Zha, W. J., et al. (2016). Corrigendum to 'Caffeic Acid Phenethyl Ester Alleviates Asthma by Regulating the Airway Microenvironment via the ROS-Responsive MAPK/Akt Pathway' [Free Radic. Biol. Med. 101C (2016) 163-175]. *Free Radic. Biol. Med.* 101, 534–175. doi:10.1016/j.freeradbiomed.2016.09.01210.1016/j.freeradbiomed.2016.10.502

Makinde, T., Murphy, R. F., and Agrawal, D. K. (2006). Immunomodulatory Role of Vascular Endothelial Growth Factor and Angiopoietin-1 in Airway Remodeling. *Curr. Mol. Med.* 6 (8), 831–841. doi:10.2174/156652406779010795

Maurer, S., Wabnitz, G. H., Kahle, N. A., Stegmaier, S., Prior, B., Giese, T., et al. (2015). Tasting *Pseudomonas aeruginosa* Biofilms: Human Neutrophils Express the Bitter Receptor T2R38 as Sensor for the Quorum Sensing Molecule N-(3-Oxododecanoyl)-l-homoserine Lactone. *Front. Immunol.* 6, 369. doi:10.3389/fimmu.2015.00369

Mori, S., Pawankar, R., Ozu, C., Nonaka, M., Yagi, T., and Okubo, K. (2012). Expression and Roles of MMP-2, MMP-9, MMP-13, TIMP-1, and TIMP-2 in Allergic Nasal Mucosa. *Allergy Asthma Immunol. Res.* 4 (4), 231–239. doi:10.4168/aair.2012.4.4.231

Mukhopadhyay, S., Malik, P., Arora, S. K., and Mukherjee, T. K. (2014). Intercellular Adhesion Molecule-1 as a Drug Target in Asthma and Rhinitis. *Respirology* 19 (4), 508–513. doi:10.1111/resp.12285

Nayak, A. P., Shah, S. D., Michael, J. V., and Deshpande, D. A. (2019). Bitter Taste Receptors for Asthma Therapeutics. *Front. Physiol.* 10, 884. doi:10.3389/fphys.2019.00884

O'Byrne, P. M., and Postma, D. S. (1999). The Many Faces of Airway Inflammation: Asthma and Chronic Obstructive Pulmonary Disease. Asthma Research Group. *Am. J. Respir. Crit. Care Med.* 159 (5 Pt 2), S41–S63.

Orsmark-Pietras, C., James, A., Konradsen, J. R., Nordlund, B., Söderhäll, C., Pulkkinen, V., et al. (2013). Transcriptome Analysis Reveals Upregulation of Bitter Taste Receptors in Severe Asthmatics. *Eur. Respir. J.* 42 (1), 65–78. doi:10.1183/09031936.00077712

Pei, Q. M., Jiang, P., Yang, M., Qian, X. J., Liu, J. B., and Kim, S. H. (2016). Roxithromycin Inhibits VEGF-Induced Human Airway Smooth Muscle Cell Proliferation: Opportunities for the Treatment of Asthma. *Exp. Cell Res.* 347 (2), 378–384. doi:10.1016/j.yexcr.2016.08.024

Pulkkinen, V., Manson, M. L., Säfholm, J., Adner, M., and Dahlén, S. E. (2012). The Bitter Taste Receptor (TAS2R) Agonists Denatonium and Chloroquine Display Distinct Patterns of Relaxation of the guinea Pig Trachea. *Am. J. Physiol. Lung Cell Mol. Physiol.* 303 (11), L956–L966. doi:10.1152/ajplung.00205.2012

Rao K, B., Malathi, N., Narashiman, S., and Rajan, S. T. (2014). Evaluation of Myofibroblasts by Expression of Alpha Smooth Muscle Actin: a Marker in Fibrosis, Dysplasia and Carcinoma. *J. Clin. Diagn. Res.* 8 (4), ZC14–7. doi:10.7860/JCDR/2014/7820.4231

Roche, W. R., Beasley, R., Williams, J. H., and Holgate, S. T. (1989). Subepithelial Fibrosis in the Bronchi of Asthmatics. *Lancet* 1 (8637), 520–524. doi:10.1016/s0140-6736(89)90067-6

Rose, C. E., Sung, S. S., and Fu, S. M. (2003). Significant Involvement of CCL2 (MCP-1) in Inflammatory Disorders of the Lung. *Microcirculation* 10 (3-4), 273–288. doi:10.1038/sj.mn.7800193

Shah, A. S., Ben-Shahar, Y., Moninger, T. O., Kline, J. N., and Welsh, M. J. (2009). Motile Cilia of Human Airway Epithelia Are Chemosensory. *Science* 325, 1131–1134. doi:10.1126/science.1173869

Sharma, P., Panebra, A., Pera, T., Tiegs, B. C., Hershfeld, A., Kenyon, L. C., et al. (2016). Antimitogenic Effect of Bitter Taste Receptor Agonists on Airway Smooth Muscle Cells. *Am. J. Physiol. Lung Cell Mol. Physiol.* 310 (4), L365–L376. doi:10.1152/ajplung.00373.2015

Sharma, P., Yi, R., Nayak, A. P., Wang, N., Tang, F., Knight, M. J., et al. (2017). Bitter Taste Receptor Agonists Mitigate Features of Allergic Asthma in Mice. *Sci. Rep.* 7, 46166. doi:10.1038/srep46166

Su, X., Shen, Z., Yang, Q., Sui, F., Pu, J., Ma, J., et al. (2019). Vitamin C Kills Thyroid Cancer Cells through ROS-dependent Inhibition of MAPK/ERK and PI3K/AKT Pathways via Distinct Mechanisms. *Theranostics* 9 (15), 4461–4473. doi:10.7150/thno.35219

Tan, X., and Sanderson, M. J. (2014). Bitter Tasting Compounds Dilate Airways by Inhibiting Airway Smooth Muscle Calcium Oscillations and Calcium Sensitivity. *Br. J. Pharmacol.* 171 (3), 646–662. doi:10.1111/bph.12460

Tanabe, T., Shimokawaji, T., Kanoh, S., and Rubin, B. K. (2014). IL-33 Stimulates CXCL8/IL-8 Secretion in Goblet Cells but Not Normally Differentiated Airway Cells. *Clin. Exp. Allergy* 44 (4), 540–552. doi:10.1111/cea.12283

Tran, H. T. T., Herz, C., Ruf, P., Stetter, R., and Lamy, E. (2018). Human T2R38 Bitter Taste Receptor Expression in Resting and Activated Lymphocytes. *Front. Immunol.* 9, 2949. doi:10.3389/fimmu.2018.02949

Wang, J., Shang, Y. X., Cai, X. X., and Liu, L. Y. (2018). Vasoactive Intestinal Peptide Inhibits Airway Smooth Muscle Cell Proliferation in a Mouse Model of Asthma via the ERK1/2 Signaling Pathway. *Exp. Cell Res.* 364 (2), 168–174. doi:10.1016/j.yexcr.2018.01.042

Wang, L., Feng, X., Hu, B., Xia, Q., Ni, X., and Song, Y. (2018). P2X4R Promotes Airway Remodeling by Acting on the Phenotype Switching of Bronchial Smooth Muscle Cells in Rats. *Purinergic Signal* 14 (4), 433–442. doi:10.1007/s11302-018-9625-4

Xu, G. N., Yang, K., Xu, Z. P., Zhu, L., Hou, L. N., Qi, H., et al. (2012). Protective Effects of Anisodamine on Cigarette Smoke Extract-Induced Airway Smooth Muscle Cell Proliferation and Tracheal Contractility. *Toxicol. Appl. Pharmacol.* 262 (1), 70–79. doi:10.1016/j.taap.2012.04.020

Xu, J., Gan, S., Li, J., Wand, D. B., Chen, Y., Hu, X., et al. (2017). Garcinia Xanthochymus Extract Protects PC12 Cells from H2O2-Induced Apoptosis through Modulation of PI3K/AKT and NRF2/HO-1 Pathways. *Chin. J. Nat. Med.* 15 (11), 825–833. doi:10.1016/S1875-5364(18)30016-5

Xu, X., Kim, J. J., Li, Y., Xie, J., Shao, C., and Wei, J. J. (2018). Oxidative Stress-Induced miRNAs Modulate AKT Signaling and Promote Cellular Senescence in Uterine Leiomyoma. *J. Mol. Med. Berl.* 96 (10), 1095–1106. doi:10.1007/s00109-018-1682-1

Yu, Q., Yu, X., Zhong, X., Ma, Y., Wu, Y., Bian, T., et al. (2020). Melatonin Modulates Airway Smooth Muscle Cell Phenotype by Targeting the STAT3/Akt/GSK-3β Pathway in Experimental Asthma. *Cell Tissue Res.* 380 (1), 129–142. doi:10.1007/s00441-019-03148-x

Yu, Y., Arora, A., Min, W., Roifman, C. M., and Grunebaum, E. (2009). EdU Incorporation Is an Alternative Non-radioactive Assay to [(3)H]thymidine Uptake for *In Vitro* Measurement of Mice T-Cell Proliferations. *J. Immunol. Methods* 350 (1-2), 29–35. doi:10.1016/j.jim.2009.07.008

Zha, W. J., Qian, Y., Shen, Y., Du, Q., Chen, F. F., Wu, Z. Z., et al. (2013). Galangin Abrogates Ovalbumin-Induced Airway Inflammation via Negative Regulation of NF-Kb. *Evid. Based Complement. Altern. Med.* 2013, 767689. doi:10.1155/2013/767689

Zhang, J., Wang, X., Vikash, V., Ye, Q., Wu, D., Liu, Y., et al. (2016). ROS and ROS-Mediated Cellular Signaling. *Oxid. Med. Cell Longev.* 2016, 4350965. doi:10.1155/2016/4350965

Zhang, W. X., and Li, C. C. (2011). Airway Remodeling: a Potential Therapeutic Target in Asthma. *World J. Pediatr.* 7 (2), 124–128. doi:10.1007/s12519-011-0264-x

Zhao, L., Wu, J., Zhang, X., Kuang, H., Guo, Y., and Ma, L. (2013). The Effect of Shenmai Injection on the Proliferation of Rat Airway Smooth Muscle Cells in Asthma and Underlying Mechanism. *BMC Complement. Altern. Med.* 13, 221. doi:10.1186/1472-6882-13-221

Conflict of Interest: The authors declare that the research was conducted in the absence of any commercial or financial relationships that could be construed as a potential conflict of interest.

Publisher's Note: All claims expressed in this article are solely those of the authors and do not necessarily represent those of their affiliated organizations, or those of the publisher, the editors and the reviewers. Any product that may be evaluated in this article, or claim that may be made by its manufacturer, is not guaranteed or endorsed by the publisher.

frontiers | Frontiers in Pharmacology

ORIGINAL RESEARCH
published: 02 June 2022
doi: 10.3389/fphar.2022.879268

Deciphering the Active Compounds and Mechanisms of HSBDF for Treating ALI *via* Integrating Chemical Bioinformatics Analysis

Yanru Wang[1†], Xiaojie Jin[1,2†], Qin Fan[3], Chenghao Li[1], Min Zhang[2], Yongfeng Wang[3], Qingfeng Wu[4], Jiawei Li[1], Xiuzhu Liu[1], Siyu Wang[1], Yu Wang[2], Ling Li[1], Jia Ling[2], Chaoxin Li[2], Qianqian Wang[5] and Yongqi Liu[1,6]**

[1]Gansu University Key Laboratory for Molecular Medicine and Chinese Medicine Prevention and Treatment of Major Diseases, Gansu University of Chinese Medicine, Lanzhou, China, [2]College of Pharmacy, Gansu University of Chinese Medicine, Lanzhou, China, [3]Gansu University of Chinese Medicine, Lanzhou, China, [4]Institute of Modern Physics, Chinese Academy of Sciences, Lanzhou, China, [5]Chronic Disease Research Center, Medical College, Dalian University, Dalian, China, [6]Key Laboratory of Dunhuang Medical and Transformation, Ministry of Education of The People's Republic of China, Lanzhou, China

OPEN ACCESS

Edited by:
Palanisamy Subramanian, Gangneung–Wonju National University, South Korea

Reviewed by:
Debasish Kumar Dey, University of Oklahoma, United States
C. Gopi Mohan FRSC, Amrita Vishwa Vidyapeetham University, India

***Correspondence:**
Qianqian Wang
wangqianqian@dlu.edu.cn
Yongqi Liu
liuyongqi73@163.com

†These authors have contributed equally to this work

Specialty section:
This article was submitted to Respiratory Pharmacology, a section of the journal Frontiers in Pharmacology

Received: 19 February 2022
Accepted: 06 April 2022
Published: 02 June 2022

Citation:
Wang Y, Jin X, Fan Q, Li C, Zhang M, Wang Y, Wu Q, Li J, Liu X, Wang S, Wang Y, Li L, Ling J, Li C, Wang Q and Liu Y (2022) Deciphering the Active Compounds and Mechanisms of HSBDF for Treating ALI via Integrating Chemical Bioinformatics Analysis. Front. Pharmacol. 13:879268. doi: 10.3389/fphar.2022.879268

The Huashi Baidu Formula (HSBDF), a key Chinese medical drug, has a remarkable clinical efficacy in treating acute lung injury (ALI), and it has been officially approved by the National Medical Products Administration of China for drug clinical trials. Nevertheless, the regulated mechanisms of HSBDF and its active compounds in plasma against ALI were rarely studied. Based on these considerations, the key anti-inflammatory compounds of HSBDF were screened by molecular docking and binding free energy. The key compounds were further identified in plasma by LC/MS. Network pharmacology was employed to identify the potential regulatory mechanism of the key compounds in plasma. Next, the network pharmacological prediction was validated by a series of experimental assays, including CCK-8, EdU staining, test of TNF-α, IL-6, MDA, and T-SOD, and flow cytometry, to identify active compounds. Molecular dynamic simulation and binding interaction patterns were used to evaluate the stability and affinity between active compounds and target. Finally, the active compounds were subjected to predict pharmacokinetic properties. Molecular docking revealed that HSBDF had potential effects of inhibiting inflammation by acting on IL-6R and TNF-α. Piceatannol, emodin, aloe-emodin, rhein, physcion, luteolin, and quercetin were key compounds that may ameliorate ALI, and among which, there were five compounds (emodin, aloe-emodin, rhein, luteolin, and quercetin) in plasma. Network pharmacology results suggested that five key compounds in plasma likely inhibited ALI by regulating inflammation and oxidative damage. Test performed *in vitro* suggested that HSBDF (0.03125 mg/ml), quercetin (1.5625 μM), emodin (3.125 μM), and rhein (1.5625 μM) have anti-inflammatory function against oxidative damage and decrease apoptosis in an inflammatory environment by LPS-stimulation. In addition, active compounds (quercetin, emodin, and rhein) had good development prospects, fine affinity, and stable conformations with the target protein. In summary, this study suggested that HSBDF and its key active components in plasma (quercetin, emodin, and rhein) can decrease levels of pro-inflammatory factors (IL-6 and

TNF-α), decrease expression of MDA, increase expression of T-SOD, and decrease cell apoptosis in an inflammatory environment. These data suggest that HSBDF has significant effect on anti-inflammation and anti-oxidative stress and also can decrease cell apoptosis in treating ALI. These findings provided an important strategy for developing new agents and facilitated clinical use of HSBDF against ALI.

Keywords: Traditional Chinese medicine, Huashi Baidu formula, acute lung injury, inflammation, oxidative stress, apoptosis

1 INTRODUCTION

Acute lung injury (ALI), an early stage of acute respiratory distress syndrome (ARDS) (Sun et al., 2020), can be caused by various intrapulmonary and extrapulmonary pathogenic factors, such as COVID-19 (Yang et al., 2020). HSBDF was recommended to treat ALI at the later stages of COVID-19 by the National Health Commission of the People's Republic of China (NHC) (Wang and Qi, 2020) and has been officially approved by the National Medical Products Administration of China for drug clinical trials due to remarkable clinical efficacy. However, its active compounds in plasma and its regulatory mechanisms are not clear yet.

Inflammatory cytokine storm is a characteristic of ALI. Previous studies indicated that interleukin 6 (IL-6) and tumor necrosis factor-α (TNF-α) were key cytokines involved in the pathological process of ALI (Gao et al., 2019). IL-6 and TNF-α were considered critical targets to prevent inflammation in treating ALI.

Molecular docking and network pharmacology are widely used in researching the material basis and mechanism of TCM in the prevention and treatment of disease (Yu R et al., 2020; Yu S et al., 2020; Chen et al., 2021a; Chen et al., 2021b; Chen et al., 2021c; Wang et al., 2021). However, owing to the complexity of TCM and the compounds in plasma remained elusive, it is necessary to make full use of the LC/MS method to conduct the research on active compounds of HSBDF in plasma in treating ALI. Therefore, based on IL-6 and TNF-α, this study aimed to uncover the regulatory mechanisms of HSBDF and its active compounds in plasma against ALI by the integrated strategy of molecular docking, LC/MS, network pharmacology, and *in vitro* approaches, which provide the basic data for further scientific research and clinical use of HSBDF in treating ALI.

2 MATERIALS AND METHODS

2.1 Materials and Reagents

Ephedra sinica (Shengmahuang, No. 190701), *Agastache rugosus* (Huoxiang, No. 200803003), Gypsum Fibrosum (Shengshigao, No. 201001), *Semen armeniacae amarum* (Kuxingren, No. 202012002), *Rhizoma Pinelliae Preparata* (Fabanxia, No. D2012128), *Magnolia officinalis* (Houpo, No. 202009002), *Atractylodes lancea* (Cangzhu, No. 20210120), *Fructus tsaoko* (Caoguo, No. 20180919), *Poria cocos* (Fuling, JZ2105009), *Astragalus membranaceus* (Shenghuangqi, No. 20210108), *Radix Paeoniae Rubra* (Chishao, No. 2103012), *Lepidium apetalum* (Tinglizi, No. 20210206), *Rheum officinale* (Shengdahuang, No. JZ2012020), and *Glycyrrhiza uralensis* (Gancao, No. 20210201) were obtained from The Affiliated Hospital of Gansu University of Chinese Medicine (Lanzhou, China) at an accurate prescription dose, and their equality control adhered to the specifications and test procedures as described in the Pharmacopoeia of the People's Republic of China (2020). HSBDF was decocted with water (1:8, w/v) for 60 min. The aqueous solutions were obtained by merging, filtrating, and concentrating to 1.23 g/ml. The extracts were kept at 4°C for preparation of a lyophilized powder for further oral administration to rats and preparation of lyophilized powder.

Methanol and acetonitrile (HPLC pure grade) were purchased from MREDA (MREDA, China), and formic acid of the same grade was provided by Thermo Fisher (Thermo Fisher, Waltham, MA, United States). Ultrapure water was obtained from Wahaha (Wahaha, China) and used throughout the study. Quercetin, luteolin, piceatannol, emodin, rhein, aloe-emodin, and physcion were all purchased from Baoji Herbest Bio-Tech Co., Ltd. (Herbest Bio-Tech, China). The purity of all reference standards was more than 98%. Other reagents of analytical grade were obtained from commercial sources.

LPS, cell counting kit-8, and Click-iT EdU-488 cell proliferation kit were purchased from Solarbio (Beijing, China), Yeasen (Yeasen Biotech, China), and Servicebio (Wuhan, China), respectively. DME/F-12, 1,640, and PBS were obtained from HyClone (HyClone, Logan, UT, United States). Annexin V−FITC/PI apoptosis detection kit was provided by Meilunbio (Dalian, China). MDA (20211202) and T-SOD (20211201) were purchased from Nanjing Jiancheng Bioengineering Institute (Nanjing, China). ELISA kits including TNF-α (2111H27) and IL-6 (2111H35) were purchased from Jiangsu Feiya Biotechnology Co., Ltd. (Jiangsu, China).

2.2 Virtual Screening and Pharmacokinetic Prediction

2.2.1 Compounds of Huashi Baidu Formula

The compounds were collected from the traditional Chinese medicine systems pharmacology (TCMSP, https://www.tcmspw.com/tcmsp.php) (Ru et al., 2014) database and Traditional Chinese Medicines Integrated Database (TCMID, http://119.3.41.228: 8000/tcmid/) (Xue et al., 2013). Meanwhile, compounds of each herb were supplemented through a literature search in the PubMed database (https://pubmed.ncbi.nlm.nih.gov/). A total of 1,613 compounds were

retrieved for 13 herbs, among which there were *E. sinica* (363), *S. armeniacae amarum* (113), *L. apetalum* (68), *R. paeoniae rubra* (119), *A. rugosus* (94), *M. officinalis* (139), *A. lancea* (49), *F. tsaoko* (59), *Astragalus membranaceus* (87), *Glycyrrhiza uralensis* (280), *R. officinale* (92), *P. cocos* (34), and *R. Pinelliae Preparata* (116). It was worth noting that Gypsum Fibrosum is a mineral drug, and its main composition was $CaSO_4 \bullet 2H_2O$. Therefore, its mechanism of action was not included in this study.

2.2.2 3D Structures of Protein

The 3D structures of IL-6R (PDB ID: 1P9M) (Ho et al., 2009), TNF-α (PDB ID: 2AZ5) (He et al., 2005), PIK3R1 (PDB ID: 4I6J) (Xing et al., 2013), SRC (PDB ID: 4U5J) (Duan et al., 2014), AKT1 (PDB ID: 4EKL) (Lin et al., 2012), TP53 (PDB ID: 5LAY) (Gollner et al., 2016), and PIK3CA (PDB ID: 7K6M) (Cheng et al., 2021) were downloaded from the RCSB Protein Data Bank (PDB, https://www.rcsb.org/).

2.2.3 Molecular Docking and Binding Free Energy Calculation

3D structures of protein in 2.2.2 were preprocessed by Protein Preparation Wizard. The compounds in 2.2.1 were prepared by the LigPrep module (Sheikh et al., 2018). A total of 1,613 compounds were docked with IL-6R and TNF-α by the Glide standard docking precision method (SP) in Schrődinger 2020-4. The corresponding low-energy conformation was obtained by MMFFs. Next, epik28 (Manchester et al., 2010) used a pH value of 7.0 ± 2.0 to conditionally allocate the ionization state and perform docking calculations.

The binding free energy was used to evaluate the affinity between the ligand and receptor. Lower binding free energy indicates a higher affinity or catalytic activity (Wu et al., 2009). In this study, MM/GBSA in the prime program was used to estimate binding energy (Hou et al., 2011). The formula is: DG bind = E_complex (minimized)—E_ligand (minimized)-E_receptor (minimized).

2.2.4 Molecular Dynamic Simulation and Binding Interaction Pattern Analysis

The initial structures of the protein complex with active compounds (emodin, rhein, and quercetin) were obtained from molecular docking. To further determine the stability of rhein and quercetin with IL-6R and rhein and emodin with the TNF-α complex in a simulated physiological solvent system, we used the Desmond module of Schrödinger to carry out molecular dynamic simulation. The molecular system was solvated with crystallographic water (TIP3P) for a 10-Å buffer region under orthorhombic periodic boundary conditions. The system charges were neutralized by adding Na^+ and Cl^-. The molecular system was solvated with crystallographic water (TIP3P) molecules under orthorhombic periodic boundary conditions for a 10 Å buffer region. The system charges were neutralized by adding Na^+ and Cl^-. The OPLS_2005 force field was used for energy calculation. After this, an ensemble (NPT) of Nose–Hoover thermostat and barostat was applied to maintain the constant temperature (300°K) and pressure (1 bar) of the systems, respectively. The complex structural dynamic simulation for the best complex was carried out with an NPT ensemble for 50°ns, and the trajectory was set at an interval of 10°ps. The RMSD (root mean square distance) was used to compare the prediction error in disparate models of specific data sets and protein–ligand contacts with the timeline. In addition, the 3D binding interaction pattern of active compounds with protein was visualized by PyMOL.

2.2.5 Pharmacokinetic Prediction of Active Compounds

The parameters of absorption, distribution, metabolism, excretion, and toxicity (ADMET) of emodin, rhein, and quercetin were calculated by using the ProTox-II data platform. In addition, active compounds that conformed to Lipinski's rule were predicted by the QikProp module of Schrödinger.

2.3 LC/MS Analysis

2.3.1 Animals and Drug Administration

A total of six male Sprague-Dawley rats (200 ± 20°g, SPF grade) were purchased from the Laboratory Animal Center of Gansu University of Chinese Medicine (Lanzhou, China) with license number: SCXK (gan) 2020-0001. All animals were housed in the Laboratory Animal Center of Gansu University of Chinese Medicine [animal license number: SCXK (gan) 2020-0009]. The rats were fed standard rodent chow and water *ad libitum* in a house with a 12 h light/dark cycle (temperature and humidity of 23°C ± 2°C and 60% ± 5%, respectively) for 10 days to adapt to the experimental environment. The experimental protocol, approved by the Committee for Ethics in the Laboratory Animal Center of Gansu University of Chinese Medicine (number: 2021-182), was conducted in strict accordance with the ethical principles in animal research.

2.3.2 Instrumentations and Analytical Conditions

The triple quadrupole LC/MS system consisted of an ExionLC (SCIEX, Framingham, MA, United States) and a SCIEX Triple Quad 5,500+ (SCIEX, Framingham, MA, United States) equipped with an ESI source. The chromatographic separation was achieved on a Kinetex C18 column (100 mm × 2.1 mm, 2.6 μm, Kinetex® C18, Phenomenex, United States). The water (containing 0.2% formic acid, solvent A) acetonitrile, and methanol (1:1, v: v, solvent B) system was used as the mobile phase. Analysis was achieved by gradient elution at a flow rate of 0.3 ml/min. The gradient elution program was: 0–2 min, 10% B; 2–5 min, 10%–40% B; 5–15 min, 40%–50% B; 15–30 min, 50%–55% B; 30–50 min, 55%–66% B; 50–63 min, 66%–80% B; and 63–73 min, 80%–100% B. The column and auto-sampler tray temperatures were kept at 30°C and 4°C, respectively. The injection volume was 2 μl. All analytes were quantified using multiple reaction monitoring (MRM) detection in the negative ion mode. The parameters of MRM are shown in **Table 1**. Other main working parameters were as follows: curtain gas (CUR), ion source gas1 (GS1), and ion source gas2 (GS2) were set at 35, 50, and 50 psi, respectively. IonSpray (IS) voltage, −4,500 V; temperature (TEM), 550°C.

TABLE 1 | Ions and fragmentations used in the MRM mode for seven compounds.

Compound	MRM fragment	Dwell time (msec)	DP (volts)	DP (volts)	Retention time (min)
Piceatannol	243.1/159	100	−122	−36.7	5.10
	243.1/201.1	100	−122.42	−31.26	
Emodin	269/225	100	−117.21	−39.04	22.39
	269/241	100	−104.02	−39.26	
Aloe-emodin	269.1/240	100	−122.91	−30.76	12.00
	269.1/183.1	100	−122.94	−44.76	
	271.3/239.1	100	−89.09	−51.73	
Rhein	283.1/239	100	−49.87	−24.24	14.77
	283.1/183.1	100	−49.93	−42.03	
	283.1/211.1	100	−50.76	−35.1	
Physcion	283.2/240.1	100	−93.21	−37.75	35.36
	283.2/211.1	100	−68.93	−47	
	283.2/183	100	−66.86	−56	
Luteolin	285.1/133.1	100	−92.87	−45.01	7.62
	285.1/151	100	−118.83	−35.17	
Quercetin	301.1/151	100	−80.95	−27.86	7.77
	301.1/179	100	−75.02	−25.84	

Note: DP, declustering potential; CE, collision energy.

2.3.3 Preparation of Standard Working Solutions, Calibration Standards, Huashi Baidu Formula Extracts, and Plasma Samples

In this study, standard working solutions were made up of mixed standard and single standard. The single standard was made up of quercetin (100 ng/ml). Piceatannol (5,000 ng/ml), emodin (90 ng/ml), rhein (15,000 ng/ml), aloe-emodin (6,000 ng/ml), physcion (150,000 ng/ml), and luteolin (300 ng/ml) were taken 10 μl each to form the mixed standard. Standard working solutions (100 μl) were added to blank plasma (100 μl) to form the calibration standards and stored at 4°C until use.

HSBDF (1.23 g/ml, 20 ml) was filtered, concentrated, dried, and dissolved in 50 ml water (containing 80% analytical-grade methanol) to collect HSBDF extracts (stored at 4°C). Also, the HSBDF extracts were filtered through a 0.22-μm syringe filter when used.

In previous studies, rats fasted overnight with free access to water. The plasma samples (~0.2 ml) were collected into heparinized microcentrifuge tubes through the caudal vein at 2 h after a single oral administration of HSBDF water decocted. The plasmas were centrifuged at 4,000 rpm for 10 min immediately after collection to obtain plasma. The plasma samples were stored at −80°C until analysis.

The calibration standards and plasma samples were treated with the protein precipitation method using methanol. The procedure was as follows: 100 μl samples were mixed with 800 μl methanol, then vortexed for 5 min, and centrifuged at 13,000 rpm for 10 min. The supernatant was transferred into a clean tube and evaporated with a stream of nitrogen. The residue was dissolved with methanol and was filtered using a 0.22-μm syringe filter to test.

2.4 Network Pharmacology Analysis

2.4.1 PPI Analysis

The similarity ensemble approach (SEA) (https://sea.bkslab.org/) (Keiser et al., 2007) was used to predict targets of the key compounds in plasma (emodin, aloe-emodin, rhein, luteolin, and quercetin). The targets were imported into the STRING database (https://string-db.org/) (Szklarczyk et al., 2017), and the organism was set to "Homo sapiens." The comprehensive score of protein interaction (confidence data >0.9) was used to obtain the PPI information of the target. The major parameter "degree" was used to evaluate its topological features for each node in the interaction network. Based on the degree, bioinformatics (http://www.bioinformatics.com.cn/) was used to visualize the key targets (top 20 targets).

2.4.2 Enrichment

GO and KEGG enrichment was carried out using DAVID (https://david.ncifcrf.gov/) databases. A total of 151 targets of key compounds in plasma were imported using the DAVID database. The select identifier was set to official gene, list type was set to gene list, species was set to "Homo sapiens," and the threshold was set at $p < 0.05$. Bioinformatics and GOChord of R language were used to construct the GO and pathway-target diagram, respectively.

2.5 Test *In Vitro*

2.5.1 Cell Culture

A549 and MLE-12 cells were purchased from Zhong Qiao Xin Zhou Biotechnology Co., Ltd. (Shanghai, China) and maintained at 37°C under 5% CO2 in DME/F-12 and 1,640 medium supplemented with 10% fetal bovine serum, respectively.

HSBDF condensed extract of 1.23 g/ml was lyophilized using a freeze dryer (EYELA, Japan). Finally, 15.38 g of lyophilized powder was obtained (yield, 11.23%). The dry powder was stored in an 80°C refrigerator until use.

2.5.2 Cell Viability Analysis

Cell viability of A549 and MLE-12 cells were measured with the CCK-8 assay after compound intervention. The cells were seeded in 96-well plates at a density of 5×10^3 cells/well in 200 μl of

culture media and grown for 4 h. Second, they were treated with different concentrations of LPS, quercetin, luteolin, emodin, rhein, aloe-emodin, and HSBDF. Subsequently, 10 μl of CCK-8 solution was added to each well, and the plates were incubated for 1 h. The optical density of each well was determined at 450 nm using a microplate reader (Bio-Rad, Hercules, CA, United States).

2.5.3 EdU Proliferation Analysis

EdU proliferation kit was employed for the determination of DNA synthetic capacity in proliferating cells. A549 cells were cultured in 96-well plates and grown for 4 h. After being treated for 24 h with compounds, the cells were strictly conducted following the instructions of the kit. Live cell imaging system (OLYMPUS, Japan, 20×) and ImageJ software were employed for calculating the number of EdU-positive cells (green cells). The percentage of EdU-positive cells to total Hoechst 33342-positive cells (blue cells) was represented as the EdU-positive rate.

2.5.4 Enzyme-Linked Immunosorbent Assay, MDA, and T-SOD Analysis

The A549 cells culture medium was gathered and centrifuged (3,000 r/min×20 min) at 4°C. The supernatant liquid was taken out for detection of MDA, T-SOD, TNF-α, and IL-6. Enzyme-Linked Immunosorbent Assay (ELISA) (TNF-α and IL-6), MDA, and T-SOD steps were followed as per the instructions of the reagent kit.

2.5.5 Flow Cytometry Analysis

FITC-conjugated annexin V was used to detect apoptosis. A549 cells were cultured in six-well plates (1×10^5 cells/well) for 4 h before treatment. After adding LPS, quercetin, emodin, rhein, and HSBDF, the cells were incubated for 24 h. Next, the cells were gathered and stained using the annexin V–FITC/PI apoptosis detection kit following the manufacturer's instructions. The resulting fluorescence signal was detected by flow cytometry (BD, FACSCelesta).

2.5.6 Statistical Analysis

Analyses were performed using GraphPad Prism 6 software. The results are expressed as mean ± standard deviation (SD) of at least three independent experiments. The statistical differences between the two groups were compared by Student's t-test. $p < 0.05$ was considered statistically significant.

3 RESULTS AND DISCUSSION

3.1 Analysis of Key Anti-Inflammatory Compounds of Huashi Baidu Formula

3.1.1 Huashi Baidu Formula Had Potential Effects to Inhibit Inflammation

To explore the anti-inflammatory effect of HSBDF, 1,613 compounds were docked with IL-6R and TNF-α by Schrődinger. The compound with a docking score of ≤ −5 Kcal/mol was known as the potentially effective compound (Hsin et al., 2013). It can be seen that the total number of compounds with potential inhibitory activities was IL-6R (96) and TNF-α (111) as shown in **Table 2**, indicating that the formula had potential effects on inhibiting inflammation by acting on IL-6R and TNF-α.

In terms of a single herb, it was found that *Glycyrrhiza uralensis*, *Ephedra sinica*, and *Rheum officinale* were the top three docking herbs with two targets, respectively. Previous studies also demonstrated that Glycyrrhiza polysaccharide (50 mg/kg) had a certain therapeutic effect on lung inflammation and oxidative damage in COPD mice (Wu et al., 2020); *Ephedra sinica* water plays an important role in distillates in arthritic rats (Yeom et al., 2006); *Rheum officinale* ethanol extract can effectively improve the pulmonary inflammation in mice infected with mycoplasma pneumonia (Gao et al., 2021). These results suggested that *Glycyrrhiza uralensis*, *Ephedra sinica*, and *Rheum officinale* were key herbs to inhibit inflammation, which was of great significance to ameliorate ALI.

3.1.2 Piceatannol, Emodin, Aloe-Emodin, Rhein, Physcion, Luteolin, and Quercetin Were Key Compounds

To determine anti-inflammatory key compounds, we selected the compounds, which conformed to Lipinski's rules (MW < 500, H-bond donor<5, H-bond acceptor<10, log P (O/W) < 5, and rotor ≤10) and docking score ≤−5 Kcal/mol, to analyze further. Based on the Pharmacopoeia of the People's Republic of China (2020) and the literature of every herb's main components, seven key compounds were selected from the top 50 compounds with high docking scores (**Table 3**). These compounds' binding free energy was further calculated in Schrődinger.

The results indicated that piceatannol, emodin, aloe-emodin, rhein, physcion, luteolin, and quercetin had potential effects on inhibiting inflammation. Therefore, these compounds were considered key compounds to explore further. Also, we found that these compounds were mainly distributed in *Glycyrrhiza uralensis*, *E. sinica*, and *R. officinale*, which further provides support that *Glycyrrhiza uralensis*, *E. sinica*, and *R. officinale* were key herbs to treat ALI.

3.2 Key Compounds in Plasma by LC/MS

In order to further analyze whether the seven key compounds (piceatannol, emodin, aloe-emodin, rhein, physcion, luteolin, and quercetin) were present in plasma, LC/MS was used. The results of preliminary experiments showed that the number of chromatographic peaks and intensity of peaks were the most strongly detected in 2 h plasma after HSBDF administration. Therefore, 2 h was selected to collect plasma after drug administration. Ion chromatograms of standards (S1) of key compounds, calibration standards (S2), HSBDF extracts (S3), and plasma sample (S4) are displayed in **Figure 1A**. LC/MS analysis showed that a total of five compounds (emodin, aloe-emodin, rhein, luteolin, and quercetin) were identified in HSBDF extracts; four compounds (emodin, aloe-emodin, rhein, and luteolin) were identified in the plasma sample at 2 h, considering that quercetin was rapidly hydrolyzed after oral administration (Jiang and Hu, 2012).

Therefore, LC/MS analysis showed that there were five key compounds in plasma of HSBDF, including emodin, aloe-

TABLE 2 | Number statistics of molecular docking.

No	Latin name of the herb	Chinese name of the herb	Number of compounds with docking score ≤–5 Kcal/mol	
			IL-6R	TNF-α
1	*E. sinica*	Shengmahuang	17	25
2	*S. armeniacae amarum*	Kuxingren	2	5
3	*L. apetalum*	Tinglizi	5	2
4	*R. Paeoniae Rubra*	Chishao	9	7
5	*A. rugosus*	Huoxiang	5	5
6	*M. officinalis*	Houpo	1	8
7	*A. lancea*	Cangzhu	0	1
8	*F. tsaoko*	Caoguo	7	6
9	*A. membranaceus*	Shenghuangqi	13	6
10	*G. uralensis*	Gancao	30	41
11	*R. officinale*	Shengdahuang	19	16
12	*P. cocos*	Fuling	0	0
13	*R. Pinelliae Preparata*	Fabanxia	8	11
Total			96	111

Note: The total number in the table is the result after weight removal.

TABLE 3 | Information of the representative compounds.

Target	Constituent	Herb	Docking score (Kcal/mol)	Binding free energy (Kcal/mol)
IL-6R	Aloe-emodin	*R. officinale*	–5.73	–38.50
	Physcion	*R. officinale*	–5.43	–39.68
	Rhein	*R. officinale*	–5.31	–23.75
	Luteolin	*E. sinica*	–5.12	–36.29
	Quercetin	*E. sinica*, *L. apetalum*, *A. rugosus*, *F. tsaoko*, *A. membranaceus*, and *G. uralensis*	–5.08	–39.35
TNF-α	Aloe-emodin	*R. officinale*	–5.57	–36.60
	Piceatannol	*R. officinale*	–5.38	–37.68
	Emodin	*R. officinale*	–5.36	–36.16
	Rhein	*R. officinale*	–5.28	–29.87
	Physcion	*R. officinale*	–5.28	–38.41
	Luteolin	*E. sinica*	–5.24	–38.38

emodin, rhein, luteolin, and quercetin. The structures of these compounds are shown in **Figure 1B**.

3.3 Network Pharmacology of Key Compounds in Plasma

3.3.1 PPI Analysis and Molecular Docking Verification

It was well known that network pharmacology contributes to exploring the potential mechanism of TCM in prevention and treatment of disease (Li et al., 2021). Therefore, in order to analyze the mechanism of key compounds in plasma, top 20 in 151 (confidence data >0.9) targets of PPI are listed in **Figure 2A**. The result showed that the top 20 targets of degree were TP53, SRC, PIK3R1, PIK3CA, AKT1, EGFR, CDK1, ESR1, PTPN11, CASP3, PTK2, FYN, MAPK8, LCK, CCNB1, CCNB2, AR, GSK3B, APP, and PTPN1.

In order to further validate the prediction of network pharmacology, five nodes, namely, TP53, SRC, PIK3R1, PIK3CA, and AKT1 with the highest degree were taken as examples to be analyzed. Their crystal structure was subjected and docked with corresponding compounds. Finally, constituent with docking score ≤ −5 (Kcal/mol) was selected to analyze. The total proportion of TP53 (5/5), SRC (5/5), PIK3R1 (5/5), PIK3CA (5/5), and AKT1 (4/5) was 96%, and the results are shown in **Figure 2B**. The results of molecular docking showed that the prediction accuracy was high, which verified the result of PPI.

It was reported that SRC could inhibit TLR4-induced inflammatory cytokines and promote anti-inflammatory cytokine IL-10, which plays an important role in the treatment of acute and chronic inflammation (Li et al., 2019). The pharmacological study suggested that *G. baccata* extract can upregulate *AKT1* gene expressions to protect the cells against oxidative damage and inflammation (Martínez et al., 2021). Moreover, the studies also suggested that TP53, PIK3R1, and PIK3CA were vital for inflammation (Eyileten et al., 2018; Busbee et al., 2021; Reske et al., 2021). Accordingly, the results indicate that emodin, aloe-emodin, rhein, luteolin, and quercetin may play an important role in inhibiting anti-inflammatory and anti-oxidative damage.

3.3.2 GO and KEGG Enrichment Analysis

To explore the regulatory mechanisms of key compounds in plasma, a total of 267 terms were enriched ($p < 0.01$), and the top five of GO enrichment were visualized, as shown in **Figure 2C**. Among which, biological processes (BP) include protein phosphorylation, peptidyl-

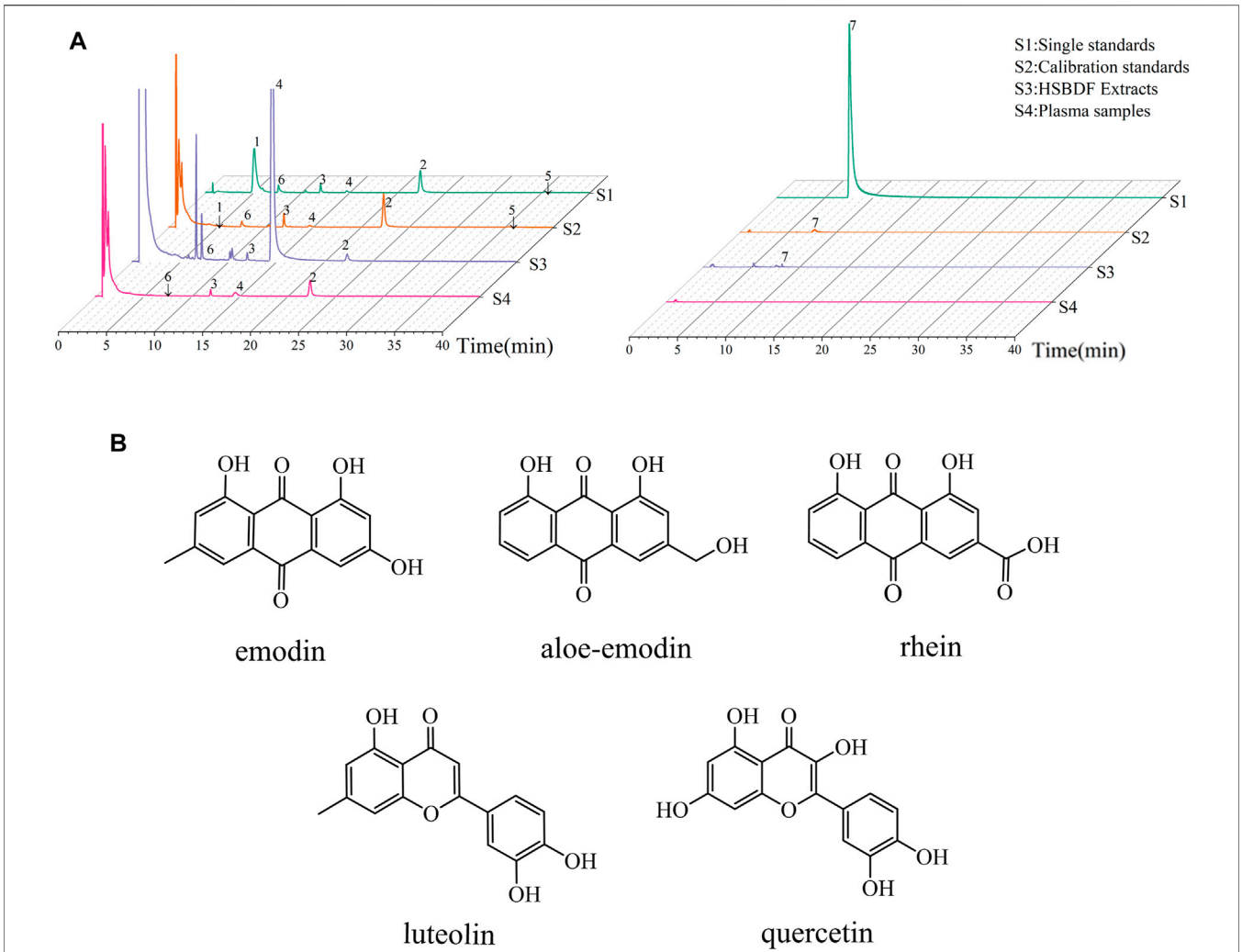

FIGURE 1 | Key compounds analysis by LC/MS. **(A)** MRM chromatograms of key compounds (1–7 represent piceatannol, emodin, aloe-emodin, rhein, physcion, luteolin, and quercetin, respectively); **(B)** structure of key compounds in plasma.

serine phosphorylation, and protein autophosphorylation, etc; cell composition (CC) includes cytosol, plasma membrane, extracellular exosome, cytoplasm, and nucleoplasm; and molecular function (MF) includes protein kinase activity, protein serine/threonine kinase activity, ATP binding, and so on.

Moreover, we had used 151 targets to enrich 107 pathways ($p < 0.05$), and the top 20 targets and top 20 pathways are shown in **Figure 2D**. It can be seen that the HIF-1 signaling pathway, the ErbB signaling pathway, the TNF signaling pathway, and so on may be the key regulated pathways of emodin, aloe-emodin, rhein, luteolin, and quercetin. Also, studies have shown that the HIF-1α signaling pathway was related to inflammation, and arginine can regulate HIF-1α to suppress the inflammatory response (Chen et al., 2020). The Er7bB signaling pathway was associated with oxidative stress, and it was reported that the ErbB4 system of the heart was activated at early stages of chronic heart failure to enhance the cardiomyocyte resistance to oxidative stress (Shchendrigina et al., 2020). The TNF signaling pathways and inflammatory pathways can suppress inflammation (Liang et al., 2021).

Network pharmacology results suggested that emodin, aloe-emodin, rhein, luteolin, and quercetin likely treated ALI by regulating the biological function and pathways related to anti-inflammatory and anti-oxidative damage.

3.4 Test *In Vitro* of Key Compounds in Plasma

3.4.1 Inflammatory Model With LPS

A549 is a human alveolar epithelial cell line. It is often used to research lung diseases, such as ARDS (Lin et al., 2020), ALI (Geiser et al., 2001; Zhao et al., 2021). Therefore, we used A549 to further study ALI. To determine the optimal concentration and time of LPS, cell counting kit-8 (CCK-8) was used to detect the viability of A549 cells in this study. As shown in **Figure 3**, LPS markedly decreased the cell viability of A549 cells in a dose- and

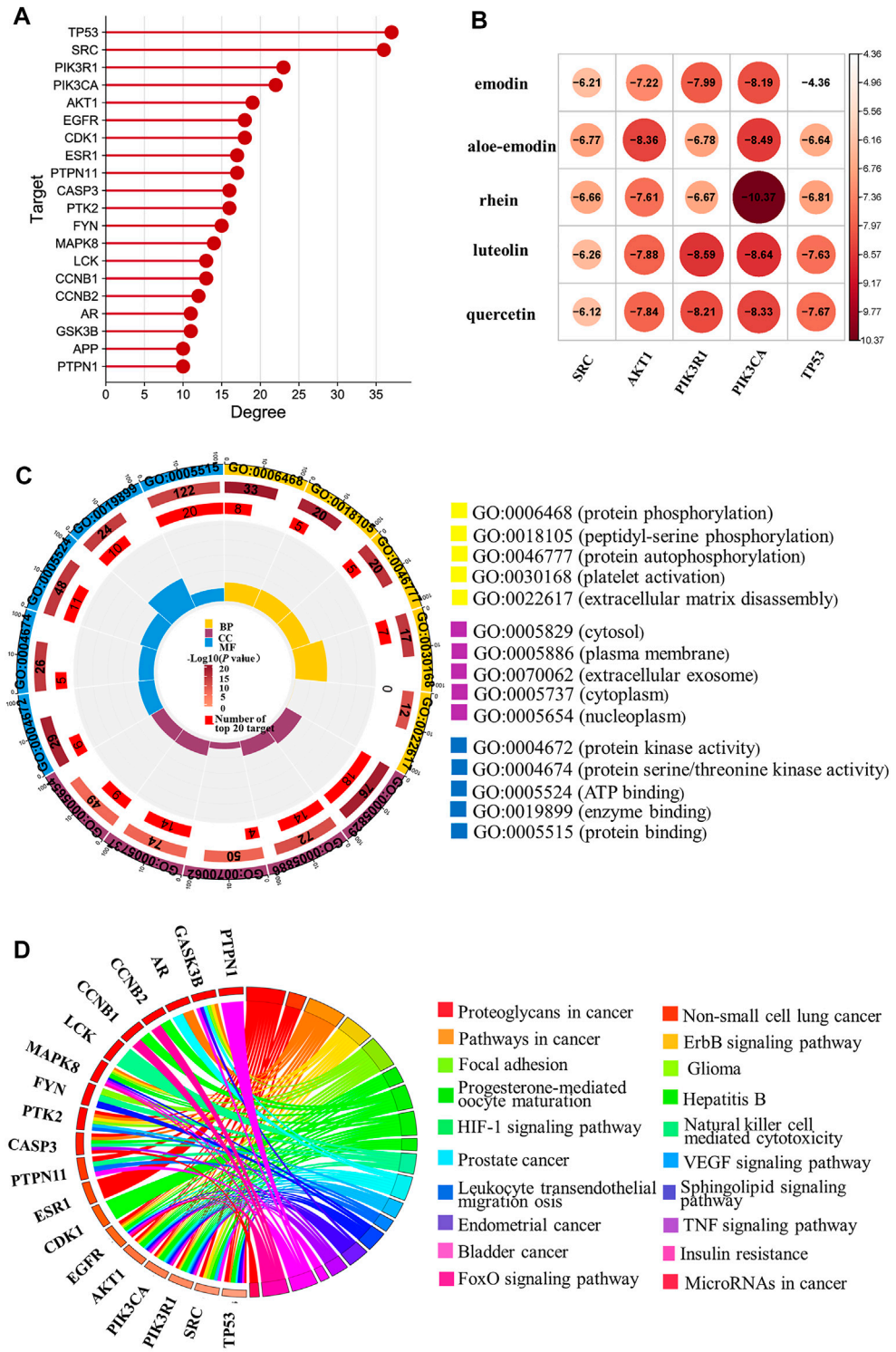

FIGURE 2 | Network pharmacology analysis of key compounds in plasma. **(A)** Top 20 targets of PPI; **(B)** molecular docking results of the key compounds in plasma with top five targets of PPI; **(C)** GO enrichment of the key compounds in plasma; **(D)** pathway-target diagram of key compounds in plasma.

time-dependent manner. The cell viability was reduced by approximately 50% when A549 was subjected to 6.25 μg/ml of LPS compared with blank ($p < 0.01$) in 24 h, indicating that 6.25 μg/ml of LPS is deleterious to the epithelial cell. LPS of 12.5, 25, 50, or 100 μg/ml decreased cell viability more prominently than 6.25 μg/ml LPS did, which demonstrated that LPS induced

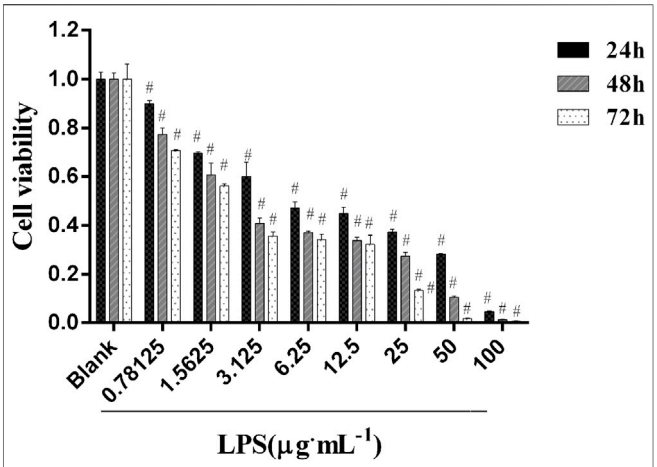

FIGURE 3 | Cell Viability after different treatments of LPS (*$p < 0.05$, #$p < 0.01$ versus blank).

cell viability loss in a dose-dependent manner and that the lowest effective injury dose of 24 h LPS treatment was 6.25 μg/ml (Liu et al., 2021). Consequently, further experiments were performed with 6.25 μg/ml of LPS at 24 h.

3.4.2 Cell Viability of the Huashi Baidu Formula and Key Compounds in Plasma

In order to determine the effect of HSBDF and key compounds in plasma on the viability of A549 cells, CCK-8 was used to detect the viability of cells treated with different concentrations of drug for 24 h (**Figure 4**). The results showed that HSBDF and key compounds in plasma can increase the cytotoxicity of A549 cells in a dose-dependent manner. Moreover, we found that A549 cell proliferation was markedly promoted with low concentration of quercetin (1.5625 μM), emodin (3.125 μM), rhein (1.5625 μM), and HSBDF (0.03125 mg/ml), whereas aloe-emodin and luteolin did not. The cell viability was further tested for normal epithelial cells (MLE12) after treating with low concentration of quercetin, emodin, and rhein. (**Supplementary Figure S1**). We found that the viability of lung epithelial cells, such as A549 and MLE-12, can be increased by these key compounds.

3.4.3 Huashi Baidu Formula and Active Compounds Promote A549 Cell Proliferation in an Inflammatory Environment

To further evaluate the effects of HSBDF, quercetin, emodin, and rhein on A549 cells grown in an inflammatory environment, the EdU proliferation kit and cck-8 were used to detect proliferating cells and the viability of cells, respectively. As shown in **Figure 5A**, we found that inflammation stimulated by LPS inhibited the proliferation of A549 cells, whereas inhibition of proliferation was decreased by quercetin (1.5625 μM), emodin (3.125 μM), rhein (1.5625 μM), and HSBDF (0.03125 mg/ml). The stimulative proliferation of quercetin (1.5625 μM), emodin (3.125 μM), rhein (1.5625 μM), and HSBDF (0.03125 mg/ml) on A549 cells cultured in an inflammatory environment was also confirmed by EdU proliferation staining (**Figures 5B1,B2**). These results demonstrate that quercetin, emodin, rhein, and HSBDF were

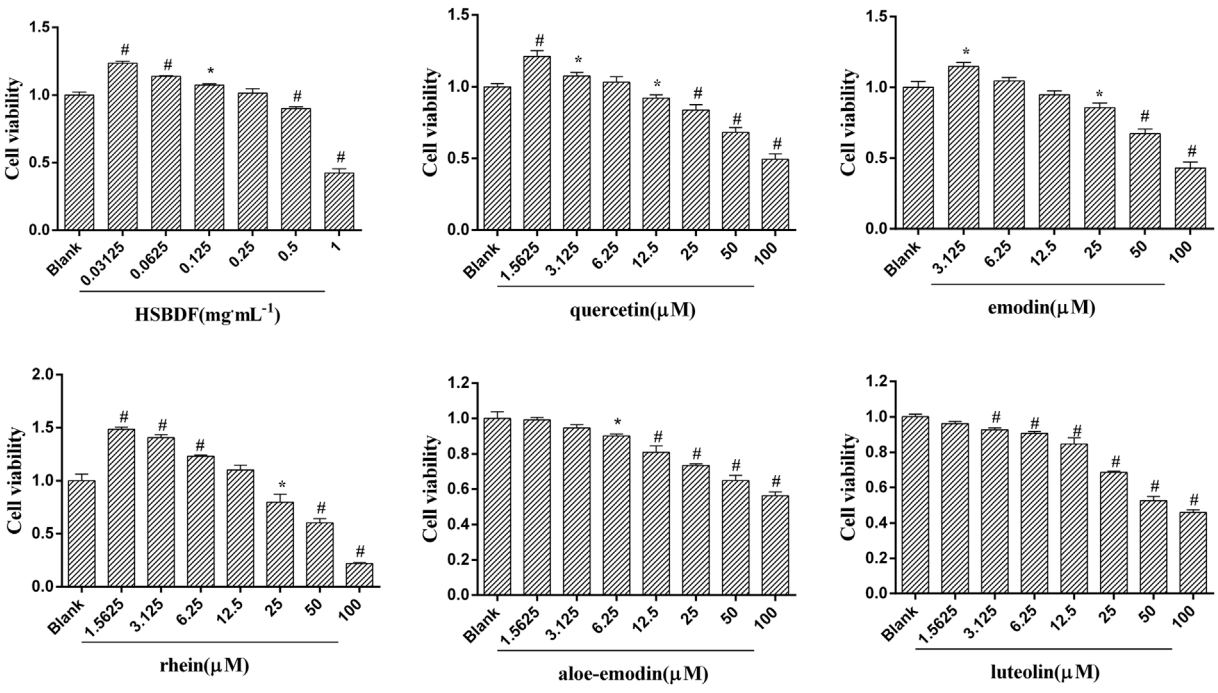

FIGURE 4 | Cell viability after treatments of HSBDF and key compounds in plasma. (cell viability was detected by CCK-8; *$p < 0.05$, #$p < 0.01$ versus blank).

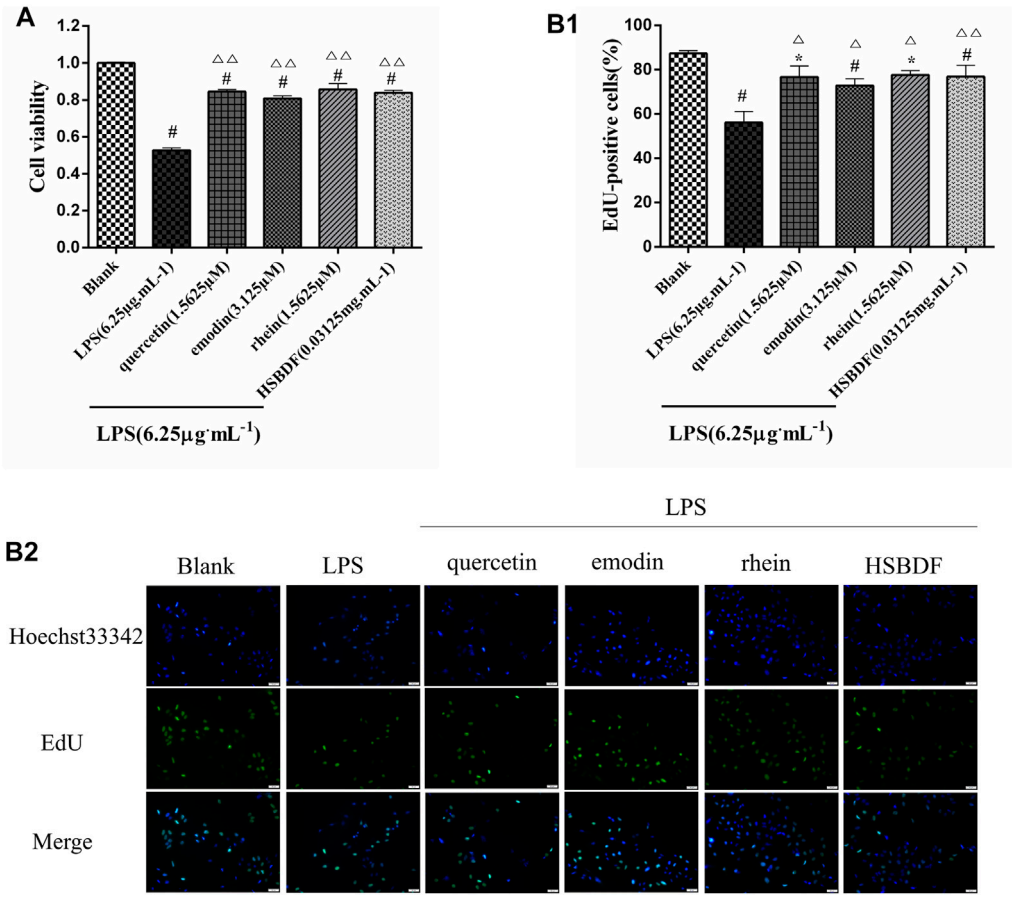

FIGURE 5 | Effect of HSBDF and active compounds treatment on cell proliferation in LPS-stimulated A549 cells. **(A)** Cell proliferation test by CCK-8; **(B1,B2)** DNA synthesis activity in cells examined by EdU staining (magnification, x20) (*$p < 0.05$, #$p < 0.01$ versus blank; △$p < 0.05$, △△$p < 0.01$ versus LPS).

effective in inhibiting inflammation. Therefore, HSBDF (0.03125 mg/ml), quercetin (1.5625 μM), emodin (3.125 μM), and rhein (1.5625 μM) were active compounds for further experiments.

3.4.4 Huashi Baidu Formula and Active Compounds Decrease Expression of TNF-α and IL-6, Decrease Expression of MDA, and Increase Expression of T-SOD in A549 Cells in an Inflammatory Environment

To determine the effect of HSBDF and active compounds on the expression of inflammatory cytokine, ELISA was used to measure the expression levels of IL-6 and TNF-α in the cell supernatant liquid. The elevated expressions of TNF-α and IL-6 induced by LPS in A549 cells were inhibited by quercetin (1.5625 μM), emodin (3.125 μM), rhein (1.5625 μM), and HSBDF (0.03125 mg/ml) (**Figure 6A**).

Simultaneously, the anti-oxidative stress of HSBDF and active compounds was further researched in an inflammatory environment. We found that the oxidative stress injury was weakened after treatment of HSBDF and active compounds. The SOD was enhanced significantly by active compounds, while the MDA was decreased (**Figure 6B**).

These results further verify that network pharmacology results indicate that emodin, rhein, and quercetin have the function of anti-inflammation and act against oxidative damage.

3.4.5 Huashi Baidu Formula and Active Compounds Inhibit A549 Cell Apoptosis in an Inflammatory Environment

LPS has been known to cause alveolar epithelial cell apoptosis that characterizes ALI (Hou et al., 2021). Therefore, the anti-apoptosis of HSBDF and active compounds was further investigated in an inflammatory environment. We investigated the effects of drugs on the apoptosis of A549 cells in an inflammatory environment by flow cytometry. We found that LPS increased A549 cell apoptosis. The apoptosis was significantly decreased after the intervention of quercetin, emodin, rhein, and HSBDF in an inflammatory environment (**Figure 7**).

4 MOLECULAR DYNAMIC SIMULATION AND BINDING INTERACTION PATTERN OF THE COMPLEX OF ACTIVE COMPOUNDS AND PROTEIN

To further confirm the molecular docking insights and analyze the conformation stability of active compounds and target proteins, molecular dynamic simulations were

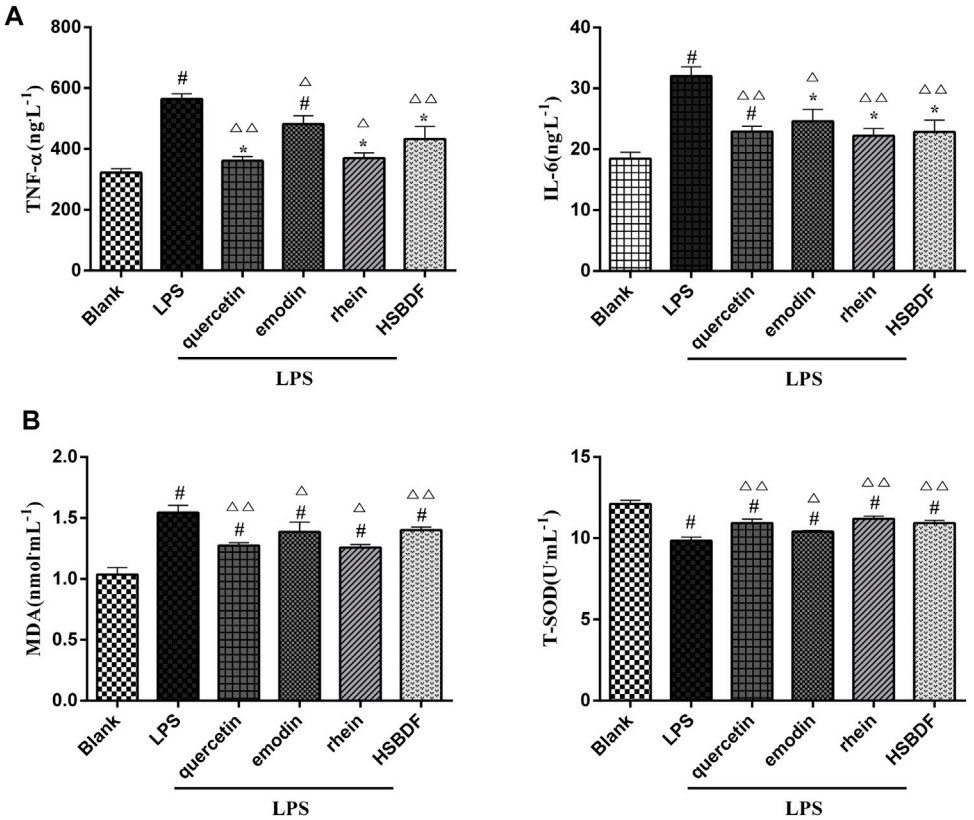

FIGURE 6 | (A) Effects of HSBDF and active compound treatment on the expression levels of inflammatory cytokine (IL-6 and TNF-α) in LPS-stimulated A549 cells by the ELISA test. **(B)** Effects of HSBDF and active compound treatment on oxidative stress (MDA and T-SOD) in LPS-stimulated A549 cells (*$p < 0.05$, #$p < 0.01$ versus blank; △$p < 0.05$, △△$p < 0.01$ versus LPS).

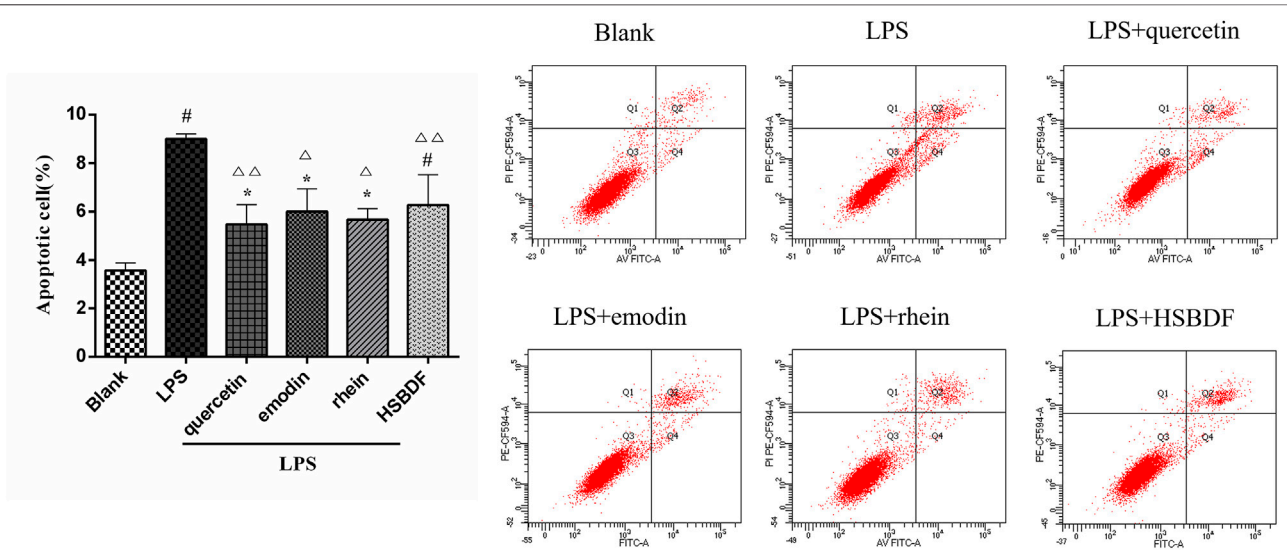

FIGURE 7 | Effects of HSBDF and active compound treatment on apoptosis in LPS-stimulated A549 cells (*$p < 0.05$, #$p < 0.01$ versus blank; △$p < 0.05$, △△$p < 0.01$ versus LPS).

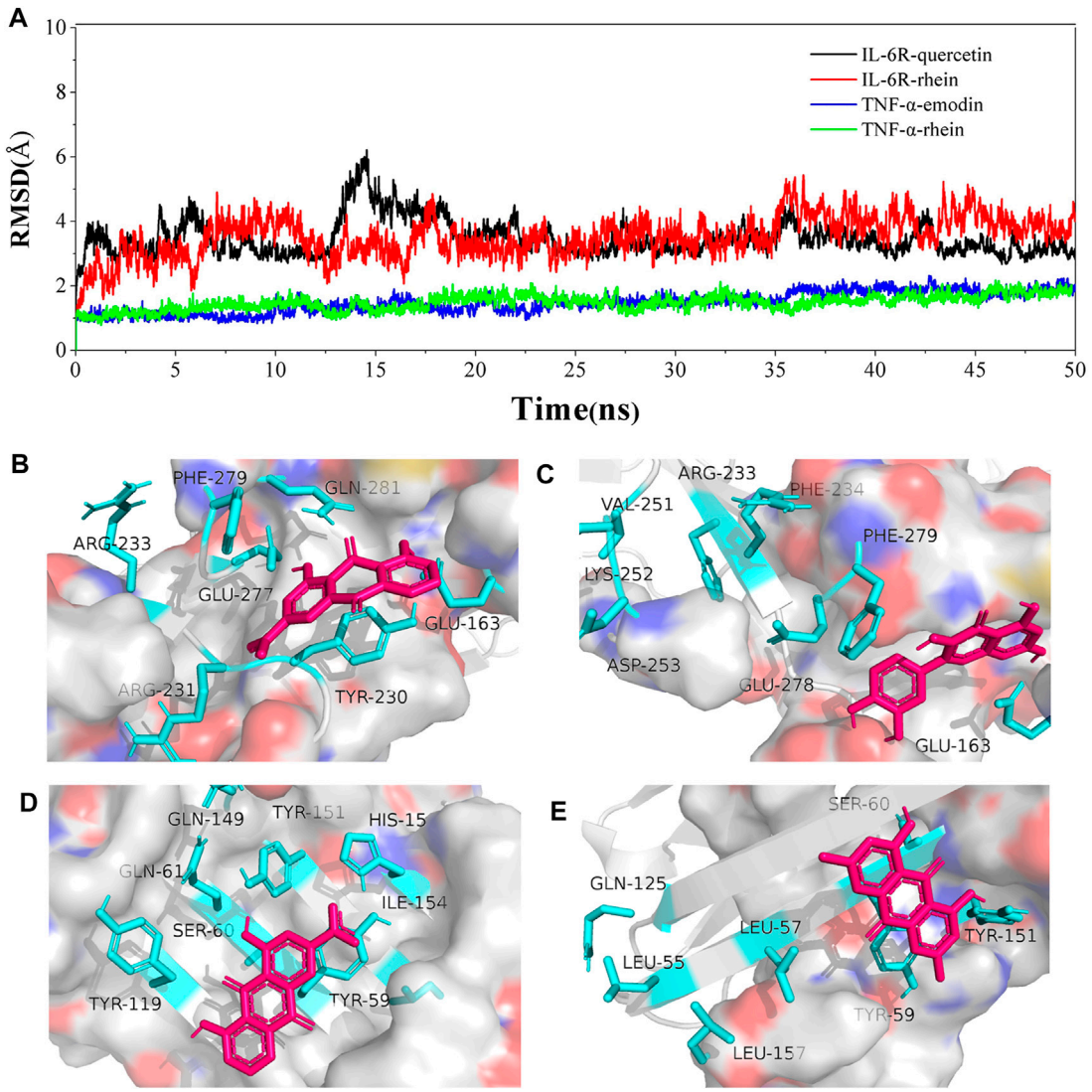

FIGURE 8 | Molecular dynamics simulation study. **(A)** RMSD of the active compound–protein complex in 50 ns, which is made up of a number of α-carbon (Cα) atoms, throughout the simulations; **(B,C)** Binding interaction patterns of rhein and quercetin with IL-6R; **(D,E)** Binding interaction patterns of rhein and emodin with TNF-α.

conducted for rhein and quercetin with IL-6R and rhein and emodin with the TNF-α complex in 50 ns by the Desmond module. The root mean square deviation (RMSD) plot in **Figure 8A** showed that the fluctuation values of RMSD of both systems were stable within a certain range by simulating 50 ns, which reveals that the simulation was well equilibrated during 50 ns and the ligand did not undergo a remarkable conformational change.

The interactions of active compounds and target proteins were further elaborated based on the hydrogen bonds, hydrophobic, ionic, and water bridges during 50-ns simulation. As shown in **Figure 8A** and **Supplementary Figure S2**, the interaction between rhein and IL-6R's residues (**Figure 8B**), such as GLU277, PHE279, GLN281, ARG233, ARG231, GLU163, and TYR230, was a stable key, for example, the H-bond and hydrophobic interaction between rhein and GLU277 and PHE29, respectively (**Figure 8C**). The interaction between quercetin and IL-6R's residues, such as ARG233, PHE234, VAL251, LYS252, ASP253, GLU278, PHE279, and GLU163, was a stable key, for example, the hydrophobic interaction betweenARG233 and quercetin. TYR59, TYR151, HIS15, GLY149, TYR119, GLN61, ILE154, and SER60 were key interacting residues of TNF-α, among which, TYR59 and TYR151 formed a stable hydrophobic and H-bond interaction with rhein, respectively (**Figure 8D**). TYR59, GLN125, TYR151, LEU157, LEU55, LEU57, and SER60 were key interacting residues of TNF-α, which mainly formed H-bond and hydrophobic and ionic interaction with emodin (**Figure 8E**).

These results suggested that binding of ligand molecules (rhein, quercetin, and emodin) stabilizes the protein structure without noticeable structural changes in native conformation.

TABLE 4 | Pharmacokinetic properties of the key compounds.

Compound	RO5[a]	% HOA[b]	CNS[c]	QPlogBB[d]	QPlogHERG[e]	LD50 (mg/kg)	Toxicity class[f]	Hepatotoxicity
Emodin	0	68.29	−2	−1.53	−4.32	5,000	V	Inactive
Rhein	0	47.47	−2	−1.97	−2.70	5,000	V	Inactive
Quercetin	0	52.20	−2	−2.40	−5.13	159	III	Inactive

[a]*Note: acceptable range: Max.4.*
[b]*acceptable range: 0–100.*
[c]*acceptable range: −2 (inactive) +2 (active).*
[d]*acceptable range: −3.0 to 1.2.*
[e]*acceptable range: <−5.*
[f]*[Class I: death after swallowing (LD50 ≤ 5); Class II: death after swallowing (5 < LD50 ≤ 50); Class III: toxic after swallowing (50 < LD50 ≤ 300); Class IV: harmful after swallowing (300 < LD50 ≤ 2000); Class V: may be harmful after swallowing (2000 < LD50 ≤ 5,000); Class VI: non-toxic (LD50 > 5,000)].*

That is the conformation of the complex was stable, and the residues are derived from stable complexes.

5 PHARMACOKINETIC PROPERTIES OF ACTIVE COMPOUNDS

The ADMET property prediction is fundamental for the selection of the most promising compounds for further development. The active compounds (quercetin, emodin, and rhein) were subjected to predictions of pharmacokinetic properties using ProTox-II and QikProp. As shown in **Table 4**, active compounds conformed to RO5 and QPlogBB, and CNS showed that a low risk of central nervous system damage. The QPlogHERG of emodin and rhein was within the specified range, indicating that the risk of cardiotoxicity of emodin and rhein was low. The toxicity level of emodin and rhein of Class V was relatively safe; the LD50 of quercetin was 159 mg/kg and belonged to Class III, indicating quercetin has potential safety risks. These suggested that emodin and rhein were the most promising compounds.

6 CONCLUSION

Based on TCM theory and documentation, HSBDF including two classical prescriptions of MXSGD (*E. sinica*, *S. armeniacae amarum*, and *Glycyrrhiza uralensis*) and HXZQP (*A. rugosus*, *M. officinalis*, *R. Pinelliae Preparata*, *A. lancea*, *P. cocos*, and *Glycyrrhiza uralensis*) was recommended to treat ALI at the later stages of COVID-19 by the NHC. Molecular docking results showed that the total number of compounds with potential inhibitory activities of MXSGD (120) against IL-6R and TNF-α was higher than that of HXZQP (110). The results indicated that MXSGD was more outstanding in anti-inflammation than HXZQP, which up to the TCM theory that MXSGD can regulate lung mechanisms such as diffuse the lung qi. Also, previous studies confirmed that MXSGD played a role in suppressing cytokine storm and immune regulation and protecting the pulmonary alveolar–capillary barrier (Wang et al., 2020).

In terms of single herb, we found that *Glycyrrhiza uralensis*, *E. sinica*, and *R. officinale* were key herbs with the potential to inhibit inflammation, which was of great significance to ameliorate ALI. These results are in accordance with the Chinese medicine theory that *Glycyrrhiza uralensis* and *E. sinica* belong to the lung channel; *R. officinale* belongs to the interior–exterior of the large intestine channel and the lung. Therefore, *Glycyrrhiza uralensis*, *E. sinica*, and *R. officinale* had properties to treat lung-related diseases. These results were a significant guide for the compatibility of TCM in the treatment of ALI.

Quercetin was outstanding in inhibiting anti-inflammation and anti-oxidative stress in this study. Considering that quercetin has potential safety risks, the structural optimization of quercetin to avoid toxicity but retain anti-inflammatory and anti-oxidant features is worth further study.

In summary, this study made good use of chemical bioinformatics analysis, including molecular docking, LC/MS, network pharmacology, test *in vitro*, molecular dynamic simulation, binding interaction pattern analysis, and pharmacokinetic properties to systematically study the regulatory mechanisms of HSBDF and its active compounds in plasma in treating ALI. Overwhelming lung inflammation, oxidative stress, and cell apoptosis were involved in the whole pathological process of ALI. Our results suggested that HSBDF and its active components in plasma (quercetin, emodin, and rhein) have significant effects on anti-inflammation, anti-oxidative stress, and decreasing cell apoptosis in treating ALI. Moreover, quercetin, emodin, and rhein, key active components in plasma, had a stable affinity with IL-6R and TNF-α, which are worthy of further development and utilization for ALI.

DATA AVAILABILITY STATEMENT

The original contributions presented in the study are included in the article/**Supplementary Material**, further inquiries can be directed to the corresponding authors.

ETHICS STATEMENT

The animal study was reviewed and approved by the Committee for Ethics in the Laboratory Animal Center of Gansu University of Chinese Medicine (number: 2021-182).

AUTHOR CONTRIBUTIONS

YrW, XJ, QqW, and YL conceived and designed the study. QF, YfW, and QfW provided the guidance of LC/MS. YrW operated the LC/MS experiment with the assistance of YL, XzL, JwL, and SyW. YrW collected the compounds of HSBDF and targets and performed the cell experiment. YrW, XJ, and YW performed the network pharmacology analysis. MZ, JL, CxL, ChL, and LL performed molecular dynamic simulation, YrW and XJ performed molecular docking and wrote the manuscript. All authors were responsible for reviewing data. All authors have read and approved the final manuscript.

FUNDING

This study was supported by the Special Project of COVID-19 Emergent TCM Treatment of National Administration of Traditional Chinese Medicine (No. 2021ZYLCYJ08-3), Provincial University Industry Support Project in Gansu (2020C-36), and National Natural Science Foundation of China (No. NSFC 82004202).

SUPPLEMENTARY MATERIAL

The Supplementary Material for this article can be found online at: https://www.frontiersin.org/articles/10.3389/fphar.2022.879268/full#supplementary-material

Supplementary Figure S1 | Cell viability for MLE12 after treatments of HSBDF and key compounds in plasma (cell viability was detected by CCK-8,*$P < 0.05$ versus blank).

Supplementary Figure S2 | Histogram and percentage graph of protein–active compound interaction in molecular dynamics simulation. **(B,C)** Protein–ligand interaction of rhein and quercetin with IL-6R; **(C,D)** protein–ligand interaction of rhein and emodin with TNF-α.

REFERENCES

Busbee, P. B., Bam, M., Yang, X., Abdulla, O. A., Zhou, J., Ginsberg, J. P. J., et al. (2021). Dysregulated TP53 Among PTSD Patients Leads to Downregulation of miRNA Let-7a and Promotes an Inflammatory Th17 Phenotype. *Front. Immunol.* 12, 815840. doi:10.3389/fimmu.2021.815840

Chen, S. F., Pan, M. X., Tang, J. C., Cheng, J., Zhao, D., Zhang, Y., et al. (2020). Arginine Is Neuroprotective through Suppressing HIF-1α/LDHA-Mediated Inflammatory Response after Cerebral Ischemia/reperfusion Injury. *Mol. Brain* 13 (1), 63. doi:10.1186/s13041-020-00601-9

Chen, Y., Jiang, F., Kong, G., Yuan, S., Cao, Y., Zhang, Q., et al. (2021a). Gasotransmitter CO Attenuates Bleomycin-Induced Fibroblast Senescence via Induction of Stress Granule Formation. *Oxid. Med. Cel Longev.* 2021, 9926284. doi:10.1155/2021/9926284

Chen, Y., Shao, X., Zhao, X., Ji, Y., Liu, X., Li, P., et al. (2021b). Targeting Protein Arginine Methyltransferase 5 in Cancers: Roles, Inhibitors and Mechanisms. *Biomed. Pharmacother.* 144, 112252. doi:10.1016/j.biopha.2021.112252

Chen, Y., Yuan, S., Cao, Y., Kong, G., Jiang, F., Li, Y., et al. (2021c). Gasotransmitters: Potential Therapeutic Molecules of Fibrotic Diseases. *Oxid. Med. Cel Longev.* 2021, 3206982. doi:10.1155/2021/3206982

Cheng, H., Orr, S. T. M., Bailey, S., Brooun, A., Chen, P., Deal, J. G., et al. (2021). Structure-Based Drug Design and Synthesis of PI3Kα-Selective Inhibitor (PF-06843195). *J. Med. Chem.* 64 (1), 644–661. doi:10.1021/acs.jmedchem.0c01652

Duan, Y., Chen, L., Chen, Y., and Fan, X. G. (2014). c-Src Binds to the Cancer Drug Ruxolitinib with an Active Conformation. *PloS one* 9 (9), e106225. doi:10.1371/journal.pone.0106225

Eyileten, C., Wicik, Z., De Rosa, S., Mirowska-Guzel, D., Soplinska, A., Indolfi, C., et al. (2018). MicroRNAs as Diagnostic and Prognostic Biomarkers in Ischemic Stroke-A Comprehensive Review and Bioinformatic Analysis. *Cells* 7 (12), 249. doi:10.3390/cells7120249

Gao, Z., Liu, X., Wang, W., Yang, Q., Dong, Y., Xu, N., et al. (2019). Characteristic Anti-inflammatory and Antioxidative Effects of Enzymatic- and Acidic-Hydrolysed Mycelium Polysaccharides by Oudemansiella Radicata on LPS-Induced Lung Injury. *Carbohydr. Polym.* 204, 142–151. doi:10.1016/j.carbpol.2018.09.073

Gao, C., Wu, Z. Q., Liu, G. H., Yu, Y., Tang, Y. M., and Qi, Y. D. (2021). Effects of Different Extraction Processed Rhei Radix et Rhizoma on Pulmonary Inflammation in Mice Infected with Mycoplasma Pneumoniae. *Chin. J. Mod. Applied Pharmacy* 38 (22), 2781–2786. (in Chinese). doi:10.13748/j.cnki.issn1007-7693.2021.22.003

Geiser, T., Atabai, K., Jarreau, P. H., Ware, L. B., Pugin, J., and Matthay, M. A. (2001). Pulmonary Edema Fluid from Patients with Acute Lung Injury Augments *In Vitro* Alveolar Epithelial Repair by an IL-1beta-dependent Mechanism. *Am. J. Respir. Crit. Care Med.* 163 (6), 1384–1388. doi:10.1164/ajrccm.163.6.2006131

Gollner, A., Rudolph, D., Arnhof, H., Bauer, M., Blake, S. M., Boehmelt, G., et al. (2016). Discovery of Novel Spiro[3H-indole-3,2'-pyrrolidin]-2(1H)-one Compounds as Chemically Stable and Orally Active Inhibitors of the MDM2-P53 Interaction. *J. Med. Chem.* 59 (22), 10147–10162. doi:10.1021/acs.jmedchem.6b00900

He, M. M., Smith, A. S., Oslob, J. D., Flanagan, W. M., Braisted, A. C., Whitty, A., et al. (2005). Small-molecule Inhibition of TNF-Alpha. *Science* 310 (5750), 1022–1025. doi:10.1126/science.1116304

Ho, J. D., Yeh, R., Sandstrom, A., Chorny, I., Harries, W. E., Robbins, R. A., et al. (2009). Crystal Structure of Human Aquaporin 4 at 1.8 A and its Mechanism of Conductance. *Proc. Natl. Acad. Sci. U S A.* 106 (18), 7437–7442. doi:10.1073/pnas.0902725106

Hou, T., Wang, J., Li, Y., and Wang, W. (2011). Assessing the Performance of the MM/PBSA and MM/GBSA Methods. 1. The Accuracy of Binding Free Energy Calculations Based on Molecular Dynamics Simulations. *J. Chem. Inf. Model.* 51 (1), 69–82. doi:10.1021/ci100275a

Hou, L., Zhang, J., Liu, Y., Fang, H., Liao, L., Wang, Z., et al. (2021). MitoQ Alleviates LPS-Mediated Acute Lung Injury through Regulating Nrf2/Drp1 Pathway. *Free Radic. Biol. Med.* 165, 219–228. doi:10.1016/j.freeradbiomed.2021.01.045

Hsin, K. Y., Ghosh, S., and Kitano, H. (2013). Combining Machine Learning Systems and Multiple Docking Simulation Packages to Improve Docking Prediction Reliability for Network Pharmacology. *PLoS One* 8 (12), e83922. doi:10.1371/journal.pone.0083922

Jiang, W., and Hu, M. (2012). Mutual Interactions between Flavonoids and Enzymatic and Transporter Elements Responsible for Flavonoid Disposition via Phase II Metabolic Pathways. *RSC Adv.* 2 (21), 7948–7963. doi:10.1039/C2RA01369J

Keiser, M. J., Roth, B. L., Armbruster, B. N., Ernsberger, P., Irwin, J. J., and Shoichet, B. K. (2007). Relating Protein Pharmacology by Ligand Chemistry. *Nat. Biotechnol.* 25 (2), 197–206. doi:10.1038/nbt1284

Li, W., Li, Y., Qin, K., Du, B., Li, T., Yuan, H., et al. (2019). Siglec-G Deficiency Ameliorates Hyper-Inflammation and Immune Collapse in Sepsis via Regulating Src Activation. *Front. Immunol.* 10, 2575. doi:10.3389/fimmu.2019.02575

Li, L., Jin, X. J., Li, J. W., Li, C. H., Zhou, S. Y., Li, J. J., et al. (2021). Systematic Insight into the Active Constituents and Mechanism of Guiqi Baizhu for the Treatment of Gastric Cancer. *Cancer Sci.* 112 (5), 1772–1784. doi:10.1111/cas.14851

Liang, X., Liu, Y., Chen, L., and Chen, S. (2021). The Natural Compound Puerarin Alleviates Inflammation and Apoptosis in Experimental Cell and Rat Preeclampsia Models. *Int. Immunopharmacol.* 99, 108001. doi:10.1016/j.intimp.2021.108001

Lin, K., Lin, J., Wu, W. I., Ballard, J., Lee, B. B., Gloor, S. L., et al. (2012). An ATP-Site On-Off Switch that Restricts Phosphatase Accessibility of Akt. *Sci. Signal.* 5 (223), ra37. doi:10.1126/scisignal.2002618

Lin, J., Li, J., Shu, M., Wu, W., Zhang, W., Dou, Q., et al. (2020). The rCC16 Protein Protects against LPS-Induced Cell Apoptosis and Inflammatory Responses in Human Lung Pneumocytes. *Front. Pharmacol.* 11, 1060. doi:10.3389/fphar.2020.01060

Liu, X., Gao, C., Wang, Y., Niu, L., Jiang, S., and Pan, S. (2021). BMSC-derived Exosomes Ameliorate LPS-Induced Acute Lung Injury by miR-384-5p-Controlled Alveolar Macrophage Autophagy. *Oxid. Med. Cel Longev.* 2021, 9973457. doi:10.1155/2021/9973457

Manchester, J., Walkup, G., Rivin, O., and You, Z. (2010). Evaluation of pKa Estimation Methods on 211 Druglike Compounds. *J. Chem. Inf. Model.* 50 (4), 565–571. doi:10.1021/ci100019p

Martínez, M.-A., Ares, I., Martínez, M., Lopez-Torres, B., Maximiliano, J.-E., Rodríguez, J.-L., et al. (2021). Brown marine Algae Gongolaria Baccata Extract Protects Caco-2 Cells from Oxidative Stress Induced by Tert-Butyl Hydroperoxide. *Food Chem. Toxicol.* 156, 112460. doi:10.1016/j.fct.2021.112460

Reske, J. J., Wilson, M. R., Holladay, J., Siwicki, R. A., Skalski, H., Harkins, S., et al. (2021). Co-existing TP53 and ARID1A Mutations Promote Aggressive Endometrial Tumorigenesis. *Plos Genet.* 17 (12), e1009986. doi:10.1371/journal.pgen.1009986

Ru, J., Li, P., Wang, J., Zhou, W., Li, B., Huang, C., et al. (2014). TCMSP: a Database of Systems Pharmacology for Drug Discovery from Herbal Medicines. *J. Cheminform.* 6, 13. doi:10.1186/1758-2946-6-13

Shchendrigina, A. A., Zhbanov, K. A., Privalova, E. V., Iusupova, A. O., Bytdaeva, A. H., Danilogorskaya, Y. A., et al. (2020). Circulating Neuregulin-1 and Chronic Heart Failure with Preserved Ejection. *Kardiologiia* 60 (11), 1222. doi:10.18087/cardio.2020.11.n1222

Sheikh, I. A., Jiffri, E. H., Ashraf, G. M., Kamal, M. A., and Beg, M. A. (2018). Structural Studies on Inhibitory Mechanisms of Antibiotic, Corticosteroid and Catecholamine Molecules on Lactoperoxidase. *Life Sci.* 207, 412–419. doi:10.1016/j.lfs.2018.06.027

Sun, X., Cheng, H., Liu, B., Du, Y., Dong, J., and Huang, J. (2020). Icariin Reduces LPS-Induced Acute Lung Injury in Mice Undergoing Bilateral Adrenalectomy by Regulating GRα. *Eur. J. Pharmacol.* 876, 173032. doi:10.1016/j.ejphar.2020.173032

Szklarczyk, D., Morris, J. H., Cook, H., Kuhn, M., Wyder, S., Simonovic, M., et al. (2017). The STRING Database in 2017: Quality-Controlled Protein-Protein Association Networks, Made Broadly Accessible. *Nucleic Acids Res.* 45 (D1), D362–D368. doi:10.1093/nar/gkw937

Wang, J., and Qi, F. (2020). Traditional Chinese Medicine to Treat COVID-19: the Importance of Evidence-Based Research. *Drug Discov. Ther.* 14 (3), 149–150. doi:10.5582/ddt.2020.03054

Wang, Y. X., Ma, J. R., Wang, S. Q., Zeng, Y. Q., Zhou, C. Y., Ru, Y. H., et al. (2020). Utilizing Integrating Network Pharmacological Approaches to Investigate the Potential Mechanism of Ma Xing Shi Gan Decoction in Treating COVID-19. *Eur. Rev. Med. Pharmacol. Sci.* 24 (6), 3360–3384. doi:10.26355/eurrev_202003_20704

Wang, Q., Shao, X., Leung, E. L. H., Chen, Y., and Yao, X. (2021). Selectively Targeting Individual Bromodomain: Drug Discovery and Molecular Mechanisms. *Pharmacol. Res.* 172, 105804. doi:10.1016/j.phrs.2021.105804

Wu, B., Zhang, Y., Kong, J., Zhang, X., and Cheng, S. (2009). In Silico predication of Nuclear Hormone Receptors for Organic Pollutants by Homology Modeling and Molecular Docking. *Toxicol. Lett.* 191 (1), 69–73. doi:10.1016/j.toxlet.2009.08.005

Wu, X. Y., Liu, D., Li, N., Hao, X. F., Chao, G. D., Liu, G. L., et al. (2020). Effects of Glycyrrhiza Polysaccharide on Inflammation and Oxidative Damage of Lung Tissue in Mice. *J. Gansu Agric. Univ.* 55 (05), 8–14+30. (in Chinese). doi:10.13432/j.cnki.jgsau.2020.05.002

Xing, W., Busino, L., Hinds, T. R., Marionni, S. T., Saifee, N. H., Bush, M. F., et al. (2013). SCF(FBXL3) Ubiquitin Ligase Targets Cryptochromes at Their Cofactor Pocket. *Nature* 496 (7443), 64–68. doi:10.1038/nature11964

Xue, R., Fang, Z., Zhang, M., Yi, Z., Wen, C., and Shi, T. (2013). TCMID: Traditional Chinese Medicine Integrative Database for Herb Molecular Mechanism Analysis. *Nucleic Acids Res.* 41 (Database issue), D1089–D1095. doi:10.1093/nar/gks1100

Yang, X., Yu, Y., Xu, J., Shu, H., Xia, J., Liu, H., et al. (2020). Clinical Course and Outcomes of Critically Ill Patients with SARS-CoV-2 Pneumonia in Wuhan, China: a Single-Centered, Retrospective, Observational Study. *Lancet Respir. Med.* 8 (5), 475–481. doi:10.1016/S2213-2600(20)30079-5

Yeom, M. J., Lee, H. C., Kim, G. H., Lee, H. J., Shim, I., Oh, S. K., et al. (2006). Anti-arthritic Effects of Ephedra Sinica STAPF Herb-Acupuncture: Inhibition of Lipopolysaccharide-Induced Inflammation and Adjuvant-Induced Polyarthritis. *J. Pharmacol. Sci.* 100 (1), 41–50. doi:10.1254/jphs.fp0050637

Yu R, R., Chen, L., Lan, R., Shen, R., and Li, P. (2020). Computational Screening of Antagonists against the SARS-CoV-2 (COVID-19) Coronavirus by Molecular Docking. *Int. J. Antimicrob. Agents* 56 (2), 106012. doi:10.1016/j.ijantimicag.2020.106012

Yu S, S., Wang, J., and Shen, H. (2020). Network Pharmacology-Based Analysis of the Role of Traditional Chinese Herbal Medicines in the Treatment of COVID-19. *Ann. Palliat. Med.* 9 (2), 437–446. doi:10.21037/apm.2020.03.27

Zhao, R., Wang, B., Wang, D., Wu, B., Ji, P., and Tan, D. (2021). Oxyberberine Prevented Lipopolysaccharide-Induced Acute Lung Injury through Inhibition of Mitophagy. *Oxid. Med. Cel Longev.* 2021, 6675264. doi:10.1155/2021/6675264

Conflict of Interest: The authors declare that the research was conducted in the absence of any commercial or financial relationships that could be construed as a potential conflict of interest.

Publisher's Note: All claims expressed in this article are solely those of the authors and do not necessarily represent those of their affiliated organizations, or those of the publisher, the editors, and the reviewers. Any product that may be evaluated in this article, or claim that may be made by its manufacturer, is not guaranteed or endorsed by the publisher.

frontiers | Frontiers in Pharmacology

ORIGINAL RESEARCH
published: 12 July 2022
doi: 10.3389/fphar.2022.921209

Number 2 Feibi Recipe Ameliorates Pulmonary Fibrosis by Inducing Autophagy Through the GSK-3β/mTOR Pathway

Haoge Liu[1], Qinglu Pang[1], Fang Cao[2], Zhaoheng Liu[1], Wan Wei[2], Zhipeng Li[1], Qi Long[3] and Yang Jiao[2]**

[1]Graduate School, Beijing University of Chinese Medicine, Beijing, China, [2]Dongfang Hospital Affiliated to Beijing University of Chinese Medicine, Beijing, China, [3]Department of Respiratory and Critical Care Medicine, Chongqing Traditional Chinese Medicine Hospital, Chongqing, China

Number 2 Feibi Recipe (N2FBR) is a traditional Chinese medicine formula for treating idiopathic pulmonary fibrosis. N2FBR inhibits H_2O_2-mediated oxidative stress damage in alveolar epithelial cells by increasing autophagy, as we previously demonstrated. However, it is unknown if similar mechanisms occur *in vivo*. We established a pulmonary fibrosis model by instilling bleomycin (BLM) from the airway to examine the effects of N2FBR on pulmonary fibrosis and investigate its probable mechanism in this work. We discovered that N2FBR treatment effectively alleviated interstitial fibrosis as well as collagen deposition, primarily in upregulating SOD, GSH-Px, T-AOC and downregulating MDA content. N2FBR also increased the expression of LC3B, Beclin-1, LAMP1, TFEB and downregulated the expression of p62, legumain. N2FBR treatment boosted the production of autophagosomes, according to the results of the TEM observation. Furthermore, we explored that N2FBR exerted its anti-oxidative stress and pro-autophagy effects via GSK-3β/mTOR signalling pathway. Therefore, these results provide further evidence for the protective effect of N2FBR in pulmonary fibrosis. Our findings could have ramifications for the development of antifibrosis therapies.

Keywords: number 2 Feibi Recipe, idiopathic pulmonary fibrosis, oxidative stress, autophagy, Chinese medicine

OPEN ACCESS

Edited by:
Arunachalam Karuppusamy, Chinese Academy of Sciences (CAS), China

Reviewed by:
Fan Yang, Jiangxi Agricultural University, China
Ganapasam Sudhandiran, University of Madras, India

****Correspondence:***
Qi Long
conlong71@126.com
Yang Jiao
yangjiao2013@sina.cn

Specialty section:
This article was submitted to Respiratory Pharmacology, a section of the journal Frontiers in Pharmacology

Received: *15 April 2022*
Accepted: *23 June 2022*
Published: *12 July 2022*

Citation:
Liu H, Pang Q, Cao F, Liu Z, Wei W, Li Z, Long Q and Jiao Y (2022) Number 2 Feibi Recipe Ameliorates Pulmonary Fibrosis by Inducing Autophagy Through the GSK-3β/mTOR Pathway. Front. Pharmacol. 13:921209. doi: 10.3389/fphar.2022.921209

INTRODUCTION

Idiopathic pulmonary fibrosis (IPF) is a progressive interstitial pneumonia illness that has no known cause, and has a median survival duration of 3–5 years after diagnosis (Lederer and Martinez, 2018). Histologically, the disease is characterized by significant destruction of the alveolar structure as well as extracellular matrix (ECM) deposition (Raghu and Richeldi, 2017). IPF patients have a median age of approximately 65 years when they are diagnosed. It is more prevalent in ex-smokers and results in dyspnea, dry cough, and progressive loss of respiratory function (Glassberg, 2019). In the last few years, several new antifibrotic agents such as pirfenidone (King et al., 2014) and nintedanib (Nasser et al., 2021) have been introduced. These medications slowed the deterioration of lung function in IPF patients but had no effect on survival or quality of life. Lung transplantation remains the only treatment that enhances patient survival. It is crucial to have a deeper understanding of the cellular processes and molecular pathways involved in order to develop effective treatments.

In comparison to other organs, the lungs are especially vulnerable to oxidate stress. Accumulating to mounting evidence, oxidative stress plays a key role in the initiation and progression of IPF. Apoptosis of alveolar epithelial cells (AEC) and apoptosis resistance in myofibroblasts are caused by excessive production of reactive oxygen species (ROS) by defective mitochondria, resulting in enhanced collagen deposition and fibrotic foci development (Tian et al., 2019). Autophagy is a process in which damaged organelles or proteins are degreed by lysosomes as a possible survival mechanism amid oxidate stress (Racanelli et al., 2018). The accumulation of p62 and low levels of LC3-II were detected in lung tissue samples from IPF patients (Patel et al., 2012). The mammalian target of rapamycin (mTOR) is an autophagy-related regulating protein kinase. Glycogen synthase kinase 3β (GSK-3β) is a serine/threonine kinase with many functions. mTOR is the downstream target of GSK-3β, according to numerous studies. SB216763 is a GSK-3β inhibitor. Simultaneously, previous research suggested that SB216763 alleviated pulmonary fibrosis by inhibiting inflammatory cytokines (Gurrieri et al., 2010) and regulating TGF-β1-induced myofibroblast differentiation (Baarsma et al., 2013). These findings proposes that autophagy plays a role in the molecular pathways that lead to the IPF development. Nevertheless, previous research on pulmonary fibrosis mainly focuses on the formation of autophagosomes. The autophagosome and lysosome fusion is significant for complete autophagic flux. Oxidative stress damages the membrane permeabilization of lysosomes, which result into lysosome dysfunction (Qin et al., 2017). Lysosomal defects disrupt the fusion of autophagosomes and lysosomes, therefore, inhibiting autophagic flux (Yu et al., 2018). The relationship between oxidative stress and autophagy in pulmonary fibrosis requires further investigation.

Number 2 Feibi Recipe (N2FBR), a Chinese medicine herbal formula, is used to treat respiratory disorders such as idiopathic pulmonary fibrosis. It is a modified formula from Feibi Recipe (FBR). FBR is comprised of eight herbs: Sheng Huangqi (Astragalus membranaceus Bge), Jin Yin Hua (Flos Lonicerae), Sheng Gan Cao (Radix Glycyrrhizae), Danggui (Angelicae Sinensis Radix), Chuan Shan Long (Discorea nipponica Makino), Zhe Bei Mu (Bulbus Fritillariae Thunbergii), and Shiwei (Pyrrosia lingua (Thunb.) Farwell), and Gua Lou Pi (Pericarpium Trichosanthes). The Feibi recipe inhibited bleomycin-induced pulmonary fibrosis through modulating TGF-β1/Smad3 Signalling Pathways (Wang et al., 2020). FBR-medicated serum crucially inhibited the production of pro-inflammatory cytokines induced by LPS in RAW264.7 macrophages *in vitro*. Additionally, treatment with FBR-medicated serum suppressed the activation of NF-κB and Smad2/Smad3 (Wei et al., 2022). N2FBR, an advanced version of FBR, comprises of the following commonly used Chinese herbs: Sheng Huangqi (Astragalus membranaceus Bge), Hong jingtian (herba rhodiolae), Jin Yin Hua (Flos Lonicerae), Huang Qin (Radix Scutellariae), Dan Shen (Radix Salviae Miltiorrhizae), and Sheng Gan Cao (Radix Glycyrrhizae). In a large body of clinical practise, N2FBR has been demonstrated to relieve symptoms and enhance the quality of life of IPF patients. N2FBR has been shown to have anti-oxidative effect of N2FBR both *in vitro* and *in vivo* (Liu et al., 2018; Gu et al., 2022). Moreover, N2FBR promoted autophagy in H_2O_2-mediated AECs. Nevertheless, the therapeutic mechanisms of N2FBR in pulmonary fibrosis are not fully understood. The goal of this study was to see if N2FBR could reduce oxidative stress in BLM-induced lung fibrosis by triggering autophagy via the GSK-3β/mTOR pathway.

MATERIALS AND METHODS

Chemicals and Reagents

Number 2 Feibi Recipe (N2FBR) comprised of six herbs, including 30 g Sheng Huangqi (Astragalus membranaceus Bge), 30 g Hong jingtian (herba rhodiolae), 30 g Jin Yin Hua (Flos Lonicerae), 20 g Huang Qin (Radix Scutellariae), 20 g Dan Shen (Radix Salviae Miltiorrhizae), and 10 g Sheng Gan Cao (Radix Glycyrrhizae). All the herbs were purchased from Beijing Kang Ren Tang, a Pharmaceutical Industry Co. The herbs had initially been soaked in water for 30 min. Afterwards, they were boiled for 1 h. Following filtration, the liquid was boiled for 0.5 h, sealed, vacuum dried, as well as stored in a glass bottle at 4°C until use. SB216763 was purchased from MedChem Express (Shanghai, China) and dissolved in a vehicle (25% dimethyl sulfoxide, 25% polyethylene glycol, and 50% saline).

Bleomycin was provided by Fresenius Kabi (Lake Zurich, United States). The HE Stain and Masson's Trichrome Stain Kit were provided by Solarbio (Beijing, China; G1120, G1340, respectively). Mice MDA, SOD, and T-AOC assay kits were purchased from Jiancheng Bioengineering Institute (Nanjing, China; A015-2-1, A003-1-2, A001-3-2, respectively). The TGF-β1 Elisa kit had been provided by Elabscience (Wuhan, China; E-EL-0162c). The rabbit anti-LC3A/B, rabbit anti-SQSTM1/p62, rabbit anti-Beclin 1, rabbit anti-LAMP1, rabbit anti-total-mTOR, rabbit anti-phospho-mTOR (Ser2448), rabbit anti-total-GSK3 beta, rabbit anti-phospho-GSK3 beta (Ser9), goat anti-rabbit IgG-HRP, as well as goat anti-rabbit IgG-FITC were purchased from Affinity (Nanjing, China; AF5402, AF5384, AF5182, DF7033, AF6308, AF3308, AF5016, AF 2016, S0001, S0008, respectively). Bioss provided the rabbit anti-Collagen alpha-1(I), rabbit anti-Legumain, and rabbit anti-TFEB antibodies (Beijing, China; bs-20124R, bs-3907R, bs-5137R, respectively).

Animals

All mice experiments were approved by the Animal Ethical Experimentation Committee of Beijing University of Chinese Medicine and performed in accordance with the guidelines of the Institutional Animal Care and Use Committee. A total of 40 C57BL/6J male mice weighing 22–24 g were purchased from Beijing Vital River Labomouseory Animal Technology Co., Ltd. (Beijing, China). The mice were housed in standard

laboratory conditions, with filtered air, ambient temperature (22°C–26°C), humidity (55 ± 10%), and light (12 h light/dark cycle). The mice were provided with sterilized water and food.

Animal Model and Experimental Design

The mice were randomly assigned into four groups (n = 10 per group): a sham group (Sham), a model group (Model), number 2 FBR group (N2FBR), and SB216763 group (SB). As previously described (Tong et al., 2021), the mice were anesthetized with isoflurane solution, and then instilled with bleomycin solution via the airway (2 u/kg), except for mice in the sham group, which received the same volume of saline solution. The N2FBR group was given the number 2 Feibi Recipe (21.02 g/kg) by gavage once a day on the second day after modelling, whereas the other group received an equivalent quantity of saline. The daily dosage of N2FBR in mice was confirmed using the conversion ratio of the surface area between mice and humans. Additionally, SB group mice were administered with SB216763 (20 mg/kg) dissolved in vehicle (25% dimethyl sulfoxide, 25% polyethylene glycol, and 50% saline) (Gurrieri et al., 2010) twice a week by intraperitoneal injection, while other group received equal volumes of vehicle intraperitoneally. Bodyweight had been measured every 3 days, and the mice were euthanized after 21 days.

Hematoxylin-Eosin and Masson Staining

The left lung was promptly fixed in 4% paraformaldehyde and embedded in paraffin. Tissue slices with a thickness of 3-μM-thick tissue sections. Histological changes as well as collagen deposition were observed using hematoxylin-eosin (H&E) staining and Masson trichrome staining. HE staining and Masson staining was performed, while dewaxing and hydration had been conducted according to the manufacturer's instructions. Alveolitis and Ashcroft scores were used to provide semi-quantitative study of inflammation. The area positive for Masson trichrome had been measured, and the ratio of the Masson trichrome-positive area to the total fibrotic area was calculated using ImageJ software.

Immunohistochemical and Immunofluorescence Staining

Tissue sections were dewaxed with xylene and rehydrated as per standard protocols. Antigen retrieval was done in a microwave oven by boiling potions in 10 mM citrate buffer (pH6). After that, sections were immersed in 3%H2O2 for 20 min and blocked with 10% goat serum. The primary antibodies against Collagen I, P62, and Legumain were then added and incubated at 4°C overnight. The following day, slides were incubated with secondary antibodies as well as stained with a DAB reagent. A light microscope was used to photograph all of the slices.

The dewaxing, rehydration, and antigen retrieval methods for immunofluorescence staining were comparable to those employed for IHC. After blocking, the sections were incubated overnight with the primary antibody against TFEB in 5% BSA/0.1% Triton X-100 PBS. The slides were stained with FITC-conjugated secondary antibody and DAPI. Images had been quantified using ImageJ software.

Determination of Oxidative Stress Biomarkers and Fibrosis Biomarkers

The contents of malondialdehyde (MDA), superoxide dismutase (SOD), glutathione peroxidase (GSH-Px), and total antioxidant capacity (T-AOC) in serum was determined using commercially available MDA, SOD, GSH-Px, and T-AOC kits. The levels of hydroxyproline (HYP), collagen III (Col III), and α-smooth muscle actin (α-SMA) in lung tissues were determined using a commercially available kit according to the manufacturer's protocol.

Western Blot

RIPA lysis buffer was used to extract total protein from lung tissues, which was then centrifugation for 15 min at 12,000 rpm at 4°C. A BCA protein concentration kit was used to determine the protein (MDL, cat. no. MD913053) concentration. Each well had been loaded with equal amounts of protein as well as separated using 10% SDS PAGE. Proteins were transferred to 0.22 μM PVDF membranes (Millipore, United States), which were blocked with 5% nonfat milk for 2 h. Membranes were incubated with specific primary antibodies overnight at 4°C. Membranes were treated with secondary antibodies conjugated with HRP for 1 h at room temperature after primary incubation. ECL reagent was used to visualise the signals. All determinations had been performed independently and repeated three times.

Transmission Electron Microscopy

The autophagy-related structure was seen using transmission electron microscopy (TEM). Lung tissues were fixed in 2.5% glutaraldehyde and post-fixed in 1% osmium tetroxide for 2 h. Dehydration was performed using a graded ethanol series. The samples were embedded in epoxy and heat-cured overnight and sliced into 90 nm-thick pieces. The sections were viewed under TEM after being stained with uranyl acetate and lead citrate (JEM-1400, JEOL, Tokyo, Japan).

Statistical Analysis

GraphPad Prism 8 was used to conduct the statistical analysis (GraphPad Software, Inc.). Each experiment was repeated at least 3 times. All results had been expressed as mean ± standard deviation (SD). One-way ANOVA or Two-way ANONA followed by Tukey's test were used for comparison between multiple groups. Brown-Forsythe test followed by the Welch ANOVA test was used for determining the Ashcroft score and inflammation. $p < 0.05$ was considered statistically significant.

RESULTS

Deaths and Body Weight Changes

As shown in **Figure 1A**, one mouse in the sham group died on day 6, while a mouse in the model group died on days 6, 14, and 16. On day 12, one mouse died in the SB group. There were no

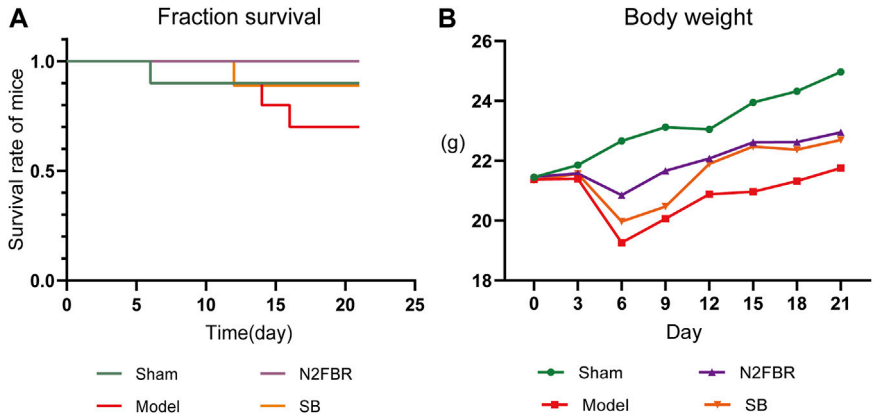

FIGURE 1 | Number of deaths and changes in body weight of mice (n = 10 mice/group). **(A)** The survival curve of mice. **(B)** Changes in body weight of mice.

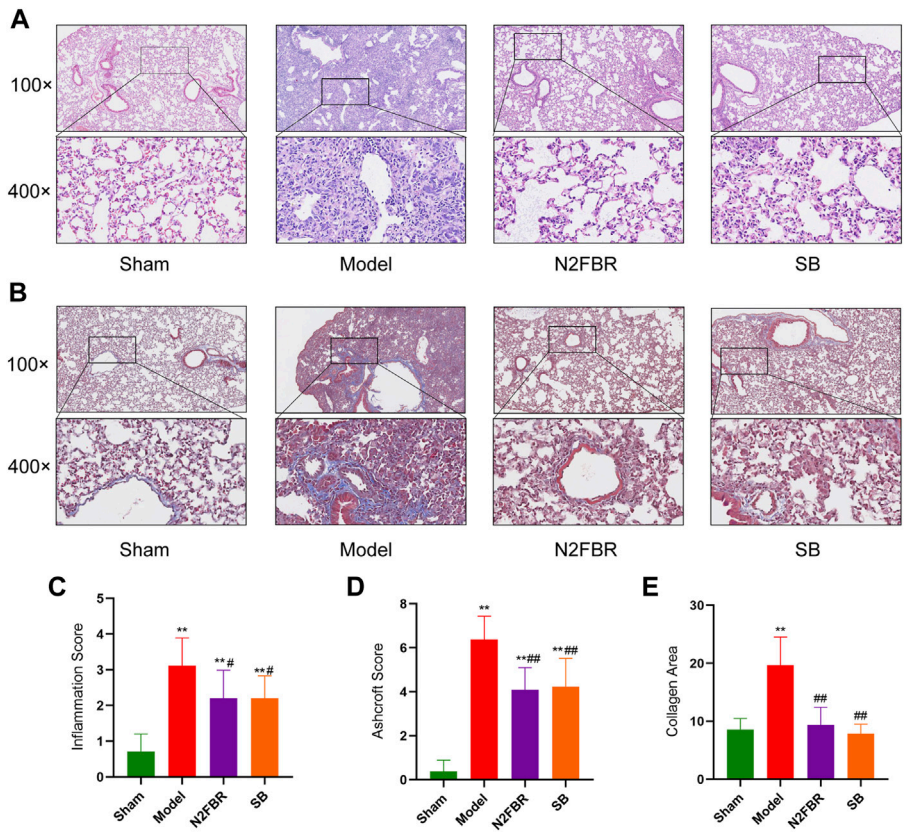

FIGURE 2 | N2FRB alleviated BLM-induced pulmonary fibrosis. **(A–B)** Representative images of HE staining, MASSON staining. **(C–E)** Quantitative analysis of Alveolitis score and Ashcroft score based on HE staining and collagen area based on MASSON staining assays. Data were analyzed using one way ANOVA (Mean ± SD): $^{**}p < 0.01$ compared with the sham group; $\#p < 0.05$, $\#\#p < 0.01$, compared with the BLM group.

deaths in the N2FBR group. There were 1, 3, and 1 death in the sham group, model group, and SB group, respectively. As illustrated in **Figure 1B**, with the exception of the Sham group, the weights of the mice were crucially reduced on day 6 after model construction. The weight of mice, on the other hand, continued to recover 9 days after the model was built. In comparison to the Sham group, the final mice weights in the model group were significantly reduced ($p < 0.01$).

Although the body weights of mice in the N2FBR and SB groups increased, no statistically significant difference was observed when made comparison with the model group.

Effects of Number 2 Feibi Recipe on the Histopathology of Bleomycin-Induced Pulmonary Fibrosis

To determine the degree of lung injury and fibrosis following treatment, sections of lung tissue were stained with H&E and Masson trichrome. Based on HE staining (**Figure 2A**), the structure of the pulmonary alveoli in the model group was severely damaged. The pulmonary alveolar walls had been thickened. A large amount of inflammatory cell infiltration was observed. Nevertheless, N2FBR and SB significantly ameliorated the effects of BLM. Meanwhile, therapy with N2FBR ($p < 0.05$, $p < 0.01$) and SB ($p < 0.05$, $p < 0.01$) significantly lowered the alveolitis score (**Figure 2C**) and Ashcroft score (**Figure 2D**), which indicate the severity of inflammation and fibrosis, respectively. The sham group's pulmonary alveoli tissues had a normal structure, with only light blue fibers observed. Unsurprisingly, large quantities of blue collagen had been deposited in the model group. Blue collagen deposition was significantly alleviated in the N2FBR ($p < 0.01$) and SB($p<0.01$) groups in contrast to the model group (**Figures 2B,E**). Taken together, treatment with N2FBR significantly reduced bleomycin-induced pulmonary fibrosis.

Number 2 Feibi Recipe Regulates the Expression of Alpha Smooth Muscle Actin, Collagen- I, Collagen-III, Hydroxyproline, and TGF-β1

The extracellular matrix's principal collagen proteins are collagen-I, collagen-III, and collagen-SMA. The immunohistochemical staining of collagen I revealed higher expression of collagen-I in the model group, which had been attenuated by N2FBR and SB treatment (**Figure 3A**). HYP levels are indicative of tissue collagen content. α-SMA, Collagen-III, and HYP were measured by ELISA. N2FBR decreased the expression levels of α-SMA, Collagen-III, and HYP in bleomycin-induced lung tissue (**Figures 3B–D**). TGF-β1 plays a crucial part in tissue fibrosis, by stimulating fibroblast proliferation and collagen synthesis (Liu et al., 2016). Compared to the model group, the TGF-β1 contents

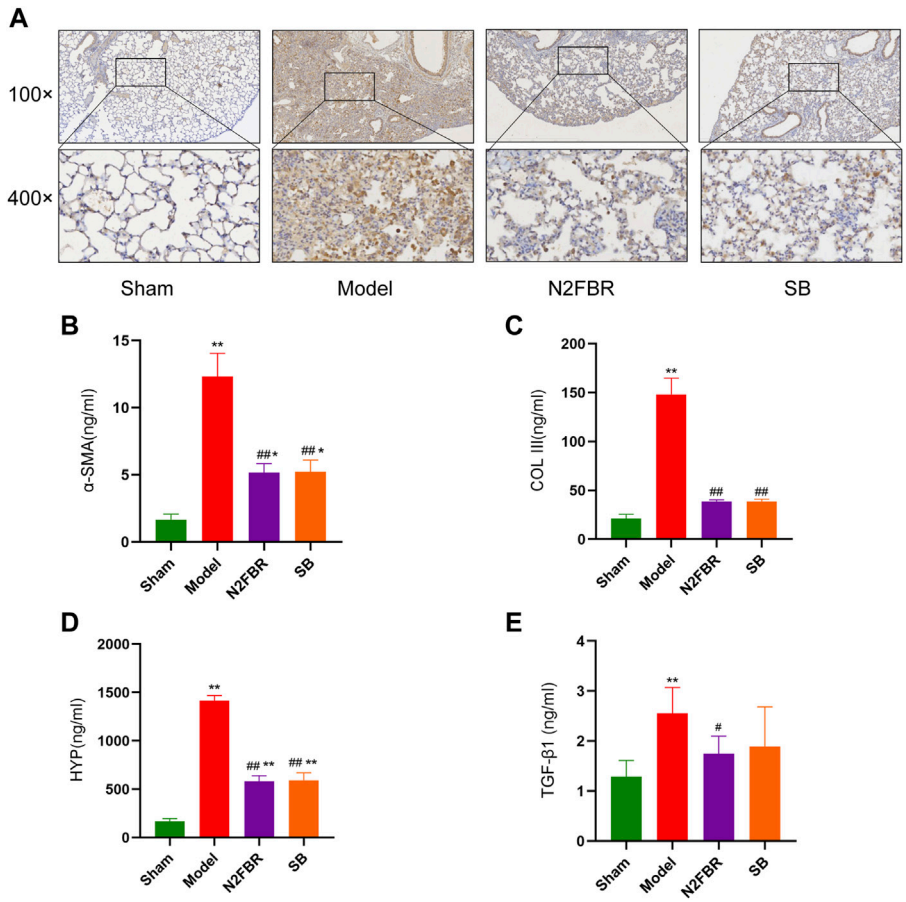

FIGURE 3 | Effects of N2FBR on fibrosis related markers. **(A)** Immunohistochemistry assays for Col I in different groups. **(B–E)** Total serum levels of α-SMA, Col III, HYP and TGF-β1. Data are expressed as Mean ± SD: $^{**}p < 0.01$, compared with sham group, $\#p < 0.05$, $\#\#p < 0.01$, compared with model group.

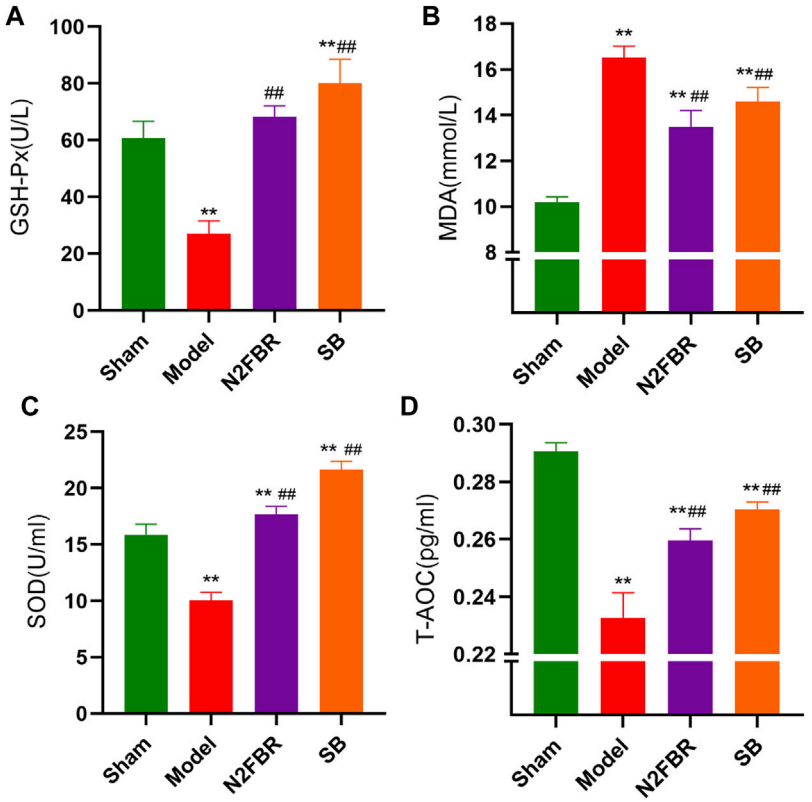

FIGURE 4 | Effects of N2FBR on oxidative stress. Total serum levels of **(A)** GSH-Px, **(B)** MDA, **(C)** SOD, **(D)** T-AOC as measured through ELISA. Data are expressed as Mean ± SD: $^{**}p < 0.01$, compared with sham group, $\#\#p < 0.01$, compared with model group.

had been significantly decreased ($p < 0.05$) in the N2FBR group (**Figure 3E**). Nevertheless, there was no statistically significant difference between the SB and model groups. It has been indicated by the findings that N2FBR is effective against the progression of lung fibrosis by reducing collagen deposition.

Number 2 Feibi Recipe Alleviates Oxidative Stress in Bleomycin-Induced Pulmonary Fibrosis Mice

To see if N2FBR contributes to anti-oxidative stress, researchers measures the activities of MDA, SOD, T-AOC, and GSH-Px. GSH-Px ($p < 0.01$), SOD ($p < 0.01$) and T-AOC($p < 0.01$) activities were significantly decreased in the serum of the model group compared to the sham group (**Figures 4A,C,D**). N2FBR increased GSH-Px ($p < 0.01$), SOD ($p < 0.01$) and T-AOC ($p < 0.01$) levels in comparison with the model group. Similarly, those antioxidant enzymes levels were increased in the SB group. Moreover, the serum MDA level, an index of lipid peroxidation, had been significantly increased in the model group than in the sham group ($p < 0.01$). BLM-mediated lipid peroxidation was significantly decreased following the administration of N2FBR and SB (**Figure 4B**) ($p < 0.01$). These data suggest that N2FBR is involved in Bleomycin-induced oxidative stress regulation.

Number 2 Feibi Recipe Promotes Autophagy in Bleomycin-Induced Pulmonary Fibrosis Mice

The expression of important autophagy-related proteins, LC3-I, LC3-II, p62, and Beclin1 was measured to confirm the N2FBR is regulated by autophagy (**Figure 5A**). p62 is a cargo receptor for autophagy. Its accumulation levels are proportional to the degree of autophagic impairment (Jiang and Mizushima, 2015). Compared to the sham group, the expression level of P62 in the model group was significantly enhanced ($p < 0.01$). P62 protein expression was significantly decreased following treatment with N2FBR ($p < 0.01$) and SB ($p < 0.01$) (**Figure 5B**). The findings had been confirmed by immunohistochemistry of P62 (**Figure 5E**). The model group had significantly lower level of beclin1 protein expression than the sham group ($p < 0.05$). Treatment with N2FBR ($p < 0.05$) and SB ($p < 0.01$) increased the level of expression of beclin1 (**Figure 5C**). The ratio of LC3-II/LC3-I is widely utilised as an indicator of autophagy. N2FBR treatment significantly accelerated the conversion of LC3B-I to LC3B-II. However, no discernible difference had been observed between the sham and model groups (**Figure 5D**). For detecting autophagic flux, TEM is the gold standard. In this study, TEM had been used for observing the morphological changes of the lung tissue. As shown in **Figure 5F**, cells from

the model group exhibited few autophagic vesicles, while numerous mitochondria were swollen, enlarged, and the cristae distorted. The use of N2FBR and SB increased the production of autophagic vesicles and reduced the number of abnormal mitochondria. Taken together, these findings proposed that N2FBR promotes autophagy, which might be responsible for its effects in the alleviation of pulmonary fibrosis.

Number 2 Feibi Recipe Relieves Lysosomal Damage in Bleomycin-Induced Pulmonary Fibrosis Mice

The expression LAMP1, Legumain, and TFEB was detected. In contrast to the sham group, the expression level of LAMP1 in the model group was inhibited (**Figure 6A**) ($p < 0.05$), while the expression in both the N2FBR ($p < 0.01$) and SB ($p < 0.05$) groups was significantly

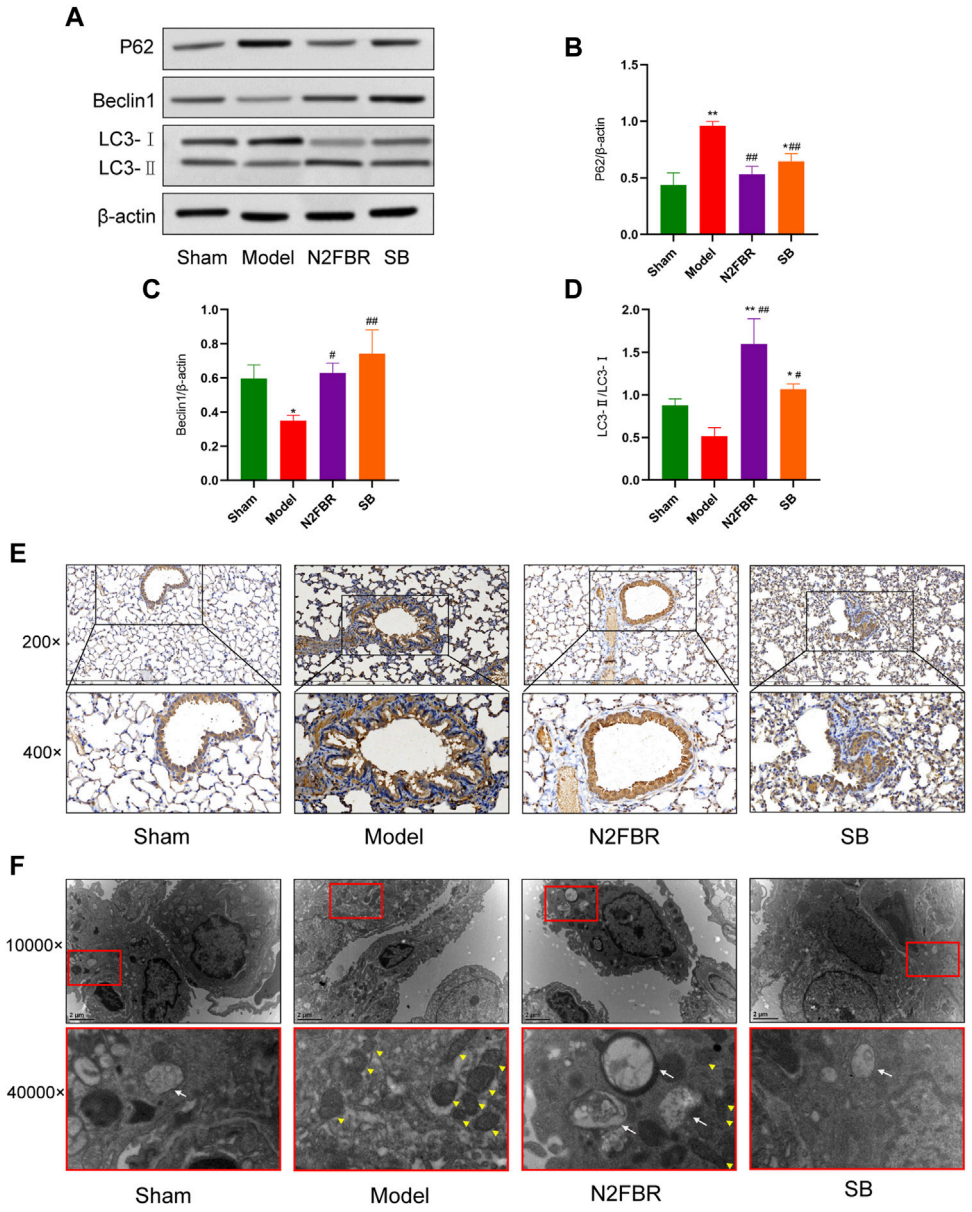

FIGURE 5 | Effects of N2FBR on autophagy. **(A)** Protein levels of beclin-1, p62, and LC3II as measured by western blotting. **(B–D)** Relative density values showing P62, beclin1, LC3- II/LC3- I expression. **(E,F)** Representative images of TEM and immunohistochemical staining for P62. The white arrows indicate autophagosomes and autolysosomes, the yellow arrowheads indicate abnormal mitochondria. Data are expressed as $^{*}p < 0.05$, $^{**}p < 0.01$, compared with sham group; $\#p < 0.05$, $\#\#p < 0.01$, compared with model group.

upregulated (**Figure 6B**). As demonstrated in **Figure 6C**, the expression level of Legumain in the model group had been significantly enhanced ($p < 0.01$). Legumain protein expression was significantly decreased following treatment with N2FBR ($p < 0.01$). Nevertheless, the level of Legumain in the SB group was not crucially different from that of the model group. Immunohistochemistry of legumain validated the findings (**Figure 6F**). Immunofluorescence confirmed that nuclear translocation and expression of TFEB was inhibited in BLM-induced mice (**Figures 6D,E**), and this phenomenon was reversed by N2FBR ($p < 0.05$) and SB ($p < 0.05$) treatment. It is implied by these findings that BLM-induced pulmonary fibrosis is caused by lysosome disorders. N2FBR alleviates BLM-induced lysosomal damage.

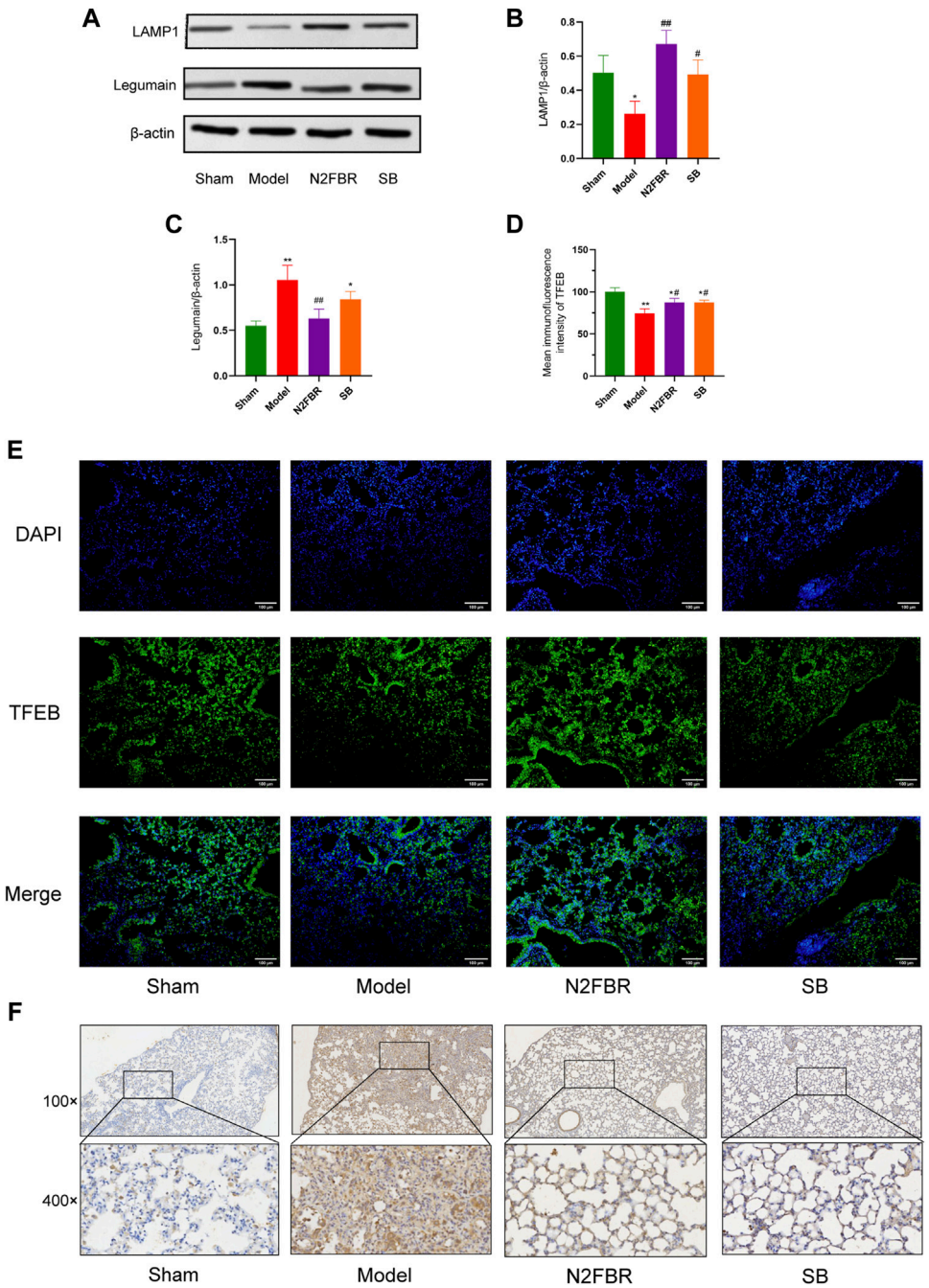

FIGURE 6 | Effects of N2FBR on lysosome injury. **(A)** Protein levels of LAMP1 and Legumain as determined by western blotting. Relative density values showing **(B)** LAMP1 and **(C)** Legumain expression. **(D)** Mean immunofluorescence intensity of TFEB. **(E)** Representative images of immunofluorescence showing the expression of TFEB. **(F)** Representative images of immunohistochemical staining for Legumain. Data are expressed as $^{*}p < 0.05$, $^{**}p < 0.01$, compared with sham group; $\#p < 0.05$, $\#\#p < 0.01$, compared with model group.

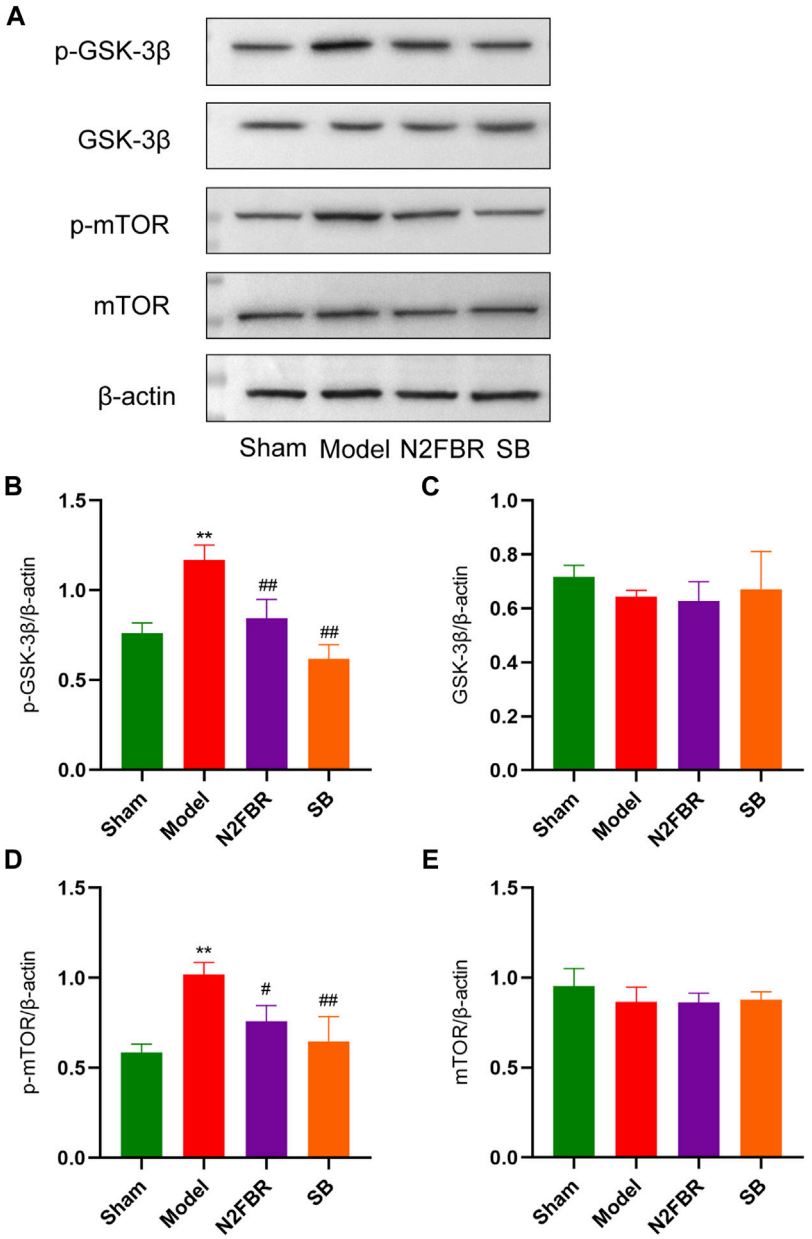

FIGURE 7 | N2FBR activated the GSK-3β/mTOR signaling pathway. **(A)** Protein levels of p-GSK-3β, GSK-3β, p-mTOR, and mTOR as quantified by western blotting. Relative density values showing **(B)** p-GSK-3β, **(C)** GSK-3β, **(D)** p-mTOR and **(E)** mTOR expression. Data are expressed as $^{**}p < 0.01$, compared with sham group; $\#p < 0.05$, $\#\#p < 0.01$, compared with model group.

Number 2 Feibi Recipe Activates the GSK-3β/mTOR Signalling Pathway to Trigger Autophagy

Western blotting was used to determine the levels of GSK-3β and mTOR, and their phosphorylation, which is the autophagy regulation mechanism, to see how N2FBR activated autophagy. As demonstrated in **Figure 7A**, the model group showed significantly increased expression levels of phosphorylated mTOR (p-mTOR) ($p < 0.01$) and phosphorylated GSK-3β(p-GSK-3β) ($p < 0.01$) in contrast to the sham group. After N2FBR ($p < 0.05$, $p < 0.01$) and SB ($p < 0.01$, $p < 0.01$) treatment, the levels of p-mTOR and p-GSK-3β were decreased (**Figures 7B,D**). Nevertheless, no discernible difference in total GSK-3β and total mTOR protein expression was observed in each group (**Figures 7C,E**). These findings indicated that N2FBR could inhibit the GSK-3β/mTOR pathway in BLM-induced pulmonary fibrosis mice.

DISCUSSION

IPF is a chronic, persistent pulmonary disease caused by a variety of factors. Unfortunately, there are not many options in terms of available pharmacological therapies. In China, Number 2 Feibi Recipe was used in clinic for the treatment of pulmonary fibrosis. Our previous study confirmed that the N2FBR decrease oxidative damage in mice exposed to PM2.5 (Liu et al., 2018). Furthermore, N2FBR reduced the level of intracellular ROS and regulated the balance of autophagy and apoptosis in H_2O_2-mediated AECs (Gu et al., 2022). In the current research, we demonstrated that N2FBR had anti-fibrotic therapeutic effects in BLM-induced pulmonary fibrosis and further explored the effector mechanisms.

In rodent models of pulmonary fibrosis, bleomycin intratracheal instillation is commonly employed. In BLM-induced mice, ECM deposition in enhanced, resulting in alveolar wall thickening and reduced ventilation function. Fibrosis could be histologically detected by day 14, with obvious responses which occur between days 21–28 (Moore and Hogaboam, 2008). Col-I and Col-III are the main components of extracellular matrix. α-SMA is a commonly recognized indicator for pulmonary fibrosis. Reduced α-SMA expression reduces fibroblasts activation, resulting in a less excessive ECM deposition (Liu T. et al., 2021). Hydroxyproline accounts for 12.5% of the amino acid content in collagen fibers. Hydroxyproline expression might be linked to the level of ECM. TGF-β1 was described as a critical signalling molecule engaged in fibrosis-induced lung injury and is considered as a key modulator of pulmonary fibrosis. TGF-β1 could activate downstream proteins and eventually initiate the induction of numerous fibrosis-related proteins (Fernandez and Eickelberg, 2012). Our findings showed that N2FBR improved the histological properties of lung tissues and slowed the advancement of fibrosis in this investigation. Moreover, N2FBR inhibited the increase in α-SMA, collagen I, collagen III, hydroxyproline, and TGF-β1 induced by bleomycin. These results comply with our previous hypotheses and further supported the anti-fibrotic effects of N2FBR. It may be a promising new agent for the treatment of pulmonary fibrosis.

Lung injury and pulmonary fibrosis are known to be linked to oxidate stress. At low concentrations, ROS could modulate signal transduction. Nevertheless, ROS at high concentrations could cause damage to lipids, proteins, and nucleic acids, resulting in cell death and tissue damage. Lung tissue as well as biological fluids from IPF patients illustrated that oxidative stress significantly contributes to IPF development and progression (Landi et al., 2014). TGF-β, the most potent pro-fibrotic factor, has been implicated in the production of reactive oxygen species (ROS), which has activated fibrogenic factors. As a result, a vicious circle is formed (Wang et al., 2022). The lung possesses an endogenous antioxidant system which protects against oxidative stress damage. In order to remove ROS, various anti-oxidant molecules and enzymes could be produced. In the present study, MDA, SOD, T-AOC, GSH-Px were selected as markers to evaluate bleomycin-induced oxidative stress damage. MDA, a lipid peroxidation product, has been utilised as an indicator of the cell damage caused by oxidative stress (Sun et al., 2020). SOD and GSH-Px are free radical scavengers that are capable of removing the active substances in oxidative damage (Poprac et al., 2017). The T-AOC is an index that measures the antioxidant capacity of the body. MDA levels were dramatically elevated after bleomycin treatment, while SOD, GSH-Px, and T-AOC levels were reduced (Dong et al., 2017). MDA expression level was decreased, while SOD, GSH-Px, T-AOC had been increased in the N2FBR group in comparison with model group. In a nutshell, N2FBR protects against oxidative damage by enhancing the activity of antioxidant enzymes in pulmonary fibrosis.

Autophagy is a homeostatic degradation process that aids in the elimination of unfolded proteins or damaged organelles and regulates cell metabolism through autophagy-related genes (Zhao et al., 2020). Beclin-1, an autophagy-related protein, has been engaged in the activation of autophagy as well as the development of autophagosome precursors. Microtubule-associated proteins 1A/1B light chain 3 (LC3) is a marker of autophagy. In the early stages of autophagy formation, LC3B-I has been converted into LC3B-II (Nieto-Torres et al., 2021). The degree of autophagy relies on the LC3II/I ratio. P62 takes part in the maturation of the autophagosome and has also been degraded during autophagy. Autophagy impairment can be confirmed by p62 accumulation. Previous research has found that the expression levels of LC3-II had been reduced in lung tissue of patients with IPF (Ricci et al., 2013). The inhibition of autophagy enhances epithelial cell senescence and myofibroblast differentiation in lung fibrosis (Araya et al., 2013). Epithelial-mesenchymal transition (EMT) is aided by abnormal autophagy in alveolar epithelial cells (Hill et al., 2019). It has been revealed by our previous research that N2FBR alleviated H_2O_2-mediated oxidative stress damage in AECs via promoting autophagy (Gu et al., 2022). In this study, we analyzed the expression of LC3-II/LC3-I, beclin1, and p62 in mice lung tissues. N2FBR administration resulted in a considerable down-regulation of p62, whereas the beclin-1 expression and LC3-I to LC3-II transformations were simultaneously stimulates as predicted. TEM is commonly recognised as the gold standard for the qualitative detection of autophagy. As apparent in the TEM images, numerous dysmorphic and enlarged mitochondria, and a few autophagic vesicles were observed in lung tissues of the model group. An increasing number of autophagic vesicles were found after N2FBR therapy. The number of abnormal mitochondria was decreased in N2FBR group compared with the model group. It is evident from these results that the functions of N2FBR on upregulating the expression of autophagy-related proteins and enhancing autophagosome formation.

Lysosomes are acid organelles for degradation at the end of the autophagic flux. The fusion of autophagosome and lysosome is the rate-limiting step of autophagy (El-Kadi et al., 2012). Excess ROS induce lysosomal permeabilization and destabilization, which lead to the disruption of autophagy-lysosome pathway. Lysosomal Associated Membrane Protein-1 (LAMP1), a major protein component of the lysosomal membrane (Eskelinen, 2006), is already established as a general marker of lysosome dysfunction. Legumain is mainly localized to the acidic lysosomal compartments. Lysosome protease is released into intracellular regions when lysosomal membranes are damaged (Akhtar et al., 2015). TFEB is a master transcriptional regulator of autophagy as well as lysosome biogenesis. Activation of TFEB is essential for lysosomal homeostasis

after lysosomal damage (Nakamura et al., 2021). Silica inhibited autophagy flux via interfering with lysosomal degradation. Overexpression of the transcription factor TFEB reduced lysosomal dysfunction and silica-induced lung fibrosis (He et al., 2020). In the current study, bleomycin treatment crucially downregulated LAMP1 expression and upregulated Legumain expression, which had been reversed by N2FBR treatment. Immunofluorescence demonstrated that N2FBR treatment promoted nuclear translocation and expression of TFEB. It is suggested by these findings that the lysosome is injured by BLM, and N2FBR treatment might protect lysosomal function as well as promote autophagic substrate degradation. Nevertheless, a recent study shown that azithromycin reduced collagen production in TGF-β treated fibroblasts by disrupting lysosomal function (Krempaska et al., 2020). These discrepancies could be related to the use of different experimental models of pulmonary fibrosis. Lysosome dysfunction might play varying roles in distinctive cells involved in IPF. Considering that little attention has been paid to this area, additional research should be conducted in future studies.

GSK-3β is involved in the control of a variety of downstream signalling pathways. SB216763, a GSK-3 inhibitor, has previously been shown to protect against BLM-induced pulmonary fibrosis. In pulmonary fibroblasts, silencing GSK-3β with siRNA decreased the TGF-β1-induced expression of α-actin and fibronectin (Baarsma et al., 2013). Additionally, the knockdown of GSK-3β reversed the induction of EMT in alveolar epithelial cells (Liu et al., 2021). GSK-3β serves a pivotal role in the regulation of mTOR pathway. The basal levels of mTORC1 and mTORC2, as well as the mTOR complexes, were shown to be up-regulated in IPF lung samples (Chang et al., 2014; Romero et al., 2016). Inhibiting mTOR accelerated autophagy, reversing apoptotic resistance in fibroblasts from IPF patients. In lung epithelial cells, Rapamycin inhibition reduced mitochondrial oxidative damage and delayed cellular senescence (Summer et al., 2019). The protein expression level of p-GSK-3β, p-mTOR, and the total of GSK-3β and mTOR in the lungs of mice were determined by Western blotting in the current study. We explored that N2FBR inhibited the activation of p-GSK-3β and p-mTOR, but had no effect on total GSK-3β and mTOR, which illustrates that the beneficial effect of N2FBR may be attributed to the inhibition of the GSK-3β/mTOR pathway.

In conclusion, the current investigation confirmed N2FBR as a promising therapy candidate for idiopathic pulmonary fibrosis collagen deposition and oxidative stress. Additionally, it activated autophagy and protected the lysosome from injury. Mechanistically, these functions may be associated with the regulation of the GSK-3β/mTOR pathway. These findings provide experimental evidence that N2FBR exert its function through promotion of autophagy and offering a new therapeutic strategy for the prevention of IPF. Nevertheless, additional research has been required to confirm whether N2FBR alleviates pulmonary fibrosis by modulating autophagy.

DATA AVAILABILITY STATEMENT

The raw data supporting the conclusions of this article will be made available by the authors, without undue reservation.

ETHICS STATEMENT

The animal study was reviewed and approved by Animal Ethical Experimentation Committee of Beijing University of Chinese Medicine.

AUTHOR CONTRIBUTIONS

HL, QP, WW, and ZL performed the experiments. HL and FC analyzed the data and wrote the manuscript. HL, ZL, and YJ participated in experimental design. HL and QL revised the manuscript. All authors gave final approval for the submitted version.

FUNDING

This study is supported by Beijing Natural Science Foundation (no. 7202118), and National Natural Science Foundation of China (no. 81573970).

REFERENCE

Akhtar, M. J., Alhadlaq, H. A., Alshamsan, A., Majeed Khan, M. A., and Ahamed, M. (2015). Aluminum Doping Tunes Band Gap Energy Level as Well as Oxidative Stress-Mediated Cytotoxicity of ZnO Nanoparticles in MCF-7 Cells. *Sci. Rep.* 5, 13876. doi:10.1038/srep13876

Araya, J., Kojima, J., Takasaka, N., Ito, S., Fujii, S., Hara, H., et al. (2013). Insufficient Autophagy in Idiopathic Pulmonary Fibrosis. *Am. J. Physiol. Lung Cell Mol. Physiol.* 304 (1), L56–L69. doi:10.1152/ajplung.00213.2012

Baarsma, H. A., Engelbertink, L. H., van Hees, L. J., Menzen, M. H., Meurs, H., Timens, W., et al. (2013). Glycogen Synthase Kinase-3 (GSK-3) Regulates TGF-β_1-Induced Differentiation of Pulmonary Fibroblasts. *Br. J. Pharmacol.* 169 (3), 590–603. doi:10.1111/bph.12098

Chang, W., Wei, K., Ho, L., Berry, G. J., Jacobs, S. S., Chang, C. H., et al. (2014). A Critical Role for the mTORC2 Pathway in Lung Fibrosis. *PLoS One* 9 (8), e106155. doi:10.1371/journal.pone.0106155

Dong, X., Li, X., Li, M., Chen, M., Fan, Q., and Wei, W. (2017). Inhibitory Effects of Thalidomide on Bleomycin-Induced Pulmonary Fibrosis in Rats via Regulation of Thioredoxin Reductase and Inflammations. *Am. J. Transl. Res.* 9 (10), 4390–4401.

El-Kadi, S. W., Suryawan, A., Gazzaneo, M. C., Srivastava, N., Orellana, R. A., Nguyen, H. V., et al. (2012). Anabolic Signaling and Protein Deposition Are Enhanced by Intermittent Compared with Continuous Feeding in Skeletal Muscle of Neonates. *Am. J. Physiol. Endocrinol. Metab.* 302 (6), E674–E686. doi:10.1152/ajpendo.00516.2011

Eskelinen, E. L. (2006). Roles of LAMP-1 and LAMP-2 in Lysosome Biogenesis and Autophagy. *Mol. Asp. Med.* 27 (5-6), 495–502. doi:10.1016/j.mam.2006.08.005

Fernandez, I. E., and Eickelberg, O. (2012). The Impact of TGF-β on Lung Fibrosis: from Targeting to Biomarkers. *Proc. Am. Thorac. Soc.* 9 (3), 111–116. doi:10.1513/pats.201203-023AW

Glassberg, M. K. (2019). Overview of Idiopathic Pulmonary Fibrosis, Evidence-Based Guidelines, and Recent Developments in the Treatment Landscape. *Am. J. Manag. Care* 25 (11 Suppl. l), S195–S203.

Gu, X., Long, Q., Wei, W., Tong, J., Li, Z., Zhang, Z., et al. (2022). Number 2 Feibi Recipe Inhibits H2O2-Mediated Oxidative Stress Damage of Alveolar Epithelial Cells by Regulating the Balance of Mitophagy/Apoptosis. *Front. Pharmacol.* 13, 830554. doi:10.3389/fphar.2022.830554

Gurrieri, C., Piazza, F., Gnoato, M., Montini, B., Biasutto, L., Gattazzo, C., et al. (2010). 3-(2,4-dichlorophenyl)-4-(1-methyl-1H-indol-3-yl)-1H-pyrrole-2,5-dione (SB216763), a Glycogen Synthase Kinase-3 Inhibitor, Displays Therapeutic Properties in a Mouse Model of Pulmonary Inflammation and Fibrosis. *J. Pharmacol. Exp. Ther.* 332 (3), 785–794. doi:10.1124/jpet.109.153049

He, X., Chen, S., Li, C., Ban, J., Wei, Y., He, Y., et al. (2020). Trehalose Alleviates Crystalline Silica-Induced Pulmonary Fibrosis via Activation of the TFEB-Mediated Autophagy-Lysosomal System in Alveolar Macrophages. *Cells* 9 (1), 122. doi:10.3390/cells9010122

Hill, C., Li, J., Liu, D., Conforti, F., Brereton, C. J., Yao, L., et al. (2019). Autophagy Inhibition-Mediated Epithelial-Mesenchymal Transition Augments Local Myofibroblast Differentiation in Pulmonary Fibrosis. *Cell Death Dis.* 10 (8), 591. doi:10.1038/s41419-019-1820-x

Jiang, P., and Mizushima, N. (2015). LC3- and P62-Based Biochemical Methods for the Analysis of Autophagy Progression in Mammalian Cells. *Methods* 75, 13–18. doi:10.1016/j.ymeth.2014.11.021

King, T. E., Jr., Bradford, W. Z., Castro-Bernardini, S., Fagan, E. A., Glaspole, I., Glassberg, M. K., et al. (2014). A Phase 3 Trial of Pirfenidone in Patients with Idiopathic Pulmonary Fibrosis. *N. Engl. J. Med.* 370 (22), 2083–2092. doi:10.1056/NEJMoa1402582

Krempaska, K., Barnowski, S., Gavini, J., Hobi, N., Ebener, S., Simillion, C., et al. (2020). Correction to: Azithromycin Has Enhanced Effects on Lung Fibroblasts from Idiopathic Pulmonary Fibrosis (IPF) Patients Compared to Controls. *Respir. Res.* 21 (1), 29. doi:10.1186/s12931-020-1304-7

Landi, C., Bargagli, E., Carleo, A., Bianchi, L., Gagliardi, A., Prasse, A., et al. (2014). A System Biology Study of BALF from Patients Affected by Idiopathic Pulmonary Fibrosis (IPF) and Healthy Controls. *Proteomics Clin. Appl.* 8 (11-12), 932–950. doi:10.1002/prca.201400001

Lederer, D. J., and Martinez, F. J. (2018). Idiopathic Pulmonary Fibrosis. *N. Engl. J. Med.* 378 (19), 1811–1823. doi:10.1056/NEJMra1705751

Liu, H., Fang, S., Wang, W., Cheng, Y., Zhang, Y., Liao, H., et al. (2016). Macrophage-derived MCPIP1 Mediates Silica-Induced Pulmonary Fibrosis via Autophagy. *Part Fibre Toxicol.* 13 (1), 55. doi:10.1186/s12989-016-0167-z

Liu, Z., Wang, W., Cao, F., Liu, S., Zou, X., Li, G., et al. (2018). Number 2 Feibi Recipe Reduces PM2.5-Induced Lung Injury in Rats. *Evid. Based Complement. Altern. Med.* 2018, 3674145. doi:10.1155/2018/3674145

Liu, S., Lv, X., Wei, X., Liu, C., Li, Q., Min, J., et al. (2021). TRIB3–GSK-3β Interaction Promotes Lung Fibrosis and Serves as a Potential Therapeutic Target. *Acta Pharm. Sin. B* 11 (10), 3105–3119. doi:10.1016/j.apsb.2021.06.017

Liu, T., Gonzalez De Los Santos, F., Hirsch, M., Wu, Z., and Phan, S. H. (2021). Noncanonical Wnt Signaling Promotes Myofibroblast Differentiation in Pulmonary Fibrosis. *Am. J. Respir. Cell Mol. Biol.* 65 (5), 489–499. doi:10.1165/rcmb.2020-0499OC

Moore, B. B., and Hogaboam, C. M. (2008). Murine Models of Pulmonary Fibrosis. *Am. J. Physiol. Lung Cell Mol. Physiol.* 294 (2), L152–L160. doi:10.1152/ajplung.00313.2007

Nakamura, S., Akayama, S., and Yoshimori, T. (2021). Autophagy-independent Function of Lipidated LC3 Essential for TFEB Activation during the Lysosomal Damage Responses. *Autophagy* 17 (2), 581–583. doi:10.1080/15548627.2020.1846292

Nasser, M., Si-Mohamed, S., Turquier, S., Traclet, J., Ahmad, K., Philit, F., et al. (2021). Nintedanib in Idiopathic and Secondary Pleuroparenchymal Fibroelastosis. *Orphanet J. Rare Dis.* 16 (1), 419. doi:10.1186/s13023-021-02043-5

Nieto-Torres, J. L., Leidal, A. M., Debnath, J., and Hansen, M. (2021). Beyond Autophagy: The Expanding Roles of ATG8 Proteins. *Trends Biochem. Sci.* 46 (8), 673–686. doi:10.1016/j.tibs.2021.01.004

Patel, A. S., Lin, L., Geyer, A., Haspel, J. A., An, C. H., Cao, J., et al. (2012). Autophagy in Idiopathic Pulmonary Fibrosis. *PLoS One* 7 (7), e41394. doi:10.1371/journal.pone.0041394

Poprac, P., Jomova, K., Simunkova, M., Kollar, V., Rhodes, C. J., and Valko, M. (2017). Targeting Free Radicals in Oxidative Stress-Related Human Diseases. *Trends Pharmacol. Sci.* 38 (7), 592–607. doi:10.1016/j.tips.2017.04.005

Qin, X., Zhang, J., Wang, B., Xu, G., and Zou, Z. (2017). LAMP-2 Mediates Oxidative Stress-dependent Cell Death in Zn(2+)-Treated Lung Epithelium Cells. *Biochem. Biophys. Res. Commun.* 488 (1), 177–181. doi:10.1016/j.bbrc.2017.05.030

Racanelli, A. C., Kikkers, S. A., Choi, A. M. K., and Cloonan, S. M. (2018). Autophagy and Inflammation in Chronic Respiratory Disease. *Autophagy* 14 (2), 221–232. doi:10.1080/15548627.2017.1389823

Raghu, G., and Richeldi, L. (2017). Current Approaches to the Management of Idiopathic Pulmonary Fibrosis. *Respir. Med.* 129, 24–30. doi:10.1016/j.rmed.2017.05.017

Ricci, A., Cherubini, E., Scozzi, D., Pietrangeli, V., Tabbì, L., Raffa, S., et al. (2013). Decreased Expression of Autophagic Beclin 1 Protein in Idiopathic Pulmonary Fibrosis Fibroblasts. *J. Cell Physiol.* 228 (7), 1516–1524. doi:10.1002/jcp.24307

Romero, Y., Bueno, M., Ramirez, R., Álvarez, D., Sembrat, J. C., Goncharova, E. A., et al. (2016). mTORC1 Activation Decreases Autophagy in Aging and Idiopathic Pulmonary Fibrosis and Contributes to Apoptosis Resistance in IPF Fibroblasts. *Aging Cell* 15 (6), 1103–1112. doi:10.1111/acel.12514

Summer, R., Shaghaghi, H., Schriner, D., Roque, W., Sales, D., Cuevas-Mora, K., et al. (2019). Activation of the mTORC1/PGC-1 axis Promotes Mitochondrial Biogenesis and Induces Cellular Senescence in the Lung Epithelium. *Am. J. Physiol. Lung Cell Mol. Physiol.* 316 (6), L1049–L1060. doi:10.1152/ajplung.00244.2018

Sun, B., Shi, Y., Li, Y., Jiang, J., Liang, S., Duan, J., et al. (2020). Short-term PM2.5 Exposure Induces Sustained Pulmonary Fibrosis Development during Post-exposure Period in Rats. *J. Hazard Mater* 385, 121566. doi:10.1016/j.jhazmat.2019.121566

Tian, Y., Li, H., Qiu, T., Dai, J., Zhang, Y., Chen, J., et al. (2019). Loss of PTEN Induces Lung Fibrosis via Alveolar Epithelial Cell Senescence Depending on NF-κB Activation. *Aging Cell* 18 (1), e12858. doi:10.1111/acel.12858

Tong, J., Wu, Z., Wang, Y., Hao, Q., Liu, H., Cao, F., et al. (2021). Astragaloside IV Synergizing with Ferulic Acid Ameliorates Pulmonary Fibrosis by TGF-β1/Smad3 Signaling. *Evid.-Based Complement. Altern. Med.* 2021, 8845798. doi:10.1155/2021/8845798

Wang, W., Liu, Z., Niu, J., Yang, H., Long, Q., Liu, H., et al. (2020). Feibi Recipe Reduced Pulmonary Fibrosis Induced by Bleomycin in Mice by Regulating BRP39/IL-17 and TGFβ1/Smad3 Signal Pathways. *Evid. Based Complement. Altern. Med.* 2020, 5814658. doi:10.1155/2020/5814658

Wang, M., Wang, L., Zhou, Y., Feng, X., Ye, C., and Wang, C. (2022). Shen Shuai Recipe Attenuates Renal Fibrosis in Chronic Kidney Disease by Improving Hypoxia-Induced the Imbalance of Mitochondrial Dynamics via PGC-1α Activation. *Phytomedicine* 98, 153947. doi:10.1016/j.phymed.2022.153947

Wei, W., Li, G., Liu, Z., Yang, H., Liu, S., Zou, X., et al. (2022). Feibi Decoction-Medicated Serum Inhibits Lipopolysaccharide-Induced Inflammation in RAW264.7 Cells and BMDMs. *Exp. Ther. Med.* 23 (1), 110. doi:10.3892/etm.2021.11033

Yu, L., Chen, Y., and Tooze, S. A. (2018). Autophagy Pathway: Cellular and Molecular Mechanisms. *Autophagy* 14 (2), 207–215. doi:10.1080/15548627.2017.1378838

Zhao, H., Wang, Y., Qiu, T., Liu, W., and Yao, P. (2020). Autophagy, an Important Therapeutic Target for Pulmonary Fibrosis Diseases. *Clin. Chim. Acta* 502, 139–147. doi:10.1016/j.cca.2019.12.016

Conflict of Interest: The authors declare that the research was conducted in the absence of any commercial or financial relationships that could be construed as a potential conflict of interest.

Publisher's Note: All claims expressed in this article are solely those of the authors and do not necessarily represent those of their affiliated organizations, or those of the publisher, the editors and the reviewers. Any product that may be evaluated in this article, or claim that may be made by its manufacturer, is not guaranteed or endorsed by the publisher.

frontiers | Frontiers in Pharmacology

ORIGINAL RESEARCH
published: 15 July 2022
doi: 10.3389/fphar.2022.928135

Photodynamic Effects of *Thuja occidentalis* on Lung Cancer Cells

Ayesha Loonat[1,2], *Rahul Chandran*[1]*, *Janice Pellow*[2] *and Heidi Abrahamse*[1]

[1]*Laser Research Centre, Faculty of Health Sciences, University of Johannesburg, Johannesburg, South Africa,* [2]*Department of Complementary Medicine, Faculty of Health Sciences, University of Johannesburg, Johannesburg, South Africa*

The global incidence and mortality rates resulting from lung cancer encapsulate a need to identify more effective treatment protocols. Photodynamic therapy (PDT) and homeopathy offer possible anticancer therapies as part of a multi-disciplinary approach. Studies have identified the anticancer effects of *Thuja occidentalis* L. plant extracts. The aim of this study was to investigate the effects of *Thuja occidentalis* (TO) homeopathic mother tincture and TO mediated PDT (TO-PDT) on A549 lung cancer cells. Commercially available A549 cells were pre-treated with TO, or laser irradiation at 660 nm, or the combined treatment (TO-PDT). Cells were analyzed morphologically by inverted light microscopy and Hoechst stain; and biochemically by lactate dehydrogenase (LDH), adenosine triphosphate (ATP), and trypan blue assays. Cells treated with TO and TO-PDT demonstrated morphological changes in the cell and cell nuclei indicative of cell death. These groups exhibited a dose dependent increase in LDH release and a decrease in ATP levels and cell viability indicating its cytotoxic and antiproliferative potential. Furthermore, at the same doses, TO when photoactivated in PDT induced enhanced anticancer responses thereby surpassing the effects of treatment with the tincture alone. Results demonstrate how the direct cytotoxic effects of TO can be improved when administered as a photosensitizer in PDT to promote cancer cell death.

Keywords: lung cancer, photodynamic therapy, homeopathy, cytotoxicity, photosensitizer

OPEN ACCESS

Edited by:
Arunachalam Karuppusamy, Chinese Academy of Sciences (CAS), China

Reviewed by:
Prabhakar Busa, Cathay General Medical Research Institute, Taiwan
Mariappan Rajan, Madurai Kamaraj University, India

***Correspondence:**
Rahul Chandran
rahulc@uj.ac.za

Specialty section:
This article was submitted to Respiratory Pharmacology, a section of the journal Frontiers in Pharmacology

Received: *25 April 2022*
Accepted: *22 June 2022*
Published: *15 July 2022*

Citation:
Loonat A, Chandran R, Pellow J and Abrahamse H (2022) Photodynamic Effects of Thuja occidentalis on Lung Cancer Cells. Front. Pharmacol. 13:928135. doi: 10.3389/fphar.2022.928135

1 INTRODUCTION

With current socio-economic developments and epidemiological transitions, there is an increase in the distribution and prevalence of the main risk factors that can initiate lung cancer. This is reflected by the continuous rise in current and expected cases of lung cancer worldwide. Unsurprisingly, patients with lung cancer also have the highest mortality rates (Bray et al., 2018). Treatment of lung cancer relies on the combined administration of surgery, radiotherapy, and chemotherapy. Despite the improvements and implementation of these therapies, it often struggles to sustain patients' expectations and treatment outcomes due to limitations of these therapies in the treatment of lung cancer. This includes lack of targeting precision, development of multi-drug resistance, and significant adverse events. These obstacles can be both a cause and a risk factor contributing to therapeutic failure and increased mortality rates (Mottaghitalab et al., 2019). Therefore, there is an expectation to continue to focus research efforts aimed at meeting crucial therapeutic demands based on highly effective treatment protocols with minimal adverse effects and long-lasting responses.

Integrative oncology embraces a multidisciplinary approach to the treatment regimen of cancer patients by administering both conventional and complementary medicines (CM) (Witt et al., 2017). The World Health Organization (WHO) defines CM as a diverse group of health care practices that

do not form a part of the country's own traditional or conventional therapies and are not fully integrated into the dominant healthcare system (Global report on traditional and, 1066). This combined approach has the potential to overcome critical challenges facing current conventional cancer therapies. This will, in turn, contribute towards improving patients' quality of life (QoL) and promoting survival (Witt et al., 2017). Homeopathy is one such CM, that is, commonly used in parallel with other conventional therapies to aid in the supportive treatment of both oncological and non-oncological diseases as part of an integrative approach (Dehghan et al., 2020). Plant-based homeopathic mother tinctures (Ø) are hydroethanolic extractions of the entire plant or parts of the plant, prepared following specific guidelines in the homeopathic pharmacopeia (Das, 2019). Different from herbal tinctures which are far more concentrated in their dilution at 1:2 or 1:1 (Romm et al., 2010); Ø's are prepared in a 1:10 dilution ratio (Steven, 2013).

Photodynamic therapy (PDT) is a photochemical process that involves the activation of a photosensitizer (PS) with an appropriate wavelength of light to produce cytotoxic reactive oxygen species (ROS) capable of initiating cell death (Chen et al., 2020). The efficacy of PDT lies in its multifunctional ability to elicit targeted cancer cell death with minimal invasiveness and drug resistance (Fan et al., 2019; Pinto da Silva et al., 2019). Successful PDT outcomes are highly dependent on selecting an appropriate PS. Currently, only a limited number of PSs are medically approved, most of which are commercially available in small amounts, and in many instances, only a few of them benefit patients entirely in clinical practice. In addition, the practical application of commonly used photophrin related PSs is limited by their slow elimination from the body, consequently resulting in adverse effects such as skin photosensitivity which may persist for weeks after the commencement of the treatment (Shi et al., 2019; Hu et al., 2020).

Natural agents are gaining much interest to determine alternative options and facilitate design strategies focused on improving safety, outcomes, and enhancing the efficacy of cancer treatments including PDT. Plant extracts contain a diverse group of bioactive compounds with anticancer capacity. These extracts can target multiple deregulated cellular pathways to induce cell death in an efficacious and selective manner and with minimal drug resistance and toxicity on healthy cells (Millimouno et al., 2014). Furthermore, these products are commercially available, environmentally sustainable, and cost-effective (Mansoori et al., 2019). Research data has provided evidence that demonstrates the presence of chromophores in various phytochemicals of plant extracts including furanocoumarins, polyacetylenic molecules, thiophenes, curcumins, xanthanoids, alkaloids, and antraquininones. These phytochemicals demonstrated photosensitizing capabilities by absorbing light at various wave-lengths within a phototherapy setting (Siewert and Stuppner, 2019). A review by Dong et al. (2021), demonstrated how hypericin-mediated PDT inhibited cell proliferation in various cancer models including colon, breast, glioma, cervical and hepatic tumour cells. Furthermore, the co-administration of hypericin-PDT and chemotherapeutic agents or other targeted therapies were able to increase the inhibitory effects of cell growth on cancer cells through the modulation of various proteins and genes (Dong et al., 2021). In an *in vitro* study on renal carcinoma cells, berberine was shown to be an effective PS in PDT (Lopes et al., 2019). The *in vitro* and *in vivo* effects of 5-Aminolevulinic acid (ALA) mediated PDT was shown to induce cell death in human colon cancer cells. In another study, ALA-PDT showed selected efficacy against aggressive adult T-cell leukemia without influencing normal lymphocytes (Sando et al., 2020). Curcumin has been extensively researched for its potential as a PS, and has demonstrated strong photocytotoxic effects in micromolar concentrations against a variety of cell lines. Furanocoumarins when photoactivated have been shown to be effective against various cancer cells through the inhibition of several pathways that play a key role in tumour development, and in the activation of proteins responsible for apoptotic induction (Kubrak et al., 2022).

Thuja occidentalis L. (TO) is a coniferous plant belonging to the Cupressaceae family with pro-apoptotic, anticarcinogenic, antiproliferative, antioxidant, and radio-protective properties. It is commonly known as the white cedar or arbor vitae and its name is Latin for tree of life (Silva et al., 2017). TO is indigenous to the north-eastern mixed and boreal forests of North America, and is grown as an ornamental tree in Europe (Danneyrolles et al., 2017). It is an important Native American ceremonial plant which has been widely utilized in ethnomedicine. The plant is greatly honoured by the Ojibwa culture by the name Nookomis Giizhik, meaning Grandmother Cedar who used the soft twigs to make soups and teas for the treatment of various ailments (Pudełek et al., 2019). In traditional medicine, TO has been used to treat diseases of the respiratory system (bronchial catarrh), urinary and reproductive systems (enuresis, cystitis, amenorrhoea), as well as rheumatic and autoimmune diseases (Stan et al., 2019). In a homeopathic clinical setting, TO mother tincture is prescribed in the treatment regimen of pathological growths such as tumours, and acute and chronic respiratory tract infections. Cell death owing to TO in cancer cells can be attributed to its primary active phytochemical thujone and to a lesser extent its polysaccharide and flavonoid fractions (Alves et al., 2014). Thujone is associated with the activation of BAX, cytochrome c, and caspase 3; all in favor of pro-apoptotic signaling (Ijaz et al., 2018). A study by Siveen and Kuttan (2011) demonstrated the immunostimulatory activity of thujone on the humoral and cell-mediated immune system during solid tumour development. The augmentation of the immune system by thujone increased natural killer (NK) cell activity, antibody-dependent cellular cytotoxicity (ADCC), and cytotoxic T lymphocyte generation (Siveen and Kuttan, 2011). Other studies have shown how thujone can exert pro-apoptotic and anti-invasive effects. The attenuating effect of thujone was further supported with the accumulation of ROS (Ijaz et al., 2018; Pudełek et al., 2019). An *in vivo* study by Sunila et al. (2011) showed the effects of TO and its polysaccharide on tumour-bearing mice which effectively stimulated cell-mediated immunity through the enhancement of NK activity, ADCC, and antibody-dependent complement-mediated cytotoxicity.

Furthermore, it also showed a decrease in pro-inflammatory cytokines, as a result inhibiting metastasis of tumour cells (Sunila et al., 2011). Mukherjee et al. (2014) demonstrated the target specific and chemopreventative role of flavonol isolated from the ethanolic leaf extracts of TO on A549 cells *in vitro* and Swiss albino mice *in vivo*. Findings demonstrated the upregulation of p53 after exposure to flavanol *in vitro* and resulted in the inhibition of cellular proliferation and tumour growth *in vivo*. Moreover, the flavonol at its specific dose was neither cytotoxic to normal L-132 lung cells *in vitro*, nor was able to raise any toxicity in mouse bodies, *in vivo* (Mukherjee et al., 2014).

To expand the anticancer potential of TO, this project aimed to be a starting point towards discovering the effects of TO mediated PDT (TO-PDT) to observe the potential synergistic benefits in enhancing cancer cell death, which will allow for further research in the field. Additionally, this study was the first to introduce the role of TO as a possible natural PS in PDT applications. Results demonstrate how the direct cytotoxic effects of TO can act synergistically with the photochemical reactions produced during PDT to promote cancer cell death, which could prove to be a promising lung cancer treatment strategy.

2 MATERIALS AND METHODS

2.1 Cell Culture

A549 lung cancer cells (ATCC CCL-185, P-17) were cultured in Roswell Park Memorial Institute 1640 Medium (RPMI, Sigma-Aldrich, R8758) supplemented with 10% foetal bovine serum (FBS, Gibco, 306-00301), 1% antibacterial (Penicillin-streptomycin, Sigma-Aldrich, P4333) and 1% antifungal (Amphotericin-B, Sigma-Aldrich, A2942) agents. Cells from passage 17 were used and taken for experimentation every four to five passages. It was made sure that all the experimental groups include cells from same passage number. Approximately 5×10^5 cells were seeded in 3.4 cm diameter culture plates. All cultures were maintained at 37°C with 5% carbon dioxide (CO_2) and 85% humidity for 24 h to allow the cells to attach. Culture plates with more than 90% confluence were used for further experiments.

2.2 *Thuja occidentalis*

The homeopathic mother tincture was bought from a reputable and registered homeopathic company (Fusion Homeopathics, South Africa). This company imports its mother tinctures from Gehrlicher Pharmaceutical Extracts (GmbH) (manufactured according to the appropriate monograph rule 3a of the German and European Homeopathic Pharmacopoeia). The tincture was stored at room temperature, away from direct sunlight. To assess for optimal dosing parameters and to identify relevant treatment-related toxicities, different doses of TO were added to culture plates for 24 h before carrying out cytotoxicity assays. TO at 5, 10, and 15 µl were selected as the final doses for further experiments.

TABLE 1 | Laser irradiation parameters.

Name and type	Diode laser
Spectrum	660 nm
Wave emission	Continuous wave
Spot size	9.1 cm^2
Power output	87.6 mW
Power density	9.3 mW/cm^2
Fluency	5 J/cm^2
Irradiation time	9 min, 3 s (s)

2.2.1 Ethanol Cytotoxicity Study

TO is prepared using a 61% ethanol solvent. To keep the concentration of the solvent in the tincture at the most suitable doses for biological experimentation, an ethanol group was included in a preliminary study as a tincture solvent control. Cells received predetermined doses of 61% ethanol (identical to the homeopathic tincture but without the active ingredients) for 24 h. An untreated group receiving neither any tincture nor ethanol was included as a control. Both groups were subjected to morphological and biochemical studies including inverted light microscopy and trypan blue staining. As the ethanol treated cells had no significant change to the untreated control at doses of 5, 10, and 15 µl, the group was not included in further experiments.

2.3 Laser Set-Up and Parameters

For treatment regimens with light, cell samples were irradiated using a diode laser supplied by the Council for Scientific and Industrial Research (CSIR), National Laser Centre (NLC) of South Africa, at a wavelength of 660 nm and a 5 J/cm^2 fluence rate. A power meter (FieldMate) was used to determine the power output of the laser at bench level in the dark. To obtain a fluency of 5 J/cm^2, the duration of laser irradiation was calculated using the following formulae:

Fluency (J/cm^2) = time (s) × [power output (W) / Surface area (cm^2)].

Culture plates were protected from extraneous light sources, and one culture dish was illuminated at a time. The culture dishes requiring irradiation were placed directly under the laser beam with their lids removed. All control and experimental culture plates were covered in foil and placed back in the incubator for 24 h before carrying out post-irradiation assays. Irradiation parameters can be found in **Table 1**.

2.4 Experimental Parameters

Culture plates were incubated for 24 h with media containing TO at concentrations of 5 µl, 10 µl, and 15 µl; irradiation alone at 660 nm (5 J/cm^2 fluence rate); or the combined treatment (5 µl TO-PDT, 10 µl TO-PDT, and 15 µl TO-PDT). An untreated control was included as a means of comparing treatment responses. All treated and untreated groups were analyzed morphologically by inverted light microscopy and the Hoechst stain assay; as well as biochemically by LDH, ATP, and the trypan blue assays.

2.4.1 Cellular Morphology- Inverted Light Microscopy

The morphology and cellular density of the treated and untreated cells were analyzed using an inverted light microscope (Wirsam, Olympus CKX41). The microscope is connected to a camera to allow for the live visualization of cells. Culture plates were placed individually under the microscope with their lids removed in a darkened room. Images were captured on a computer using the GetIT analysis program.

2.4.2 Nuclear Morphology- Hoechst Stain Assay

Any alterations in the nuclear morphology of the treated and untreated cells were assessed by the Hoechst stain assay. Cells were seeded in 3.4 cm diameter culture dishes over sterile coverslips and allowed to reach above 80% confluence. Once confluent, cells were exposed to the different treatments. After 24 h of incubation at 37°C with 5% CO_2 and 85% humidity, each coverslip was stained with 200 µl of the Hoechst working stock solution (Hoechst 33258, Invitrogen, H1398) and incubated at room temperature for 30 min. The solution was removed from each coverslip, and cells were rinsed with phosphate-buffered saline (PBS, Sigma-Aldrich, R8758) to remove any remaining stain. Fluorescence was observed in a dark room with a fluorescent microscope (Axio observer Z1, Carl Zeiss) using a broadband 4′,6-Diamidino-2-Phenylindole (DAPI) filter set, measured at an excitation wavelength of 352 nm and an emission wavelength of 455 nm.

2.4.3 Cytotoxicity-Lactate Dehydrogenase Assay

The membrane integrity of cells was assessed by estimating the amount of LDH pre-sent in the culture media. The cytosolic enzyme LDH is released into the media due to cell membrane damage. The CytoTox 96® Non-Radioactive Cytotoxicity Assay (Anatech Promega, G400) is a quantitative method used to measure the LDH released in all control and experimental groups. Equal volumes (50 µl) of reconstituted LDH reagent and cell culture medium were micro pipetted in a clear bottom 96 well plate. The entire 96 well plate was covered with tin foil, mixed, and incubated in the dark at room temperature for 15 min. The colorimetric mixture was measured spectrophotometrically at 490 nm (Perkin–Elmer, Separation Scientific, VICTOR3™).

2.4.4 Cellular Proliferation- Adenosine Triphosphate Luminescent Assay

The ATP Cell Titer-Glo® luminescent assay (Anatech Promega, G7570) is a homogeneous method for the determination of cellular proliferation and quantification of ATP present in metabolically active cells. Equal volumes (50 µl) of reconstituted ATP reagent and the cell suspension were micro pipetted into an opaque-walled luminescent 96 well plate (white). The entire plate was covered with foil and the cells and reagent mixture were mixed on a shaker for 5 min to induce cell lysis. The cells were incubated in the dark at room temperature for 30 min to stabilize the luminescent signal. The luminescent signal was read using the 1420 multilabel counter victor3 (Perkin-Elmer, Separation Scientific, VIC-TOR3™) in relative light units (RLU).

2.4.5 Cellular Viability- Trypan Blue Assay

Cell viability in all groups was quantified using the trypan blue dye exclusion assay. Trypan blue (Sigma-Aldrich, T8154) was used to stain the cells by diluting 10 µl of the cell suspension into 10 µl of 0.4% trypan blue dye. A volume of 10 µl of stained cells was loaded into each side of a plastic, disposable cell counting chamber slide. Cells with damaged membranes (non-viable) will take in the blue chromophore dye, whereas the cells with intact cell membranes (viable) will not absorb the dye and hence, remain clear. An automated cell counter (CountessTM Automated Cell Counter, Thermo Fischer, AMQAX1000) was used for the cell count and viability estimation.

2.5 Statistical Analysis

Data were obtained from representative independent experiments and expressed as the mean ± standard error (SE). Experiments were repeated in triplicate, and assays were run in duplicate ($n = 6$). The SPSS Data Analysis Software was used to collect and process the results. Data were statistically analyzed using the one-way ANOVA and Dennett's multiple comparison test. Statistical significance was set at $^*p < 0.05$ when compared to the control.

3 RESULTS

3.1 Ethanol Cytotoxicity Study on A549 Cells

To investigate the cytotoxic effects of ethanol, A549 cells were pre-treated with 61% ethanol for 24 h at different doses and compared to untreated control cells. The cytotoxic and antiproliferative effects were observed morphologically by an inverted light microscope and biochemically by trypan blue staining.

3.2.1 Cellular Morphology by Inverted Light Microscopy

An inverted light microscope was used to assess any morphological changes in the cell and cell density of A549 cells treated with 61% ethanol at the selected doses that may be indicative of apoptosis and hence cell death. Cells treated with ethanol at doses up to 15 µl demonstrated no significant change in cell morphology and density compared to the control. Cells at these doses remained attached to their respective culture plates at high densities and retained their normal morphological shape. **Figure 1A** demonstrates the morphological changes in A549 cells treated with 61% ethanol at different doses compared to untreated control cells.

3.2.2 Cellular Viability by Trypan Blue Assay

The trypan blue assay was used to assess the viability of A549 cells treated with 61% ethanol at different doses. Cells treated with ethanol at doses up to 15 µl demonstrated no significant change in cell viability when compared to the control and is thus associated with the absence of cytotoxicity. **Figure 1B** shows the viability of A549 cells treated with 61% ethanol at different doses compared to the untreated control.

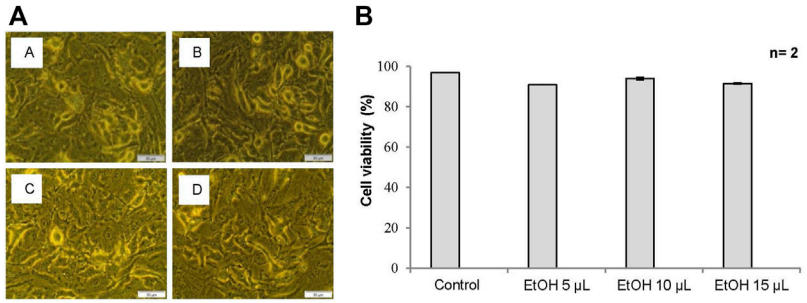

FIGURE 1 | (A) Cell morphology of A549 cells after exposure to different doses of 61% ethanol (EtOH) under an inverted light microscope (x200 Magnification). **Figure 1A** Untreated control, **(B)** 5 µl EtOH, **(C)** 10 µl EtOH, and **(D)** 15 µl EtOH. Scale bar 50 µm. **(B)** The percentage (%) of viable cells using trypan blue assay in A549 cells treated with 61% EtOH. Data is represented as the mean standard error (±SE).

3.3 Experimental Study

To investigate the cytotoxic and antiproliferative effects of the treatment, A549 cells were pre-treated with TO, TO-PDT, and irradiation alone for 24 h and compared to untreated control cells. TO was delivered to cells in doses of 5, 10, and 15 µl. A 660 nm diode laser was used to deliver treatment regimens with light at a fluence rate of 5 J/cm^2. To obtain this fluency, the duration of laser irradiation was calculated using the power output from the 660 nm laser. The power output for the 660 nm laser was 87.6 mW. Therefore, the time calculated to deliver a fluence of 5 J/cm^2 to a culture plate requiring irradiation was 9 min and 3 s. The cytotoxic and antiproliferative effects were observed morphologically and biochemically using various assays. Statistically significant at $^*p < 0.05$, $^{**}p < 0.01$, and $^{***}p < 0.001$.

3.3.1 Cellular Morphology by Inverted Light Microscopy

Cells in all control and experimental groups were observed under an inverted light microscope to assess any changes in the cell that may be attributed to cell death. Cells treated with TO and TO-PDT demonstrated significant morphological changes when compared to the control. Cells in the control group retained their normal shape and remained attached to their respective culture plates in high densities. Cell detachment, rounding up of cells, and cell debris were observed in cells treated with TO and TO-PDT, with increasing evidence of cell death in cells treated with 15 µl of TO-PDT. Cells treated with irradiation alone demonstrated no observable changes in cell morphology when compared to the control. **Figure 2** demonstrates the morphology of the A549 cells in the control and experimental cell groups.

3.3.2 Nuclear Morphology by Hoechst Stain Assay

Alterations in the nuclear morphology of the treated cells were explored using the Hoechst fluorescent stain assay and compared to the control cells. Changes in the nuclei morphology associated with apoptosis; including abnormally shaped nuclei, nuclei shrinkage, chromatin condensation, and nuclei fragmentation were observed in cells treated with TO and TO-PDT. Cells treated with irradiation alone demonstrated no observable changes in the cell nuclei when compared to the control. **Figure 3** shows the morphology of the cell nuclei in all experimental and control groups.

3.3.3 Cytotoxicity by Lactate Dehydrogenase Assay

The lactate dehydrogenase (LDH) CytoTox96® colorimetric assay was used to investigate the *in vitro* cytotoxic effects of the different treatments on A549 cells compared to the control cells. Cell death is accompanied by a loss of cell membrane integrity which allows the intracellular LDH to release into the extracellular media. The extracellular LDH was quantified 24 h post-treatment. Cells treated with TO at 5 ($p < 0.05$), 10 ($p < 0.01$), and 15 ($p < 0.001$); and TO-PDT ($p < 0.05$) demonstrated significant dose-dependent decreases in LDH levels when compared to the control. The highest cytotoxic effects were observed in A549 cells after using a dose of 15 µl TO-PDT. Cells treated with irradiation alone demonstrated no significant change in comparison to the control. **Figure 4A** demonstrates the levels of LDH in all experimental and control groups.

3.3.4 Cellular Proliferation by Adenosine Triphosphate Luminescent Assay

The adenosine triphosphate (ATP) Cell Titer-Glo® luminescent assay was used to determine the antiproliferative potential of the different treatment groups on A549 cells when compared to the control. Metabolically active cells are associated with higher levels of ATP due to the increased proliferation of cells compared to metabolically inactive cells. Cells treated with TO at 5 ($p < 0.01$), 10, and 15 ($p < 0.001$); and TO-PDT ($p < 0.001$) demonstrated significant dose-dependent decreases in the levels of intracellular ATP when compared to the control. Results demonstrate the antiproliferative potential of both therapies against the A549 cells. Cells treated with irradiation alone, demonstrated no significant change in ATP levels when compared to the control. **Figure 4B** shows the levels of ATP in all experimental and control groups.

3.3.5 Cellular Viability by Trypan Blue Assay

The trypan blue assay was used to investigate the viability of cells in all experimental and control groups. A decrease in cell viability is directly associated with cell death and vice versa. Cells treated with TO ($p < 0.001$) and TO-PDT ($p < 0.001$) demonstrated a dose-dependent decrease in the viability of the cells when compared to the control. Cells treated with irradiation alone,

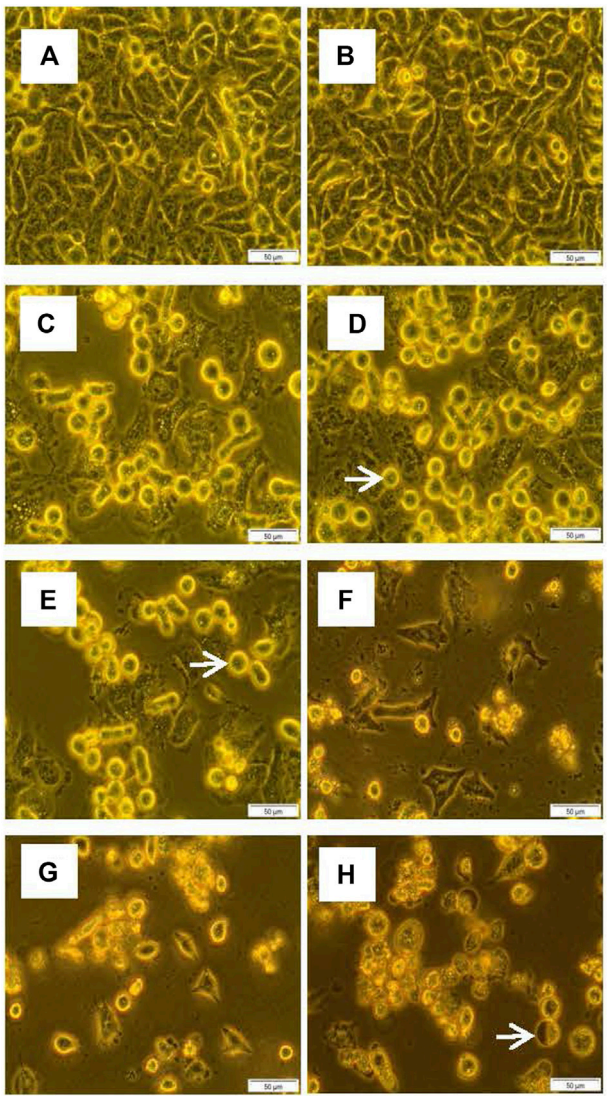

FIGURE 2 | Cell morphology of A549 cells after exposure to different doses of *Thuja occidentalis* homeopathic mother tincture (TO) and TO mediated photodynamic therapy (TO-PDT) under an inverted light microscope (x200 Magnification). **Figure 3 (A)** Untreated control, **(B)** Irradiation only, **(C)** 5 µl TO, **(D)** 10 µl TO, **(E)** 15 µl TO, **(F)** 5 µl TO-PDT, **(G)** 10 µl TO-PDT, **(H)** 15 µl TO-PDT. Scale bar 50 µm. White arrows indicate examples of rounded up dead cells.

demonstrated no significant change in the viability of cells when compared to the control and both maintained an average viability rate above 90%. **Figure 4C** shows the viability of cells in all experimental and control groups.

4 DISCUSSION

Lung cancer is at the forefront of cancer-related mortality worldwide, and despite advances in current treatments it still has a 5-year survival rate estimated at 15% of all stages combined (Duruisseaux and Esteller, 2018). This highlights the need for further investigations that may identify alternative treatment pathways that provide more efficient solutions for diverse situations. This study introduced and proposed the combinatory role of PDT and homeopathy in an attempt to provide new perspectives in the search for optimal lung cancer therapeutics. Studies carried out *in vivo* and *in vitro* have demonstrated and maintained the role of TO as an effective anticancer agent that can act as a natural obstacle in limiting cancer cell growth and progression. To expand the cytotoxic potential of TO, this study investigated the effects of TO homeopathic mother tincture when used as a PS in PDT on A549 lung cancer cells to observe any additive value of the combined treatment in enhancing cancer cell death.

Ethanol above its toxic threshold can alter the cellular environment and cause disruptions in the physical activities of cells. Thus, ethanol at toxic dosages can promote cell death which

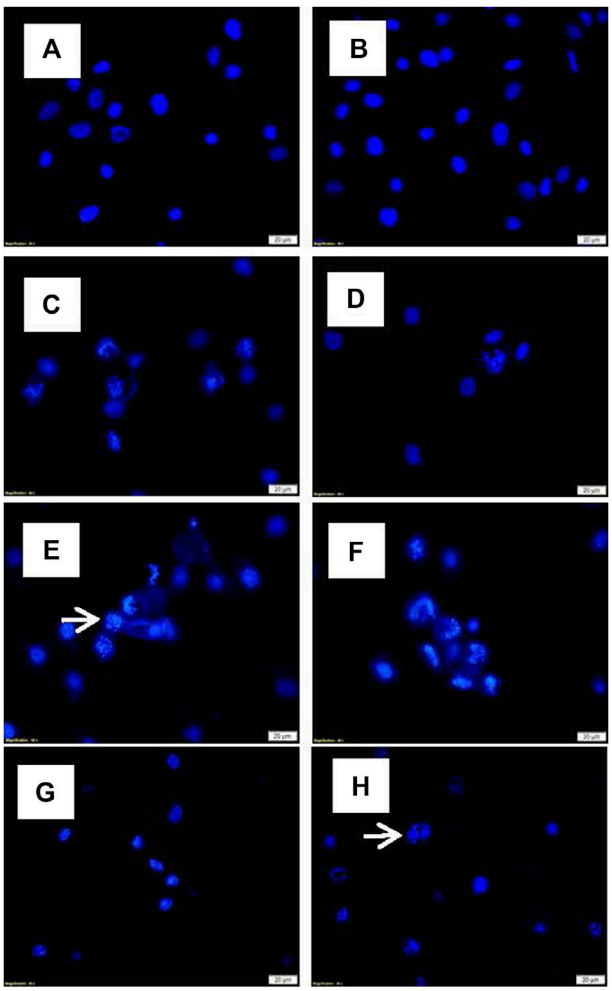

FIGURE 3 | Nuclei morphology of A549 cells after exposure to different doses of TO and TO-PDT under a fluorescent microscope (x400 Magnification). **(A)** Untreated control, **(B)** Irradiation only, **(C)** 5 µl TO, **(D)** 10 µl TO, **(E)** 15 µl TO, **(F)** 5 µl TO-PDT, **(G)** 10 µl TO-PDT, **(H)** 15 µl TO-PDT. Scale bar 20 µm. White arrows indicate examples of abnormal cell nuclei.

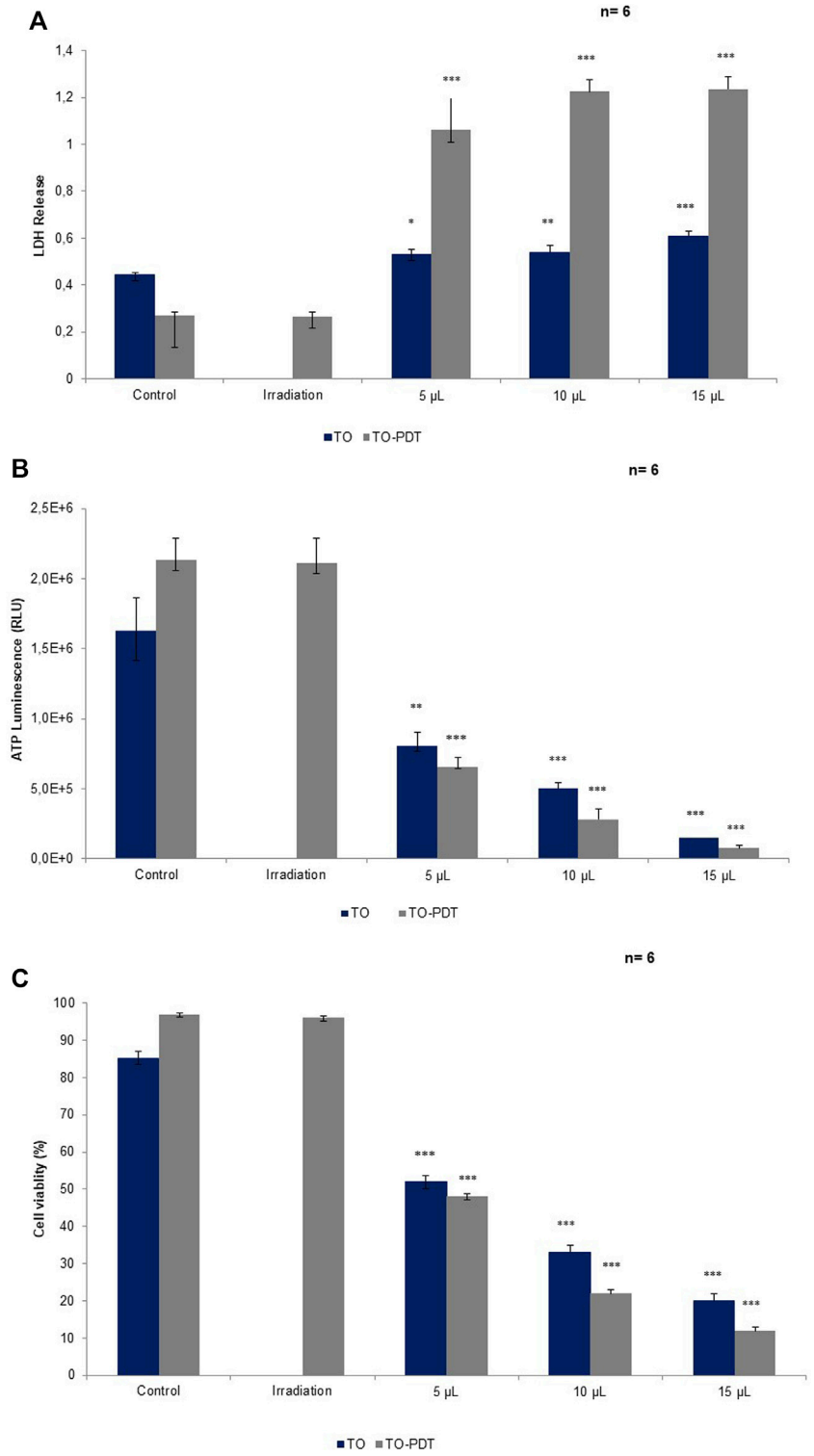

FIGURE 4 | A comparison of **(A)** LDH, **(B)** ATP, and **(C)** cell viability levels on A549 cells treated with *Thuja occidentalis* homeopathic mother tincture (TO) and TO mediated photodynamic therapy (TO-PDT) at the same doses of the tincture. At the same doses, TO when used as a photosensitizer in PDT, produced amplified antiproliferative and cytotoxic responses on A549 cells compared to cells treated with TO alone.

can consequently alter experimental outcomes and results (Timm et al., 2013). TO is pre-pared in a 61% hydroethanolic solvent; therefore to attribute the anticancer effects of the treatment to its plant actives, the solvent at its selected dose had to be biocompatible and non-toxic to cells. Both the morphological and viability studies demonstrated that ethanol in doses up to 15 µl had no significant observable differences when compared to the untreated control. This would imply that 61% ethanol in optimized doses (5, 10, and 15 µl) had no direct cytotoxic effects on A549 cells, and any signs of cell death can be attributed to TO.

Cells treated with TO and TO-PDT displayed significant morphological changes under an inverted light microscope which provided preliminary evidence of cell death. This included loss of cell-to-cell contact, cell shrinkage, reduced cellular density, rounding up of cells, and cell detachment from their respective culture plates; all associated with features indicative of apoptosis and hence, cell death. Results are consistent with nuclear morphology studies, which demonstrate the ability of the treatments in inducing DNA damage. On the Hoechst stain, cells treated with TO and TO-PDT displayed irregularly shaped nuclei, chromatin condensation, nuclear fragmentation, and shrinkage; all of which are associated with the typical features of apoptosis and negative consequences for cell survival and progression. Cells treated with irradiation alone were unable to elicit any significant change morphologically or biochemically compared to the control cells and are hence, associated with the absence of any positive anticancer effects. Results from the morphological studies correlate with results obtained from biochemical parameters. Cells treated with TO and TO-PDT demonstrated a statistically significant dose-dependent increase in LDH levels. The LDH results are complemented by the dose-dependent decrease in ATP and cell viability, which confirms the antiproliferative and cytotoxic potential of the therapies. The decline in ATP is associated with a decrease in the metabolic activity of the cells meaning that the cells can no longer sustain growth signaling and cell proliferation. ATP deprivation is a common feature occurring in apoptosis, necrosis, and autophagic cell death mechanisms (Nikoletopoulou et al., 2013; Kim, 2018).

These results validate previous research studies that elucidate and demonstrate the independent ability of TO herbal and homeopathic extracts in inducing cancer cell death. In the *in vitro* study by Biswas et al., TO homeopathic mother tincture was shown to decrease cell viability and proliferation and induce cell death through apoptotic induction in A375 cancer cells by favouring mitochondrial transmembrane collapse, internucleosomal DNA fragmentation, increased ROS generation, and the activation of caspase-3 (Biswas et al., 2011). Torres et al. (2016) provided a detailed mechanism of the pro-apoptotic and anti-angiogenic properties of the thujone fractions isolated from TO extracts on glioblastoma cells *in vitro*. The thujone components induced their anticancer effects through the inhibition of angiogenic factor production, decrease in the tube formation of endothelial cells, and decreased expressions of vascular endothelial growth factors (VEGF) and angiopoietin-4. These factors are essential for tumour growth and survival in a hypoxic environment (Torres et al., 2016). In an *in vitro* study by Saha et al. (2014), TO extracts were shown to induce apoptosis in a ROS-P53 feedback loop on breast cancer cells (Saha et al., 2014). These studies showed the preferential induction of the cytotoxic effects on cancer cells while maintaining the intact structure and integrity of healthy cells.

TO when photoactivated, revealed higher anticancer activity levels on A549 cells compared to cells treated with TO only (**Figure 4**). At the same doses, cells treated with TO-PDT had the ability to remarkably enhance the cytotoxic and antiproliferative potential in A549 lung cancer cells 24 h post-irradiation by favouring higher LDH release and lower ATP production and cell viability, thereby surpassing the effects of treatment with TO alone. This indicates how the direct cytotoxic effects of TO can act synergistically with the photochemical reactions produced during PDT to promote cell death. This implies that TO has a positive absorption wavelength at the red region specifically at 660 nm, which falls within the therapeutic window of biological tissue where increased transmission and high ROS production are at its maximum (Donohoe et al., 2019). Cell death after PDT is mediated predominantly through apoptosis which is associated with irreversible cell death (Villacorta et al., 2017). According to phytochemical studies, TO based preparations contain various active constituents including essentials oils, coumarins, flavonoids, tannins and proanthocyanidines (Caruntu et al., 2020). In a PDT setting, coumarins and its derivatives play an active role in research as a naturally occurring organic PS due its strong photophysical and photochemical properties (Köksoy et al., 2019). A study by Gangopadhyay et al. (2015), revealed the photodynamic effects of a titanium dioxide-coumarin nanoconjugate on MDA-MB-231 breast cancer cells. Coumarin derivatives were selected as the chromophore in the complex due to its photophysiochemical abilities (Gangopadhyay et al., 2015). In TO, coumarins are present in the form of p-coumaric acid (PCA), and umbelliferone (7-hydroxycoumarin) (Caruntu et al., 2020). PCA is a phenolic compound with antioxidant, anticancer and anti-inflammatory properties. Kianmehr et al. (2020) demonstrated the anticancer activity of PCA and low-level irradiation against human malignant melanoma cells. The combined treatment was able to decrease cell viability, possibly through apoptotic pathways (Kianmehr et al., 2020). 7-hydroxycoumarins have been shown to exhibit anticancer, anti-inflammatory, and antimutagenic properties. These agents are considered to be common precursors of furanocoumarin derivatives depending on the prenylation position of the 7-hydroxycoumarin. At the C6 position, 7-hydroxycoumarin gives rise to the psoralen derivative and at the C8 position it gives rise to the angelicin derivative (Karamat et al., 2014). Further studies should aim to discover the exact phytochemicals that could be responsible for its interactions and contributions in a PDT setting.

While TO-PDT may be an effective treatment strategy against lung cancer, further and more complex investigations are needed to determine the mechanism of action of the therapy and to establish optimal dosimetric, treatment, and safety parameters that would allow for wider-ranging interpretations of the current findings.

5 CONCLUSION

This study has corroborated previous research that demonstrates the cytotoxic and antiproliferative properties of TO and has implicated its efficacy as a potential anticancer agent. This study was also the first to introduce the role of TO as a possible natural PS in PDT applications, which by this study has been revealed to be far more effective in inducing cancer cell death than that produced by TO independently. A549 cells treated with TO and TO-PDT showed a dose-dependent increase in LDH with a concomitant decrease in ATP and cell viability levels that were statistically significant and biologically plausible. Furthermore, changes in the cell and cell nuclei indicative of apoptosis were observed under morphological analyses. The implementation of TO in PDT applications presents a possible anticancer strategy in the treatment of lung cancer. The experiment can be replicated on different types of cell lines to determine the efficacy of TO and TO-PDT on other types of cancer. However, an extensive amount of research is encouraged and needed to validate the laboratory findings in both *in vitro* and *in vivo* studies before treatment regimens with TO-PDT become discernible. Further research will aim to compare the photodynamic effects of TO to other medically approved PSs, to determine if TO-PDT has any additional and synergistic benefits aimed at overcoming the limitations of current conventional PSs.

DATA AVAILABILITY STATEMENT

The original contributions presented in the study are included in the article/supplementary materials, further inquiries can be directed to the corresponding author.

AUTHOR CONTRIBUTIONS

Conceptualization, RC and AL; methodology, RC; validation, AL, RC, JP, and HA; formal analysis, AL and RC; investigation, AL and RC; resources, AL, RC, and HA; data curation, AL and RC; writing—original draft preparation, AL; writing—review and editing, AL, RC, JP, and HA; visualization, AL, RC, and JP; supervision, RC and JP; project administration, RC; funding acquisition, RC and HA All authors have read and agreed to the published version of the manuscript.

FUNDING

This research was funded by the South African Research Chairs Initiative of the Department of Science and Technology and National Research Foundation of South Africa (Grant No 98337), as well as grants received from the University of Johannesburg (URC), the National Research Foundation, and the Council for Scientific and Industrial Research National Laser Centre Laser Rental Pool Program.

REFERENCES

Alves, L. D. S., Figueirêdo, C. B. M., Silva, C. C. A. R., Marques, G. S., Ferreira, P. A., Soares, M. F. R., et al. (2014). *Thuja occidentalis* L. (Cupressaceae): Review of Botanical, Phytochemical, Pharmacological and Toxico-Logical Aspects. *Int. J. Pharm. Sci. Res.* 5, 1163–1177. doi:10.13040/IJPSR.0975-8232.5

Biswas, R., Mandal, S. K., Dutta, S., Bhattacharyya, S. S., Boujedaini, N., and Khuda-Bukhsh, A. R. (2011). Thujone-Rich Fraction of *Thuja occidentalis* Demonstrates Major Anti-Cancer Potentials: Evidences from *In Vitro* Studies on A375 Cells. *Evidence-Based Complementary Altern. Med.* 2011, 568148. doi:10.1093/ecam/neq042

Bray, F., Ferlay, J., Soerjomataram, I., Siegel, R. L., Torre, L. A., and Jemal, A. (2018). Global Cancer Statistics 2018: GLOBOCAN Estimates of Incidence and Mortality Worldwide for 36 Cancers in 185 Countries. *CA Cancer J. Clin.* 68, 394–424. doi:10.3322/caac.21492

Caruntu, S., Ciceu, A., Olah, N. K., Don, I., Hermenean, A., and Cotoraci, C. (2020). *Thuja Occidentalis* L. (Cupressaceae): Ethnobotany, Phytochemistry and Biological Activity. *Molecules* 25 (22), 5416. doi:10.3390/molecules25225416

Chen, J., Fan, T., Xie, Z., Zeng, Q., Xue, P., Zheng, T., et al. (2020). Advances in Nanomaterials for Photodynamic Therapy Applications: Status and Challenges. *Biomaterials* 237, 119827. doi:10.1016/j.biomaterials.2020.119827

Danneyrolles, V., Dupuis, S., Arseneault, D., Terrail, R., Leroyer, M., de Römer, A., et al. (2017). Eastern White Cedar Long-Term Dynamics in Eastern Canada: Implications for Restoration in the Context of Ecosystem-Based Management. *For. Ecol. Manag.* 400, 502–510. doi:10.1016/j.foreco.2017.06.024

Das, E. (2019). Understanding the Principles of Homeopathy on a Research Perspective. *Jcmah* 9, 555756. doi:10.19080/JCMAH.2019.09.555756

Dehghan, M., Namjoo, Z., Bahrami, A., Tajedini, H., Shamsaddini-Lori, Z., Zarei, A., et al. (2020). The Use of Complementary and Alternative Medicines, and Quality of Life in Patients under Hemodialysis: A Survey in Southeast Iran. *Complement. Ther. Med.* 51, 102431. doi:10.1016/j.ctim.2020.102431

Dong, X., Zeng, Y., Zhang, Z., Fu, J., You, L., He, Y., et al. (2021). Hypericin-mediated Photodynamic Therapy for the Treatment of Cancer: a Review. *J. Pharm. Pharmacol.* 73 (4), 425–436. doi:10.1093/jpp/rgaa018

Donohoe, C., Senge, M. O., Arnaut, L. G., and Gomes-da-Silva, L. C. (2019). Cell Death in Photodynamic Therapy: From Oxidative Stress to Anti-tumor Immunity. *Biochim. Biophys. Acta Rev. Cancer* 18721872, 188308. doi:10.1016/j.bbcan.2019.07.003

Duruisseaux, M., and Esteller, M. (2018). Lung Cancer Epigenetics: From Knowledge to Applications. *Semin. Cancer Biol.* 51, 116–128. doi:10.1016/j.semcancer.2017.09.005

Fan, H. Y., Yu, X. H., Wang, K., Yin, Y. J., Tang, Y. J., Tang, Y. L., et al. (2019). Graphene Quantum Dots (GQDs)-Based Nanomaterials for Improving Photodynamic Therapy in Cancer Treatment. *Eur. J. Med. Chem.* 182, 111620. doi:10.1016/j.ejmech.2019.111620

Gangopadhyay, M., Mukhopadhyay, S. K., Karthik, S., Barman, S., and Pradeep Singh, N. D. (2015). Targeted Photoresponsive TiO2-Coumarin Nanoconjugate for Efficient Combination Therapy in MDA-MB-231 Breast Cancer Cells: Synergic Effect of Photodynamic Therapy (PDT) and Anticancer Drug Chlorambucil. *Med. Chem. Commun.* 6 (5), 769–777. doi:10.1039/C4MD00481G

Global Report on Traditional and Complementary Medicine. Available online: https://apps.who.int/iris/bitstream/handle/10665/312342/9789241515436-eng.pdf?ua=1. [Accessed 3 April 2021].

Hu, J.-J., Lei, Q., and Zhang, X.-Z. (2020). Recent Advances in Photonanomedicines for Enhanced Cancer Photodynamic Therapy. *Prog. Mater. Sci.* 114, 100685. doi:10.1016/j.pmatsci.2020.100685

Ijaz, S., Akhtar, N., Khan, M. S., Hameed, A., Irfan, M., Arshad, M. A., et al. (2018). Plant Derived Anticancer Agents: A Green Approach towards Skin Cancers. *Biomed. Pharmacother.* 103, 1643–1651. doi:10.1016/j.biopha.2018.04.113

Karamat, F., Olry, A., Munakata, R., Koeduka, T., Sugiyama, A., Paris, C., et al. (2014). A Coumarin-specific Prenyltransferase Catalyzes the Crucial Biosynthetic Reaction for Furanocoumarin Formation in Parsley. *Plant J.* 77 (4), 627–638. doi:10.1111/tpj.12409

Kianmehr, Z., Khorsandi, K., Mohammadi, M., and Hosseinzadeh, R. (2020). Low-level Laser Irradiation Potentiates Anticancer Activity of P-Coumaric Acid

against Human Malignant Melanoma Cells. *Melanoma Res.* 30 (2), 136–146. doi:10.1097/CMR.0000000000000603

Kim, S. Y. (2018). Cancer Energy Metabolism: Shutting Power off Cancer Factory. *Biomol. Ther. Seoul.* 26, 39–44. doi:10.4062/biomolther.2017.184

Köksoy, B., Durmuş, M., and Bulut, M. (2019). Potential Photosensitizer Candidates for PDT Including 7-Oxy-3-Thiomethylphenyl Coumarino-Phthalocyanines. *Inorganica Chim. Acta* 498, 119137. doi:10.1016/j.ica.2019.119137

Kubrak, T. P., Kołodziej, P., Sawicki, J., Mazur, A., Koziorowska, K., and Aebisher, D. (2022). Some Natural Photosensitizers and Their Medicinal Properties for Use in Photodynamic Therapy. *Molecules* 27 (4), 1192. doi:10.3390/molecules27041192

Lopes, T. Z., de Moraes, F. R., Tedesco, A. C., Arni, R. K., Rahal, P., and Calmon, M. F. (2019). Berberine Associated Photodynamic Therapy Promotes Autophagy and Apoptosis via ROS Generation in Renal Carcinoma Cells. *Biomed. Pharmacother.* 123, 109794. doi:10.1016/j.biopha.2019.109794

Mansoori, B., Mohammadi, A., Amin Doustvandi, M., Mohammadnejad, F., Kamari, F., Gjerstorff, M. F., et al. (2019). Photodynamic Therapy for Cancer: Role of Natural Products. *Photodiagnosis Photodyn. Ther.* 26, 395–404. doi:10.1016/j.pdpdt.2019.04.033

Millimouno, F. M., Dong, J., Yang, L., Li, J., and Li, X. (2014). Targeting Apoptosis Pathways in Cancer and Perspectives with Natural Compounds from Mother Nature. *Cancer Prev. Res. (Phila)* 7, 1081–1107. doi:10.1158/1940-6207.CAPR-14-0136

Mottaghitalab, F., Farokhi, M., Fatahi, Y., Atyabi, F., and Dinarvand, R. (2019). New Insights into Designing Hybrid Nanoparticles for Lung Cancer: Diagnosis and Treatment. *J. Control Release* 295, 250–267. doi:10.1016/j.jconrel.2019.01.009

Mukherjee, A., Sikdar, S., Bishayee, K., Boujedaini, N., and Khuda-Bukhsh., A. R. (2014). Flavonol Isolated from Ethanolic Leaf Extract of *Thuja occidentalis* Arrests the Cell Cycle at G2-M and Induces ROS-independent Apoptosis in A549 Cells, Targeting Nuclear DNA. *Cell Prolif.* 47 (1), 56–71. doi:10.1111/cpr.12079

Nikoletopoulou, V., Markaki, M., Palikaras, K., and Tavernarakis, N. (2013). Crosstalk between Apoptosis, Necrosis and Autophagy. *Biochim. Biophys. Acta* 1833, 3448–3459. doi:10.1016/j.bbamcr.2013.06.001

Pinto da Silva, L., Núnez-Montenegro, A., Magalhães, C. M., Ferreira, P. J. O., Duarte, D., González-Berdullas, P., et al. (2019). Single-molecule Chemiluminescent Photosensitizer for a Self-Activating and Tumor-Selective Photodynamic Therapy of Cancer. *Eur. J. Med. Chem.* 183, 111683. doi:10.1016/j.ejmech.2019.111683

Pudełek, M., Catapano, J., Kochanowski, P., Mrowiec, K., Janik-Olchawa, N., Czyż, J., et al. (2019). Therapeutic Potential of Monoterpene α-thujone, the Main Compound of *Thuja occidentalis* L. Essential Oil, against Malignant Glioblastoma Multiforme Cells *In Vitro*. *Fitoterapia* 134, 172–181. doi:10.1016/j.fitote.2019.02.020

Romm, A., Ganora, L., Hoffmann, D., Yarnell, E., Abascal, K., and Coven, M. (2010). "Fundamental Principles of Herbal Medicine," in *Botanical Medicine for Women's Health* (Saint Louis: Churchill Livingston), 24–74. doi:10.1016/b978-0-443-07277-2.00003-9

Saha, S., Bhattacharjee, P., Mukherjee, S., Mazumdar, M., Chakraborty, S., Khurana, A., et al. (2014). Contribution of the ROS-P53 Feedback Loop in Thuja-Induced Apoptosis of Mammary Epithelial Carcinoma Cells. *Oncol. Rep.* 31, 1589–1598. doi:10.3892/or.2014.2993

Sando, Y., Matsuoka, K. I., Sumii, Y., Kondo, T., Ikegawa, S., Sugiura, H., et al. (2020). 5-aminolevulinic Acid-Mediated Photodynamic Therapy Can Target Aggressive Adult T Cell Leukemia/lymphoma Resistant to Conventional Chemotherapy. *Sci. Rep.* 10 (1), 17237. doi:10.1038/s41598-020-74174-x

Shi, S., Cho, H., Sun, Q., He, Y., Ma, G., Kim, Y., et al. (2019). Acanthopanacis Cortex Extract: A Novel Photosensitizer for Head and Neck Squamous Cell Carcinoma Therapy. *Photodiagnosis Photodyn. Ther.* 26, 142–149. doi:10.1016/j.pdpdt.2019.02.020

Siewert, B., and Stuppner, H. (2019). The Photoactivity of Natural Products - an Overlooked Potential of Phytomedicines? *Phytomedicine* 60, 152985. doi:10.1016/j.phymed.2019.152985

Silva, I. S., Nicolau, L. A. D., Sousa, F. B. M., Araújo, S., Oliveira, A. P., Araújo, T. S. L., et al. (2017). Evaluation of anti-inflammatory potential of aqueous extract and polysaccharide fraction of *Thuja occidentalis* L. in mice. *Int. J. Biol. Macromol.* 105, 1105–1116. doi:10.1016/j.ijbiomac.2017.07.142

Siveen, K. S., and Kuttan, G. (2011). Augmentation of humoral and cell mediated immune responses by Thujone. *Int. Immunopharmacol.* 11 (12), 1967–1975. doi:10.1016/j.intimp.2011.08.006

Stan, M. S., Voicu, S. N., Caruntu, S., Nica, I. C., Olah, N. K., Burtescu, R., et al. (2019). Antioxidant and Anti-Inflammatory Properties of a *Thuja occidentalis* Mother Tincture for the Treatment of Ulcerative Colitis. *Antioxidants (Basel)* 8 (9), 416. doi:10.3390/antiox8090416

Steven, D. Botanical Basics: Botanical Extracts: Not Single Chemical Ingredients. Understanding botanical extracts requires understanding solvents, extract ratios and extract semi-purification. Available at: https://www.nutraceuticalsworld.com/issues/2013-04/view_columns/botanical-basics-botanical-extracts-not-single-chemical-ingredients/[Accessed on 22 April 2022].

Sunila, E. S., Hamsa, T. P., and Kuttan, G. (2011). Effect of *Thuja occidentalis* and its polysaccharide on cell-mediated immune responses and cytokine levels of metastatic tumor-bearing animals. *Pharm. Biol.* 49 (10), 1065–1073. doi:10.3109/13880209.2011.565351

Timm, M., Saaby, L., Moesby, L., and Hansen, E. W. (2013). Considerations regarding use of solvents in *In Vitro* cell based assays. *Cytotechnology* 65, 887–894. doi:10.1007/s10616-012-9530-6

Torres, A., Vargas, Y., Uribe, D., Carrasco, C., Torres, C., Rocha, R., et al. (2016). Pro-apoptotic and anti-angiogenic properties of the α/β-thujone fraction from *Thuja occidentalis* on glioblastoma cells. *J. Neurooncol* 128, 9–19. doi:10.1007/s11060-016-2076-2

Villacorta, R. B., Roque, K. F. J., Tapang, G. A., and Jacinto, S. D. (2017). Plant extracts as natural photosensitizers in photodynamic therapy: *In Vitro* activity against human mammary adenocarcinoma MCF-7 cells. *Asian Pac. J. Trop. Biomed.* 7, 358–366. doi:10.1016/j.apjtb.2017.01.025

Witt, C. M., Balneaves, L. G., CardosoCohenH Johnstone P KücükMailmanMao, M. J. L. GreenleeO. J. J. J., Cohen, L., Greenlee, H., Johnstone, P., et al. (2017). A comprehensive definition for integrative oncology. *J. Natl. Cancer Inst. Monogr.* 2017, 52. doi:10.1093/jncimonographs/lgx012

Conflict of Interest: The authors declare that the research was conducted in the absence of any commercial or financial relationships that could be construed as a potential conflict of interest.

Publisher's Note: All claims expressed in this article are solely those of the authors and do not necessarily represent those of their affiliated organizations, or those of the publisher, the editors and the reviewers. Any product that may be evaluated in this article, or claim that may be made by its manufacturer, is not guaranteed or endorsed by the publisher.

Advantages of publishing in Frontiers

OPEN ACCESS
Articles are free to read for greatest visibility and readership

FAST PUBLICATION
Around 90 days from submission to decision

HIGH QUALITY PEER-REVIEW
Rigorous, collaborative, and constructive peer-review

TRANSPARENT PEER-REVIEW
Editors and reviewers acknowledged by name on published articles

Frontiers
Avenue du Tribunal-Fédéral 34
1005 Lausanne | Switzerland

Visit us: www.frontiersin.org
Contact us: frontiersin.org/about/contact

REPRODUCIBILITY OF RESEARCH
Support open data and methods to enhance research reproducibility

DIGITAL PUBLISHING
Articles designed for optimal readership across devices

FOLLOW US
@frontiersin

IMPACT METRICS
Advanced article metrics track visibility across digital media

EXTENSIVE PROMOTION
Marketing and promotion of impactful research

LOOP RESEARCH NETWORK
Our network increases your article's readership